Fall 1998

Experimental Description of Flow at an Open-Channel Junction

Eric Dean Shumate
University of Iowa

EXPERIMENTAL DESCRIPTION OF FLOW AT AN OPEN-CHANNEL JUNCTION

by

Eric Dean Shumate

A thesis submitted in partial fulfillment of the requirements
for the Master of Science degree in
Civil and Environmental Engineering
in the Graduate College of
The University of Iowa

December 1998

Thesis supervisor: Assistant Professor Larry J. Weber

Graduate College
The University of Iowa
Iowa City, Iowa

CERTIFICATE OF APPROVAL

MASTER'S THESIS

This is to certify that the Master's thesis of

Eric Dean Shumate

has been approved by the Examining Committee for the thesis requirement for the Master of Science degree in Civil and Environmental Engineering at the December 1998 graduation.

Thesis committee: _____
Thesis supervisor

_____
Member

_____
Member

ACKNOWLEDGMENTS

I would first like to thank Dr. Larry Weber for the continual guidance and funding he provided throughout the duration of my graduate education. His encouragement and guidance has allowed me to achieve goals I would never have believed possible. I am fortunate to have found both a good advisor and a good friend.

I need to thank the entire IIHR shop staff for the prompt assistance when any problems arose during the completion of this project. A special thanks to Jim Goss, Steve Laszczak, Jeff King, and Terry Lehman for the design and construction of the flume in which this experiment was carried out and for the hours of torment that they seemed so happy to provide. Mike Kundert also deserves thanks for his ability to produce construction drawings and report illustrations on short notice.

I would like to thank my family for the continuous support that they have given me not only in my education, but also throughout my life.

Above all, I want to thank Michelle for all the patience and faith she has had in me. She has unfailingly supported me through all the long hours away and nights full of studying. The sacrifices she has made to keep our home and family together throughout my education will never be forgotten.

TABLE OF CONTENTS

LIST OF TABLES

LIST OF FIGURES

LIST OF SYMBOLS

E_1	energy in the upstream main channel
E_2	energy in the branch channel
F_d	Froude number in the downstream channel
F_{n3}	Froude number in the downstream channel
H	width of the zone of separation
K	turbulent kinetic energy
K_e	energy loss coefficient
k_2	ratio of branch channel velocity head to branch channel depth
L	length of the zone of separation
n	number of samples
n_q	ratio of branch channel flow to downstream combined flow
n_q	ratio of upstream main channel flow to downstream combined flow
n_y	ratio of upstream main channel depth to downstream combined depth
q	ratio of branch channel flow to downstream combined flow
q	ratio of upstream main channel flow to downstream combined flow
q^*	ratio of upstream main channel flow to downstream combined flow
Q_b	branch channel flow
Q_m	upstream main channel flow

Q_t	downstream combined flow
R_q	ratio of branch channel flow to downstream combined flow
s	sample standard deviation
u	velocity in the x-direction
u′	turbulent velocity fluctuation in the x-direction
v	velocity in the y-direction
v′	turbulent velocity fluctuation in the y-direction
w	velocity in the z-direction
w′	turbulent velocity fluctuation in the z-direction
W	channel width
x	longitudinal distance from upstream junction corner, positive upstream
x^*	longitudinal distance non-dimesionalized by channel width
y	lateral distance from upstream junction corner, positive toward outer wall
y^*	lateral distance non-dimensionalized by channel width
y_1	depth in upstream main channel
y_c	depth at critical section
Y	ratio of upstream main channel depth to downstream combined depth
z	vertical distance from bed at upstream junction corner, positive up
z^*	vertical distance non-dimesionalized by channel width
α	kinetic energy correction coefficient
β	momentum correction coefficient
δ	angle between centerline of branch channel and centerline of upstream channel

ΔE junction energy loss

γ angle between centerline of branch channel and centerline of upstream channel

μ contraction coefficient

θ angle between centerline of branch channel and centerline of upstream channel

CHAPTER 1

INTRODUCTION

The junction of two open channels is a common occurrence in many hydraulic structures ranging from wastewater treatment facilities to fish passage conveyance structures. While open-channel junctions are present in many hydraulic systems, only limited research has been conducted on the topic. In recent years more focus has been given to the combining open-channel junction problem, yet very little data exist on the detailed flow conditions present in junction flow. Prior studies have focused on simplified mathematical approximations of different junction flow characteristics with limited data collected to compare with the theoretical models. The collected data in previous studies are limited to one-dimensional or two-dimensional velocities and often dependent on dye trace visualization for flow description.

The difficulty in addressing the problem theoretically is the numerous variables present at the junction of two open channels. One set of variables can be described as geometry variables, such as the size, shape, slope, and angle between the combining channels. One can see that infinite combinations of these four variables are possible. A second set of variables are flow variables, such as the Froude number present in the downstream flow, the channel roughness, the division of flow between the two tributary channels, and the variation of fluid properties. It is readily apparent that a simplified

mathematical model can not fully describe the complex flow conditions present at the junction of two open channels. The difficulty of describing the open-channel junction with simplified mathematical models leads to the possibility of using a three-dimensional computational fluid dynamics (CFD) code to describe the flow conditions in a combining flow junction. To date, most CFD codes have been developed for internal flows and use a rigid lid approximation for free surface flows. Therefore, the compilation of a complete data set for validation of three-dimensional, free water surface CFD codes is timely. However, currently there does not exist such a data set necessary to validate a numerical model.

The goal of this project is to compile a data set that fully describes the complex, three-dimensional flow conditions present in open-channel junction flow. The purpose for the collection of this data is to provide a benchmark experimental data set for the validation of future numerical models. The data set presented in this paper is composed of three-dimensional velocity, turbulence, and water surface mapping in the immediate area of the channel junction. The experiment focuses on a 90°, sharp-edged junction of identically sized channels. The experimental facility used in this study is of a much larger scale than that of previous studies. This allows for a detailed set of measurements to be taken across the width and depth of the tributary channels and the downstream combined channel.

The purpose of this thesis is to present the data from this experimental study of a 90° open-channel junction and describe the general junction flow features. This data set will be posted on the internet to broaden its use as validation data for numerical models.

Chapter 2 provides a review of the work previously completed in the field of combining flow at open-channel junctions. Chapter 3 discusses the specifics of the experimental facility used and the testing program implemented for this study. The collected data are presented in Chapter 4 along with a discussion of the junction flow characteristics seen in the data set. Chapter 5 provides conclusions from this study and recommendations for future work.

CHAPTER 2

REVIEW OF EXISTING LITERATURE

2.1 Introduction

While open-channel junctions have been integral in numerous hydraulic systems, there currently exists only limited data on the detailed flow conditions at open-channel junctions. The complex flow characteristics encountered in an open-channel junction coupled with the numerous variables needed to describe the junction problem has inhibited attempts to describe the flow with a mathematical model.

Open-channel junctions are characterized by the combining of incoming flow from two channels, typically a main "through" channel and a branch channel, to form a single channel conveying the combined flow downstream. These junctions may be natural or man-made. Current work has not addressed the natural channel junctions, as the addition of changing channel cross section and loose boundary further complicates the problem. However, the current work does apply to natural systems by showing general flow characteristics that are evident in all channel junctions.

The variables involved in an open-channel junction flow are numerous. The Froude number of the downstream combined channel, F_d, divides open-channel junction studies into two classes. The downstream channel may be either subcritical, the majority of published studies, or supercritical. The channel junction can act as a hydraulic control

and be the location of a flow transition from subcritical to supercritical. The flow behavior in a subcritical open-channel junction has been shown to be greatly dependent on F_d. Other junction variables include: a flow ratio describing the amount of the total flow entering the downstream combined channel from each of the contributing channels, junction angle, channel sizes, channel roughness, channel slope, bed elevations, and the variation of fluid properties. This range of variables makes a simplified mathematical model quite difficult.

The distinctive characteristics of an open-channel junction flow are a zone of separation immediately downstream of the junction, a contracted flow region due to the separation zone, a stagnation point immediately upstream of the junction, a shear layer developed between the two combining flows, and an increase in depth from the downstream channel to the upstream contributing channels (Figure 2.1). The zone of separation is created due to the momentum of the entering branch flow causing the flow

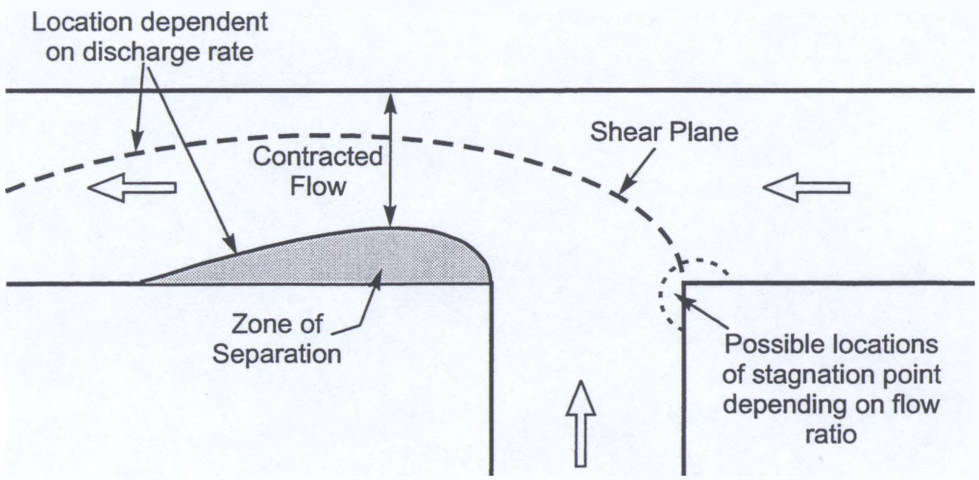

Figure 2.1. Open-Channel Junction Characteristics

to detach at the downstream corner of the junction.

In the subcritical open-channel junction, the downstream depth is generally known in design due to the backwater characteristics of the channel, however the prediction of the upstream depths required to pass the two combining flows through the junction is often needed in channel design. This depth can be found by describing the energy loss characteristics of the channel junction. The attempt to produce an expression for these individual characteristics in relation to certain junction variables is the focus of most previous studies in this field. Although these depth relationships will be reviewed in this thesis in the interest of completeness, developing a new relationship is not one of the goals of this work.

2.2 Subcritical Open-Channel Junction Flow

Subcritical open-channel junction flow is described as flow that is subcritical throughout the junction region. This definition implies that the flow in both the tributary channels and the downstream combined flow channel remains subcritical at all times in the junction region and that the zone of separation therefore does not create a critical contraction as is possible in some junction configurations. In subcritical junction flow the junction geometry, as well as, the downstream channel characteristics and downstream flow conditions create significant differences in the junction flow. The subcritical junction flow forms the majority of the research completed to date in the open-channel junction field, this is partly because most designed open-channel junctions will be carrying this type of flow.

Taylor (1944) first addressed the topic of open-channel junction flow. His work attempted to create an empirical relationship for the prediction of the tributary channel depths upstream of the junction. The work was completed in a rectangular flume, all channels 0.33 ft wide, and with junction angles of both 45° and 135°, measured from the centerline of the upstream channel to the centerline of the branch channel. Taylor suggested that for any channels other than rectangular, the design should be dependent on a physical model study of the junction in question. The author based his work on assumptions that have become common throughout open-channel junction studies: "(1) The flow is parallel to the channel walls immediately above and below the junction, (2) ordinary wall friction is negligible in comparison with other forces involved, and (3) the depths in channels 1 and 2 (the tributary channels) are equal immediately above the junction." The results are a momentum analysis that yields a predictive equation for the depth ratio between the upstream channels and the downstream channel.

$$k_2 = \frac{n_q^{\,2}\left(n_y^{\,2}-1\right)}{4n_y^{\,2}\left(2n_q - n_q^{\,2}\left(1+\cos\theta\right)+n_y-1\right)}$$

Where: k_2 = the ratio of the branch channel velocity head to the branch channel depth.

n_q = the ratio of the branch channel flow to the downstream combined flow

n_y = the ratio of the upstream main channel depth and the downstream combined flow depth

θ = junction angle

Comparison of the experimental results with the theoretical equation is good for the junction angle of 45° and not for the angle of 135°. Taylor's paper is important for its identification of the need of theoretical description of the open-channel junction and the groundwork it formed for future investigations.

Webber and Greated (1966) implemented the method of conformal mapping to define a theoretical flow pattern. Using this method, they were able to locate the stagnation point at the upstream corner of the channel junction and delineate the zone of separation. The solution was applicable to a junction where one of the tributary channels lied in a straight line with the downstream channel and that all channels have the same width. An approach was defined for the determination of the flow depth ratio, which could be reduced to the equation derived by Taylor (1944). The authors did add an equation to estimate the relative energy loss occurring in the junction.

$$\frac{\Delta E}{E_1 + E_2} = 1 - \frac{n_y^{\,2}\left(2 + F_{n3}^{\,2}\right)}{2n_y^{\,3} + F_{n3}^{\,2}\left(3n_q^{\,2} - 3n_q + 1\right)}$$

Where: ΔE = junction energy loss

E_1 = energy in the upstream channel

E_2 = energy in the branch channel

n_q = the ratio of the branch channel flow to the downstream combined flow

n_y = the ratio of the upstream main channel depth and the downstream combined flow depth

F_{n3} = downstream Froude number

The relative energy loss equation and the depth ratio equation were compared to experimental results collected in a small flume (0.42 ft wide) for junction angles of 30°, 60°, and 90°, measured between the centerline of the upstream channel and the branch channel. The agreement between theoretical and experimental depth ratio was best for the 30° junction and worsened as the junction angle increased. For each junction angle the agreement was much better for cases where less than half the total combined flow entered through the branch channel. The relative energy loss was overestimated for all junction angles. An efficient, curved 90° channel junction was designed and tested based on the theoretical flow patterns.

Lin and Soong (1979) compare the energy loss in the open-channel junction to the energy loss found in pipe flow. The total energy loss was divided into two terms, a boundary friction loss, found by using Manning's formula, and a turbulent mixing loss. The turbulent mixing loss was found to be slightly larger than the turbulent mixing loss in pipes. Lin and Soong found the mixing loss and the friction loss to be comparable in magnitude. Experimental results were taken from a 90° junction flume with channel widths of 1.50 ft.

Joy and Townsend (1981) presented a study on the velocity patterns, shear stress distribution, and energy correction coefficients, α, for a 90° junction. The measurements were taken in a flume with a main channel width of 1.00 ft and a branch channel width of 0.33 ft. The one-dimensional velocity measurements were taken with a propeller-type current meter. The grid for the velocity data collection was not discussed. Junction

modifications tested were a flared downstream junction corner, a deflector installed on the upstream junction corner, guide vanes placed in the main channel, and a reverse slope at the outlet of the branch channel. The results showed that the flared downstream corner performed the best by reducing the flow distortion in the junction. This flare minimized the separation zone and thereby reduced velocities and shear stress in the contracted region. The paper also introduced that a unit coefficient (α=1.00) on the kinetic energy term in the energy equation underestimates the actual kinetic energy.

Modi et al. (1981) applied the method of conformal mapping to approximate the flow pattern in the junction. However, assumptions necessary to implement this method require that the fluid be treated as inviscid, irrotational flow and that junction energy loss is neglected. The results are the location of the stagnation point in either the lateral channel or the main upstream channel depending on the flow ratio between the two channels. However, the results show the size of the separation zone to approach 75% of the channel width when 80% of the entering flow comes from the branch channel. This value is much higher than any results from a physical study.

Best and Reid (1984) focused solely on the separation zone in a physical study. Photography of surface dye traces and particle traces was used to delineate the separation zone in a junction composed of 0.50 ft wide channels and was performed for varying junction angles and flow ratios. In this study velocity measurements were taken at one point in a vertical section by a miniature current meter. A separation zone shape index (H/L) was defined as the ratio of the width of the separation zone, H, and the length of the separation zone, L. The study showed that for a 90° junction the maximum width of

the separation zone as a percentage of the overall downstream channel width is approximately 40%, much less than the value predicted by Modi et al. (1981).

Ramamurthy et al. (1988) investigates the transfer of lateral momentum from the branch channel to the main channel. This investigation was performed by measuring wall pressure at the junction entrance of the branch channel along with the depth difference from upstream side of the branch channel entrance to the downstream side of the branch channel entrance. The experimental facility was composed of channels that were 0.81 ft wide.

Biron et al. (1996) studied the previously neglected effects of bed discordance on the effects of the channel junction flow. The experiment was performed in a flume with a main channel width of 0.40 ft and a branch channel width of 0.25 ft with a junction angle of 30°. Velocity measurements were taken using a two-component fiber optic laser Doppler anemometer (LDA). The LDA provided a streamwise velocity measurement and a vertical velocity measurement. The velocity measurements were taken along 82 vertical profiles throughout the junction region, with each vertical profile consisting of 8 data points. The study investigated the difference between the downstream flow patterns created by a junction with concordant beds, vertical step discordant beds, and a 45° slope between the discordant beds. The results show considerable differences in the flow patterns along the downstream junction adjacent wall. The concordant bed junction showed a separation zone extending from the bed to the surface along the downstream junction adjacent wall. In the discordant bed tests, there was no flow separation near the channel bed. However, the velocities near the bed had a significant vertical component

as the near-bed flow entered the separation zone above. The paper also related flow patterns depicted in this study to naturally occurring channel confluences.

Gurram et al. (1997) provide a thorough background of the open-channel junction problem and a presentation of many junction characteristics. The experiments in this study were completed in a flume with a 1.64 ft wide main channel and branch channel widths of both 1.00 ft and 1.64 ft were tested. Velocities were taken using a miniature propeller meter at half of the local flow depth. An angle meter was used to determine local streamline angle. The study is composed of branch channel wall pressures, continuous wall flow profiles, separation zone measurements, branch inflow angles, and backwater effects. Data-fit equations are provided for each characteristic for both, varying angles and flow ratios. The original paper should be examined for these data-fit equations, as they are too numerous to list. An explicit solution, using a momentum approach, for small depth ratios is provided that is dependent upon downstream Froude number, discharge ratio, and junction angle.

$$Y = 1 + \frac{qF_d^{\,2}(2 - q - \cos\gamma)}{1 - F_d^{\,2}}$$

Where: Y = the ratio of the upstream main channel depth and the downstream combined flow depth

q = the ratio of the branch channel flow to the downstream combined flow

F_d = downstream Froude number

γ = angle between centerline of upstream main channel and branch channel

This equation was compared to the data collected by Webber and Greated (1966). The results for the 90° junction are better than that of the 30° junction angle. The agreement between data and theory is best for low downstream Froude number.

Hsu et al. (1998a) provided an approach to solving for the upstream/downstream depth ratio and for the contraction coefficient at the point of maximum flow constriction due to the separation zone. The experimental setup consists of identical 0.50 ft width main and branch channels. Velocity measurements were taken using a two-component electromagnetic current meter with a cylindrical sensor 5 mm in diameter and 25 mm high. Velocity measurements were taken at eight sections in the junction region, with six to eight vertical profiles taken at each section. The vertical profiles consisted of eight evenly spaced data points. While a number of velocity points are present, their validity is questionable. The flow depths in this study varied from 6 cm to 10 cm (60 mm to 100 mm). Measurements were not taken within 14 mm of the bed or water surface. Thus the true spacing of the velocity measurements is between 4 mm and 10 mm vertically. Separation zone delineation was determined using dye trace observations. The authors provided a combined momentum and energy based solution to solving for upstream depth and contraction coefficient based on a control volume surrounding an area significantly upstream of the junction in each tributary and passing through the point of maximum contraction in the downstream channel. These equations are quite lengthy and can be found in the original work. The author provides data-fit equations for the prediction of energy correction coefficient, α, and momentum correction coefficient, β, applicable at the maximum contracted section.

Hsu et al. (1998b) added to the previous study by including junction angles of 30°, 45°, and 60°. Energy and momentum correction coefficients were calculated at the downstream end of the separation zone. Their data show the depth-averaged angle of entry across the width of the branch channel flow. An equation describing a coefficient of energy loss, including eddy loss and friction loss, was formed and compared to experimental data from their study.

$$K_e = \frac{n_y^{\,3} + \frac{1}{2}F_d^{\,2}\left[n_q^{\,3} + (1-n_q)^3\right]}{\left(1+\frac{1}{2}F_d^{\,2}\right)n_y^{\,2}}$$

Where: K_e = energy loss coefficient

n_y = the ratio of the upstream main channel depth and the downstream combined flow depth

n_q = ratio of upstream main channel flow to downstream total flow

F_d = downstream Froude number

It was shown that for each junction angle the equation significantly over-estimated the energy loss coefficient for all range of flow ratios. The authors did produce a finite-difference approximation which solves for the depth ratio for a given flow ratio, junction angle, and downstream Froude number. This finite-difference approximation must be seen in the original paper to understand the solution approach. The finite-difference approach provides a close estimation of the depth ratio without the need for analytically solving the differential equation previously used by the authors.

2.3 Transitional Open-Channel Junction Flow

Transitional flow in channel junctions occurs when the contraction due to the separation zone is great enough to force the passing flow to critical depth. The downstream channel must be able to support supercritical flow immediately downstream of the junction region for transitional flow to be present. The topic of transitional open-channel flow has seen much less research than the related subcritical junction flow.

Ramamurthy et al. (1988) investigated the upstream depth given that critical depth was achieved at the section of maximum contraction. The study covered 90° channel junctions only and provided a momentum based analytical approach to solving for the upstream depth.

$$\left(\frac{y_1}{y_c}\right)^3 + (0.48R_q - 3)\frac{y_1}{y_c} + \frac{1 - R_q}{0.63 + 0.25R_q} = 0$$

Where: y_1 = upstream depth

y_c = depth at critical section

R_q = ratio of branch channel flow to the downstream combined flow

The tests were performed only in cases with less than 60% of the flow entering from the branch channel. The results show, that in the range of flow conditions tested, the solution for the depth ratio was within +/-5% of the measured depths. The author also states that transitional flow was not possible in cases where less than 23% of the total flow was entering from the branch channel.

Hager (1989) provides a combined energy and momentum approach to solving for the upstream depth in a transitional channel junction. Hager's approach is based on energy and longitudinal momentum acting on a control volume that passes through the maximum contracted section, as is necessary when studying a transitional channel. The theoretical analysis utilizes a contraction coefficient for the constricted section, assumes the presence of a pressure correction coefficient to account for the absence of hydrostatic pressure throughout the junction region, and neglects the energy losses upstream of the maximum contracted section. The result of the theoretical analysis produces two equations with two unknowns.

$$\mu = Y\left\{\frac{(3-2Y)}{\left[(1-q)^3+q^3\right]}\right\}^{1/2}$$

$$Y^3(1-\cos\delta)+3Y(\cos\delta-\mu)+2\mu^2q^2+2\cos\delta\left(\mu^2(1-q)^2-(1-2q+2q^2)\right)=0$$

Where: μ = contraction coefficient

Y = ratio of upstream depth to depth at critical section

q = ratio of upstream main channel flow to the downstream combined flow

δ = angle between branch channel centerline and upstream channel centerline

The theoretical equations do not agree with the experimental data from his study. The experimental data were collected in a 0.31 ft wide channels. The streamline directions were determined using a miniature angle meter and velocities were found using a current meter aligned along the previously determined streamline directions. The author does not include the vertical location of collected velocities. The author does

provide a simplified design equation that estimates a depth ratio given a flow ratio and junction angle, based on a fit of the recorded data.

$$Y = 1 + 0.92\left\{(1.1-q)\left[q + (1-q)sin^{3/2}\left(\frac{\delta}{2}\right)\right]\right\}^{1/2}$$

Where: Y = ratio of upstream depth to depth at critical section

q = ratio of upstream main channel flow to the downstream combined flow

δ = angle between branch channel centerline and upstream channel centerline

The above equation provides a description of the authors collected depth ratio data to within +/-3%. The results of Hager's study show that a transitional flow becomes impossible when less than 15% of the total combined flow enters from the branch channel, which is in reasonable agreement with the results found by Ramamurthy et al. (1988).

Kumar (1993) investigated the same problem as Hager (1989). However, Kumar disagreed with two assumptions made in the previous work. First, the assumption of no energy loss upstream of the maximum contracted section is questioned in light of the impingement of the branch channel flow and the significant momentum transfer from the branch flow. The author also challenges the inclusion of the pressure correction factor in Hager's one-dimensional approach. The author's assumptions produce a simplified theoretical depth ratio equation.

$$Y^3 - 3Y + 2\left(q^2 + (1-q)^2 \cos\theta\right) = 0$$

Where: Y = ratio of upstream depth to depth at critical section

q = ratio of upstream main channel flow to the downstream combined flow

θ = angle between branch channel centerline and upstream channel centerline

When compared with Hager's theoretical equation and data, this simplified equation proves to be a better predictor of measured results.

2.4 Summary

The existing research of open-channel junction flow centers on the attempt to define the depth ratio through either a theoretical or empirical one-dimensional model. Most of these models provide an estimated depth ratio for a given flow ratio, junction angle, and downstream Froude number. The accuracy of these predictive models varies widely. However, there are some trends apparent throughout the entire body of work completed to date on the junction depth ratio. First, as the majority of the flow enters the junction from the branch channel, the accuracy of these models decreases. There is very little agreement between theoretical approximations and experimental results for cases with more than 80% of the junction flow entering from the branch channel. In practice, however, the need to design a channel junction where such a large percentage of the discharge enters from the branch channel should be uncommon. Second, the accuracy of the predictive models is good for junction angles less than 45°, and steadily decreases as the junction angle approaches 90°. Unlike the problem encountered with large branch channel flow ratios, the 90° channel junction will most likely be encountered in practical

problems. The increased materials and consumed space causes low angle junctions to be uncommon in practical applications.

Some authors, as mentioned, provide descriptive equations for some flow features found in the open-channel junction based on collected data. These features include separation zone size, momentum and energy coefficients, and angle of entering branch channel flow. The separation zone data were collected in all cases by visual dye traces. This method of delineation of the separation zone is questionable due to the turbulent flow along the separation zone boundary mixing the dye and making accurate visual delineation difficult. With the exception of Biron et al. (1996), the velocity data collected in these studies are minimal. The velocity data often consist of a single measurement at a predefined depth to describe the entire vertical profile. The complex flow patterns created in the open-channel junction make the description of an entire vertical profile by a single point inaccurate.

The available literature does not present data that are adequate for the validation of a three-dimensional numerical model. There currently exists no truly three-dimensional data describing the junction flow. Biron et al. (1996) did record vertical velocities, but these were taken by aligning a two-component LDA along streamlines defined by dye visualization. Also, in most instances where multiple data points were taken along a vertical profile, the testing grid does not sufficiently cover the entire junction region. Finally, there does not exist any complete water surface mapping for the junction region.

The open-channel junction problem has recently begun to attract more attention and research focused on the complexities involved in this flow. To date, the studies have focused mostly on a one-dimensional study of the flow and in some cases a two-dimensional look at streamlines. Dye-trace or particle-trace visualization have provided the description of the surface flow features of the open-channel junction.

CHAPTER 3

EXPERIMENTAL DETAILS

3.1 Physical Description

The experiments discussed in this study were performed in a 90° combining flow flume located at the Iowa Institute of Hydraulic Research. The main channel is 72 ft long and the junction occurs 18 ft downstream of the flume entrance, as shown in Figure 3.1. The branch channel is 12 ft long. The tributary channels and the downstream combined flow channel are all 3.00 ft in width and 1.67 ft in depth as can also be seen in Figure 3.1. The channels are constructed with stainless steel beds except in the immediate junction region, where the bed is Plexiglas for flow visualization. The channel bed is horizontal at all locations. The main channel walls are glass to allow for flow visualization. The side channel walls are made of plywood to allow realignment of the side channel to achieve differing junction angles. As Figure 3.1 shows, the side channel walls can be arranged such that junction angles from 45° to 90° can be tested. The current study is concerned only with the sharp-edged 90° junction.

Each channel begins with a head tank, that in conjunction with perforated plate and 4 in thick honeycomb at the channel entrances, ensures properly developed flow before entering into the channel junction. A 50 horsepower variable speed pump provides water from an underground sump to the flume through a 12 in supply pipe.

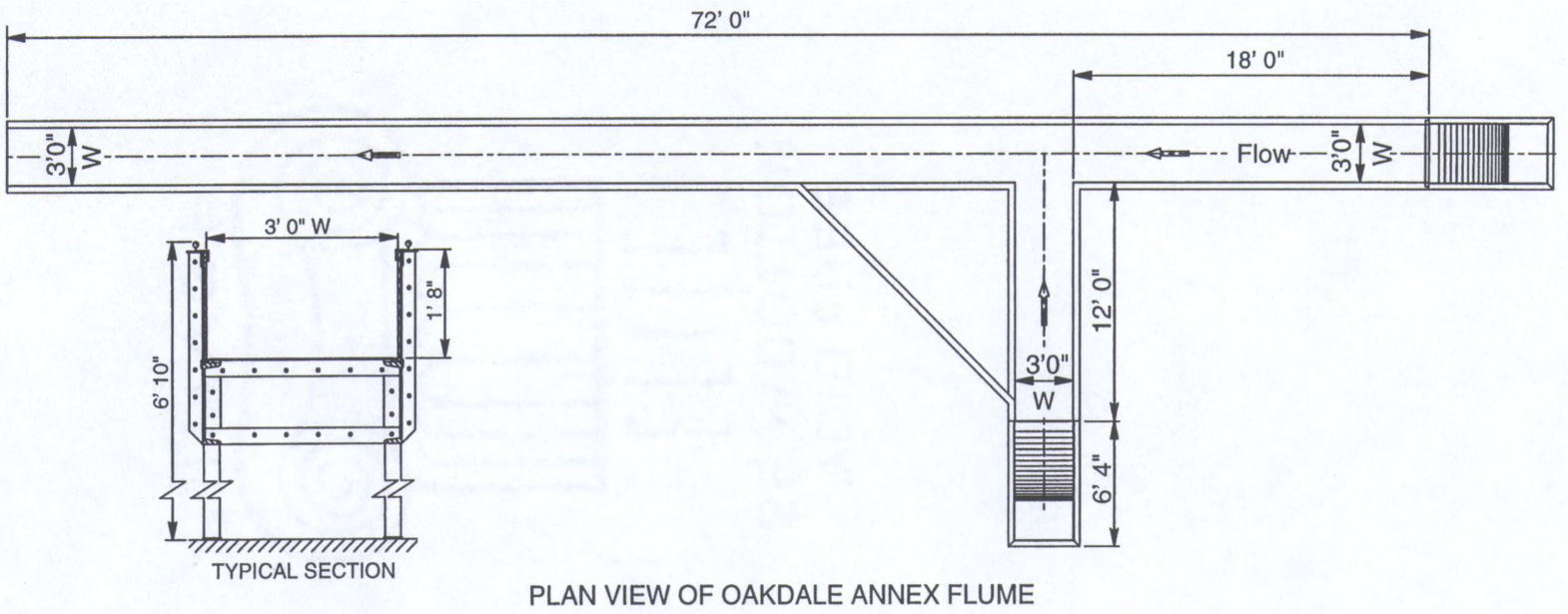

Figure 3.1. Layout of Experimental Flume

Volumetric measurements were made with manometer readings from calibrated 8 in orifices in each of the 12 in supply pipes. The tailwater depth in the downstream channel is controlled by an adjustable tailgate. Mike Kundert, draftsman at the Iowa Institute of Hydraulic Research, prepared the construction drawings for this flume that are included in Appendix A.

3.2 Experimental Procedures

The coordinate system defined for this testing has the positive x-direction oriented in the upstream direction of the main channel. The positive y-direction points to the main channel wall opposite of the channel junction. Thus the positive z-direction is upward in the vertical direction. The origin from which all points are measured is the bed at the upstream corner of the channel junction. All distances are non-dimensionalized by the channel width, W = 3.00 ft. This non-dimensionalization allows the results of this test to be applied in general to any 90° equal width channel junction. The non-dimensionalized coordinates are called x^*, y^*, and z^* for x/W, y/W, and z/W, respectively. All test sections in this study are denoted by the distance in channel widths measured positive in the x-direction for upstream main channel measurements, negative in the x-direction for downstream combined flow measurements, or negative in the y-direction for measurements in the branch channel.

The upstream main channel, branch channel, and total combined flow are denoted as Q_m, Q_b, and Q_t, respectively. The flow ratio, q^*, is defined as the ratio of the upstream main channel flow, Q_m, to the total flow, Q_t. In this study, the total combined flow, 6.0

cfs and downstream depth, 0.97 ft, were held constant. This constant downstream flow rate and depth produced a constant downstream Froude number, $F_d = 0.37$. The flow conditions tested are listed in Table 3.1.

Table 3.1. Experimental Flow Conditions

Q_m (cfs)	Q_b (cfs)	q^*
0.5	5.5	0.083
1.5	4.5	0.250
2.5	3.5	0.417
3.5	2.5	0.583
4.5	1.5	0.750
5.5	0.5	0.917

A three-component Acoustic Doppler Velocimeter (ADV) was used to measure velocities and turbulence intensities. The velocity measurements were taken at each sampling location for 60 seconds at a sampling rate of 10 Hz. The manufacturer's specifications state that the measuring accuracy of the ADV is +/-1% of the measured velocity or 0.008 ft/s, whichever is greater. The time series of velocity at each data point was analyzed to produce an average velocity and turbulence intensity. The velocity measurements were taken at the channel cross-sections as shown in Figure 3.2. A channel cross-section consisted of seven evenly spaced vertical profiles with two

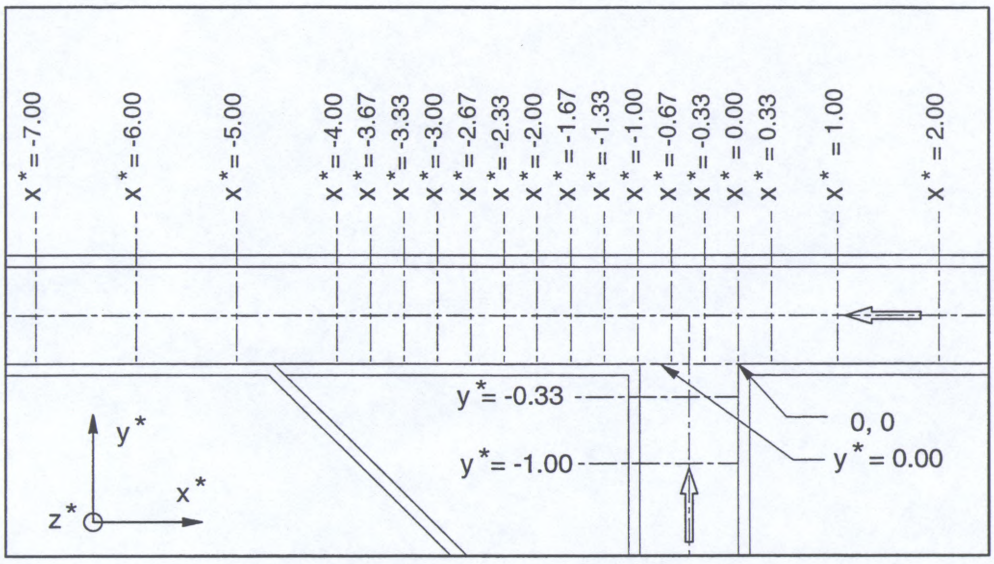

Figure 3.2. Cross-Section Locations

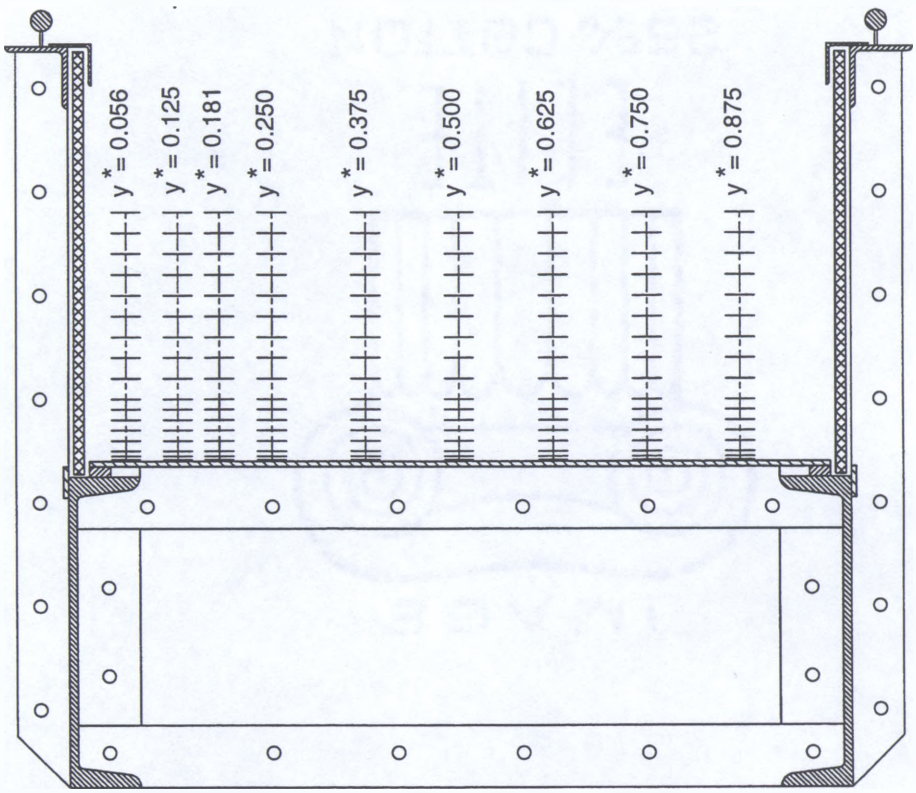

Figure 3.3. Data Collection Locations

additional vertical profiles, $y^* = 0.056$ and $y^* = 0.181$, taken near the branch-side wall on sections immediately downstream of the junction (Figure 3.3). Seventeen points were measured on each vertical, with the near bed points being more closely spaced (Figure 3.3). This testing grid produced approximately 2,850 velocity measurement locations for each tested flow condition.

Depth measurements for this study were made using a point gauge with an accuracy of 0.005". The water surface mapping was performed on a 0.25 ft square grid in the junction region. The water surface for a given flow condition was completely mapped in one day by the same individual without changing any flow settings during the time of the water surface data collection. These precautions ensure that the flow structure was continuous throughout the mapping and that uniform measurement techniques were employed.

CHAPTER 4

RESULTS AND DISCUSSION

4.1 Introduction

The goal of this project is to compile a data set that fully describes the flow conditions occurring in open-channel junction flow. For this goal to be achieved, channel sizes were chosen which are considerably larger than previous studies of junction flow. The larger channel size enabled more velocity measurements to be taken at a meaningful spacing across the entire cross-section. The data set is comprised of three-dimensional velocity and turbulence measurements. The test grid produces approximately 120 data points to describe the flow at a given channel cross-section, for a total of approximately 2850 data points describing each tested flow condition. The resulting data set provides a detailed representation of three-dimensional flow occurring at the junction of two open channels. This chapter focuses on the presentation of the collected data and discusses the resultant flow features. All data are plotted in Appendices B through G. Only representative data plots are included and discussed in this chapter.

4.2 Longitudinal Velocity

The longitudinal velocity, u, is the velocity in the x-axis direction. The x-axis is positive upstream and therefore a velocity in the downstream direction is defined as

negative. Figure 4.1 displays u isovels near the bed for $q^* = 0.417$. The separation zone can be seen as the area of low velocity along the junction adjacent wall immediately downstream of the channel junction. Recirculation inside the separation zone is shown as the region of positive velocity, indicating upstream motion. The highest velocities are seen just downstream of the junction in the sections contracted by the zone of separation.

The longitudinal velocity isovels for flow at the surface (Figure 4.2) have some differences from the near bed velocity patterns that are common in all the flow conditions. The separation zone is larger near the surface, both in length and width. The separation zone size varies from top to bottom because of the angle of entrance of the branch channel flow and will be discussed later. There is also more recirculation inside the separation zone near the surface. In the constricted reach immediately downstream of the junction, higher velocities occur near the bed. This effect is also attributed to the entrance angle of the lateral flow and will be discussed later. However, once the contracted region is passed, the velocities return to the normal state of higher velocities near the surface. As can be seen in the surface velocities, the flow has not recovered from the junction effects even at $x^* = -6.00$. This could complicate the design of successive junctions, because any theoretical solution would not be accurate without properly developed flow entering the junction.

Figure 4.3 displays the u velocity patterns at the surface for a condition with more flow entering the junction from the main channel, $q^* = 0.750$. Comparing these velocity patterns with those in Figure 4.2 display the flow changes caused by the ratio of the incoming flows. As more flow enters from the main channel, q^* increases, the separation

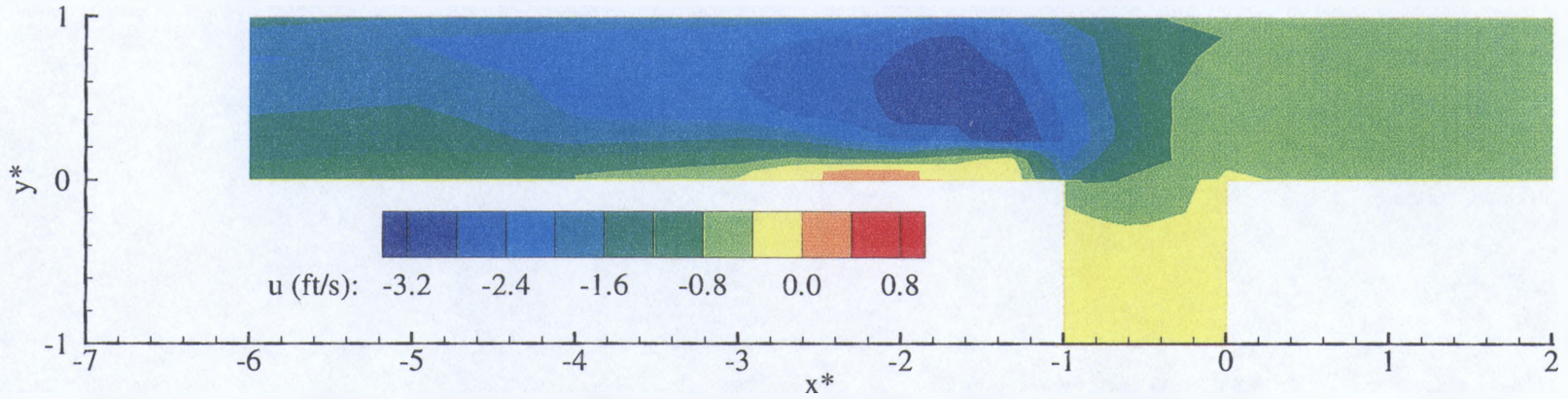

Figure 4.1. u Velocity, z* = 0.014, q* = 0.417

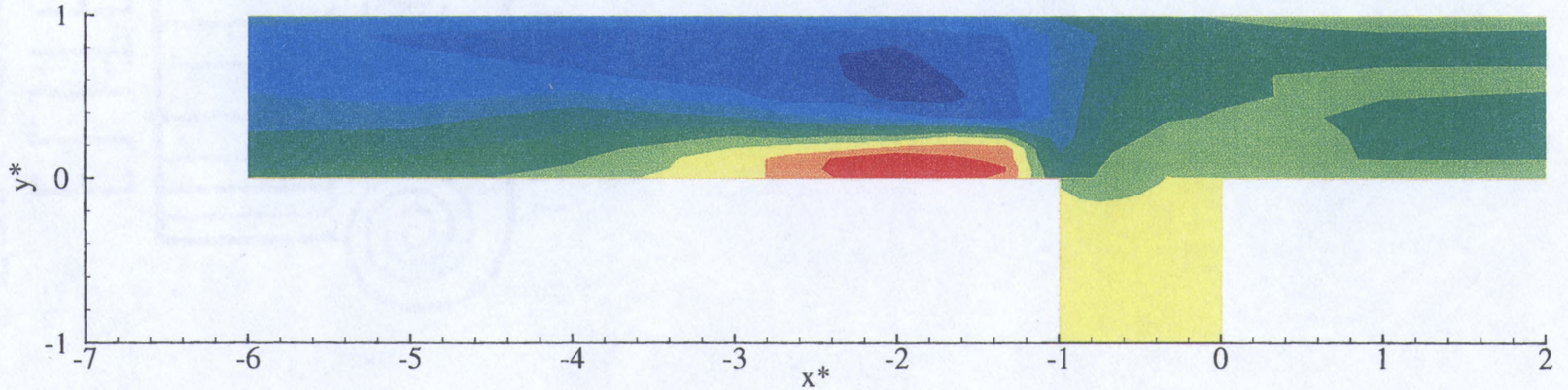

Figure 4.2. u Velocity, z* = 0.278, q* = 0.417

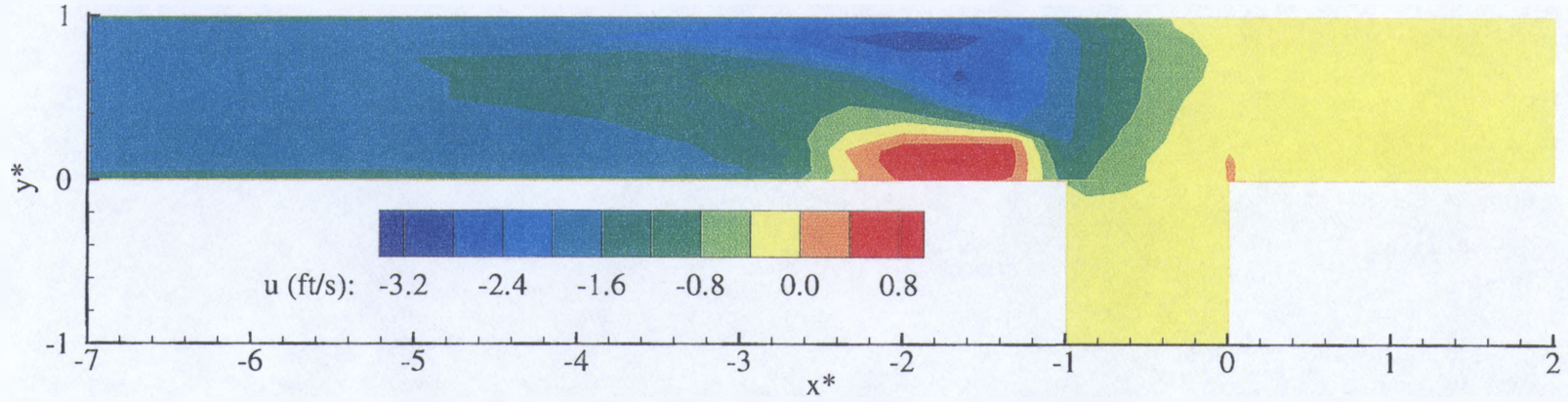

Figure 4.3. u Velocity, z* = 0.278, q* = 0.750

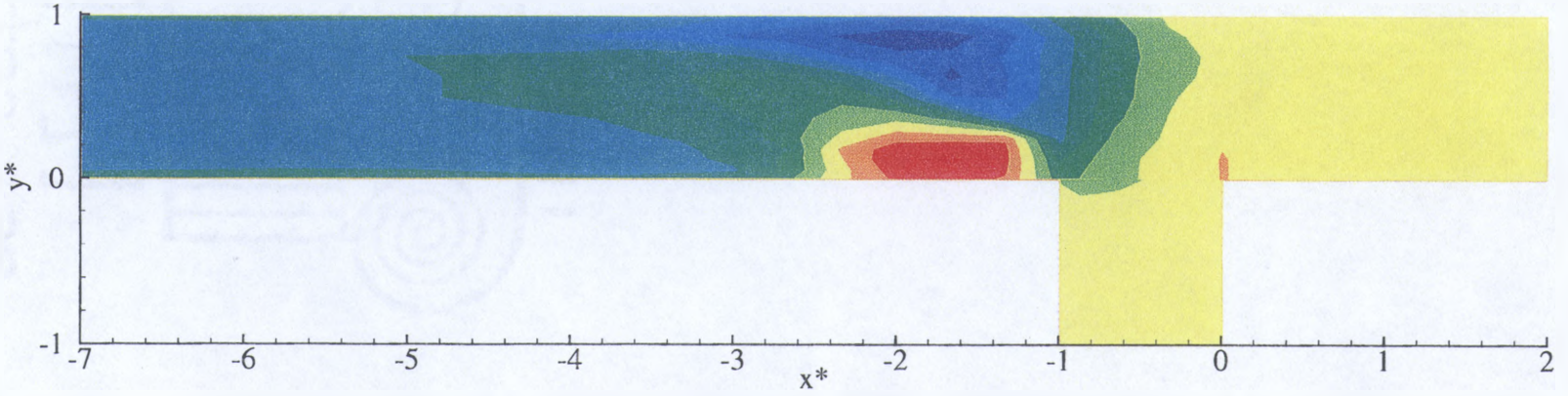

Figure 4.4. u Velocity, z* = 0.278, q* = 0.083

zone decreases in width and length. This can be expected by considering the limiting condition of all flow entering the junction from the main channel, $q^* = 1.00$, which obviously would have no separation occurring. Lower velocities in the junction region result from the reduced channel constriction by the smaller zone of separation. However, there is an exception to the increased separation size as q^* decreases. There is a point that so much flow enters from the branch channel that the reflection of the entering branch flow off of the opposite wall engulfs the downstream end of the separation zone, effectively shortening it. This only occurs at a very low q^*. In this series of experiments, only $q^* = 0.083$ (Figure 4.4) exhibited this feature as the separation zone is much shorter than that of $q^* = 0.417$ (Figure 4.2). Previous studies do not address this occurrence, and consider that the length of the separation zone continually increases as more flow enters from the branch channel. It does appear that the zone of separation continuously widens as q^* decreases.

A cross-sectional view of the longitudinal velocity patterns offers a different insight into the junction flow patterns. Figure 4.5 displays a cross-sectional view of the u velocity upstream of the junction. At this location the velocity is evenly distributed across the section with slightly higher velocities located near the surface. Approaching the junction, the main channel flow is deflected toward the wall opposite of the junction and stagnation begins to form on the left hand side (Figure 4.6). Just downstream of the junction, the separation zone can be clearly seen in Figure 4.7. As previously mentioned, the separation zone extends further into the width of the channel near the surface than at the bed. There is more area of high velocities near the bed as is attributed to the angle of

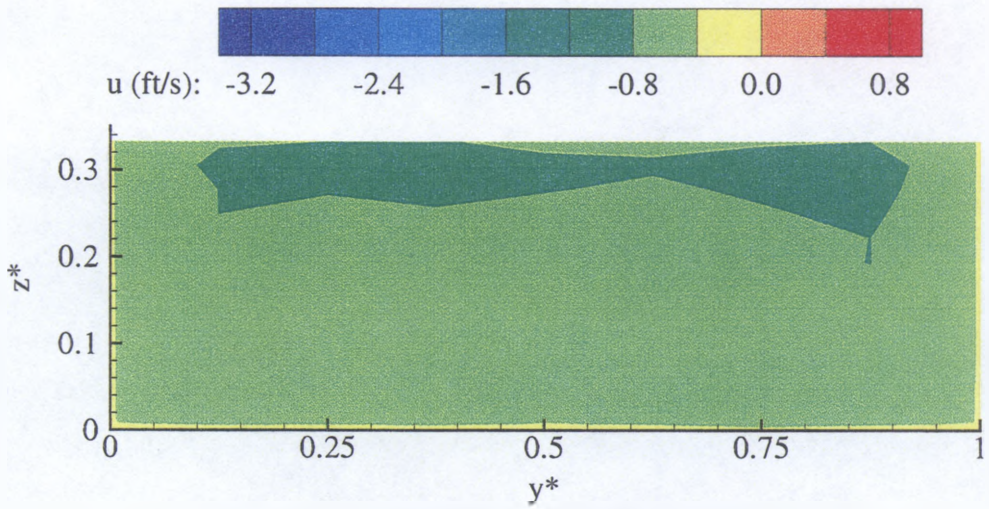

Figure 4.5. u Velocity, x* = 2.00, q* = 0.417

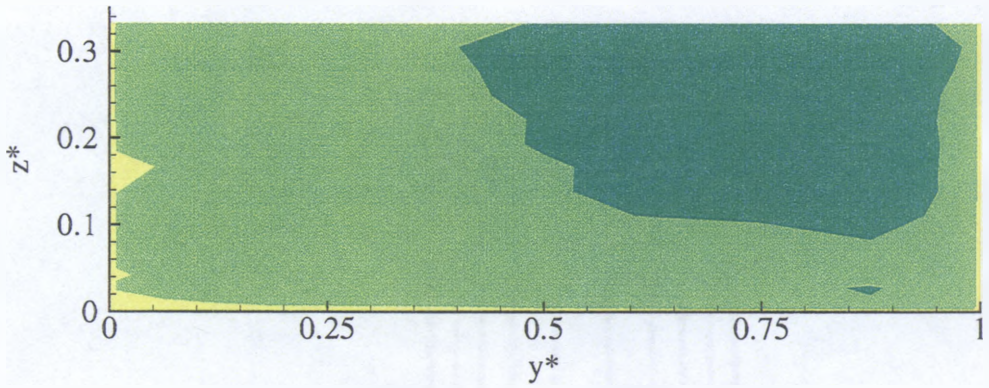

Figure 4.6. u Velocity, x* = 0.00, q* = 0.417

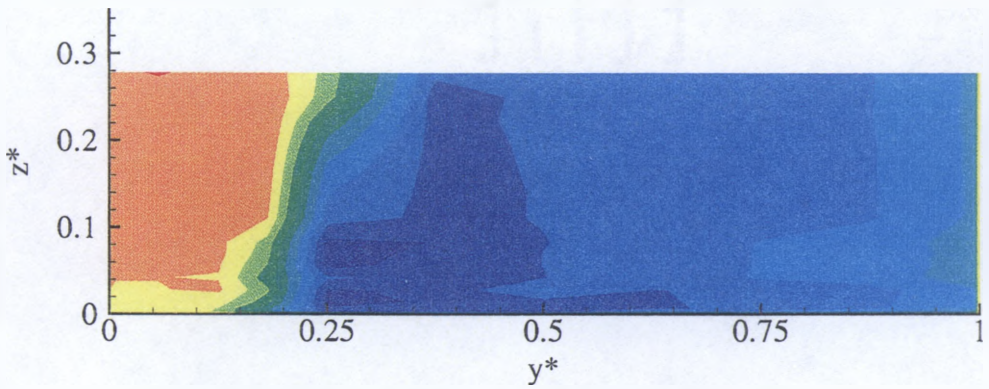

Figure 4.7. u Velocity, x* = -1.33, q* = 0.417

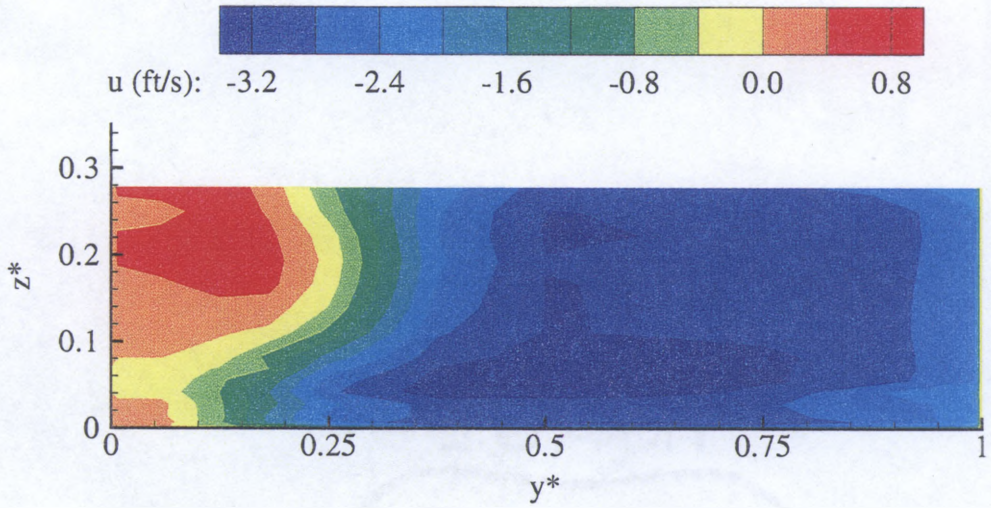

Figure 4.8. u Velocity, x* = -2.00, q* = 0.417

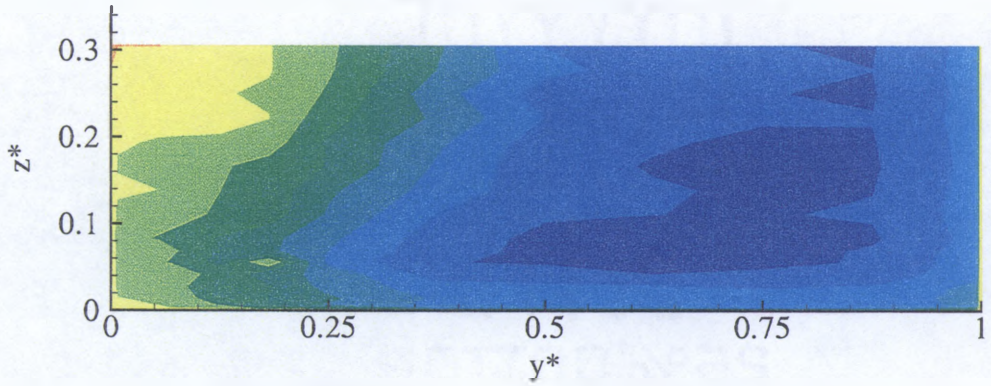

Figure 4.9. u Velocity, x* = -3.00, q* = 0.417

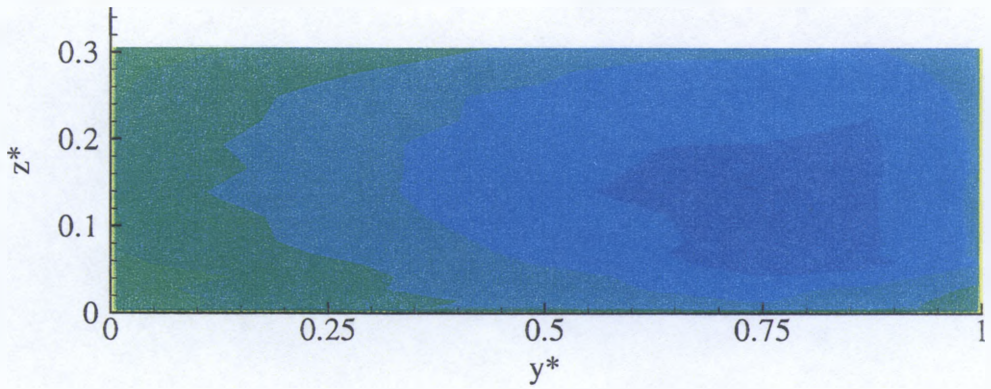

Figure 4.10. u Velocity, x* = -6.00, q* = 0.417

entrance of the branch channel flow. Section $x^* = -1.33$ is near the junction and therefore the flow is concentrated near the separation zone as the lateral component of the entering flow is still directing the branch flow toward the outer wall. Approximately midway through the contracted region (Figure 4.8) the flow is now concentrated on the outer half of the channel width. The separation zone still consumes much of the channel cross-section a full channel width downstream from the junction. Two channel widths downstream of the junction (Figure 4.9), the separation zone is receding. The flow is still concentrated on the outer half of the channel but beginning to distribute more evenly over the cross-section. Figure 4.10 displays the farthest downstream collected data for this flow condition. It is evident that the flow has still not completely recovered from the junction effects but the entire channel cross-section is carrying flow downstream again.

Comparing the cross-sectional u velocity patterns from different flow ratios displays the dependence of junction flow characteristics on flow ratio. Figure 4.11 depicts the flow at the beginning of the channel junction where 75% of the flow is entering from the main channel. A slight deflection of the entering flow is evident, as the velocities are slightly skewed toward the wall opposite of the junction. It is apparent, in comparison with Figure 4.6, that the upstream flow deflection is more significant as more flow enters from the branch channel. The separation zone, as seen in the section immediately downstream of the channel junction, extends much further into the width of the channel for $q^* = 0.417$ (Figure 4.7) than that of $q^* = 0.750$ (Figure 4.12). This is caused by the decreased momentum of the entering branch channel flow as q^* increases. The higher momentum for the low q^* condition allows the branch channel flow to extend

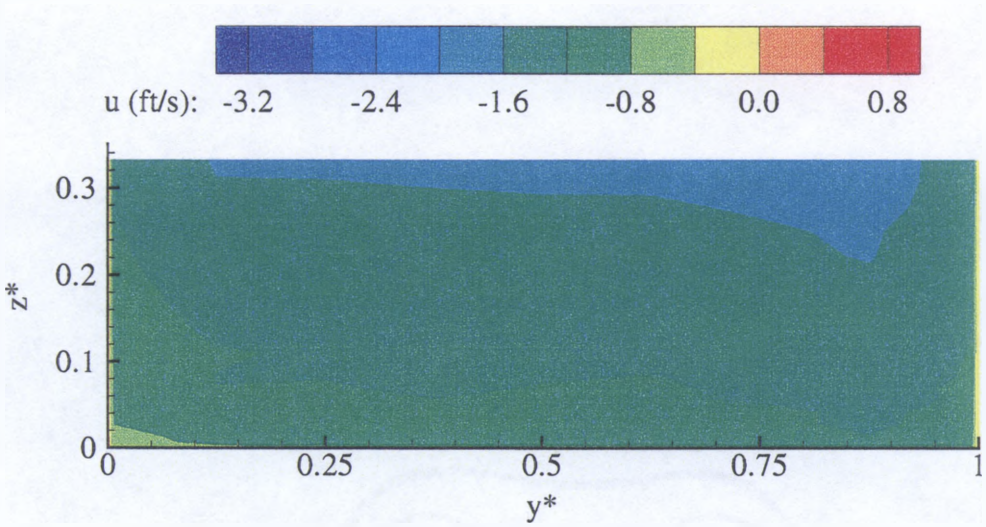

Figure 4.11. u Velocity, x* = 0.00, q* = 0.750

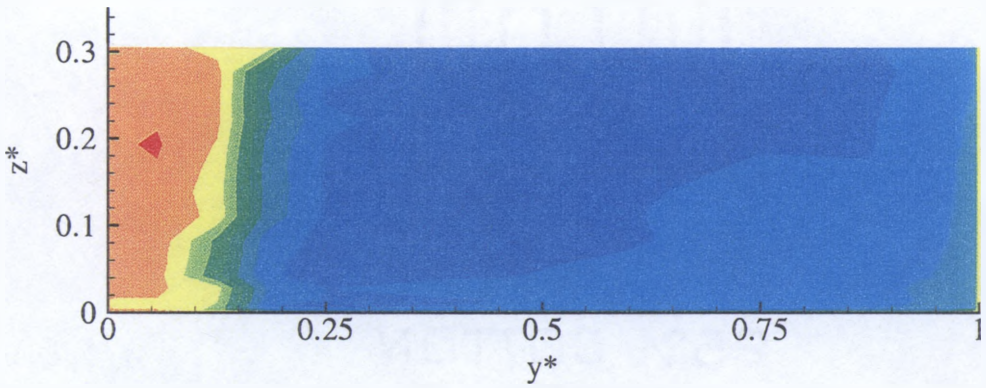

Figure 4.12. u Velocity, x* = -1.33, q* = 0.750

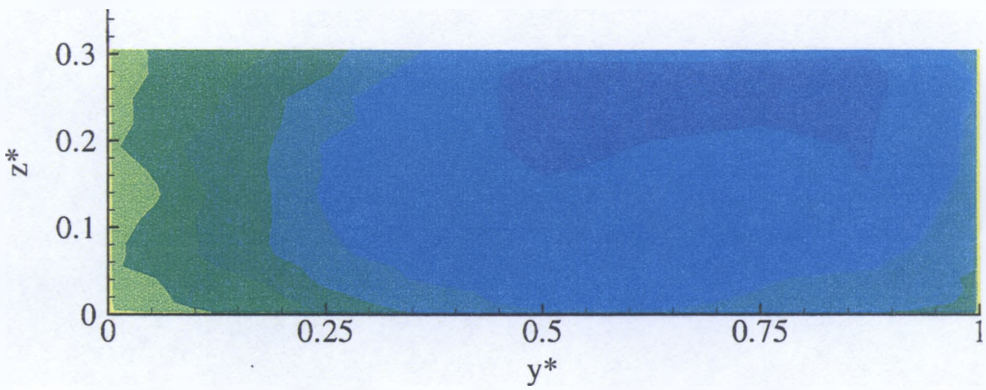

Figure 4.13. u Velocity, x* = -3.00, q* = 0.750

further into the main channel before being directed downstream, therefor causing a wider zone of separation. The reduced constriction in the case of $q^* = 0.750$ allows the flow to pass at lower velocities, as is evident in Figure 4.12. Comparing the sections two channel widths downstream of the junction, it is evident that the downstream effects of the channel junction are greatly reduced as the flow ratio increases. In the case of $q^* = 0.750$ (Figure 4.13), the separation zone is completely absent at $x^* = -3.00$. While the flow is still deflected toward the outer wall, the entire channel is again conveying flow downstream. For the lower flow ratio (Figure 4.9), the separation zone is still present at section $x^* = -3.00$ and the flow is concentrated nearly three-quarters of the distance across the channel.

The distribution of u velocities provides a description of open-channel junction flow characteristics. Studying the u velocity patterns the separation zone is evident as is the effects of constriction on the passing flow. It was seen that up to a threshold, the separation zone lengthens as q^* decreases. The separation zone did continually widen as q^* decreased. In the region of the channel constriction, there were high velocities at the bed as well as the surface. At the bed, much of the channel width carried higher velocity flow. This feature of open-channel junction flow could be a cause of concern in the design of erodible channels. More u velocity data are presented in Appendices B through G for all flow conditions tested.

4.3 u-v Vector Field

As shown by the longitudinal velocities, the flow patterns are very different at the bed and the surface. The two-dimensional u-v vector field displays that the entrance conditions of the branch flow is very different between the surface and the bed. Figure 4.14 shows that the entering branch flow is significantly skewed toward the downstream direction. Comparing the angle of entry with that of the surface flow, Figure 4.15, it is apparent that the surface flow is entering at a larger angle to the main channel. The reduced angle of entry results in an even lower lateral momentum at the bed. This results in a narrower separation zone at the near bed depths than at the surface. A secondary effect is that the reduced channel constriction coupled with the downstream deflection of the near bed branch flow results in the concentration of high velocities near the bed. At approximately $x^* = -1.33$, nearly 75% of the channel width is conveying flow downstream near the bed compared to approximately 50% of the channel width for the surface flows. The difference in length of the separation zone is also clearly evident when comparing the surface and near bed flows at the section $x^* = -3.00$. This flow ratio also displays stagnation occurring at the upstream corner of the junction at the bed.

For the dependency of the u-v velocity field upon q^* the vector fields from $q^* = 0.417$ and $q^* = 0.750$ are used. Figure 4.16 and Figure 4.17 display the $q^* = 0.750$ u-v velocity vectors for the near bed velocities and the surface velocities, respectively. The difference between the branch channel entrance angle is less between the near bed and surface for the condition $q^* = 0.750$ than for that of the $q^* = 0.417$ in Figures 4.14 and 4.15. The velocity vectors for the higher q^* show less deflection toward the outer wall in

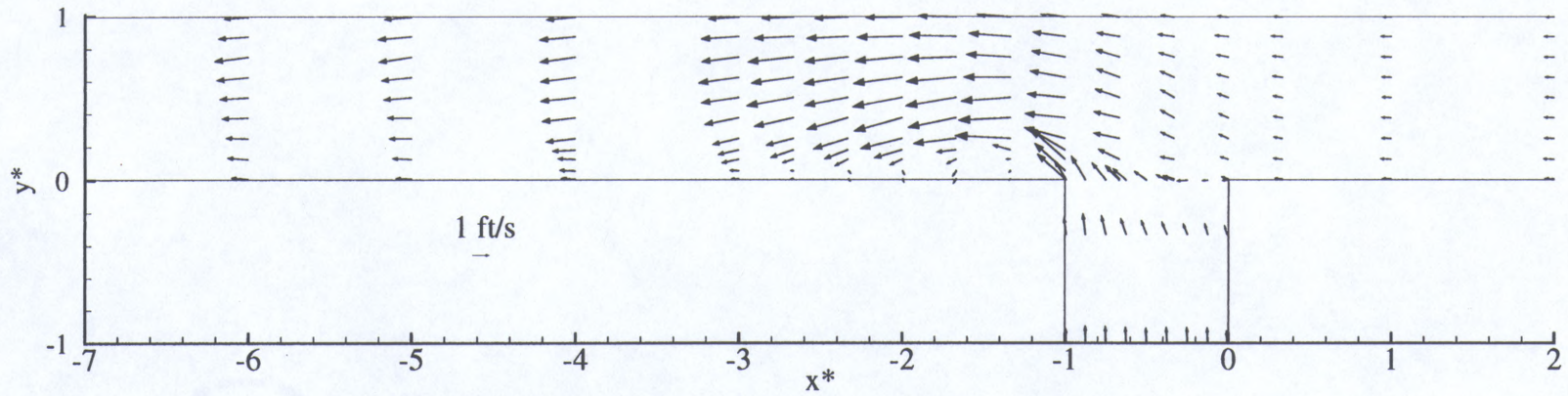

Figure 4.14. u-v Vector Field, z* = 0.014, q* = 0.417

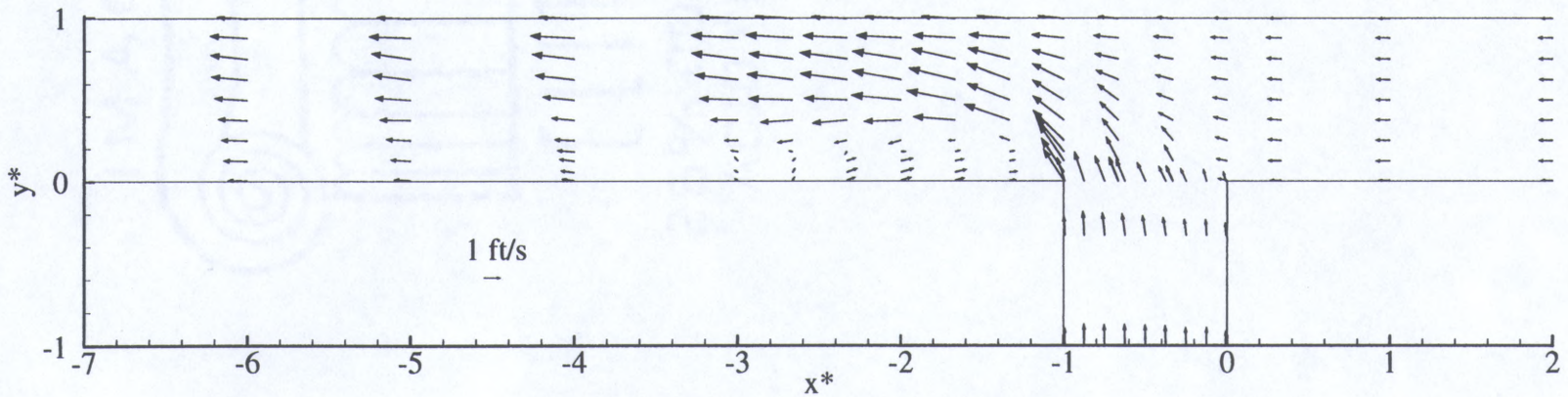

Figure 4.15. u-v Vector Field, z* = 0.278, q* = 0.417

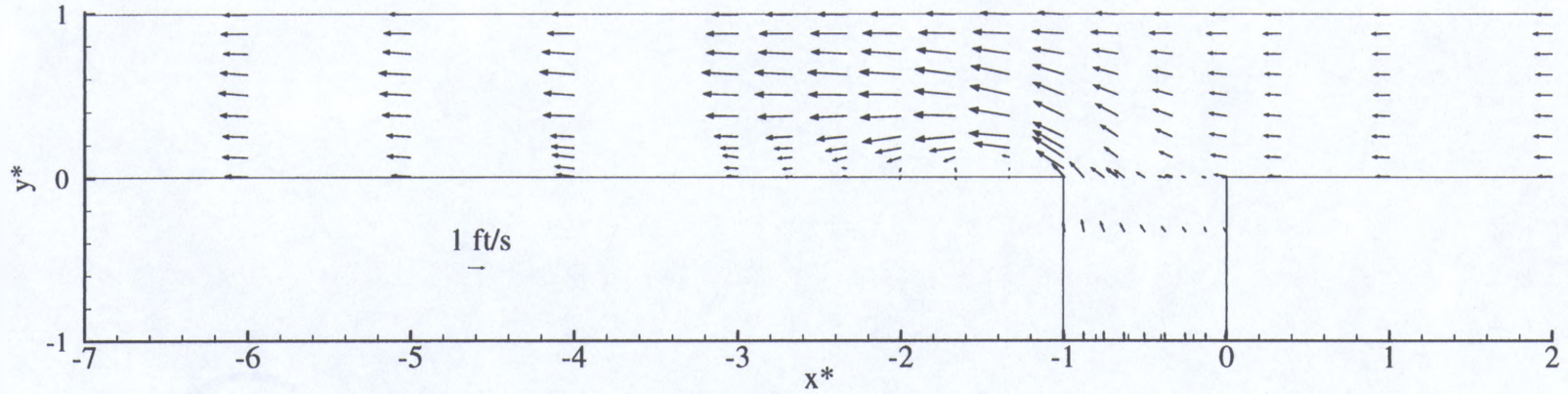

Figure 4.16. u-v Vector Field, z* = 0.014, q* = 0.750

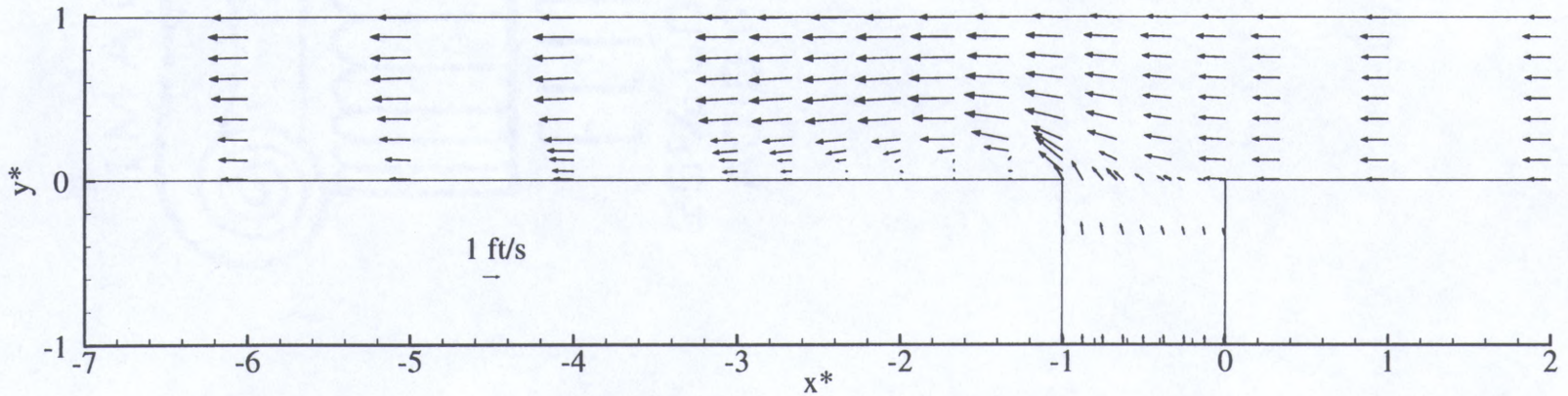

Figure 4.17. u-v Vector Field, z* = 0.278, q* = 0.750

the junction region. The velocity field is more uniform across the channel at a shorter distance downstream from the junction for both the near bed and surface with the higher q^* than those of the lower q^*. The stagnation point has also moved into the branch channel near the upstream junction corner for $q^* = 0.750$ as opposed to the location at the junction corner for $q^* = 0.417$. The stagnation point migrates from the branch channel at the upstream junction corner for large q^* to the main channel for small q^*.

The differences between the near bed velocities and the surface velocities are most dramatic for the flow condition $q^* = 0.083$. As noted in the previous section with respect to the length of the separation zone, the condition of $q^* = 0.083$ does not follow the general trends present for the other tested flow ratios. The near bed velocity vectors are seen in figure 4.18. An interesting feature is that the flow is actually directed toward the branch channel in the junction area. Looking at the surface velocity vectors, Figure 4.19, the reason for this is evident. The surface flow impinges directly on the junction opposite wall. This flow is then reflected at the bed due to the lower lateral momentum of the bed flow. The surface vectors display a region of low velocity at the center of the channel just downstream of the separation zone. The cause of this effect is the significant secondary current developed downstream of the junction returning the bed flow to the surface at the junction adjacent wall. The secondary current will be clearly apparent when looking at the v-w vector field. A curious result of the mixing caused by the secondary current is that the flow is more evenly distributed across the channel in a shorter distance downstream than for a higher q^*, Figure 4.15. For this lower flow ratio,

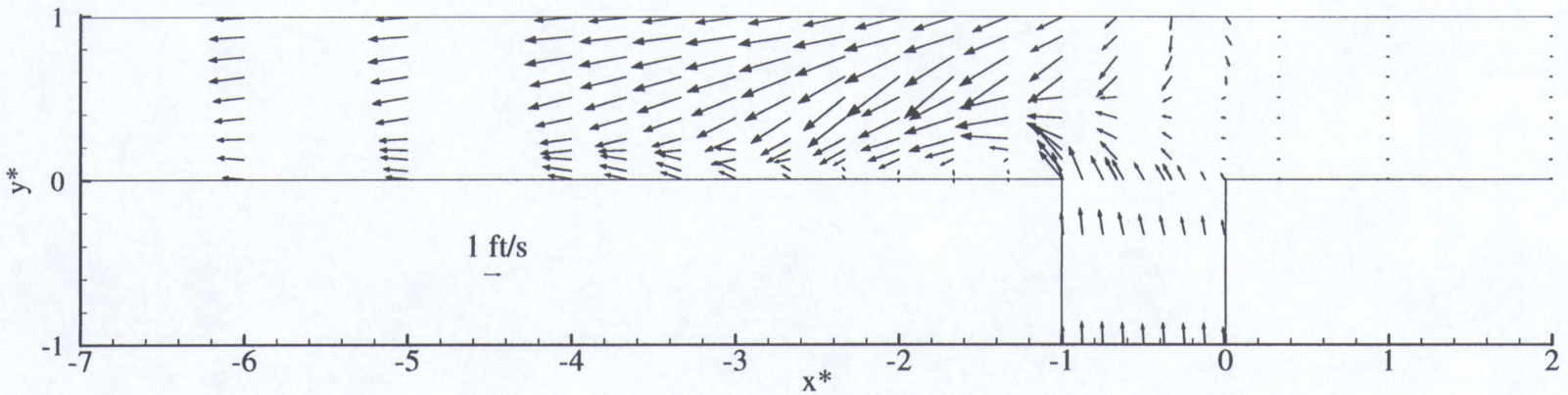

Figure 4.18. u-v Vector Field, z* = 0.014, q* = 0.083

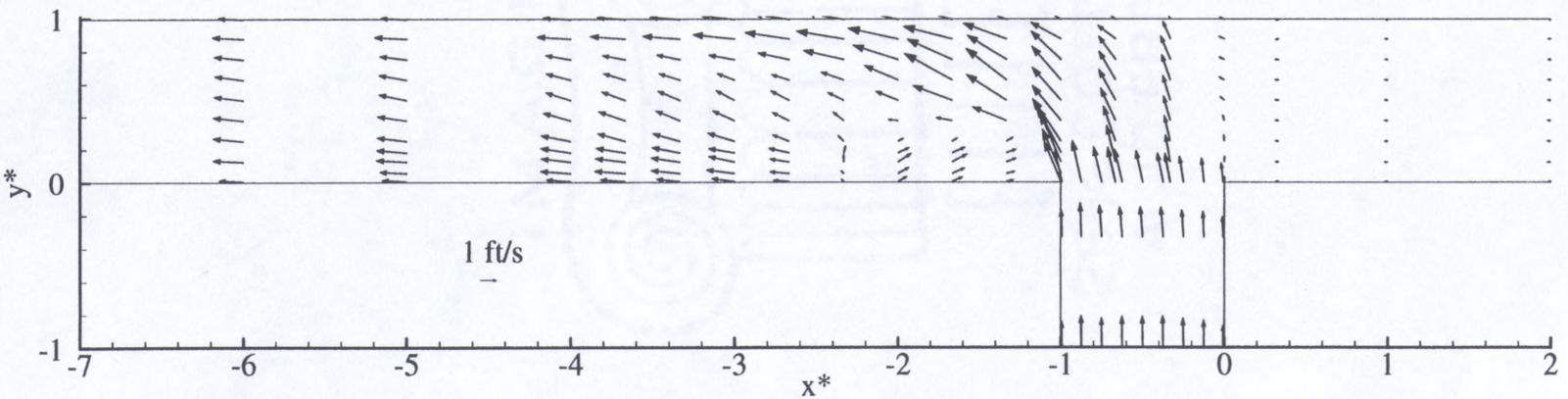

Figure 4.19. u-v Vector Field, z* = 0.278, q* = 0.083

it should be noted that the stagnation point occurs near the upstream junction corner inside the main channel.

The u-v velocity vector field displays insight into the differences between the bed and surface momentum of the entering branch channel flow. It is apparent that in developed entering flow the higher velocities at the surface provide an increased momentum over that of the bed. The result of this momentum difference causes variance in the amount of deflection toward the downstream direction of the entering branch channel flow. As a result of this difference in momentum and direction of the branch channel flow the velocity patterns, separation zone, and flow recovery are very different between the bed and the surface for a given flow condition. Additional u-v velocity field plots can be located in Appendices B through G.

4.4 v-w Vector Field

The three-dimensional nature of the open-channel junction flow problem has been only briefly addressed in any previous work on the topic. While a two-dimensional look at the junction flow will provide insight to the general flow patterns, a true model of an open-channel junction would have to be three-dimensional as vertical velocity gradients and secondary currents are a significant portion of the junction flow. This study has included the three-dimensional velocity and turbulence data to provide a benchmark data set for numerical models which can address the junction flow in three-dimensions.

The v-w vector field is shown for $q^* = 0.250$ as it propagates downstream from $x^* = -1.33$ through $x^* = -7.00$ (Figures 4.20 – 4.25). The flow at $x^* = -1.33$ is showing that

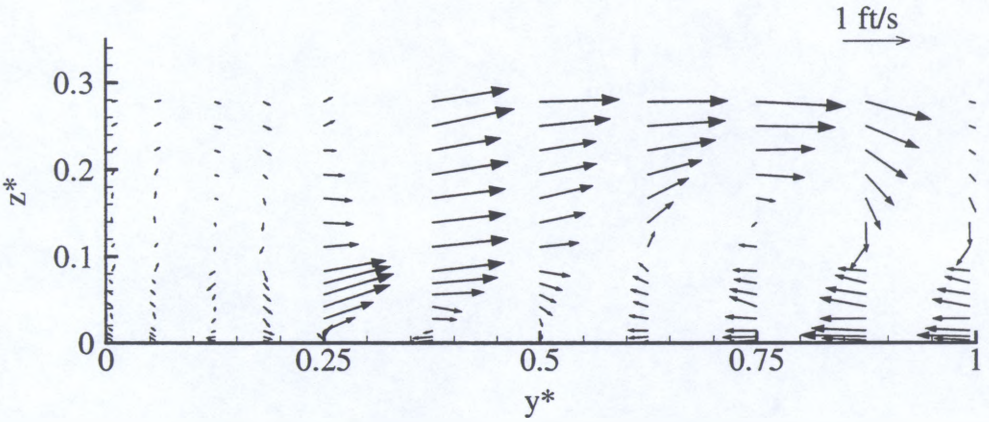

Figure 4.20. v-w Vector Field, x* = -1.33, q* = 0.250

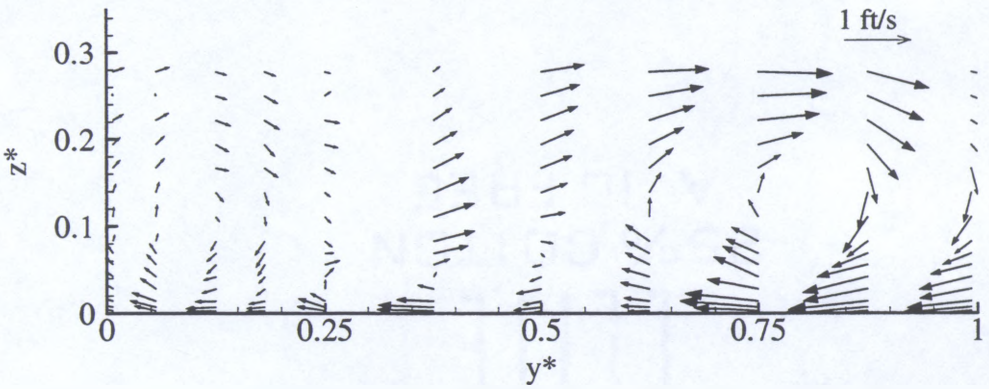

Figure 4.21. v-w Vector Field, x* = -1.67, q* = 0.250

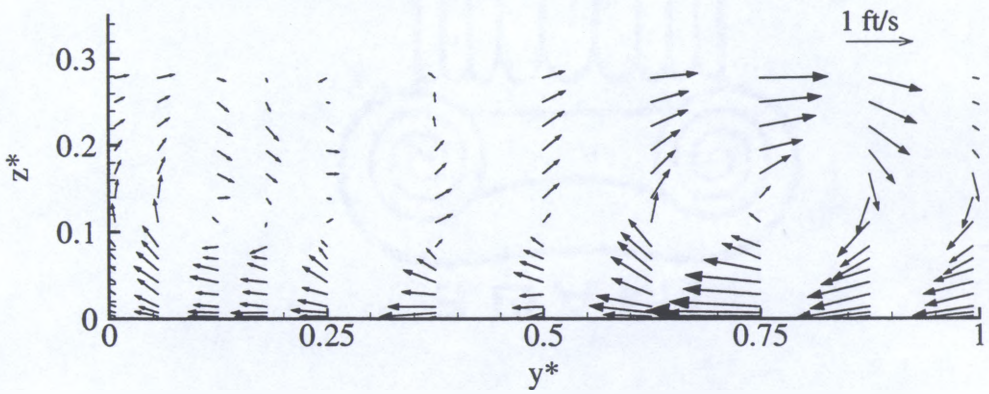

Figure 4.22. v-w Vector Field, x* = -2.00, q* = 0.250

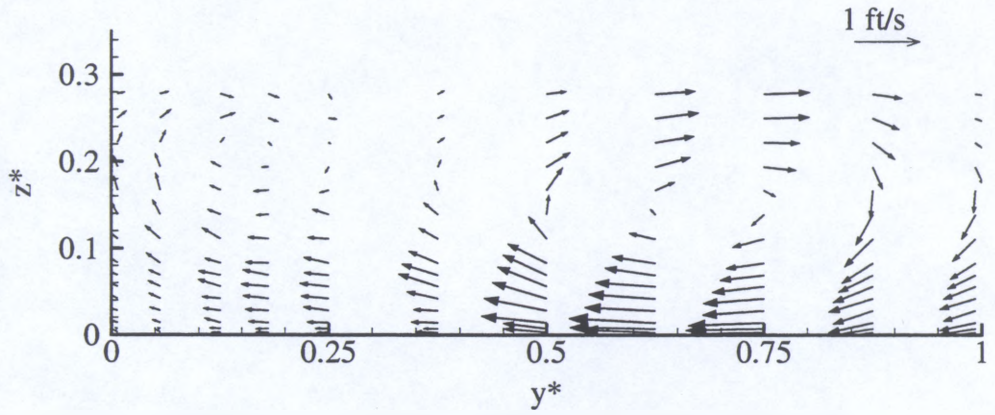

Figure 4.23. v-w Vector Field, x* = -3.00, q* = 0.250

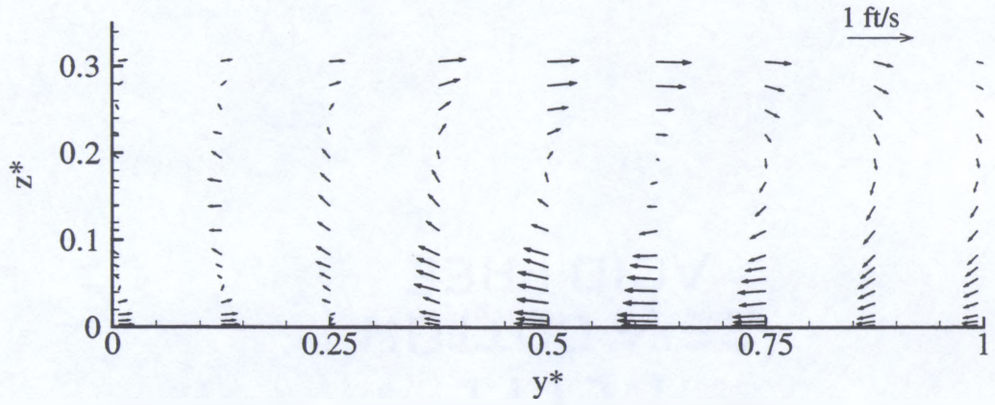

Figure 4.24. v-w Vector Field, x* = -5.00, q* = 0.250

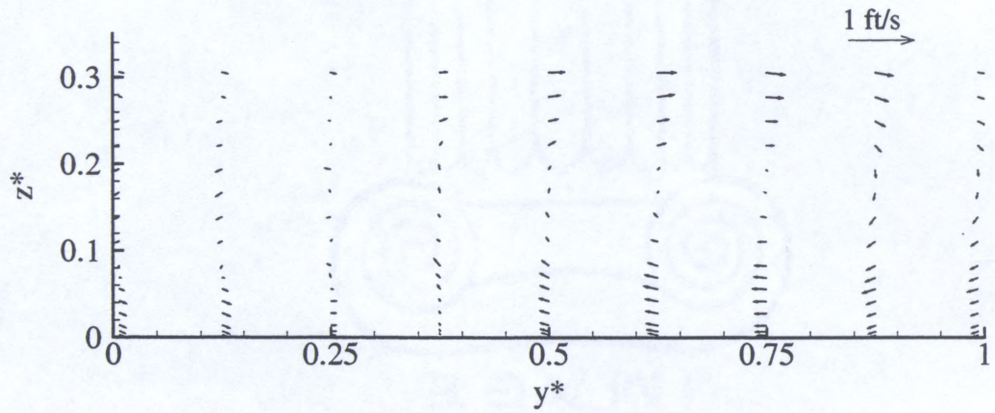

Figure 4.25. v-w Vector Field, x* = -7.00, q* = 0.250

the lateral momentum of the surface being greater than that of the near bed allows the surface water to approach the junction opposite wall. As the surface water has a significant v component into the wall, continuity dictates that the flow can not go into the wall. The surface water is then deflected slightly downstream by the oncoming main channel water, note the diminishing v components as the flow travels downstream, and downward by the weight of the water itself, note the negative w component along the junction opposite wall. This motion creates a secondary current that is evident along the outer half of the channel in Figures 4.20 through 4.23. The first portion of the junction flow to enter the separation zone along the junction adjacent wall is the near bed flow due to the negative v component of the flow as it comes to the bed from the surface. As is evident by the v-w vectors in Figure 4.22 and 4.21, the upper portion of the separation zone does not get filled by lateral flow, but rather by vertical flow. The near bed flow as it approaches the junction adjacent wall must again be redirected and, similar to the surface flow, some of this is in the downstream direction. However, the bed flow is also deflected upward into the zone of separation. Eventually, the entire channel is engulfed in a large clockwise secondary current as seen in Figure 4.24. By the section at $x^* = -7.00$ the secondary current has significantly diminished. Similar secondary flow patterns are evident in the cases of $q^* = 0.083$ and $q^* = 0.417$, but the three-dimensional significance diminishes greatly as q^* increases, as seen in Figure 4.26.

The significance of the w velocity component can be judged by the relative magnitude of the w component of the velocity with respect to a reference velocity. The reference velocity in this study was chosen to be the average velocity in the section if the

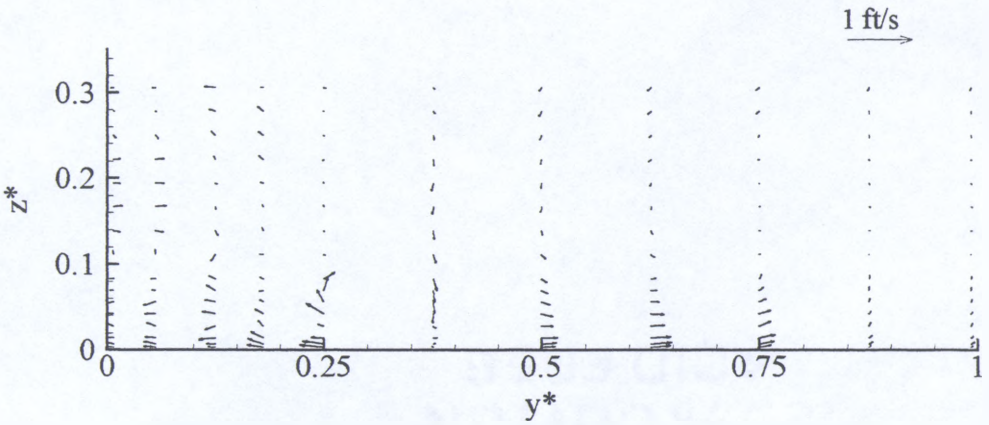

Figure 4.26. v-w Vector Field, x* = -1.67, q* = 0.750

entire section were conveying flow at a depth of 11 in ($z^* = 0.306$), an average depth in the junction region for this study. The resulting reference velocity for 6.0 cfs passing at this depth is 2.40 ft/s. Figures 4.27 through 4.32 show the relative magnitude of the vertical velocity component at $x^* = -1.67$ for the entire range of q^* tested. Section $x^* = -1.67$ was chosen because that section displayed some of the largest w velocities recorded in the study. Figure 4.27 shows that the three-dimensionality of low q^* junctions is an important factor, with the w component composing more than 30% of the total velocity at certain points. The similar is true for the condition of $q^* = 0.250$ and for $q^* = 0.417$ to a lesser extent. However, when q^* is large the three-dimensional nature of the channel junction flow is reduced.

Studying the complete set of velocity data and observing flow in the flume, allows one to visualize the complete flow structure in the vicinity of the junction. Figure 4.33

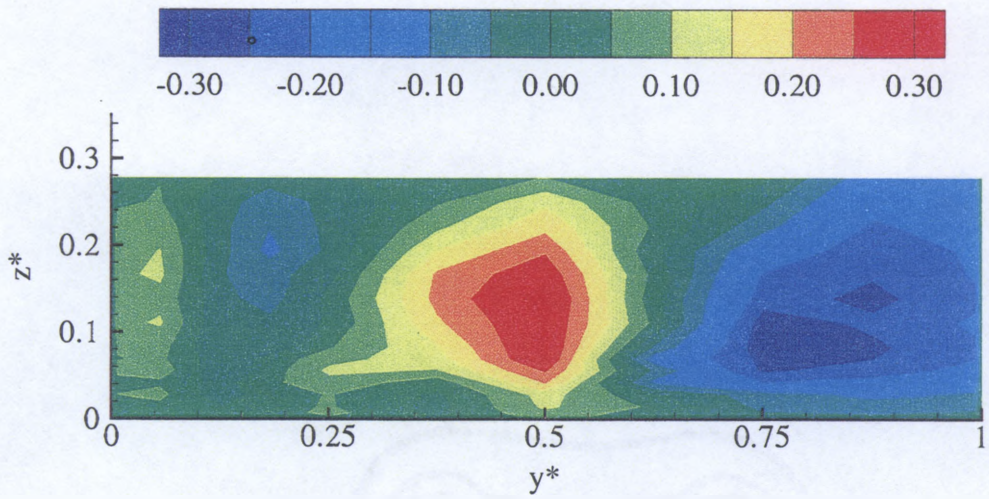

Figure 4.27. Relative Magnitude of w, x* = -1.67, q* = 0.083

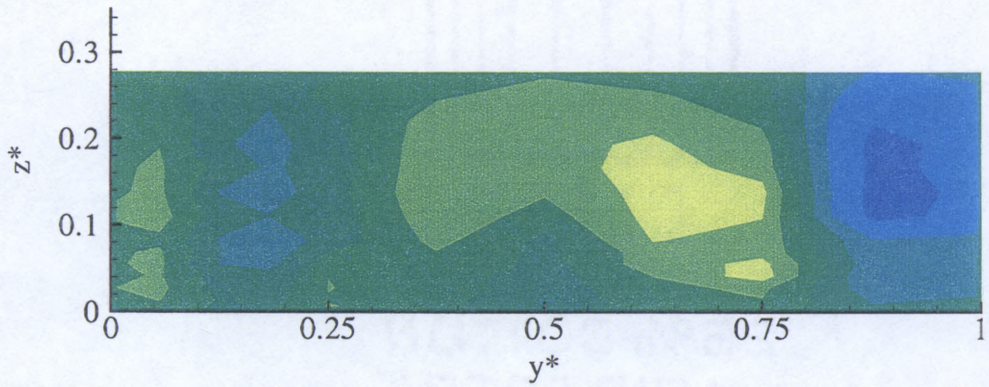

Figure 4.28. Relative Magnitude of w, x* = -1.67, q* = 0.250

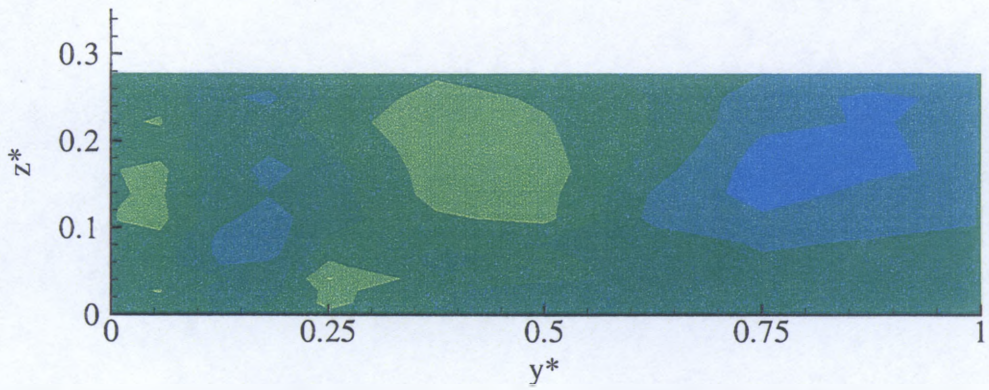

Figure 4.29. Relative Magnitude of w, x* = -1.67, q* = 0.417

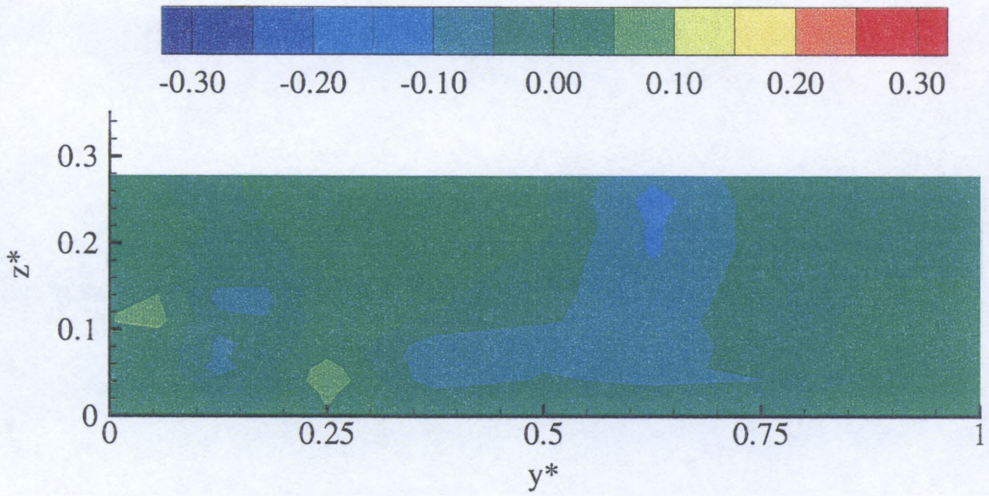

Figure 4.30. Relative Magnitude of w, x* = -1.67, q* = 0.583

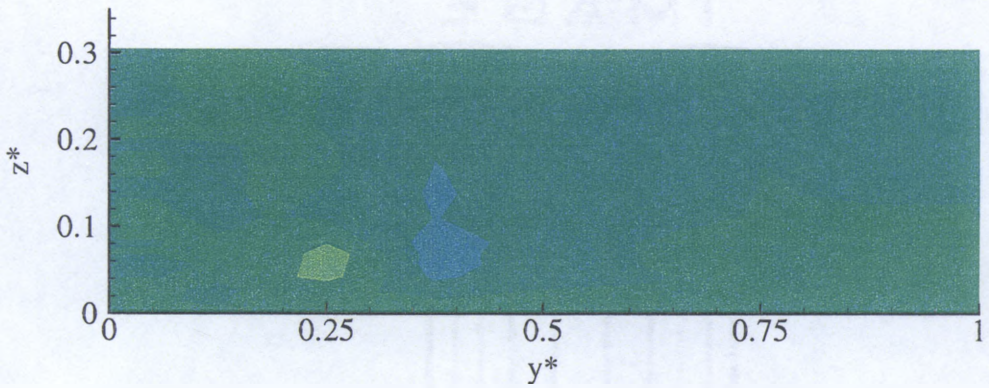

Figure 4.31. Relative Magnitude of w, x* = -1.67, q* = 0.750

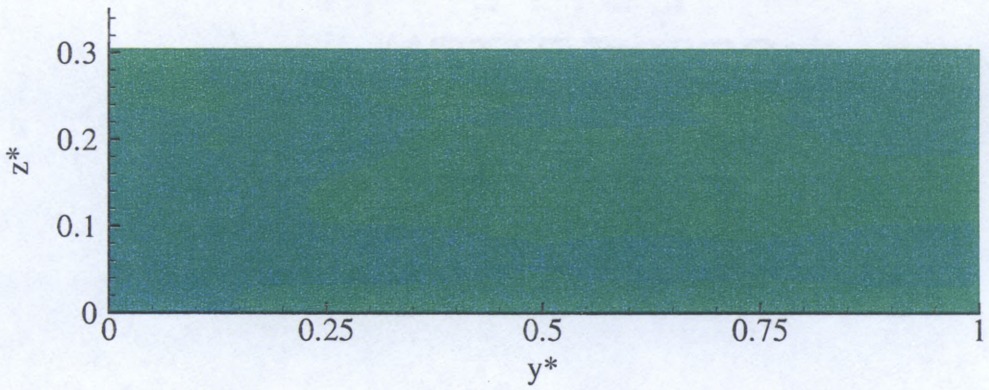

Figure 4.32. Relative Magnitude of w, x* = -1.67, q* = 0.917

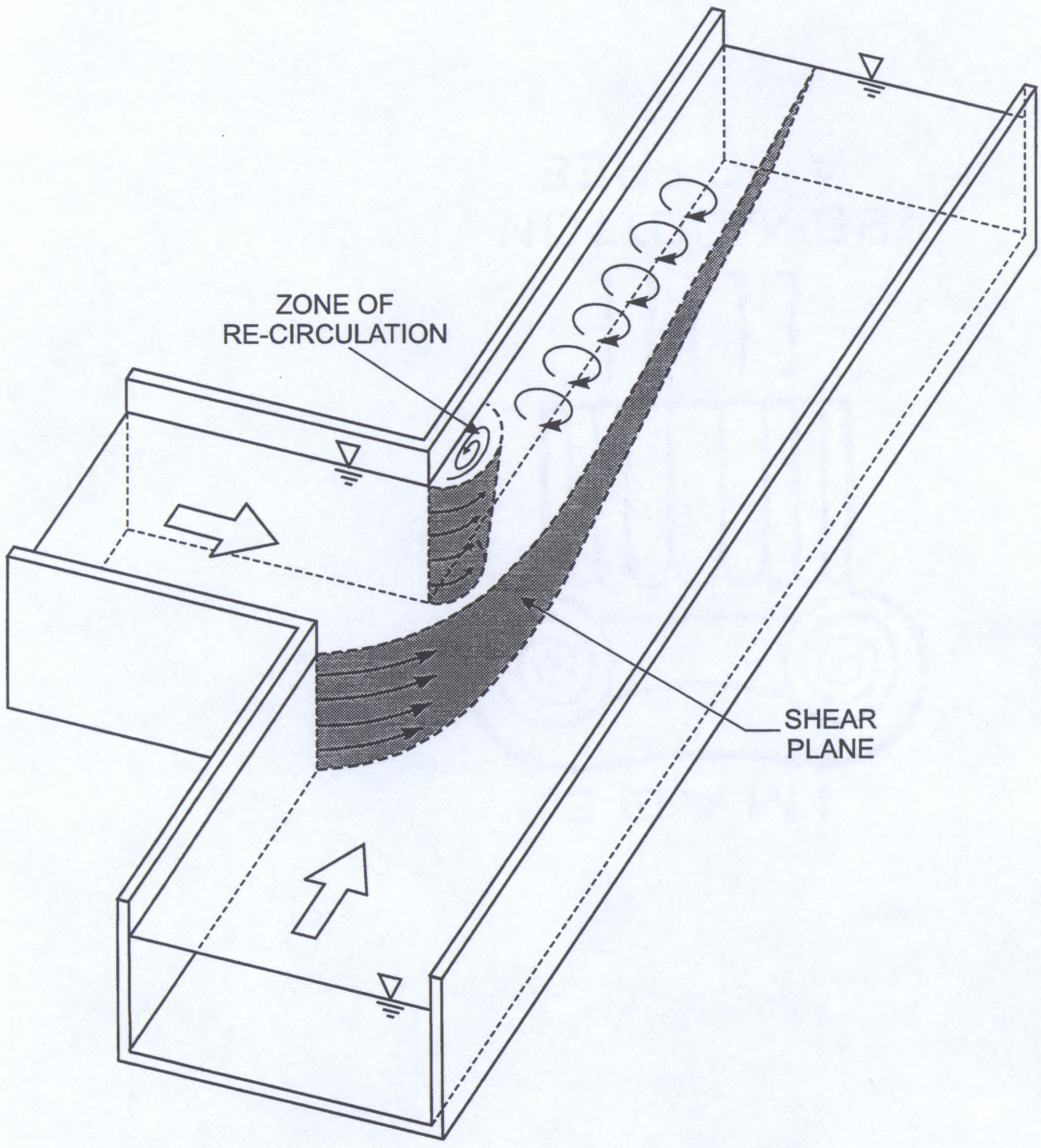

Figure 4.33. Combining Flow Schematic, q* = 0.750

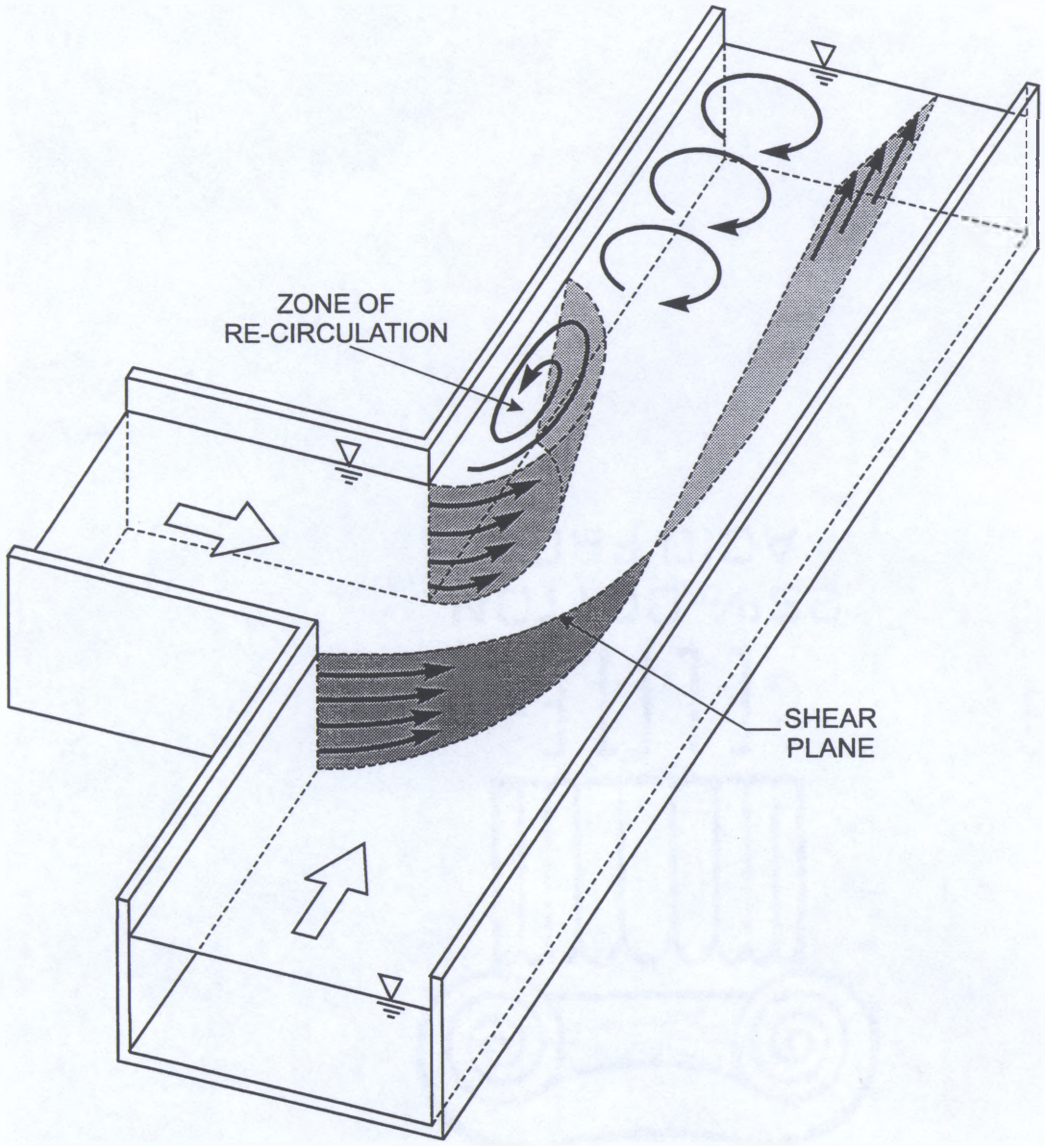

Figure 4.34. Combining Flow Schematic, q* = 0.250

shows a schematic of the flow structures present for the flow $q^* = 0.750$ and Figure 4.34 displays the flow structures present for $q^* = 0.250$.

4.5 Turbulent Kinetic Energy

As mentioned in section 3.2, the measurements at one point in a cross-section consist of 60 seconds of instantaneous velocities collected at 10 Hz. The mean of the set of the individual velocity samples produced the average velocities discussed in the previous sections of this chapter. The sample standard deviation, s, of this set of velocity samples can be shown to be approximately equal to the root-mean-square of the turbulent velocity fluctuation, u′.

$$s = \sqrt{\frac{\sum (u - \bar{u})^2}{n-1}}$$

$$u' = u - \bar{u}$$

$$RMS\ u' = \sqrt{\frac{\sum (u')^2}{n}} = \sqrt{\frac{\sum (u - \bar{u})^2}{n}}$$

It is apparent, that for a large sample set, the sample standard deviation is approximately equal to the root-mean-square of the turbulent velocity fluctuations. The above equations are also true for v′ and w′. From the root-mean-square of the turbulent velocity fluctuations the turbulent kinetic energy, K, is calculated.

$$K = \frac{1}{2}\left[(RMS\ u')^2 + (RMS\ v')^2 + (RMS\ w')^2\right]$$

The final data set includes the three-dimensional turbulent velocity fluctuations and the turbulent kinetic energy for each data point.

It should be noted that it is unclear from the literature how turbulence measurements obtained from an ADV compare with similar measurements from an LDV or hot film anemometry. However, it is likely that variances will result from differences in sampling rate, measurement volume, and physics of the measurement devices. Therefor, these data should be used with appropriate understanding.

The turbulent kinetic energy, K, for the condition $q^* = 0.417$ is displayed in Figure 4.35 for the near bed flow and Figure 4.36 for the surface flow. It is evident that the most turbulent region occurs along the boundary of the passing flow and the downstream portion of the separation zone. It is interesting to note that, while the branch channel is impinging on the main channel flow, both flows pass through the channel junction without significant turbulent mixing between the two flows. However, as the higher velocity passing flow begins to enter the lower velocity separation zone downstream of the junction, significant turbulence occurs. The relative position of the highest turbulent kinetic energies with respect to the separation zone is similar for all flow conditions as seen in Figure 4.37 and Figure 4.38 showing the turbulent kinetic energy for $q^* = 0.750$. The position of the highest turbulent flow is again located at the boundary of the separation zone. The magnitude of the highest turbulent kinetic energy along the separation zone remains fairly constant for the middle flow conditions, $q^* = 0.250$ through $q^* = 0.750$. The cross-sectional views of K, Figure 4.39 through 4.41 display that turbulent kinetic energy is approximately constant along the vertical.

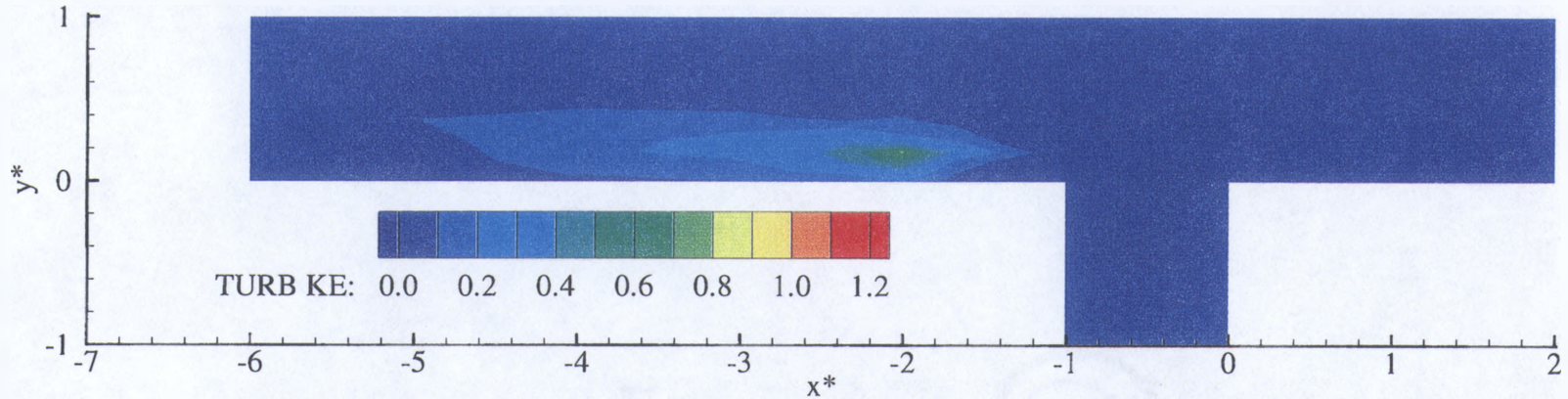

Figure 4.35. Turbulent Kinetic Energy, z* = 0.014, q* = 0.417

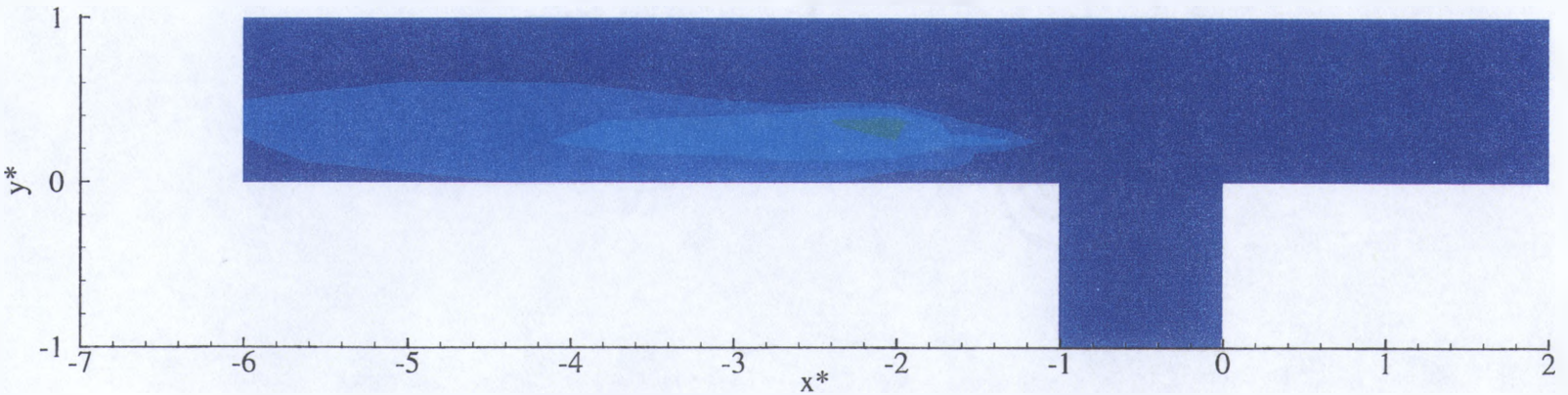

Figure 4.36. Turbulent Kinetic Energy, z* = 0.278, q* = 0.417

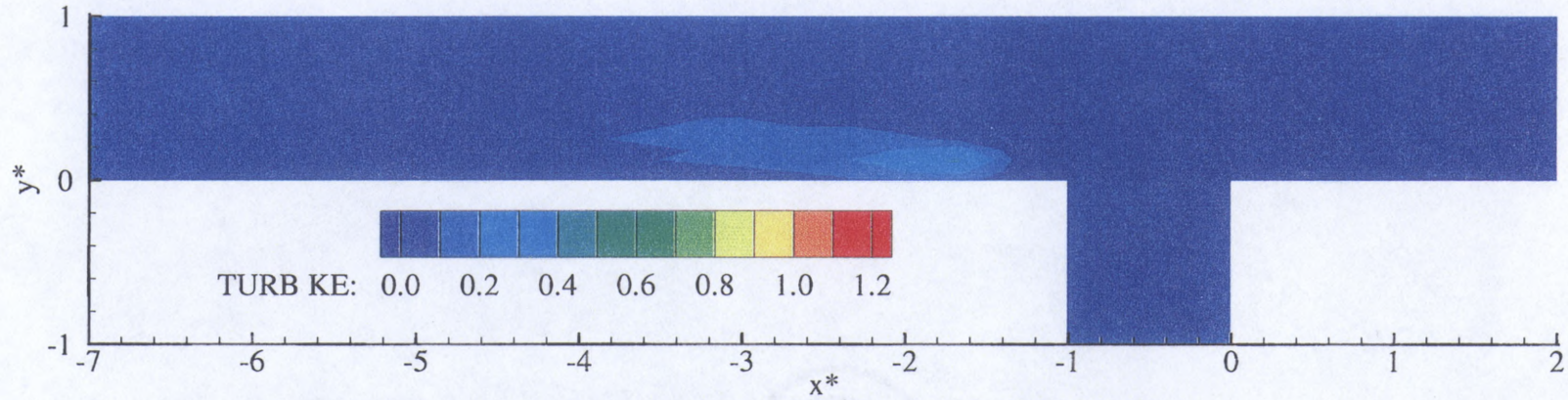

Figure 4.37. Turbulent Kinetic Energy, z* = 0.014, q* = 0.750

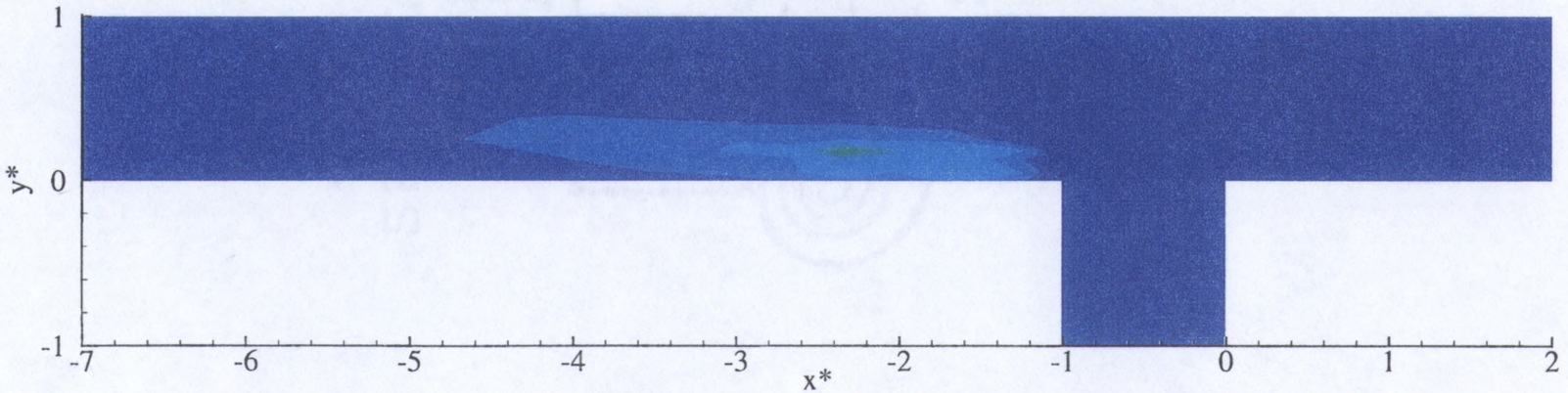

Figure 4.38. Turbulent Kinetic Energy, z* = 0.278, q* = 0.750

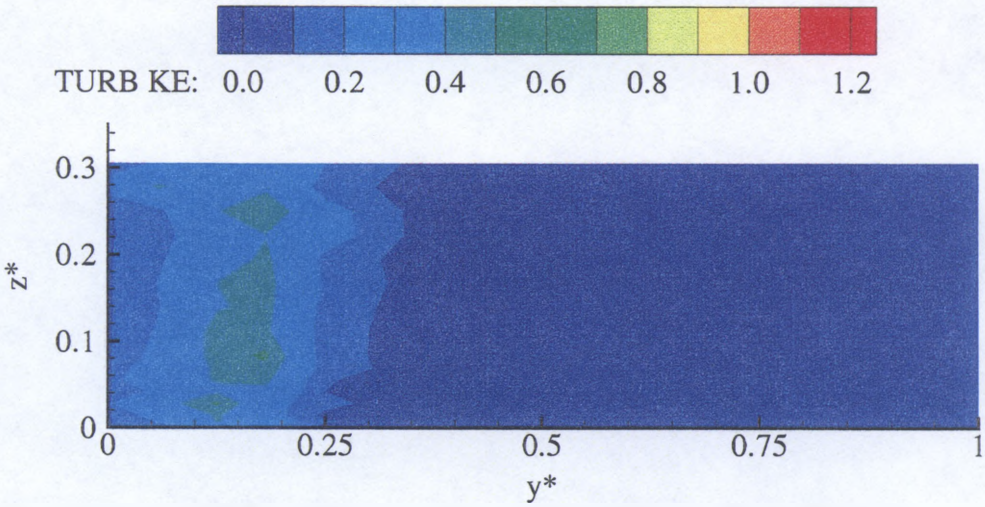

Figure 4.39. Turbulent Kinetic Energy, x* = -1.67, q* = 0.750

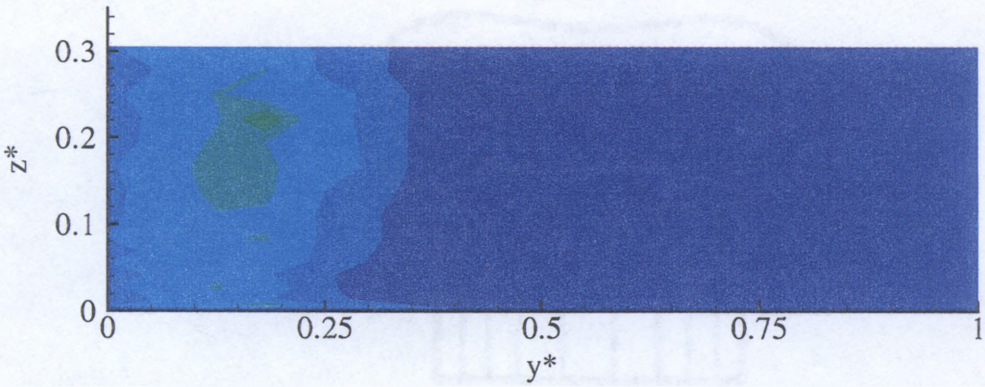

Figure 4.40. Turbulent Kinetic Energy, x* = -2.00, q* = 0.750

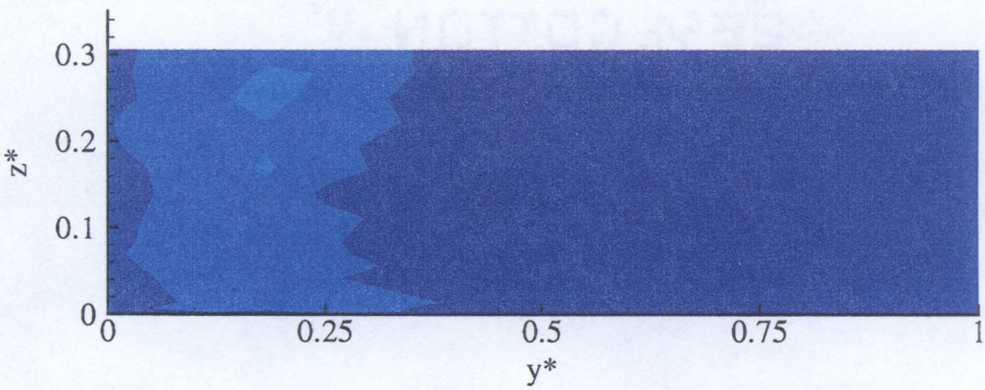

Figure 4.41. Turbulent Kinetic Energy, x* = -3.00, q* = 0.750

Turbulent kinetic energy plots for all flow conditions can be found in Appendices B through G.

4.6 Uncertainty Analysis

To ascertain the repeatability of the measurements, a simple uncertainty analysis was performed. The ADV probe was positioned to measure the velocity components at a position in the flume with highly three-dimensional flow (i.e., at $x^* = -2.00$, $y^* = 0.50$, $z^* = 0.20$, and $q^* = 0.417$). Ten measurements of velocity were recorded with the setup and the flow stabilized. The pertinent information presented in Table 4.1. Additionally, to ascertain the uncertainty of the measurements resulting from the setting of the pumps, inlet valves, positioning of the probe, and stability of the flow structures, ten measurements were repeated with the flume being restarted and the probe being repositioned between each measurement. These data are shown in Table 4.2. As can be seen from the tabulated data the experimental uncertainty is relatively small compared to the mean values of velocity and turbulence intensity.

Table 4.1. Repeatability of Measurements From a Single Test Session

	u velocity	v velocity	w velocity	RMS u'	RMS v'	RMS w'
Minimum	-2.830	0.092	-0.022	0.105	0.110	0.060
Maximum	-2.762	0.117	-0.007	0.126	0.129	0.071
Mean	-2.779	0.102	-0.012	0.112	0.120	0.064
Std. Dev.	0.020	0.009	0.005	0.007	0.006	0.004

Table 4.2. Repeatability of Measurements From Multiple Test Sessions

	u velocity	v velocity	w velocity	RMS u'	RMS v'	RMS w'
Minimum	-2.873	-0.031	-0.122	0.118	0.114	0.066
Maximum	-2.782	0.125	0.048	0.160	0.186	0.112
Mean	-2.824	0.070	-0.053	0.127	0.138	0.092
Std. Dev.	0.029	0.056	0.063	0.013	0.021	0.014

4.7 Water Surface Mapping

The water surface was mapped for $q^* = 0.750$ and allows visualization of the dynamics of the water surface through the channel junction region. Figure 4.42 displays contours of constant water surface elevation.

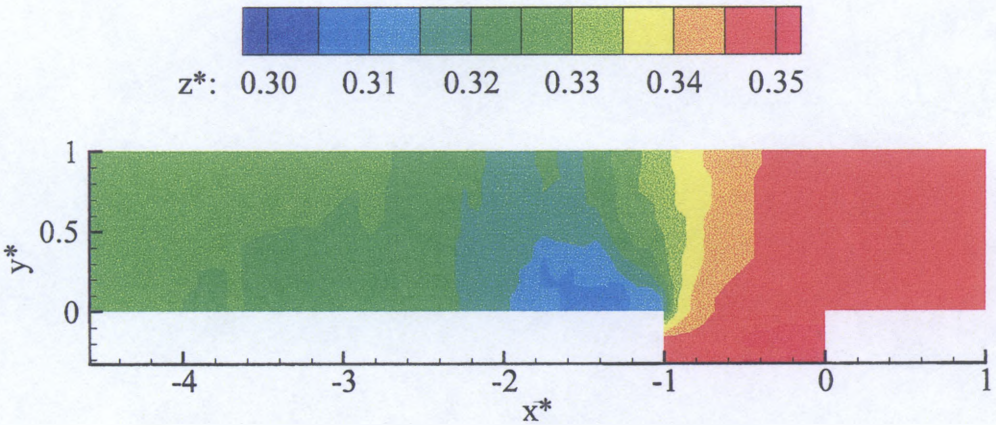

Figure 4.42. Water Surface Mapping, $q^* = 0.750$

The depth change from the flow downstream of the junction to the flow upstream of the junction is apparent in the water surface map. The difference in the upstream and downstream water surface elevation is approximately 1 in. This depth ratio is the focus of most previous work on open-channel junction flow, as mentioned in Chapter 2. The water surface displays a drawdown as the flow enters the contracted region and a depth increase as the flow expands to the entire channel width downstream of the separation zone.

CHAPTER 5

CONCLUSIONS AND RECOMMENDATIONS

5.1 Conclusions

This thesis presents data taken at a 90° open-channel junction in a large, combining flow flume. The data are composed of three-dimensional velocity and turbulence measurements, along with some water surface mapping. The result of this project is a thorough description of the flow patterns and characteristics found in the combining flow junction of two open channels, which until the presentation of this data set has not been available. From this project, the following conclusions can be made:

1.) A detailed set of data exists that contains three-dimensional velocities and turbulence measured on a sufficiently dense grid to allow the validation of a numerical model of an open-channel junction. The complete data set is available for download from the IIHR website (http://www.iihr.uiowa.edu) and in hard copy format in an IIHR Report in preparation.

2.) The three-dimensional nature of open-channel combining flow is important to the general flow conditions present in the junction region.

3.) Significant vertical velocities are present in the junction flow.

4.) Secondary currents develop as the branch channel flow enters the main channel along a curvilinear path.

5.) The surface and near-bed flows show two different flow patterns, with higher velocities located near the bed immediately downstream of the junction.

6.) The region of highest turbulence occurs at the downstream end of the separation zone, where the contracted flow is expanding to the full width of the channel.

7.) The separation zone increases in length as a larger percentage of the total flow enters from the branch channel, until a threshold value is reached, after which the length of the separation zone begins to decrease.

5.2 Recommendations for Future Work

The following recommendations for future work are made for furthering the knowledge and design of open-channel junctions:

1.) The application of a three-dimensional, free water surface, computational fluid dynamics code to the open-channel junction problem.

2.) Detailed experimental descriptions, similar to the presented data set, of combining flow at open-channel junctions with junction angles other than 90°.

3.) Detailed experimental descriptions, similar to the presented data set, of combining flow at open-channel junctions with varying downstream Froude number.

APPENDIX A

EXPERIMENTAL FLUME CONSRUCTION DRAWINGS

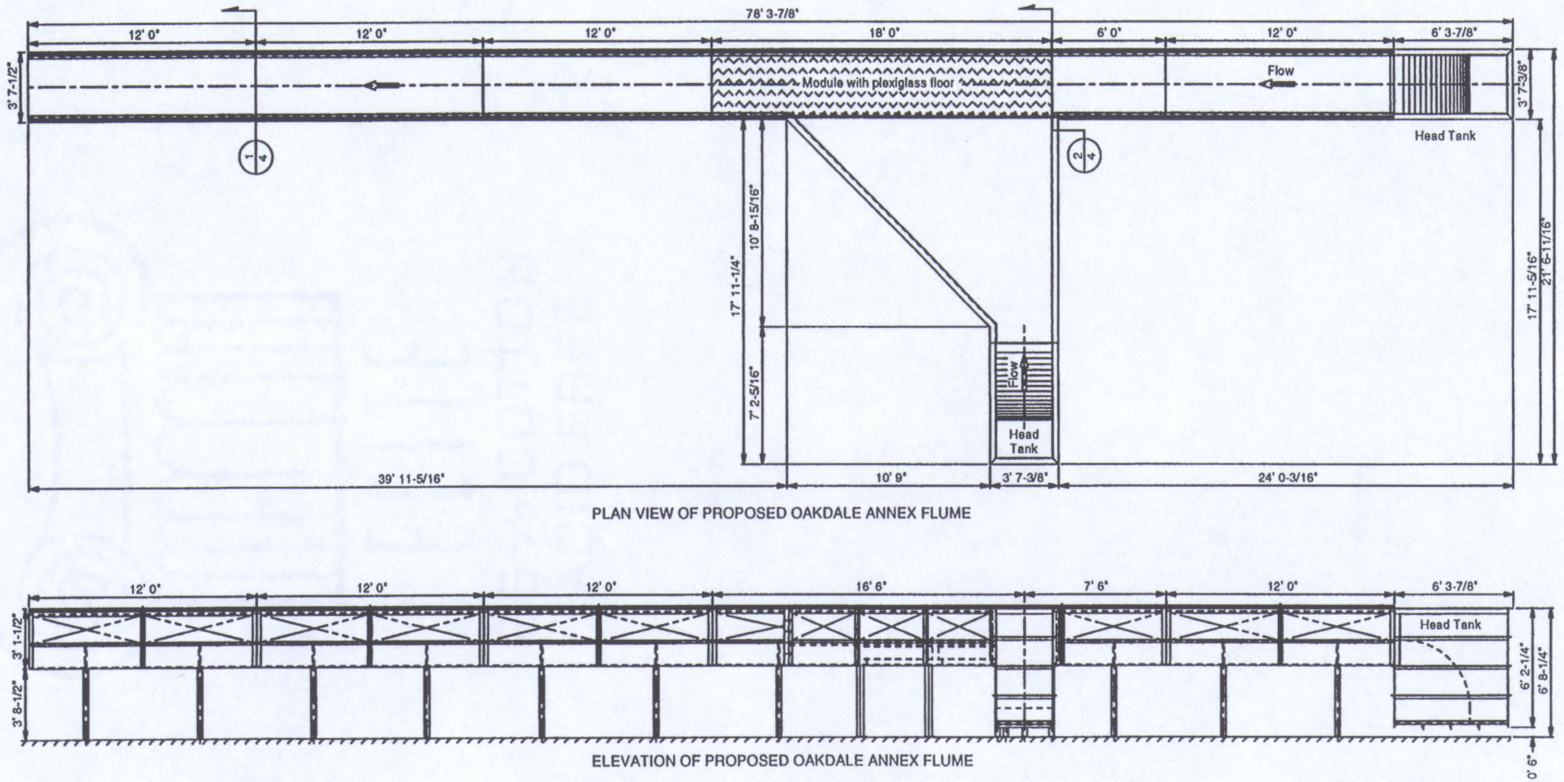

Figure A.1. Experimental Flume Construction Drawings

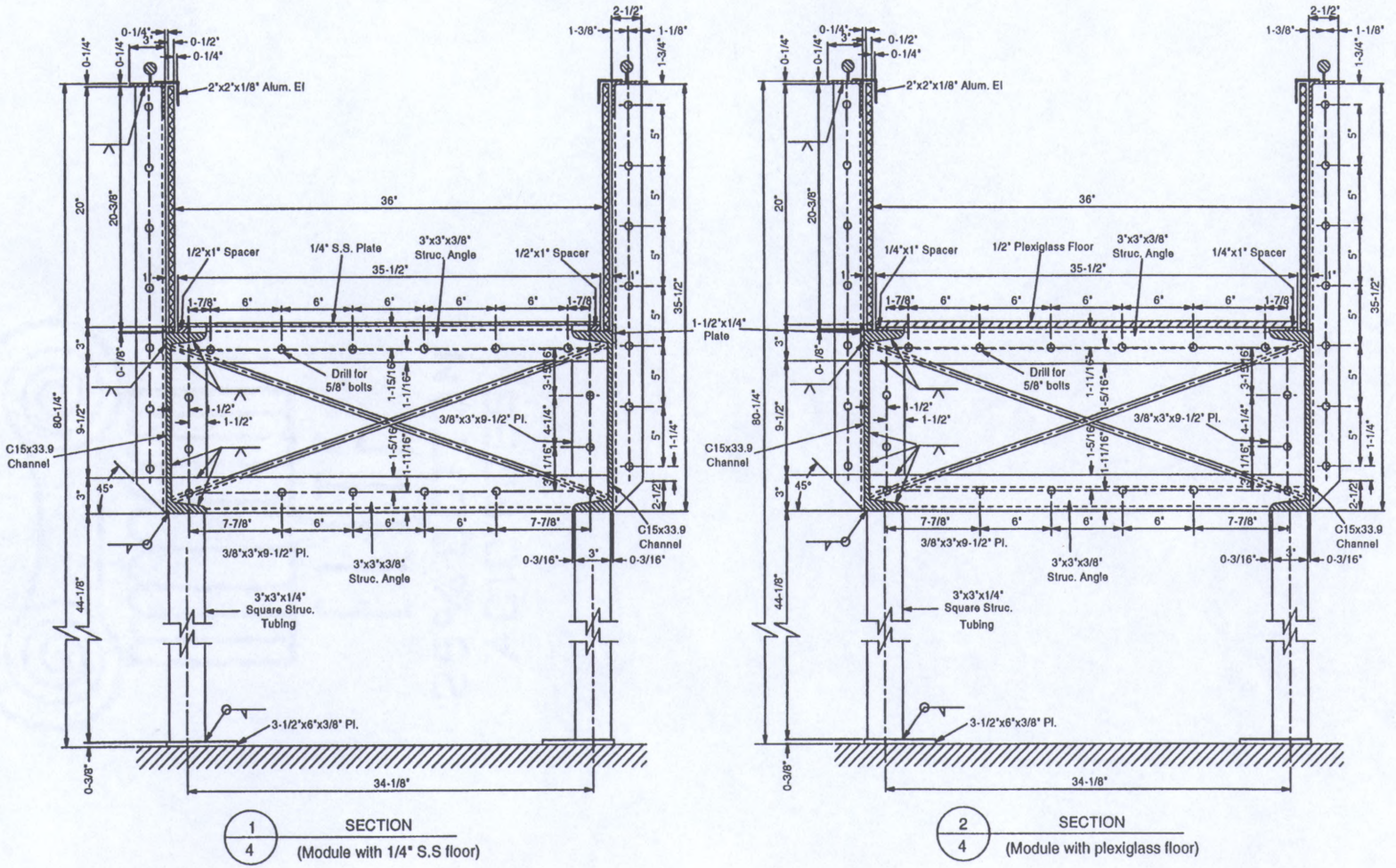

Figure A.1. Continued

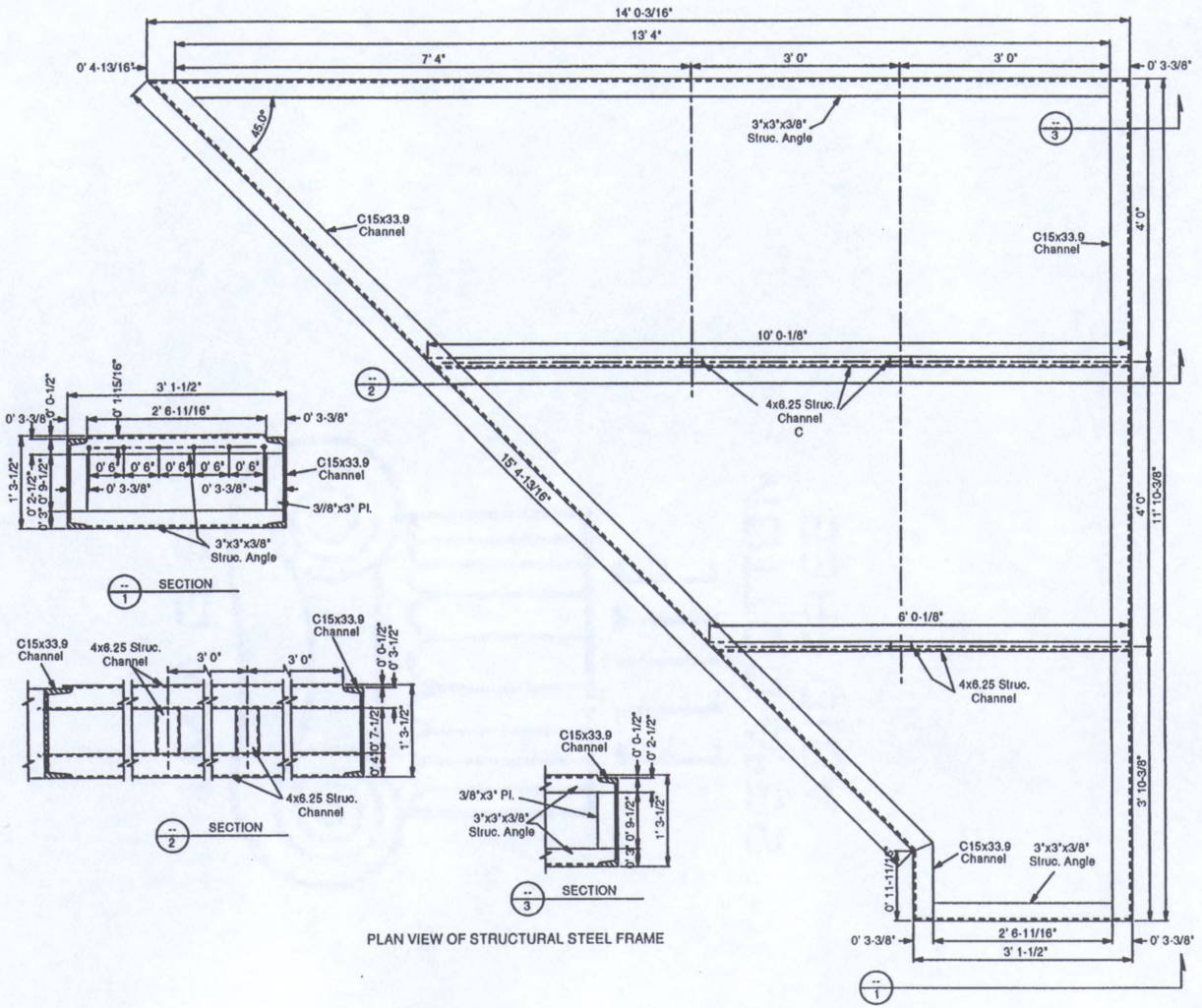

Figure A.1. Continued

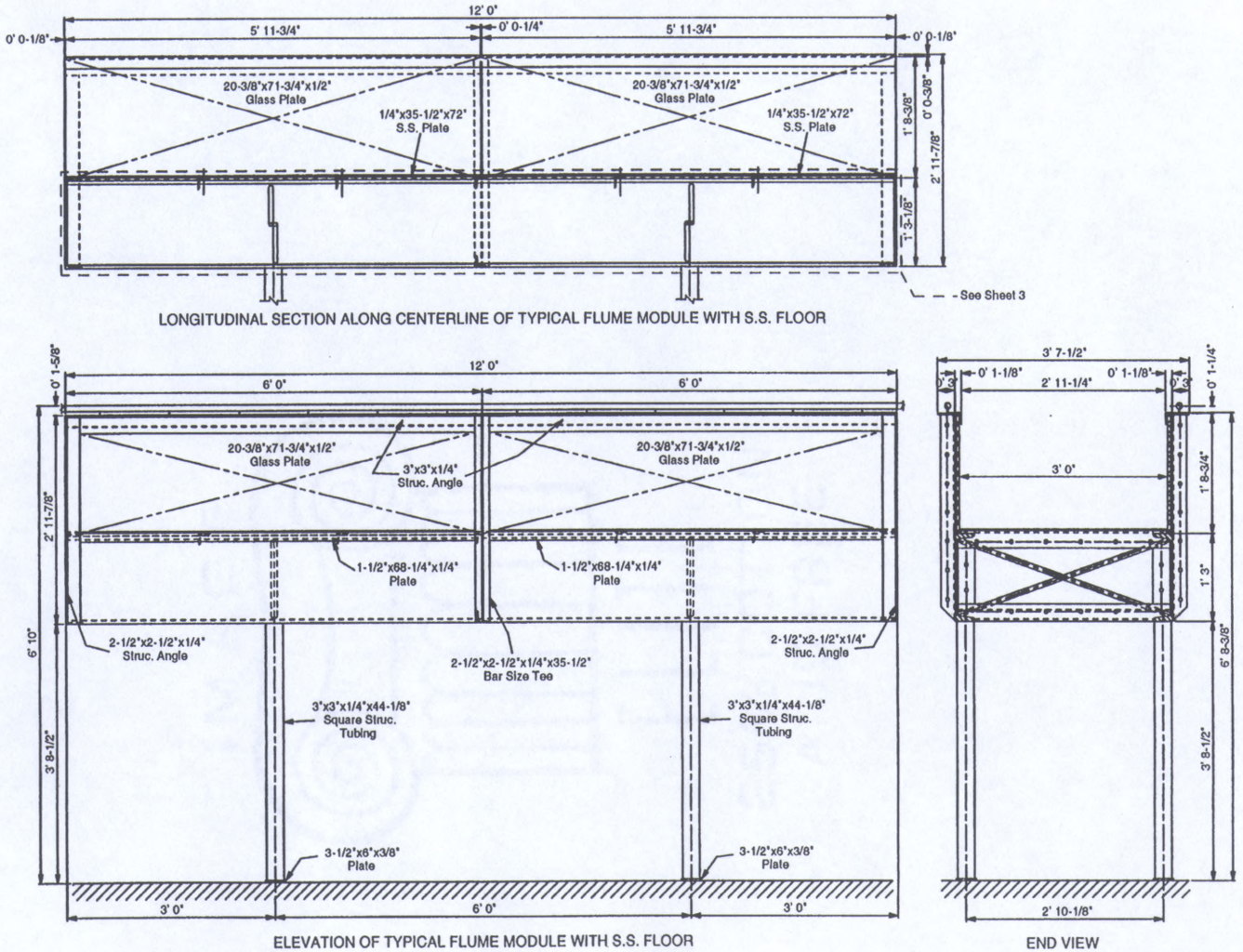

Figure A.1. Continued

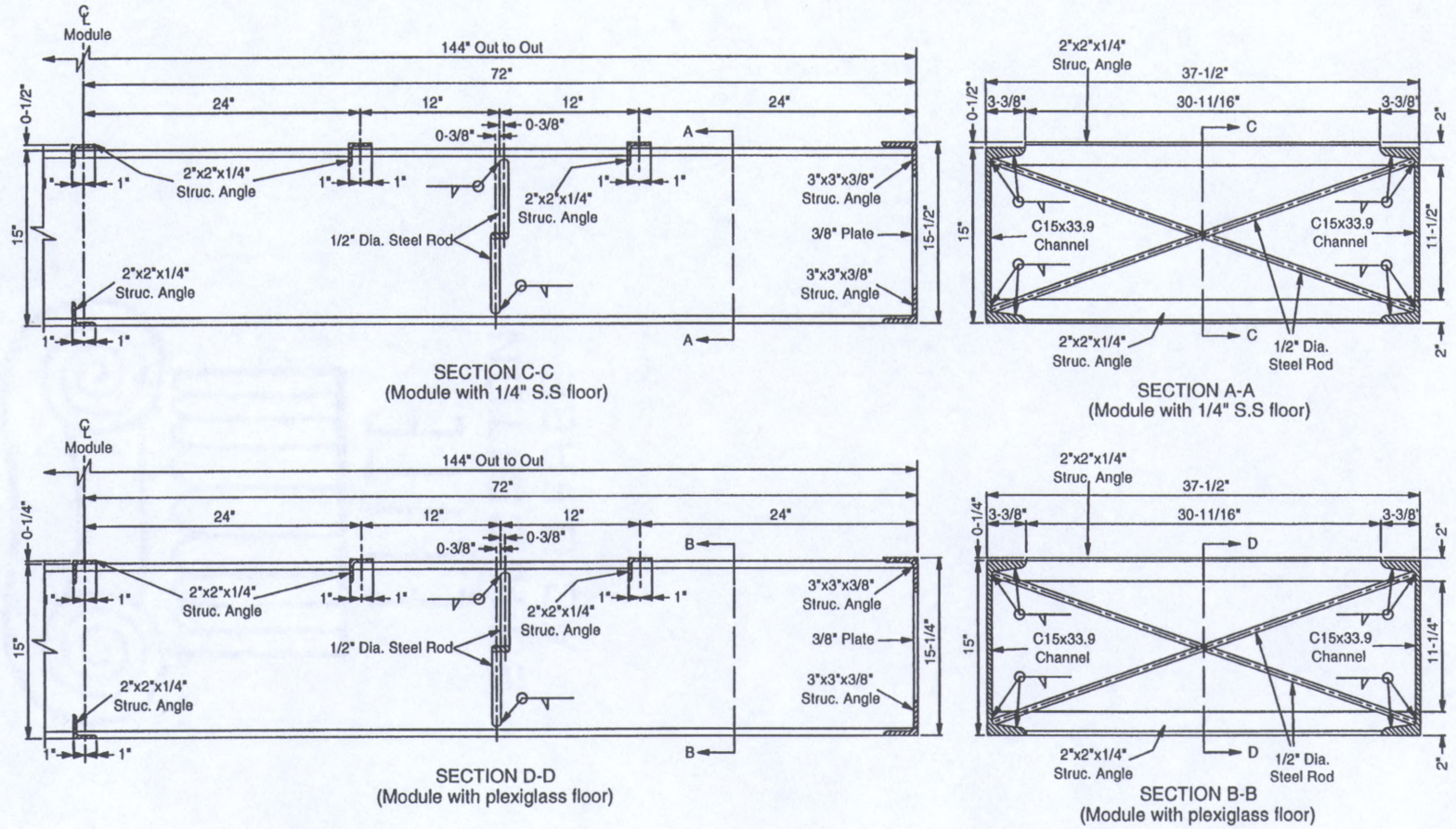

Figure A.1. Continued

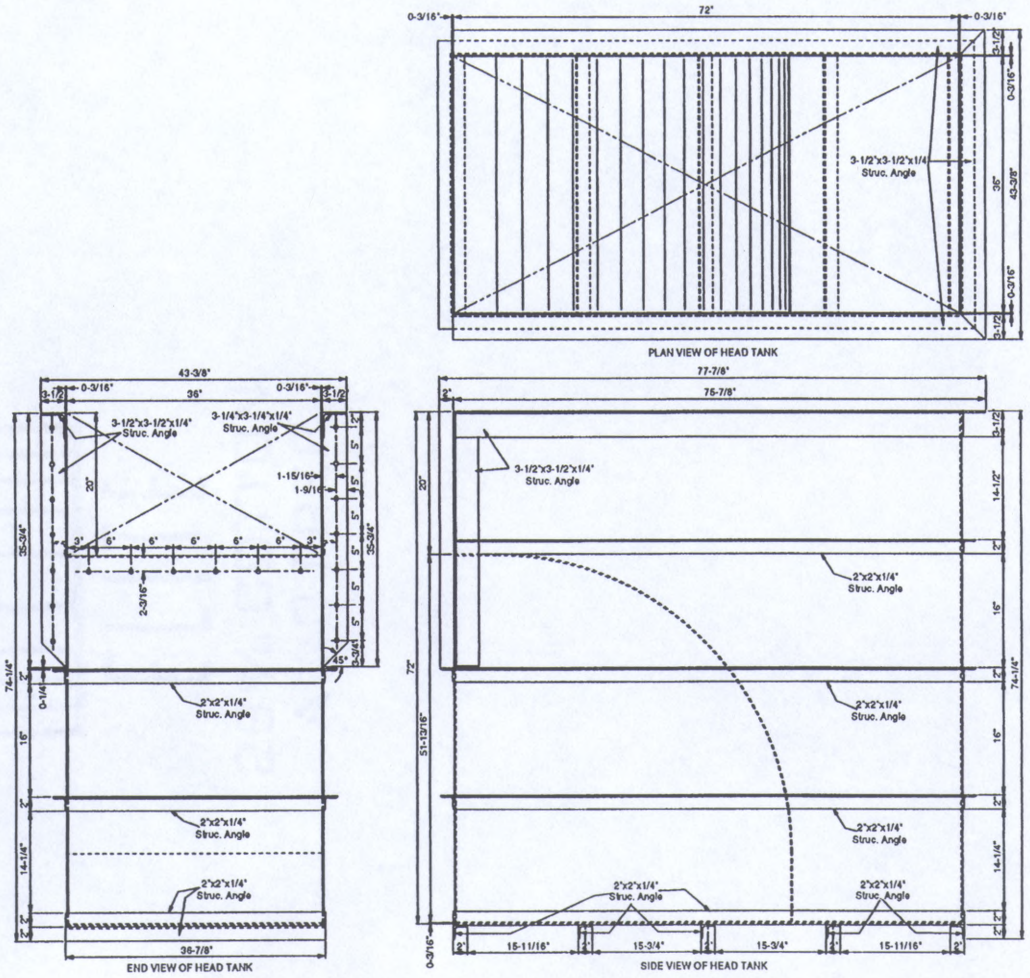

Figure A.1. Continued

APPENDIX B

DATA PLOTS FOR $q^* = 0.917$

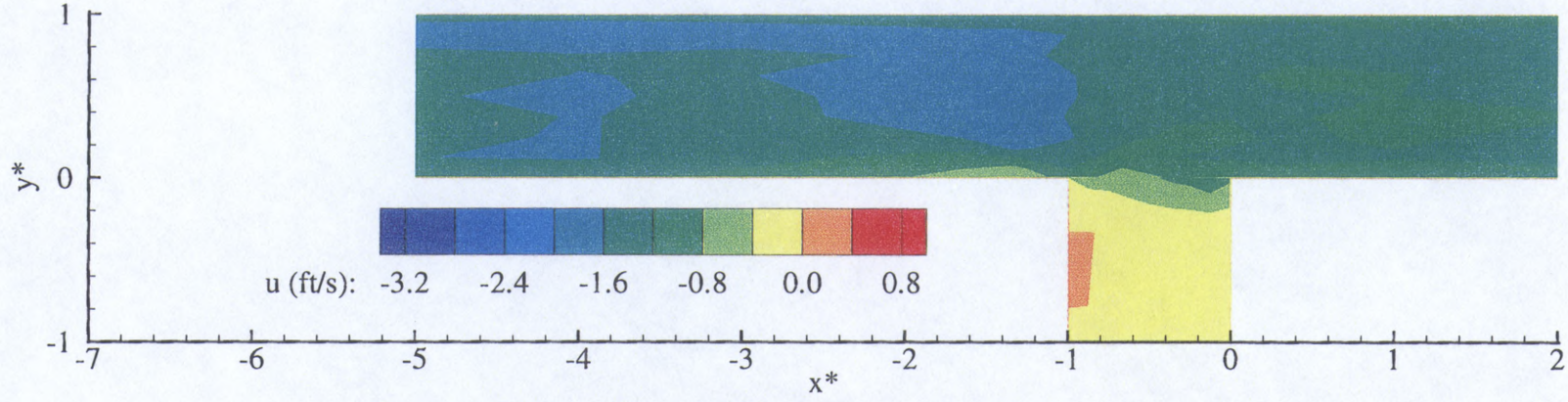

a) z* = 0.014

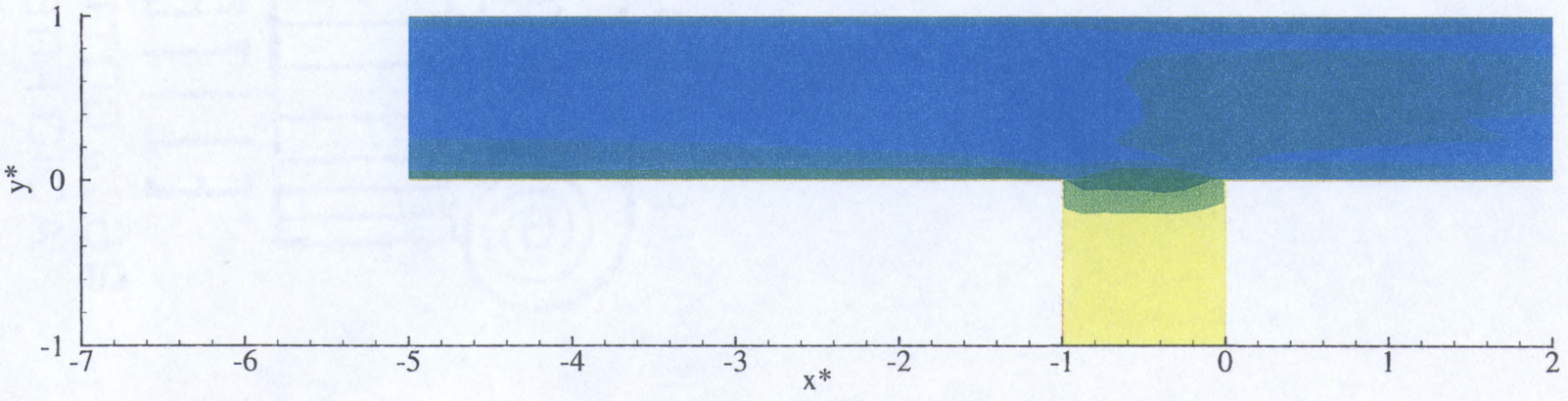

b) z* = 0.278

Figure B.1. u Velocity Plan View, q* = 0.917

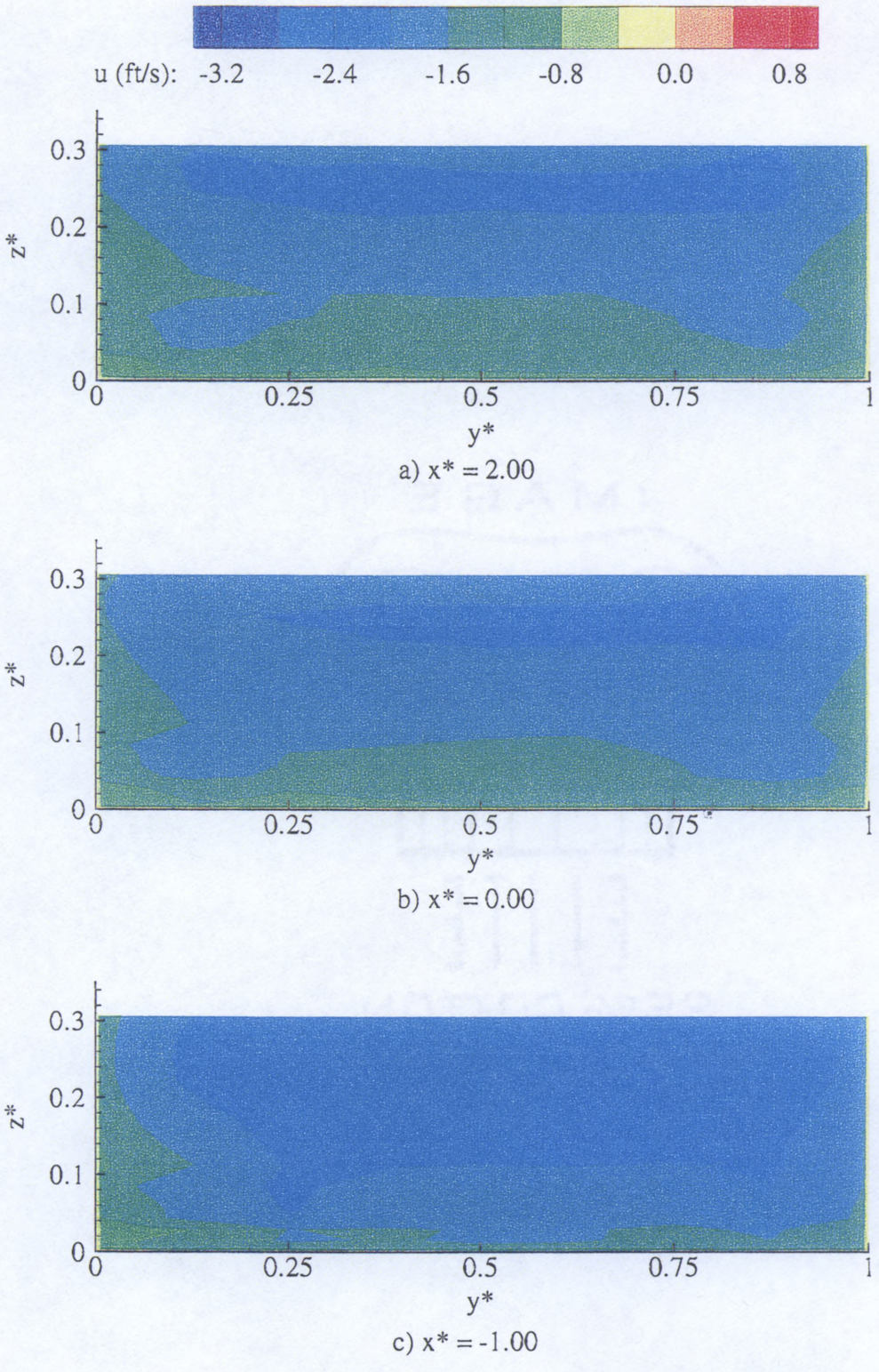

Figure B.2. u Velocity Cross-Sections, q* = 0.917

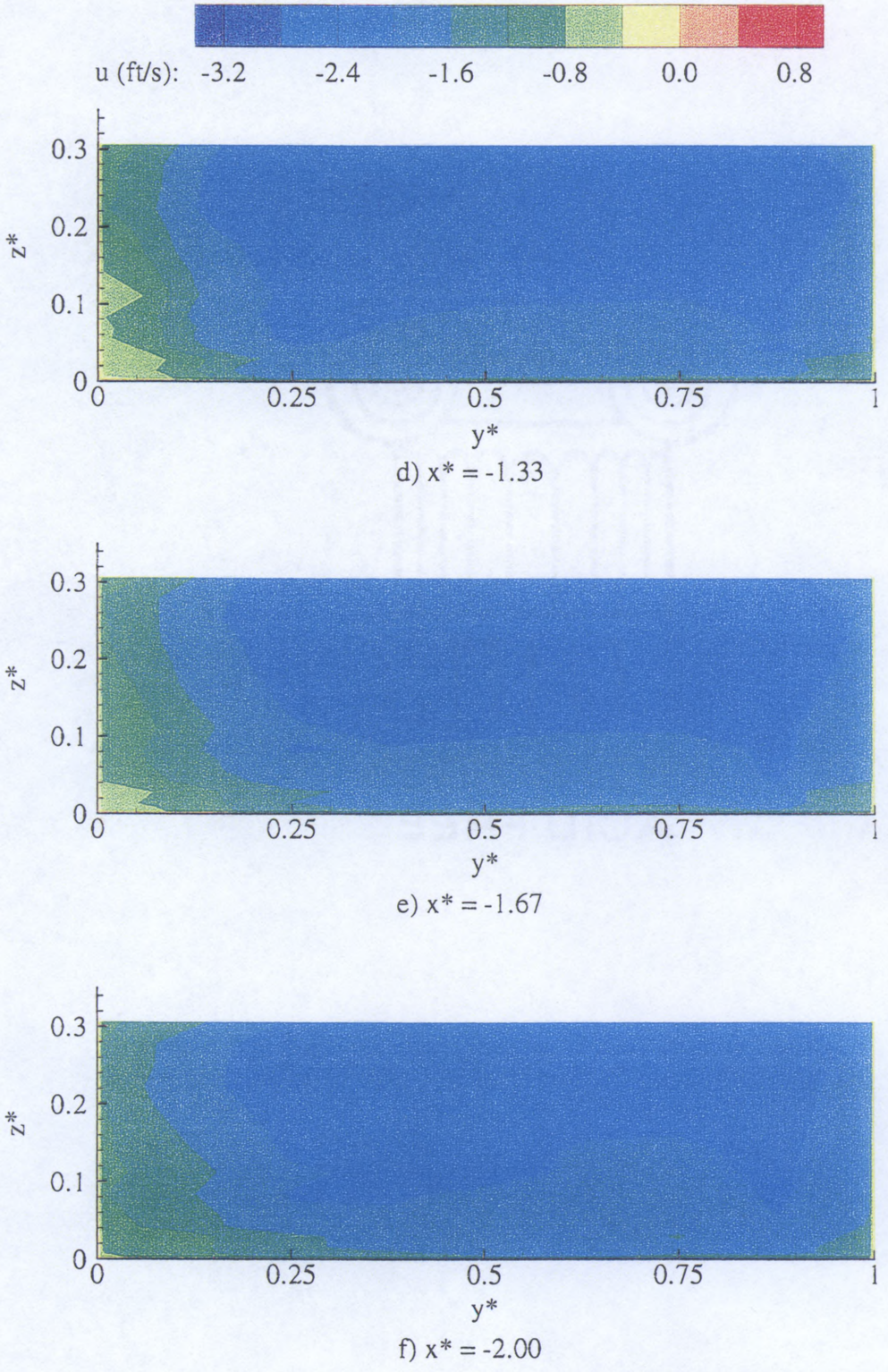

Figure B.2. Continued

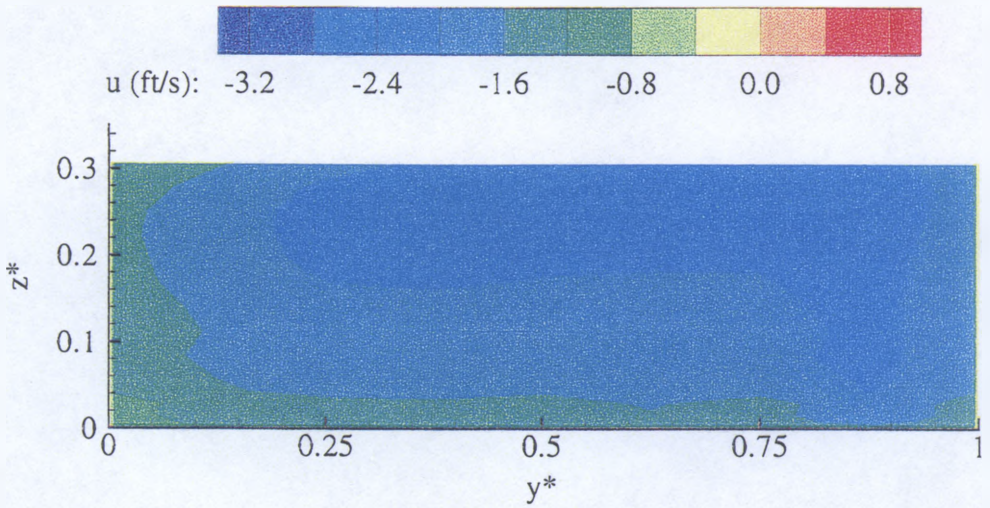

g) x* = -3.00

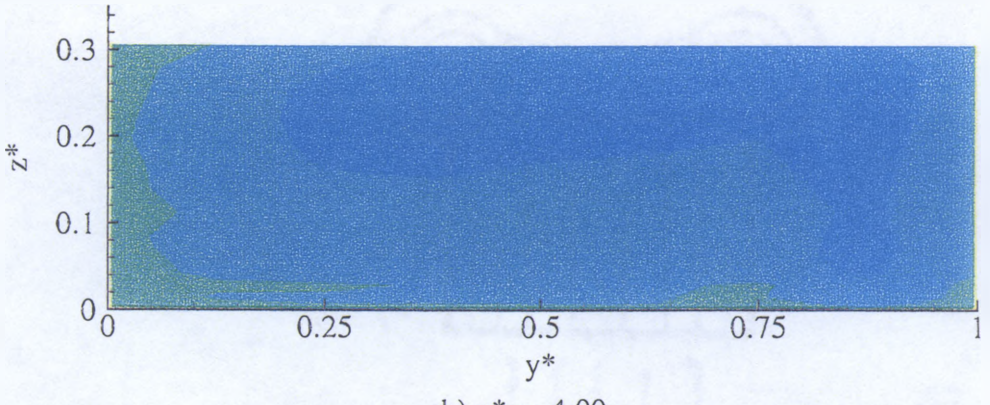

h) x* = -4.00

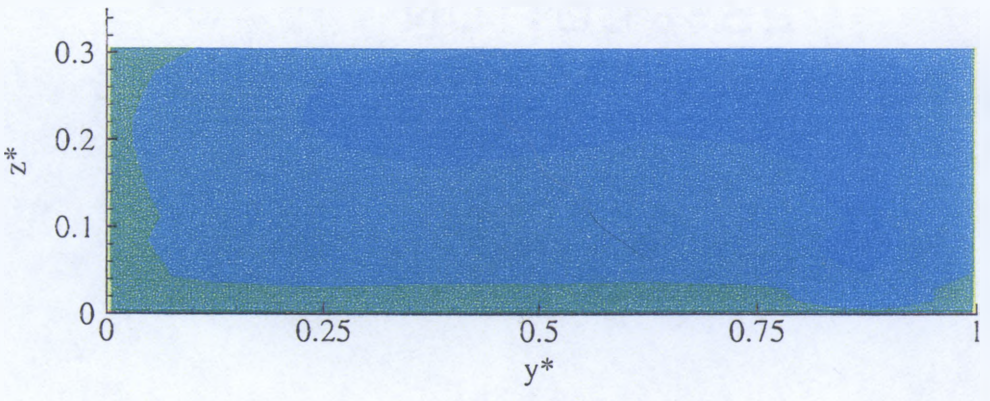

i) x* = -5.00

Figure B.2. Continued

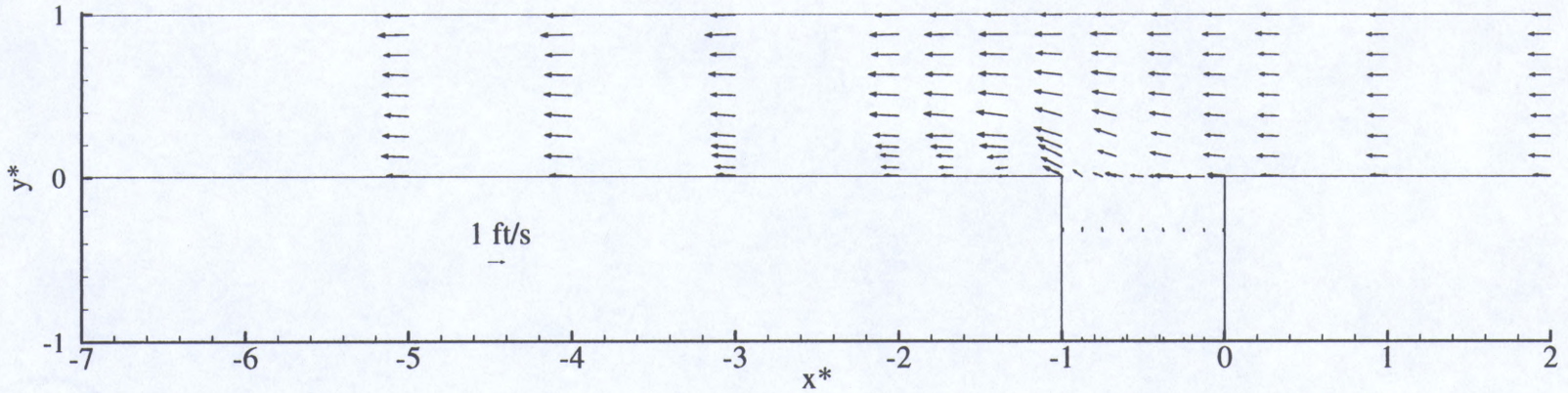

a) z* = 0.014

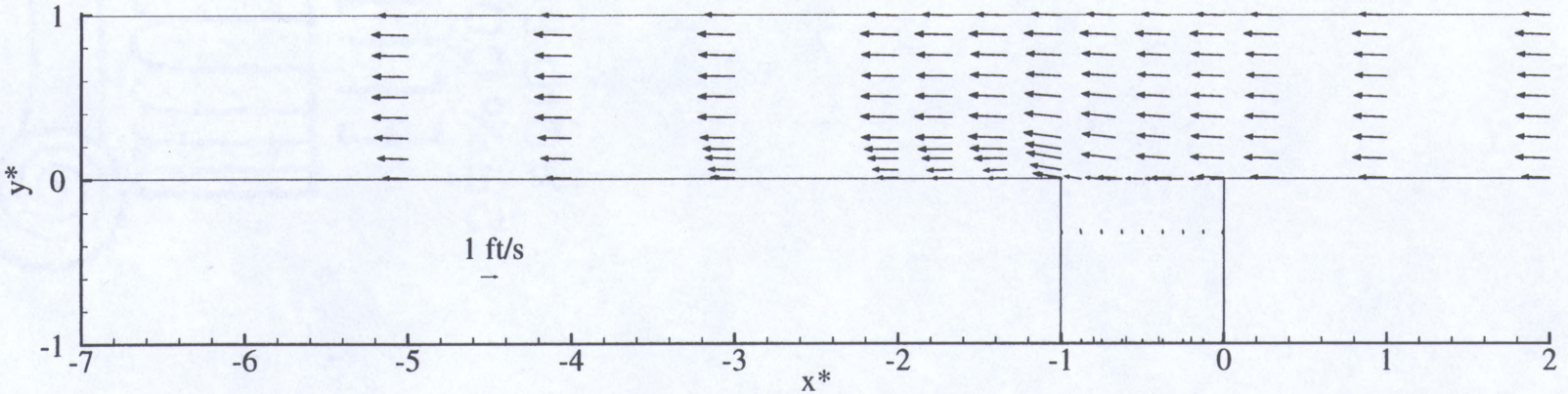

b) z* = 0.278

Figure B.3. u-v Vector Fields, q* = 0.917

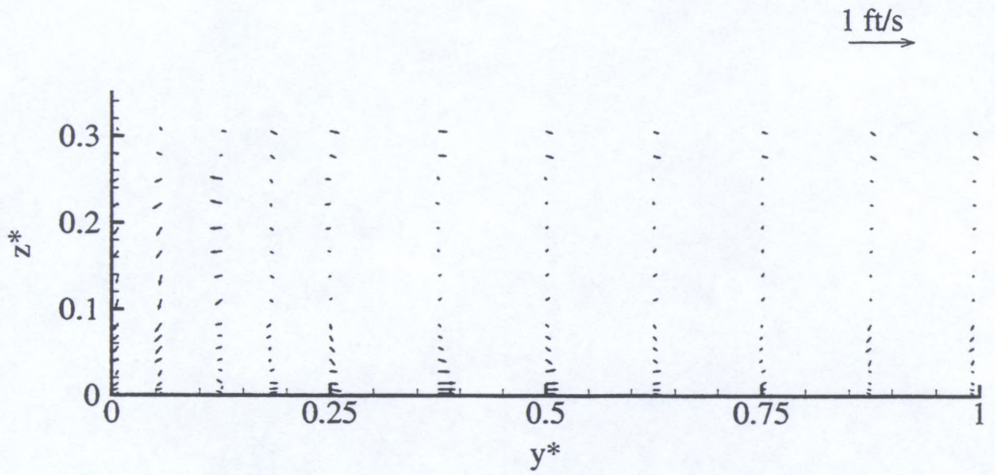

a) x* = -1.33

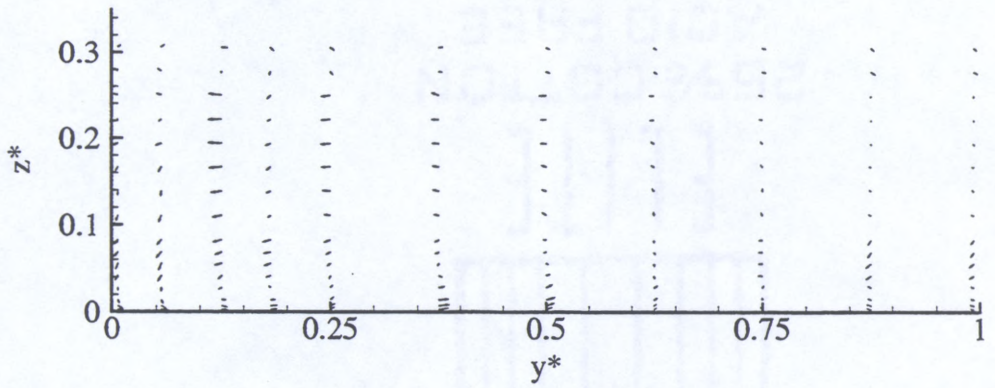

b) x* = -1.67

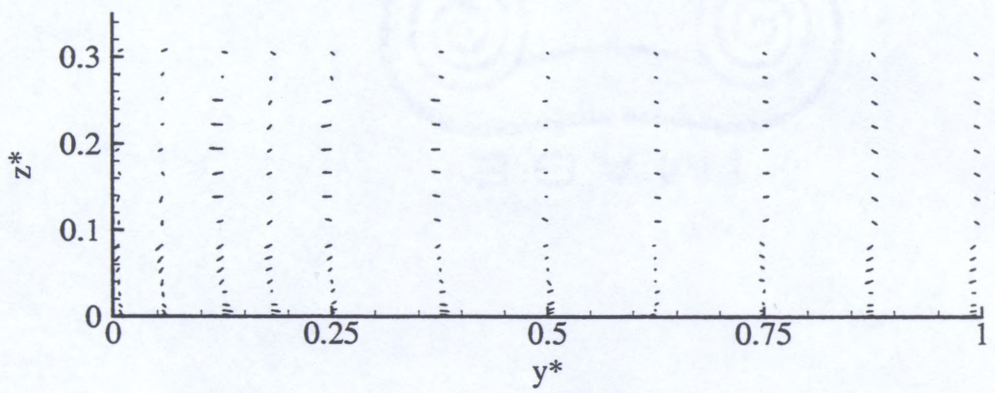

c) x* = -2.00

Figure B.4. v-w Vector Fields, q* = 0.917

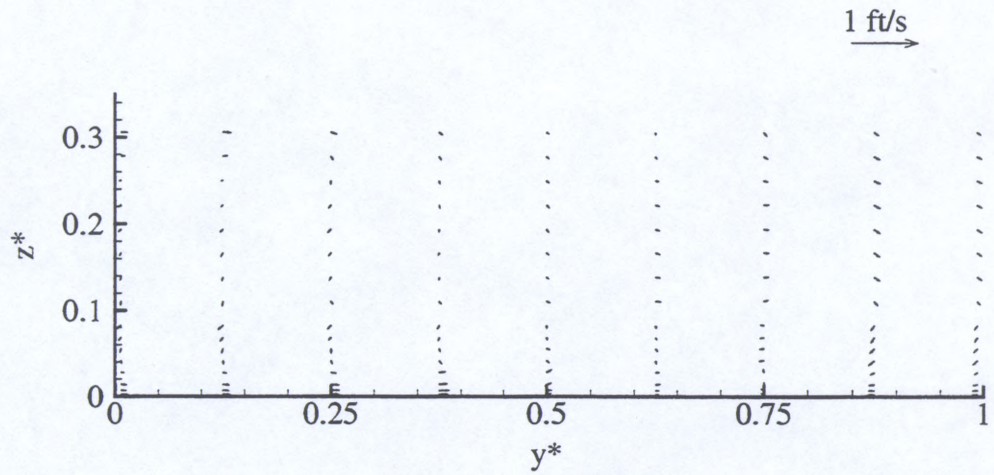

d) x* = -3.00

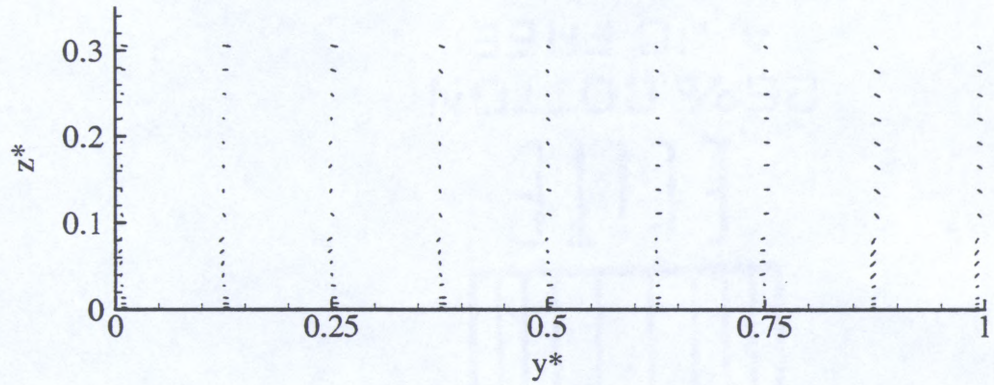

e) x* = -5.00

Figure B.4. Continued

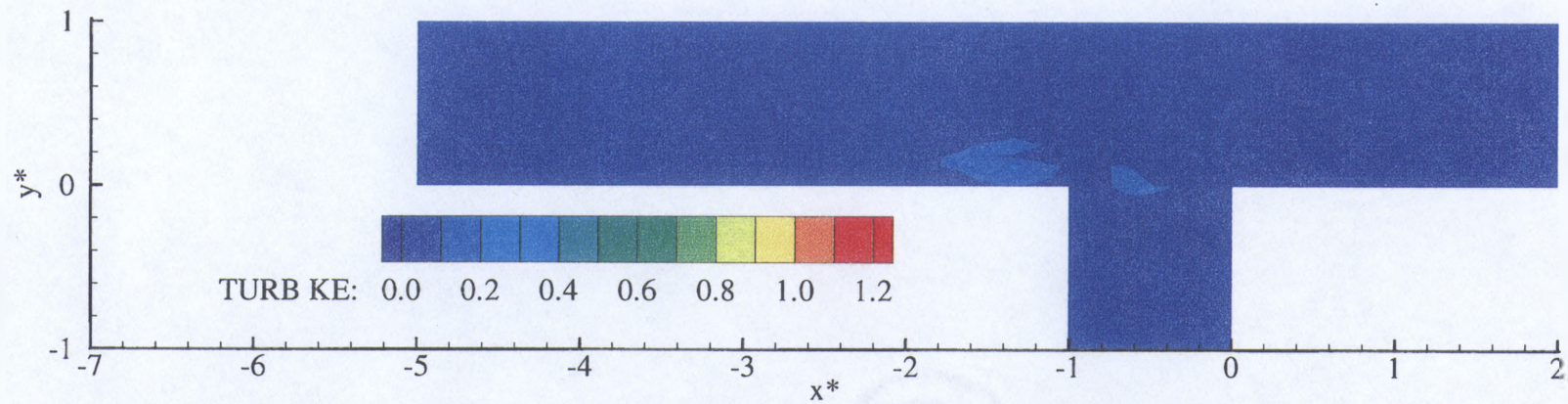

a) z* = 0.014

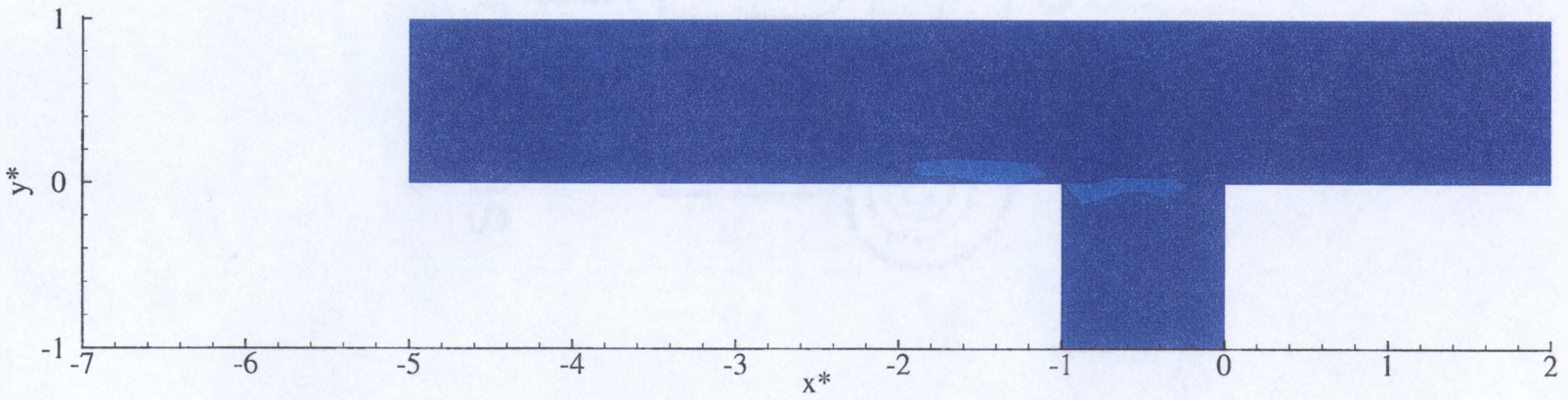

b) z* = 0.278

Figure B.5. Turbulent Kinetic Energy Plan View, q* = 0.917

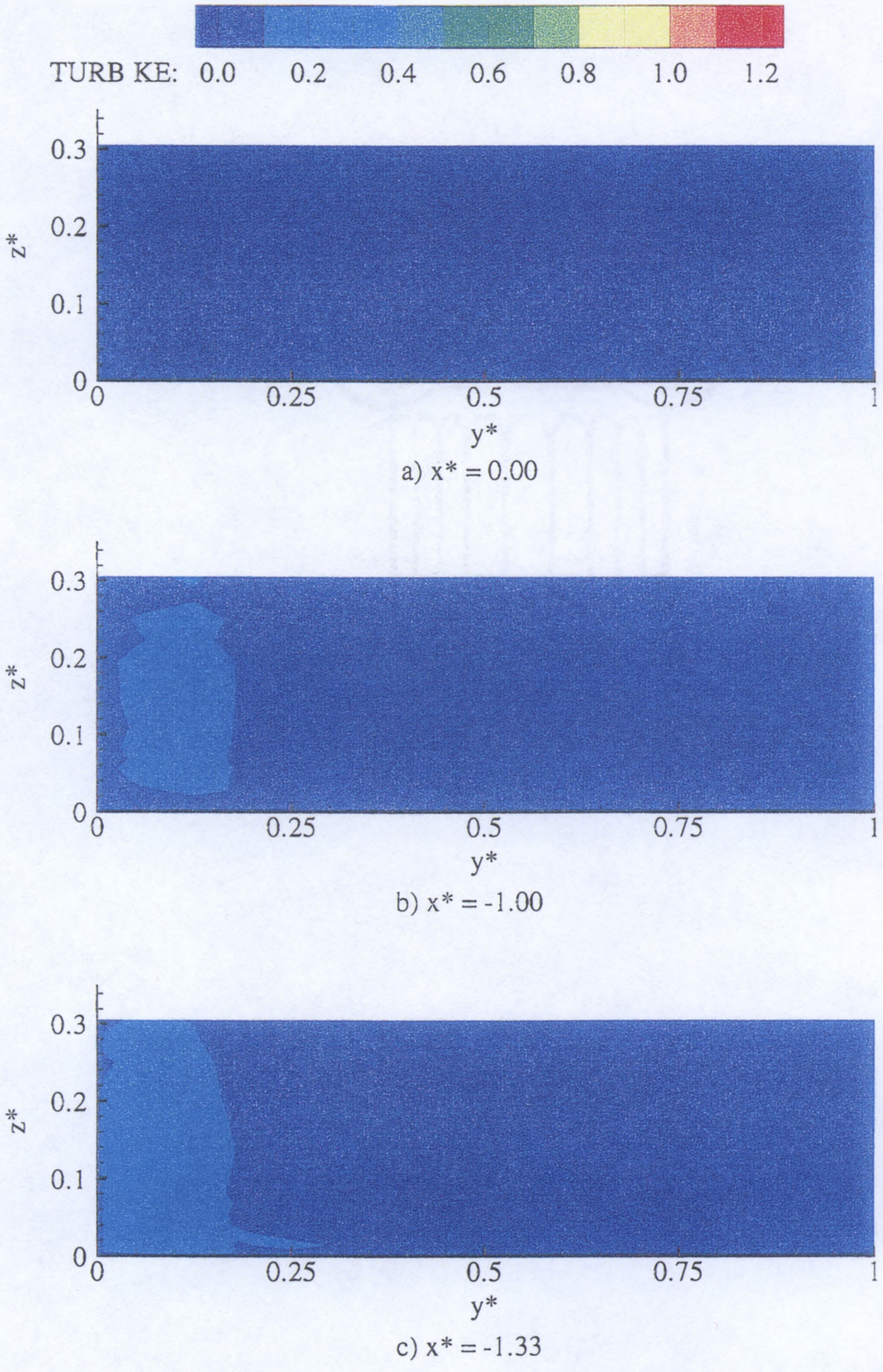

Figure B.6. Turbulent Kinetic Energy Cross-Sections, q* = 0.917

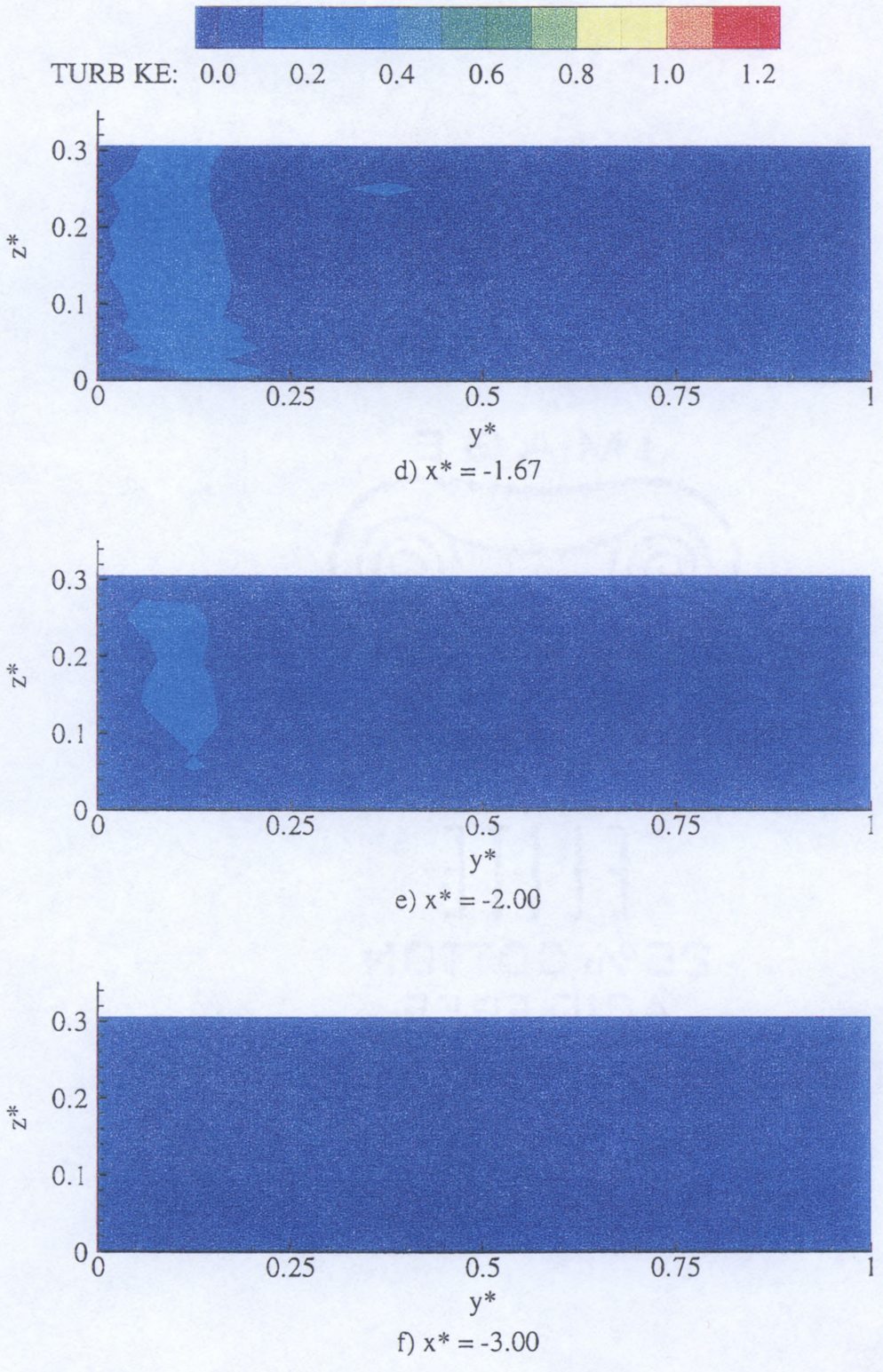

Figure B.6. Continued

APPENDIX C

DATA PLOTS FOR q* = 0.750

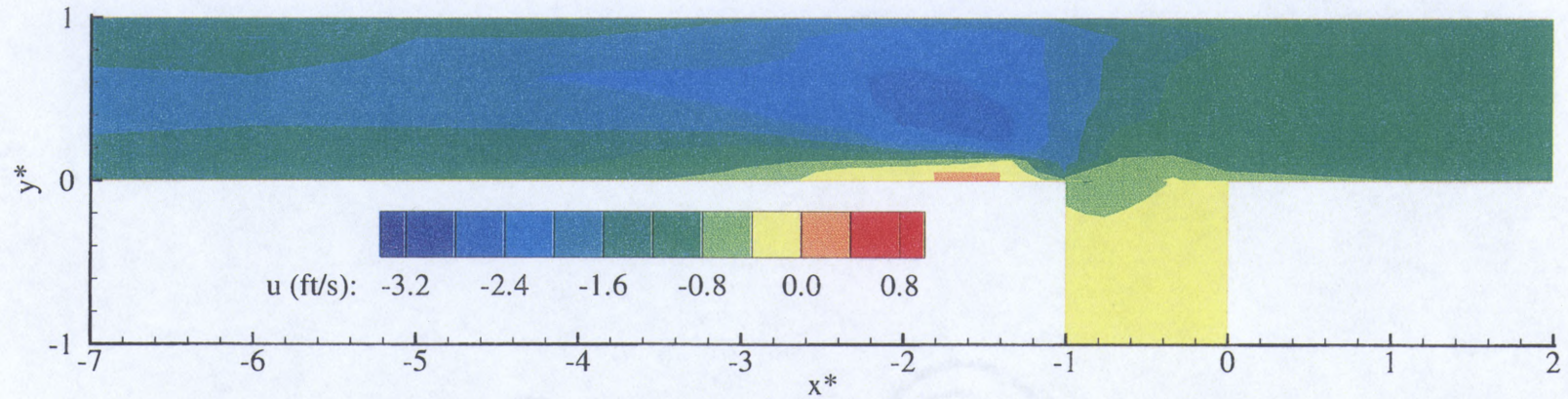

a) z* = 0.014

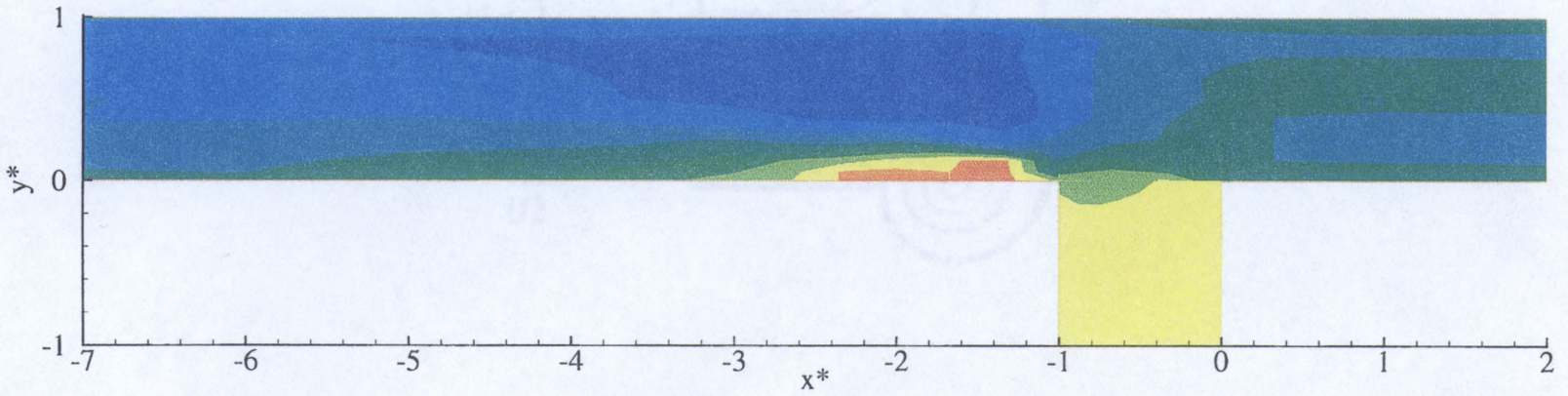

b) z* = 0.278

Figure C.1. u Velocity Plan View, q* = 0.750

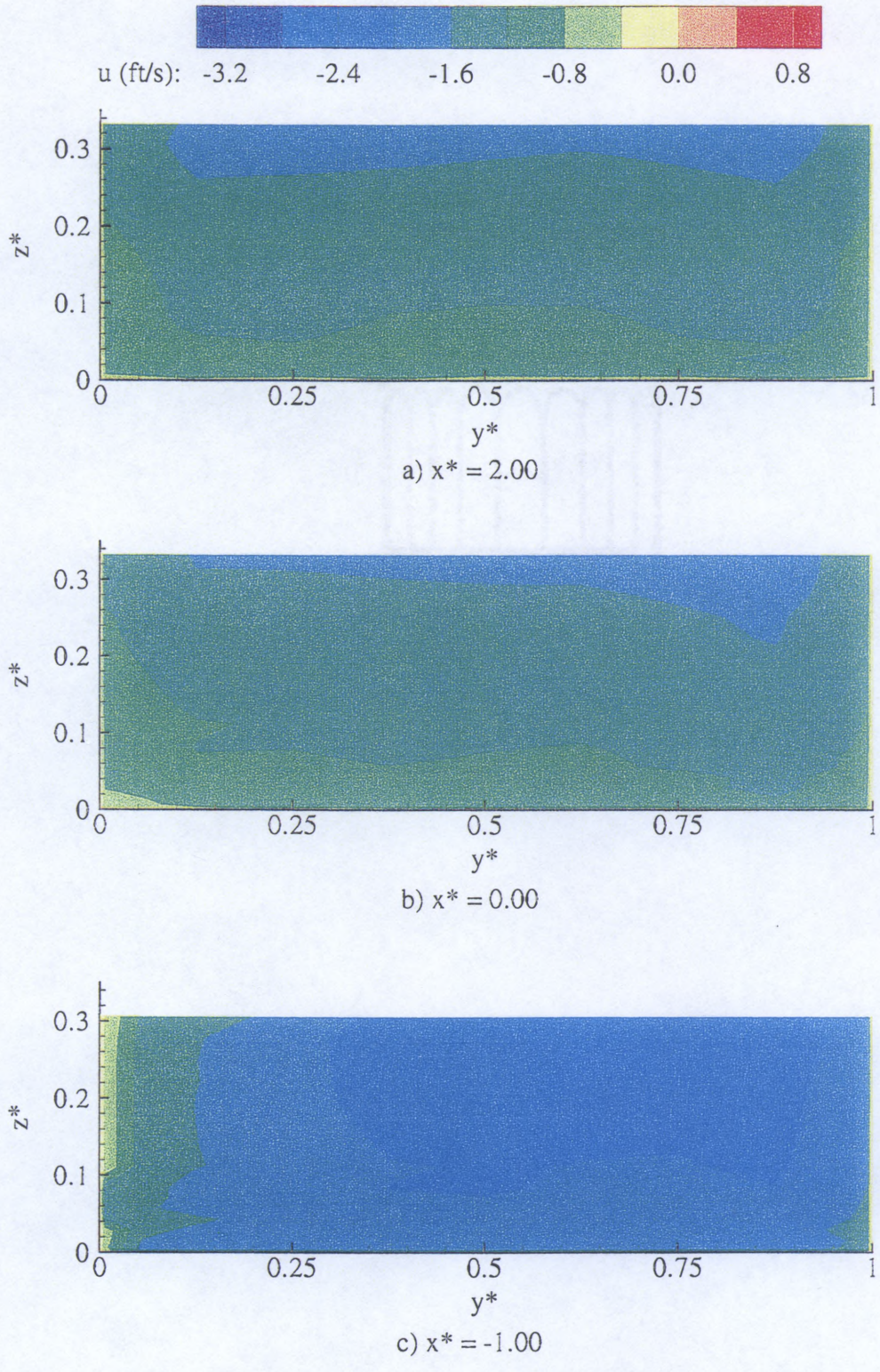

Figure C.2. u Velocity Cross-Sections, q* = 0.750

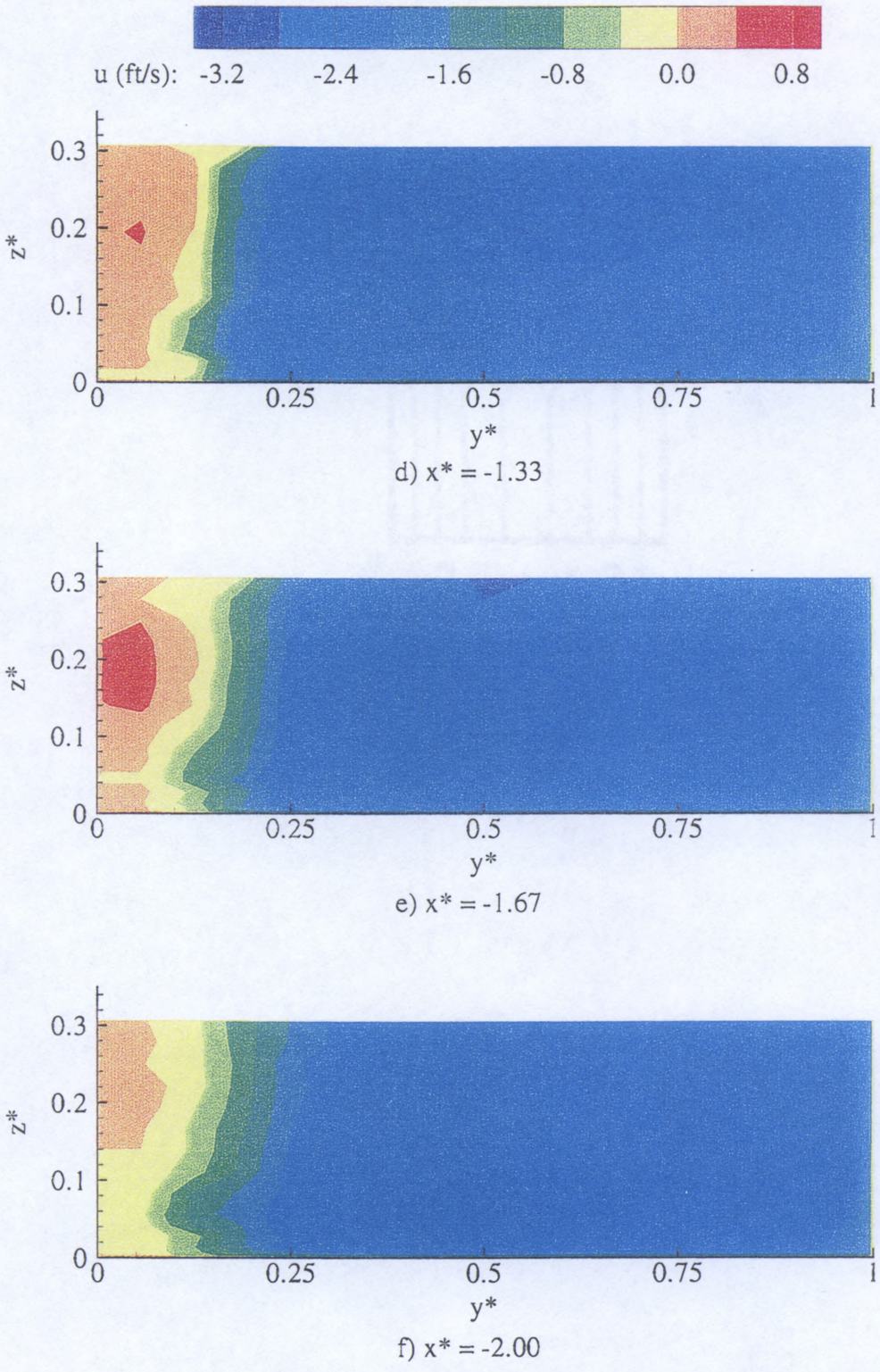

Figure C.2. Continued

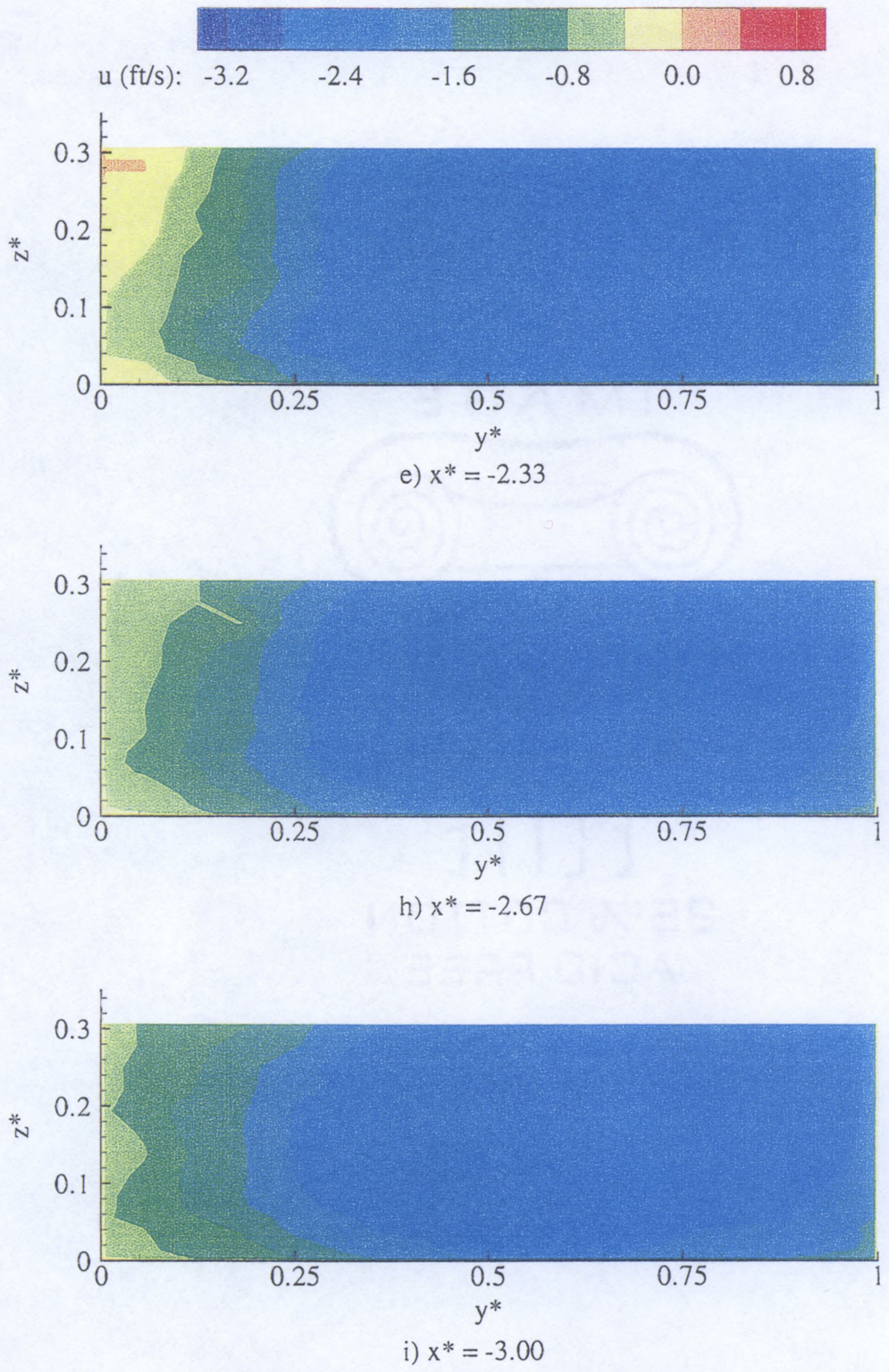

Figure C.2. Continued

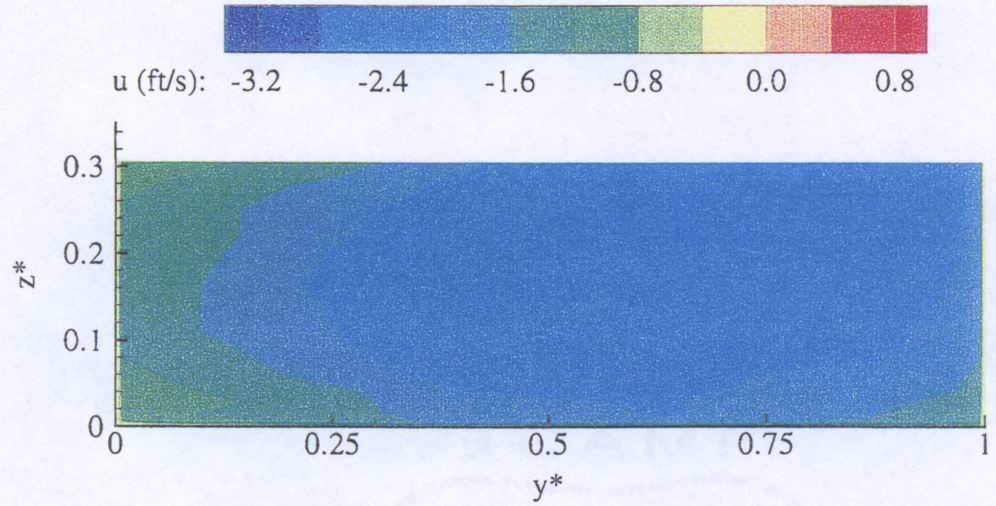

j) x* = -4.00

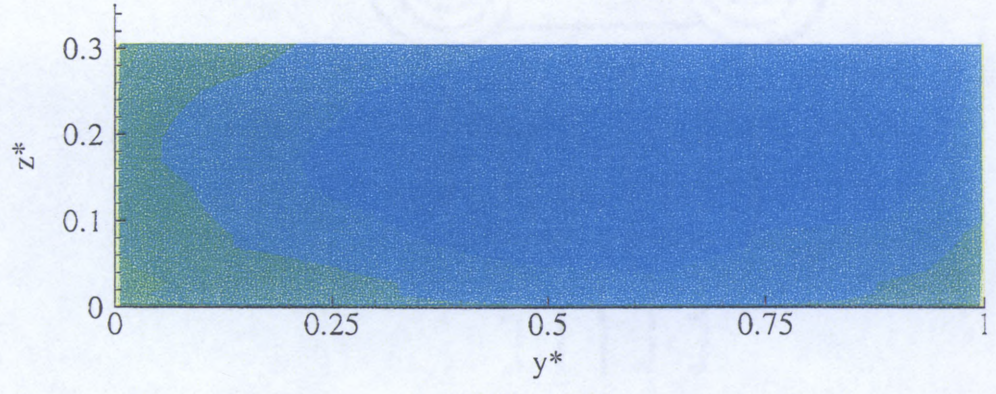

k) x* = -5.00

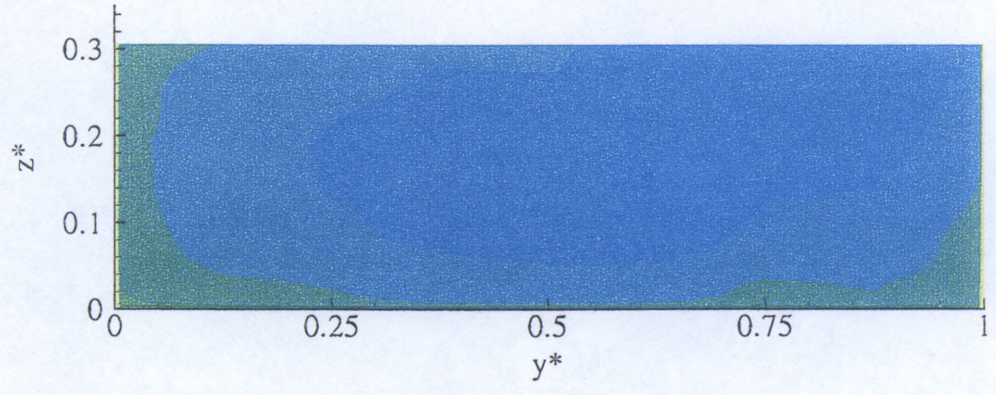

l) x* = -7.00

Figure C.2. Continued

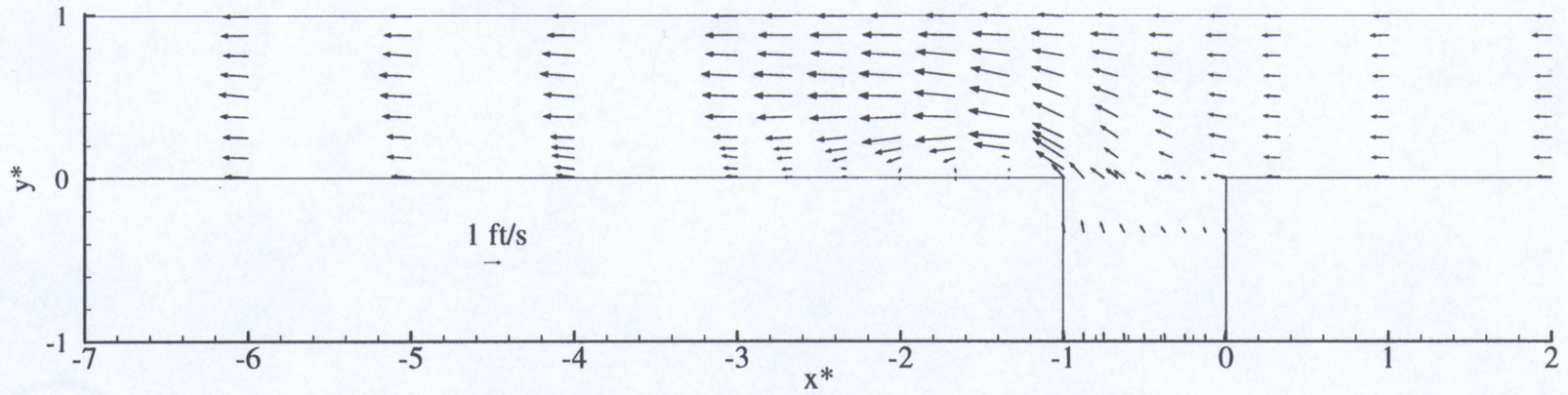

a) z* = 0.014

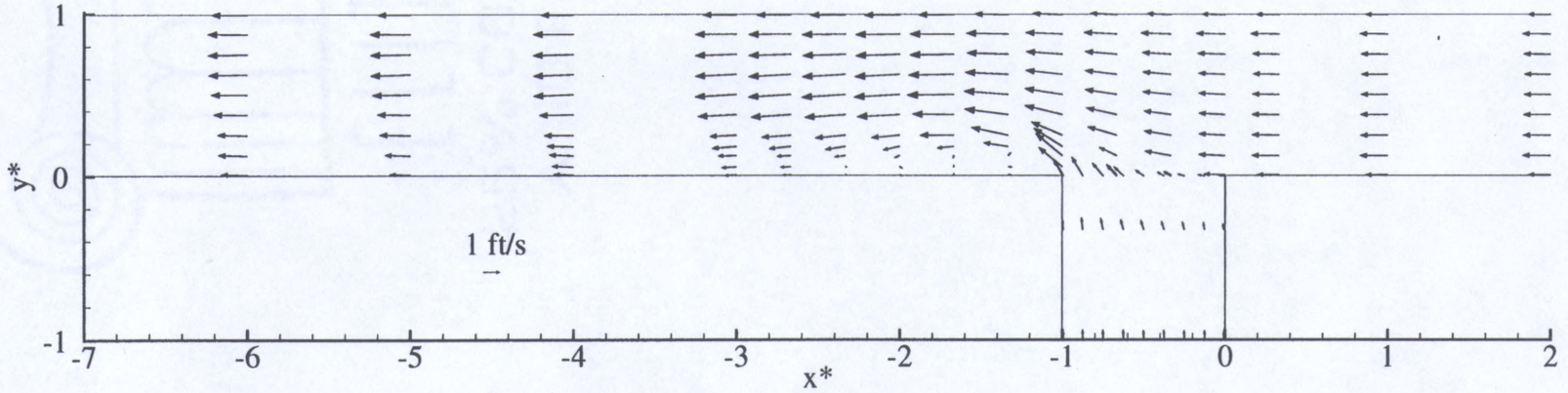

b) z* = 0.278

Figure C.3. u-v Vector Fields, q* = 0.750

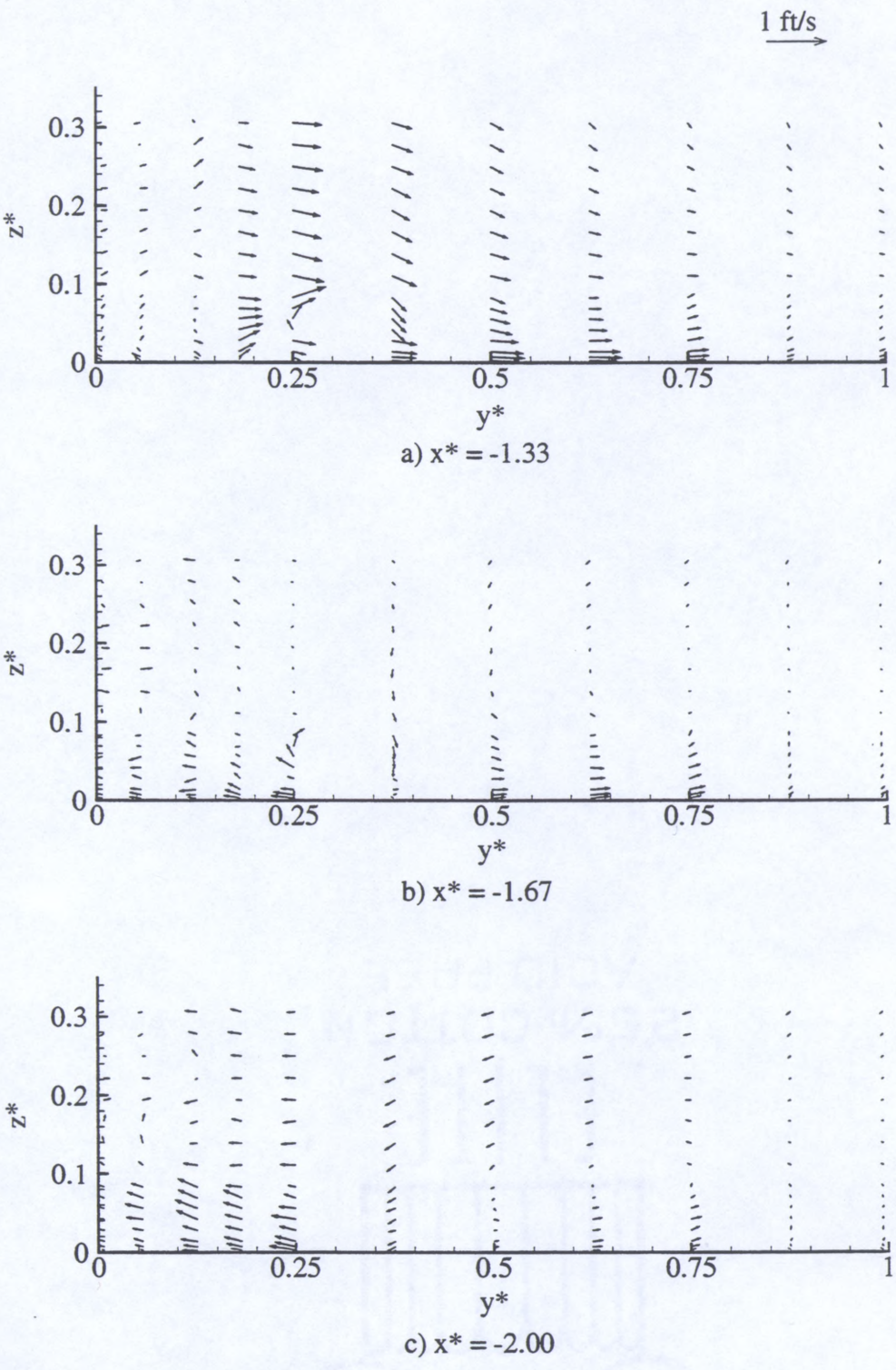

Figure C.4. v-w Vector Fields, q* = 0.750

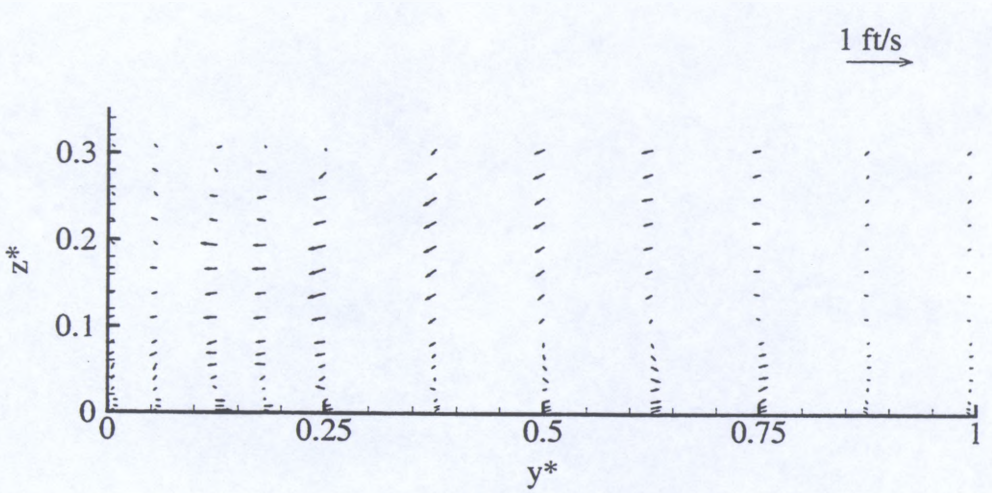

d) x* = -3.00

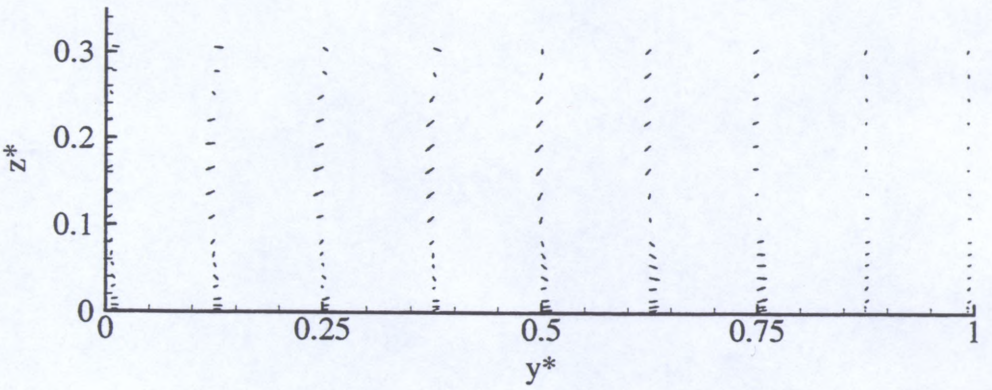

e) x* = -5.00

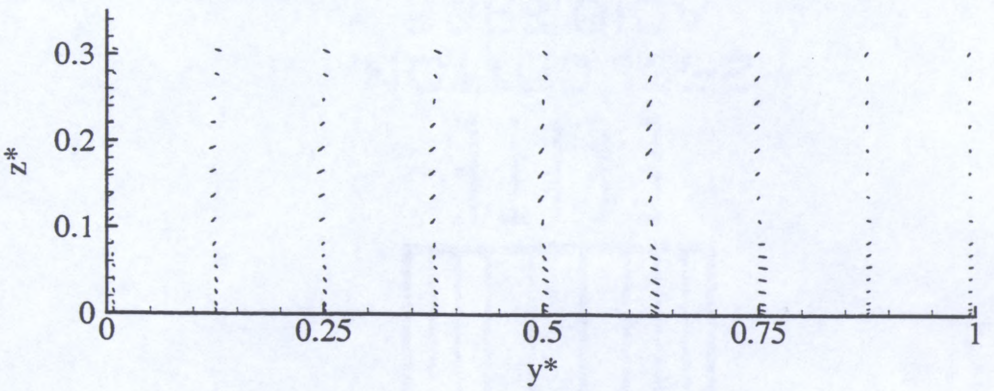

f) x* = -7.00

Figure C.4. Continued

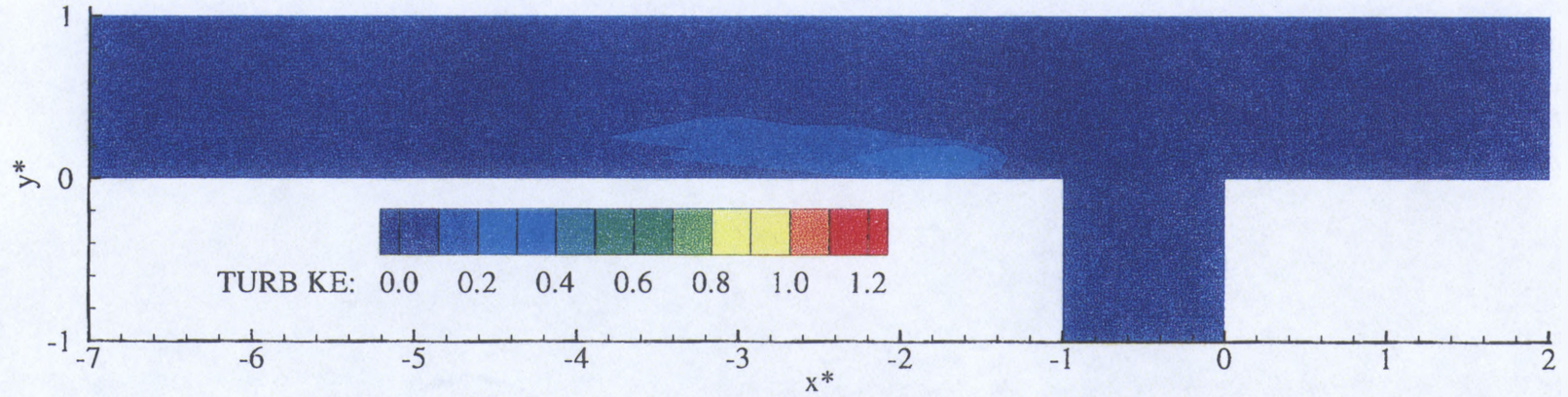

a) z* = 0.014

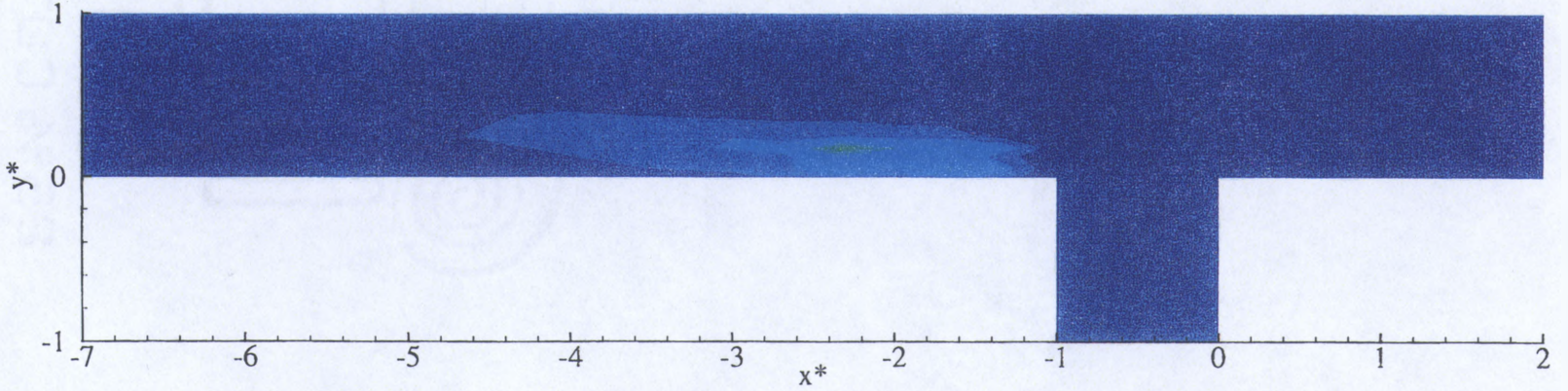

b) z* = 0.278

Figure C.5. Turbulent Kinetic Energy Plan View, q* = 0.750

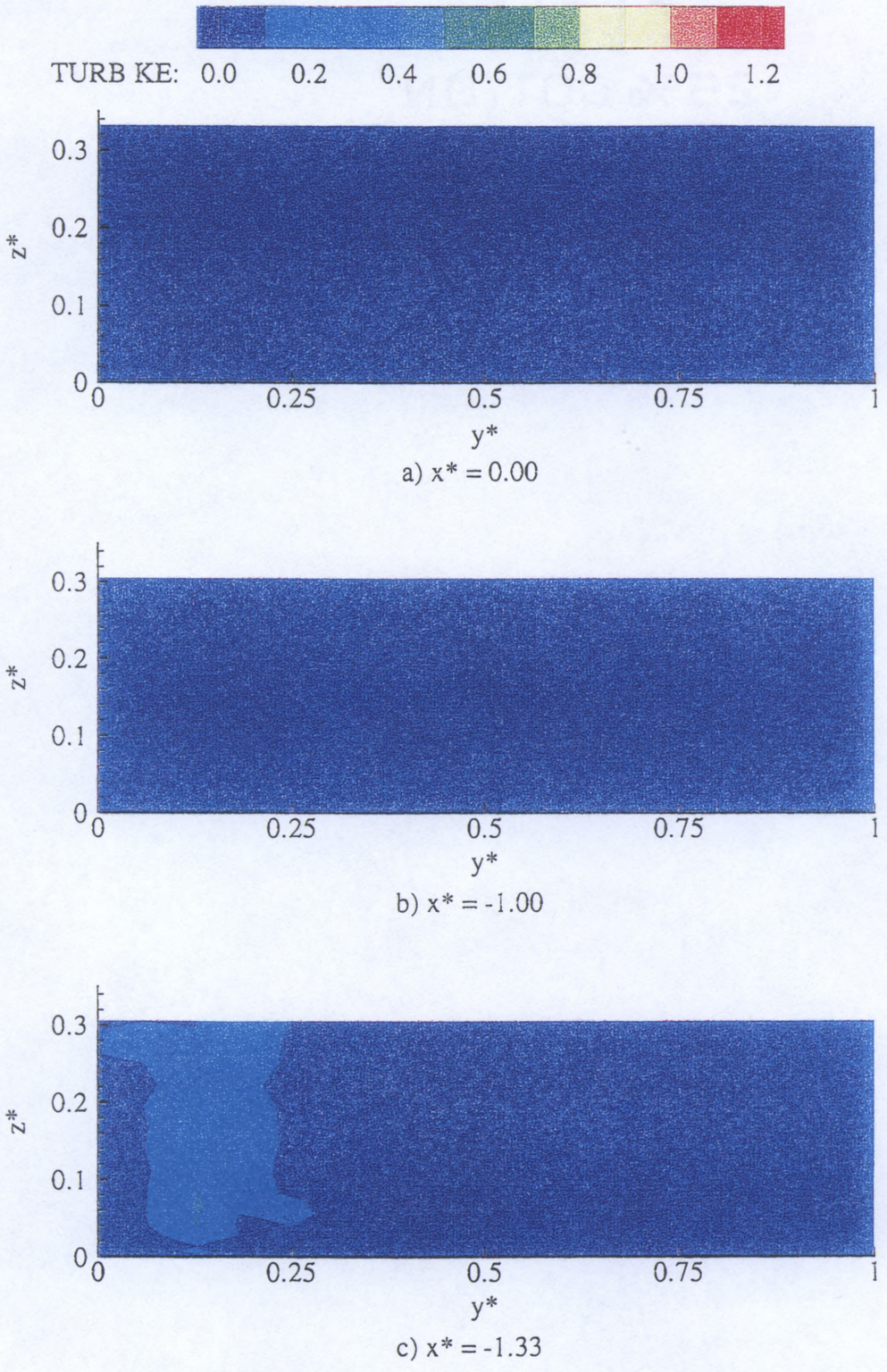

Figure C.6. Turbulent Kinetic Energy Cross-Sections, q* = 0.750

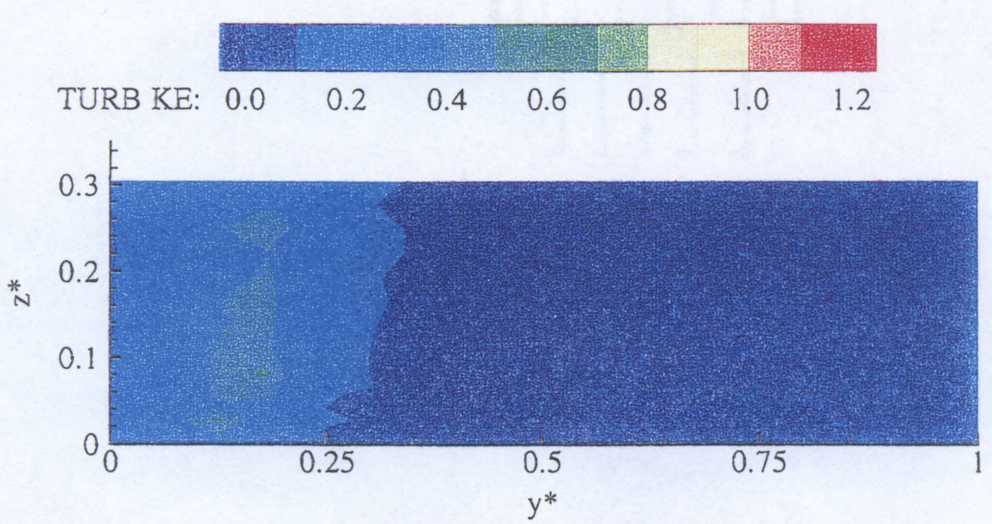

d) x* = -1.67

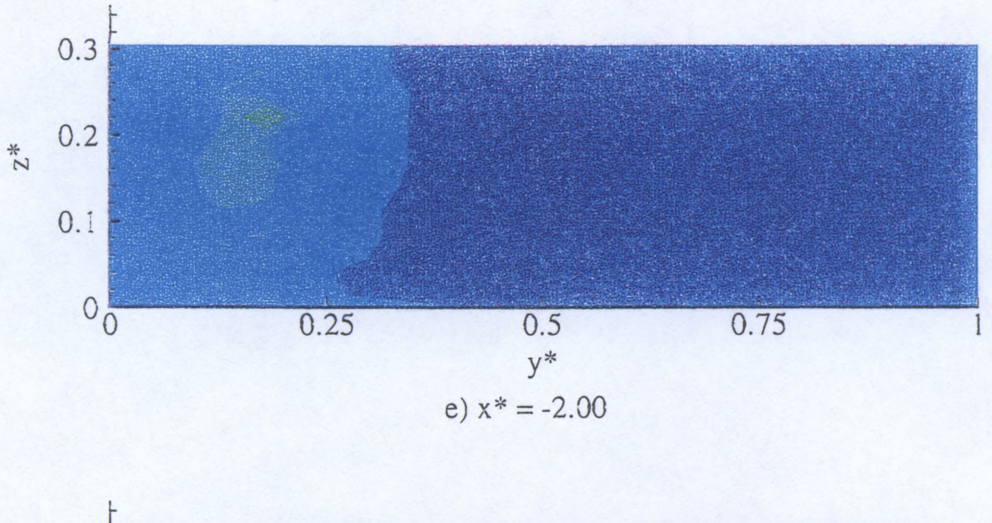

e) x* = -2.00

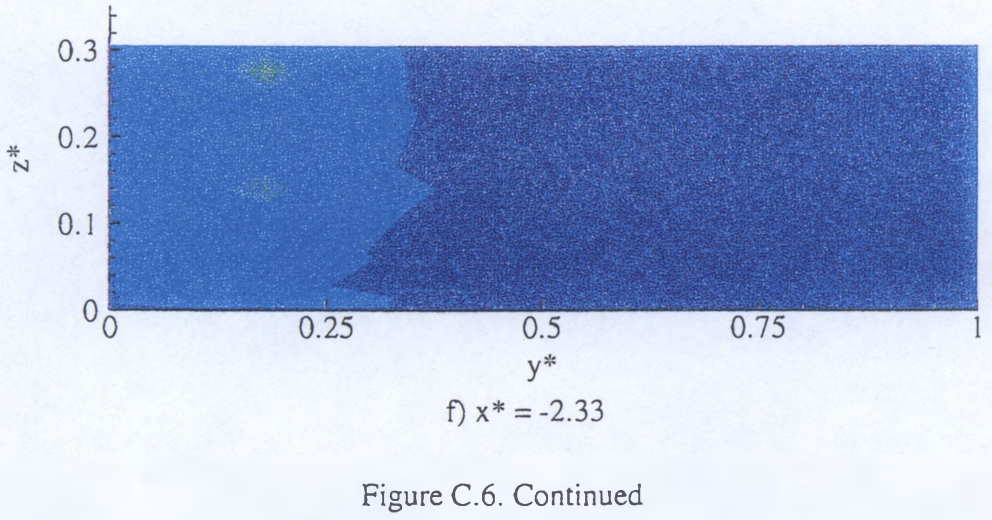

f) x* = -2.33

Figure C.6. Continued

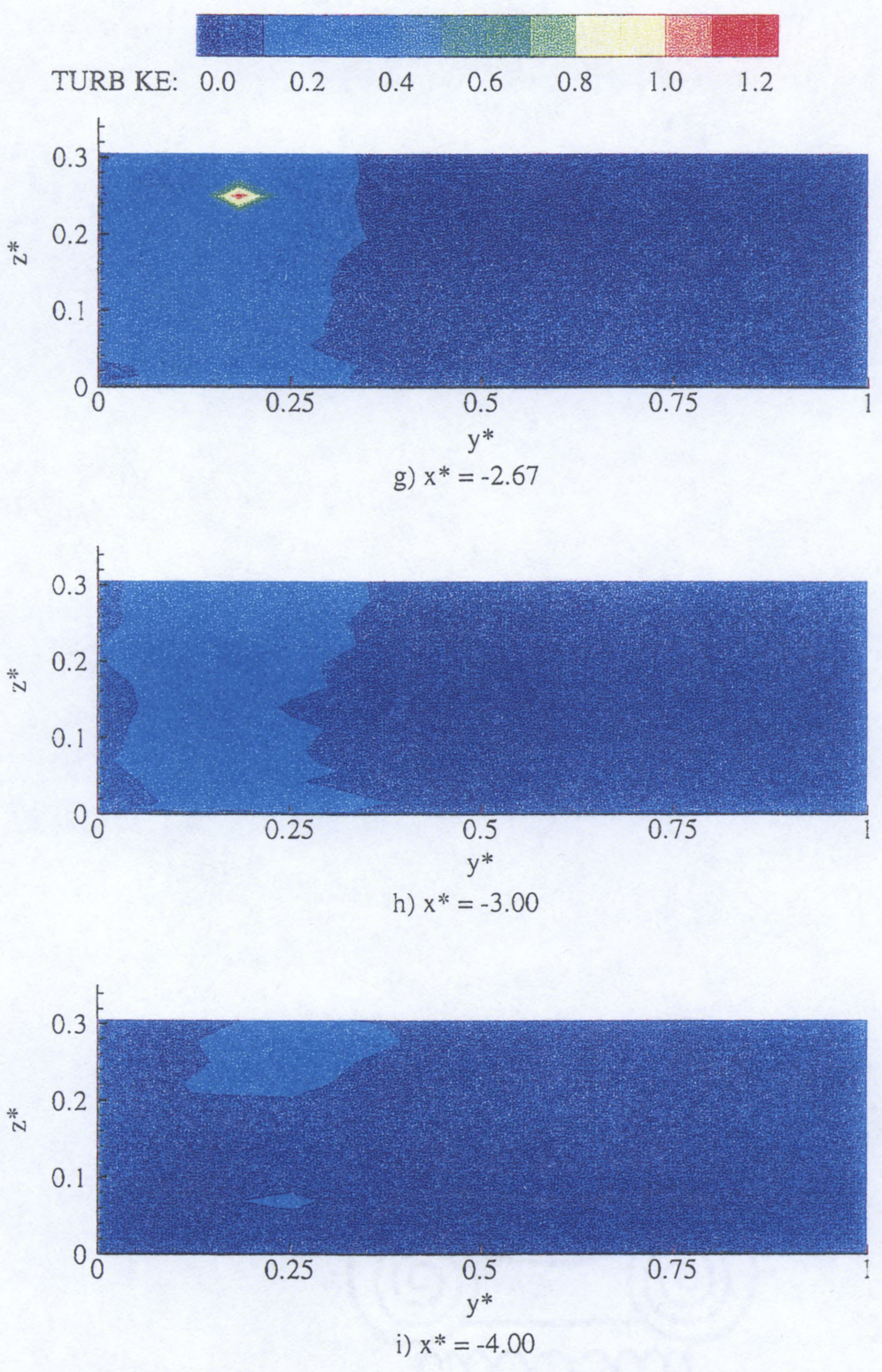

Figure C.6. Continued

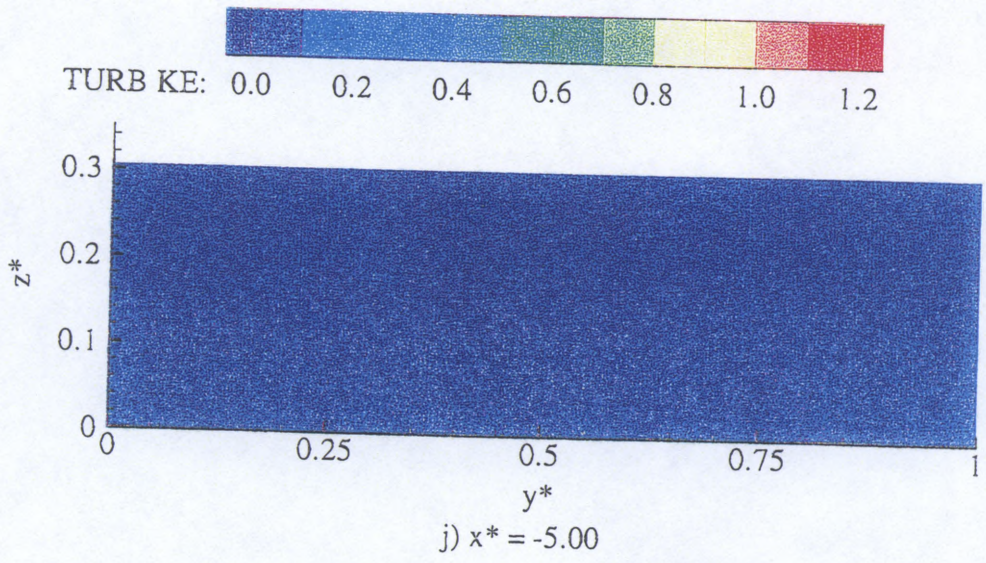

Figure C.6. Continued

APPENDIX D

DATA PLOTS FOR $q^* = 0.583$

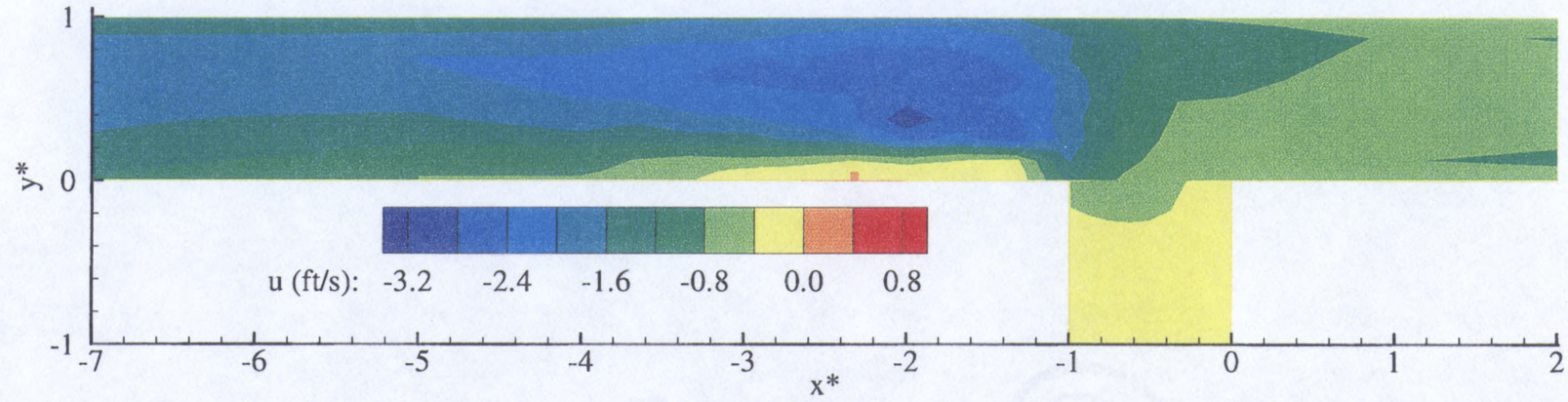

a) z* = 0.014

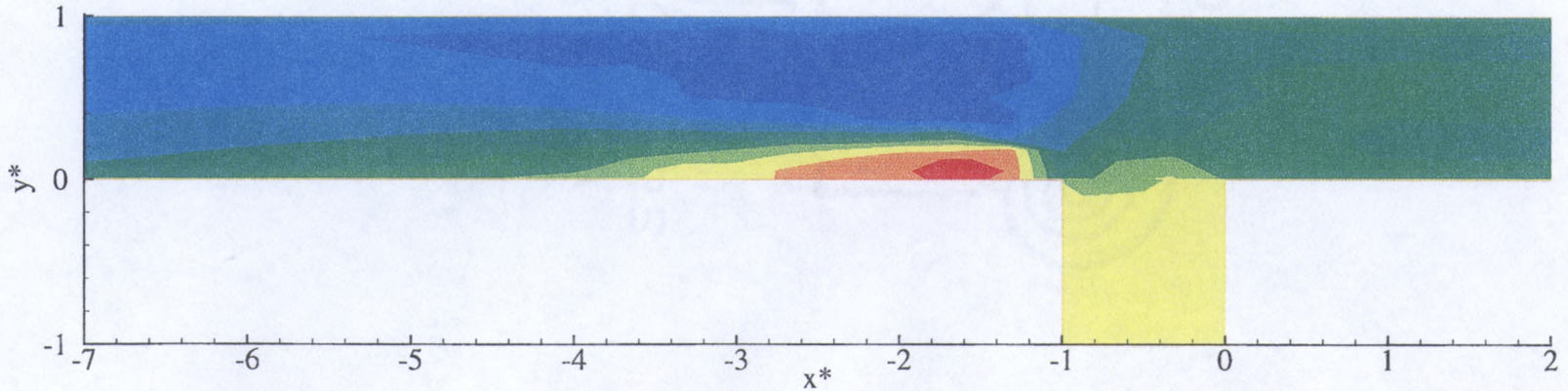

b) z* = 0.278

Figure D.1. u Velocity Plan View, q* = 0.583

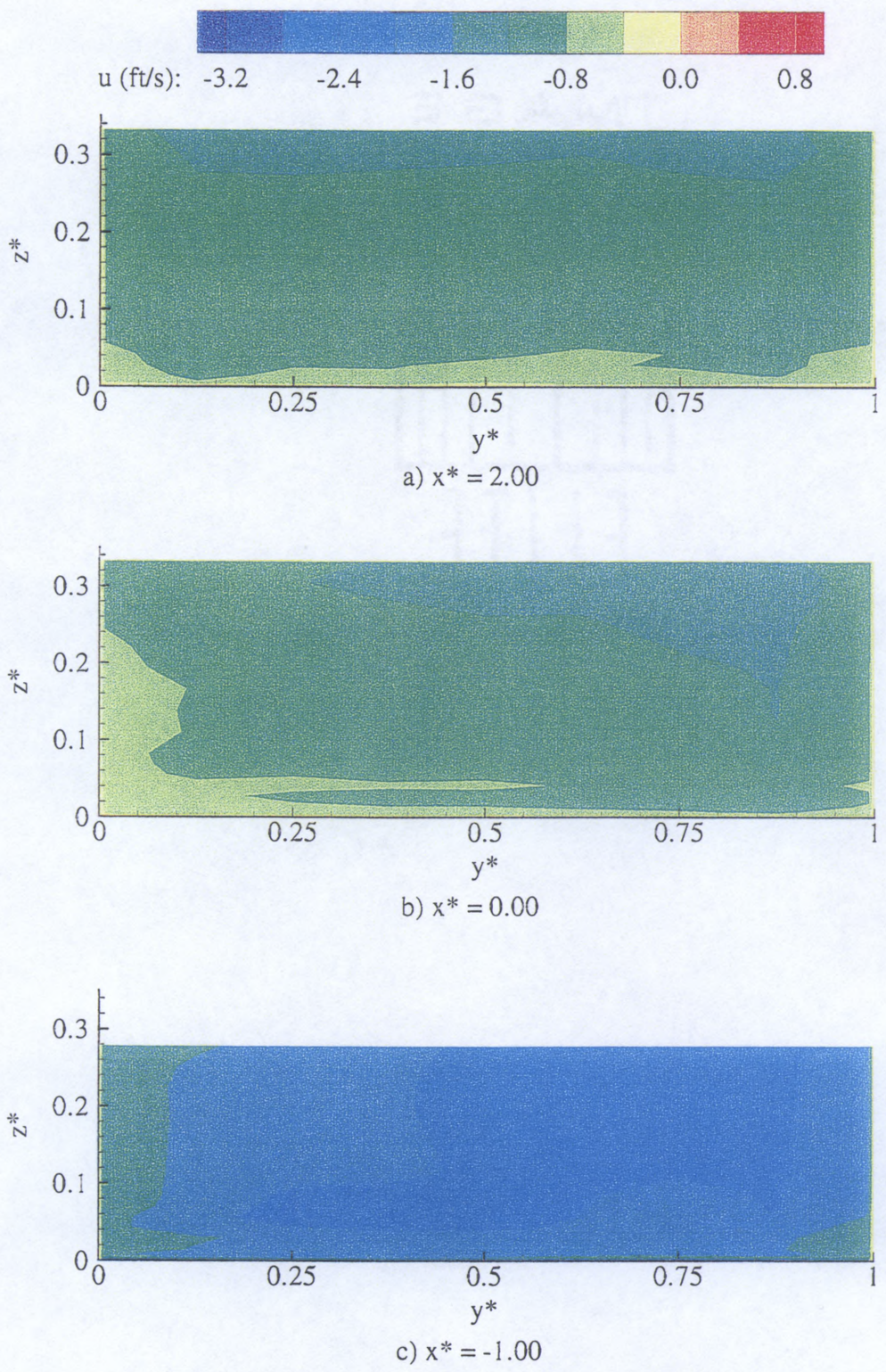

Figure D.2. u Velocity Cross-Sections, q* = 0.583

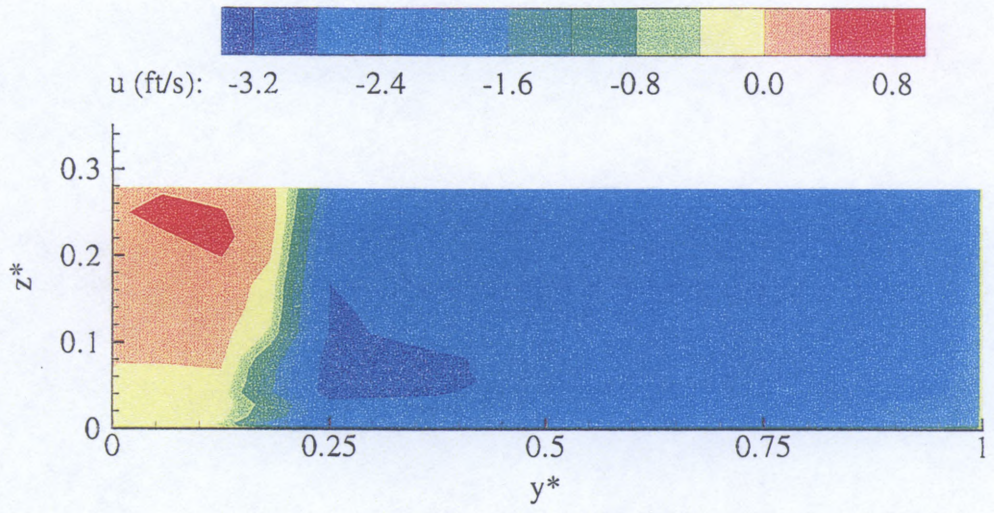

d) x* = -1.33

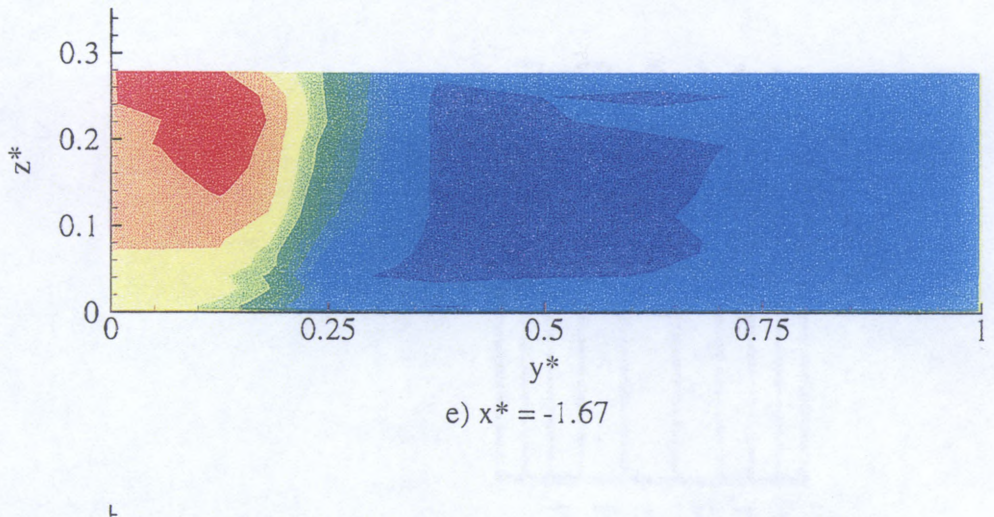

e) x* = -1.67

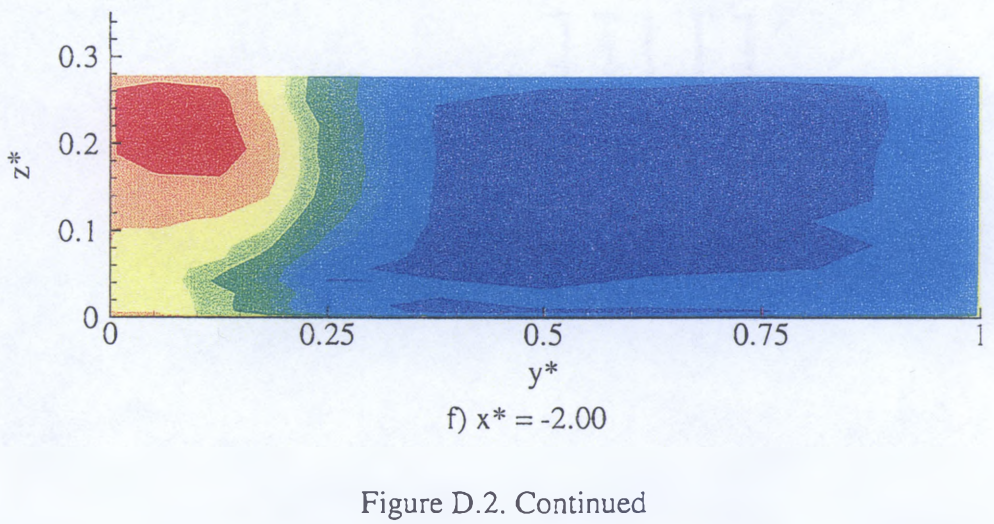

f) x* = -2.00

Figure D.2. Continued

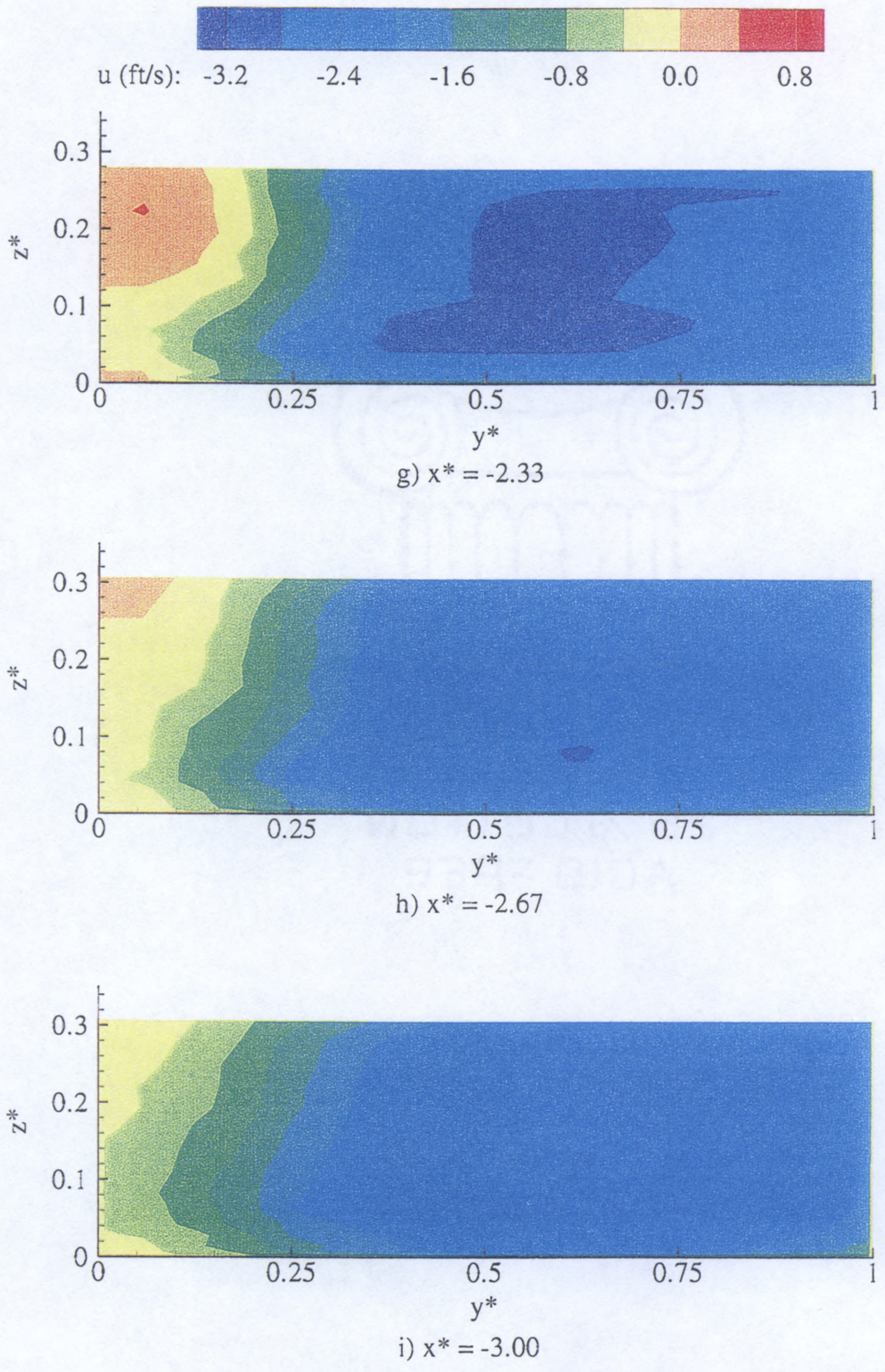

Figure D.2. Continued

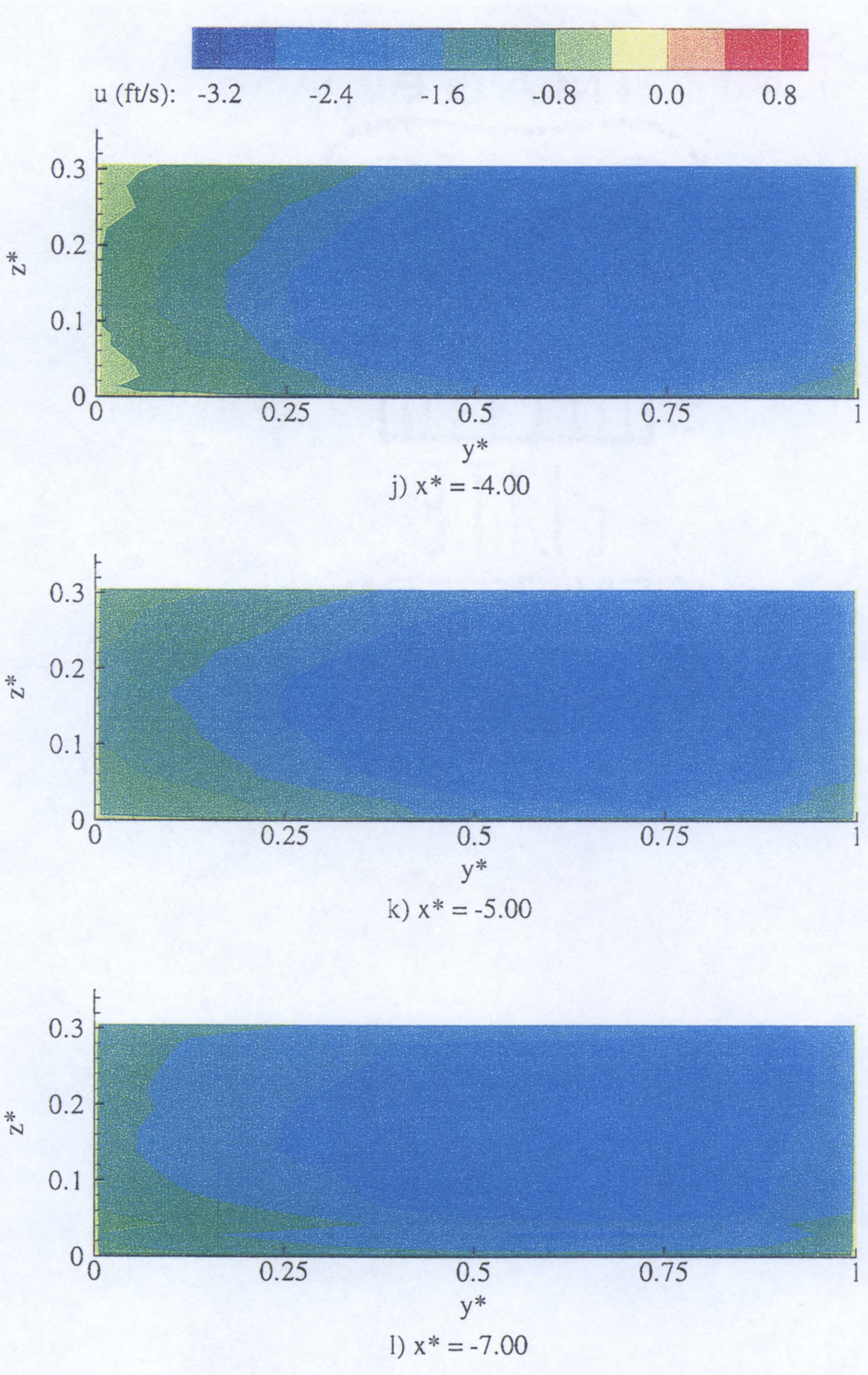

Figure D.2. Continued

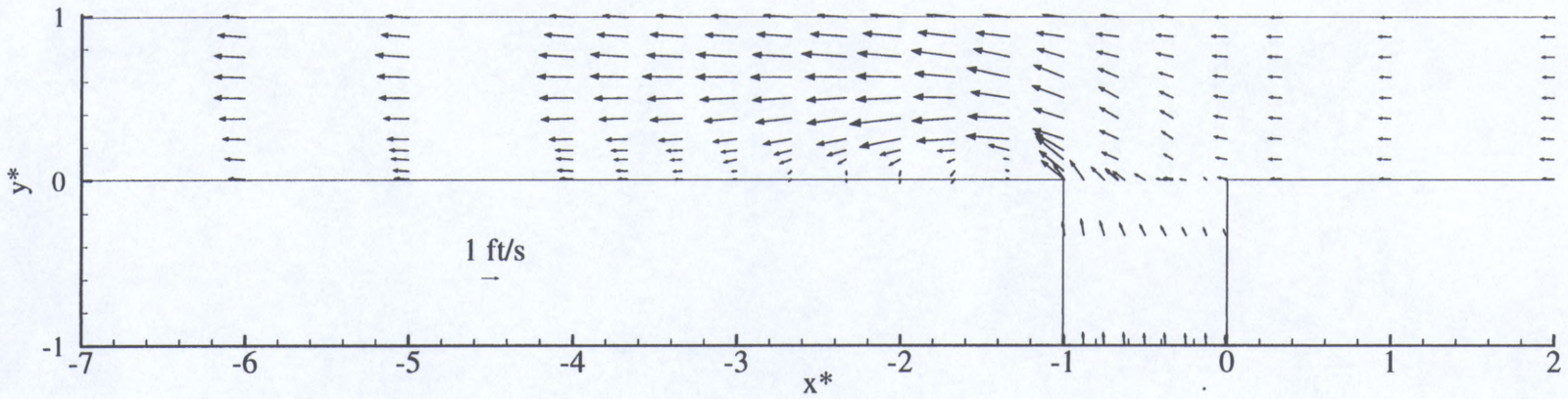

a) z* = 0.014

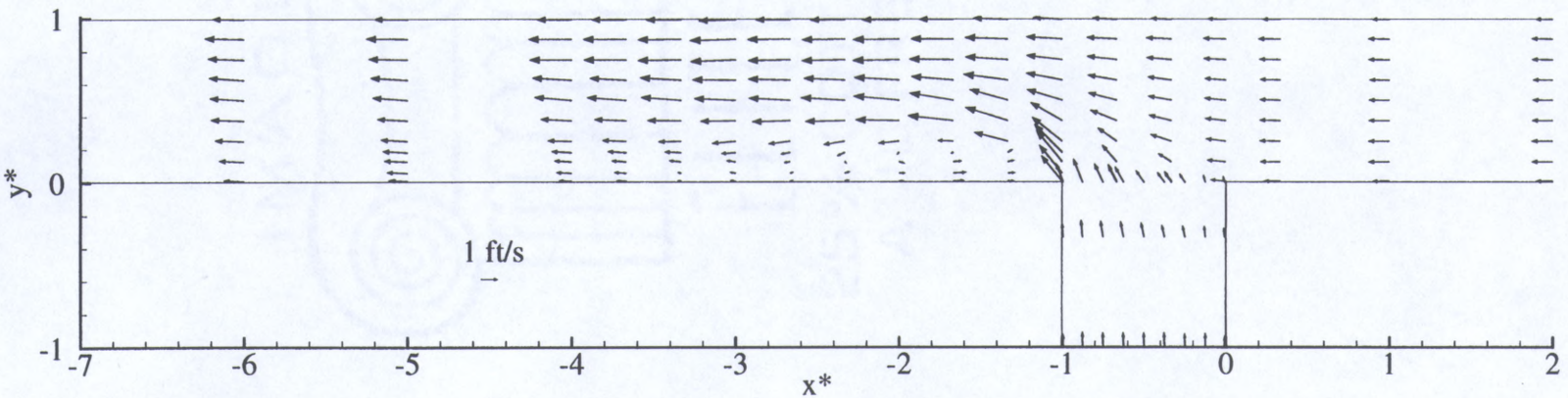

b) z* = 0.278

Figure D.3. u-v Vector Fields, q* = 0.583

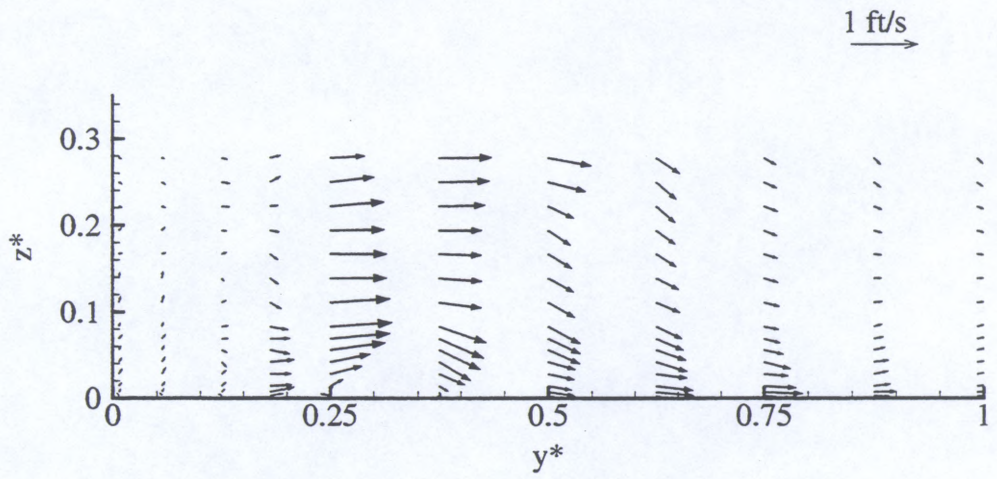

a) x* = -1.33

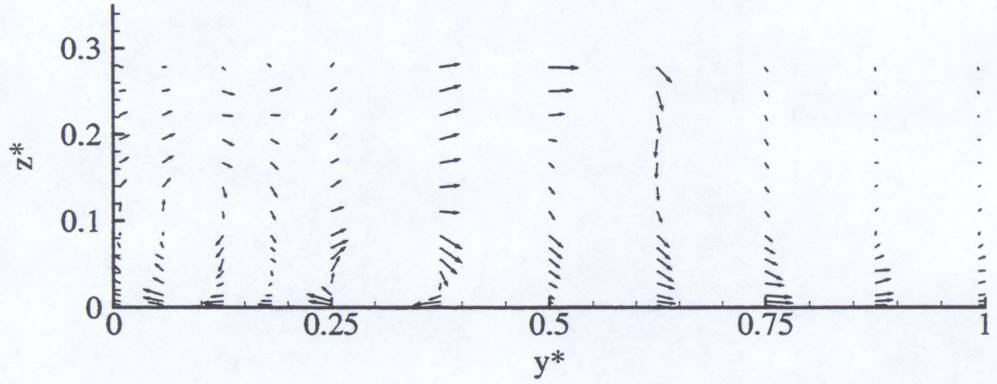

b) x* = -1.67

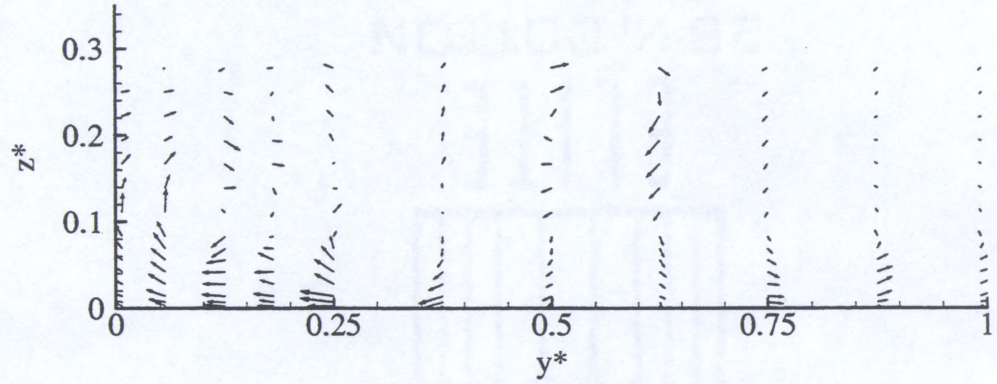

c) x* = -2.00

Figure D.4. v-w Vector Fields, q* = 0.583

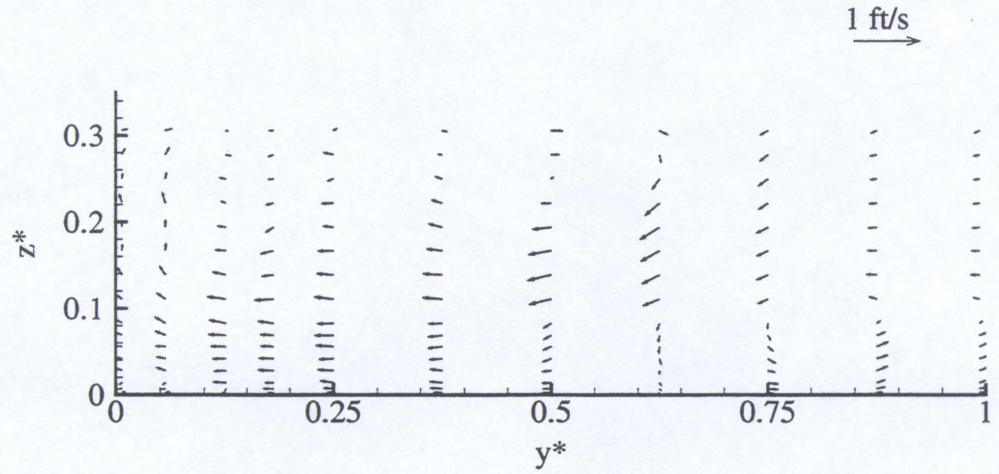

d) x* = -3.00

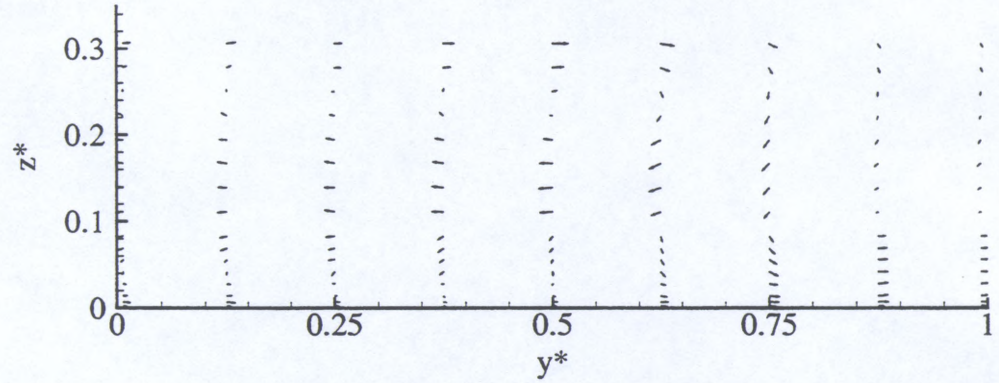

e) x* = -5.00

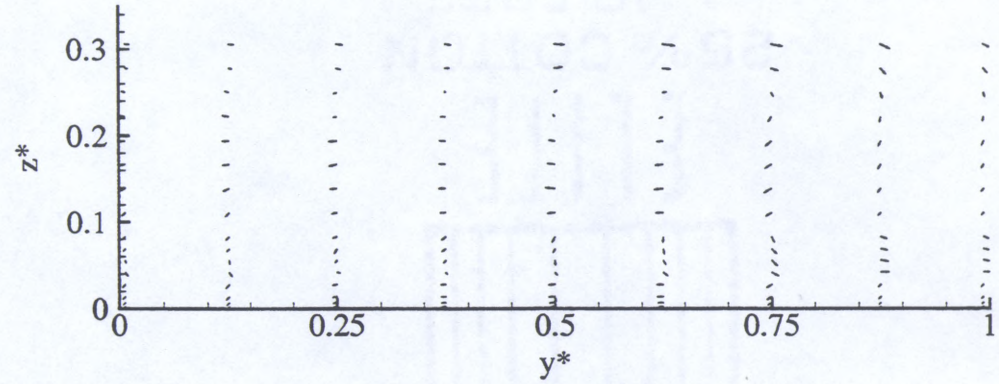

f) x* = -7.00

Figure D.4. Continued

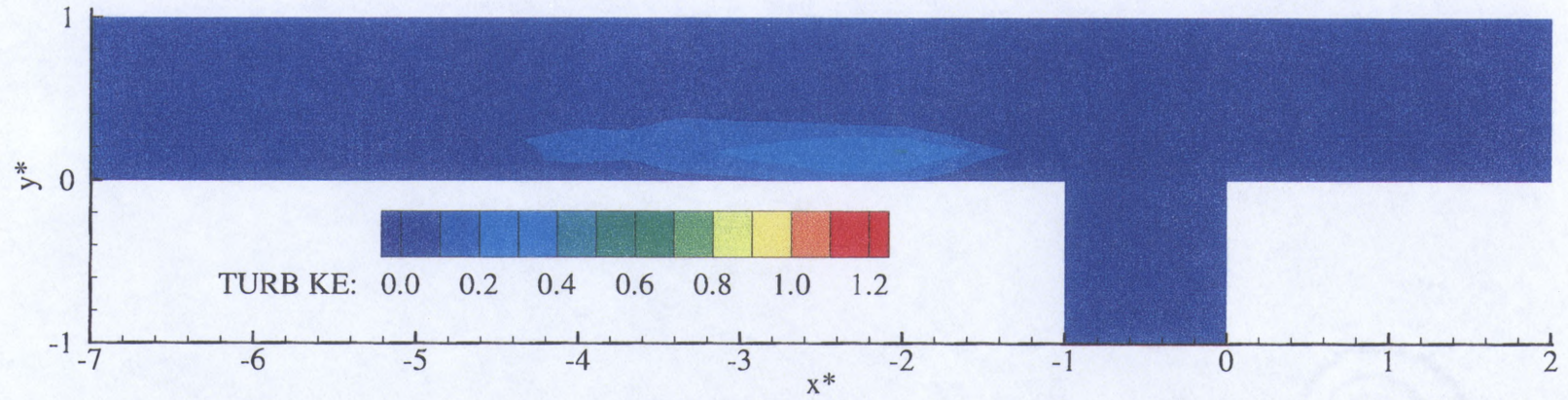

a) z* = 0.014

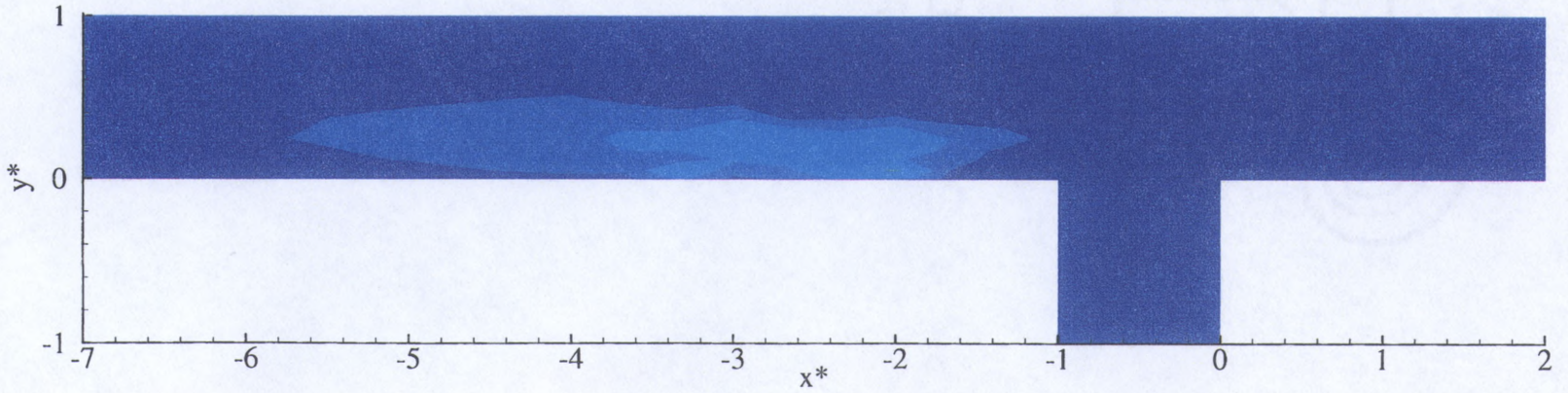

b) z* = 0.278

Figure D.5. Turbulent Kinetic Energy Plan View, q* = 0.583

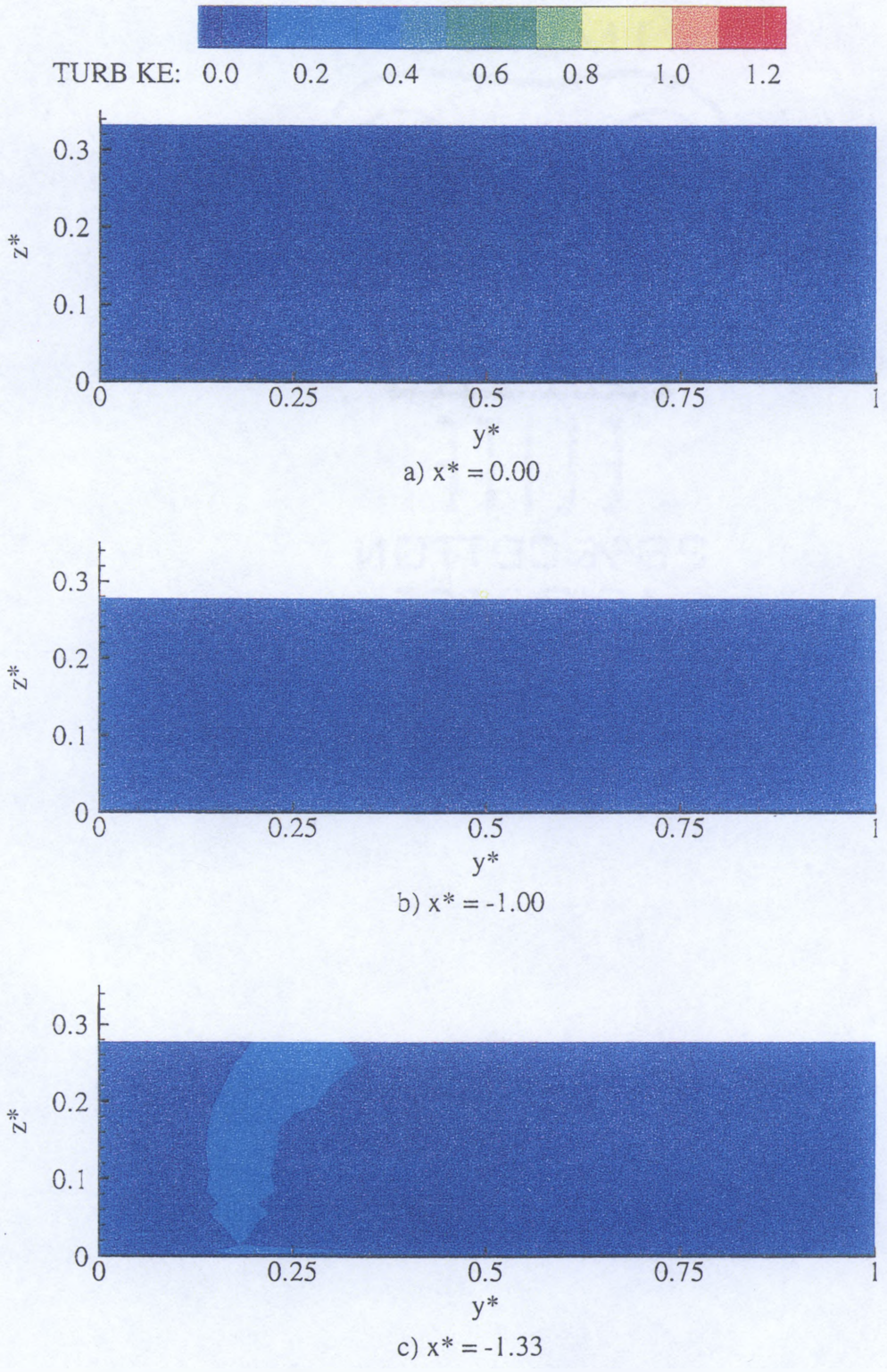

Figure D.6. Turbulent Kinetic Energy Cross-Sections, q* = 0.583

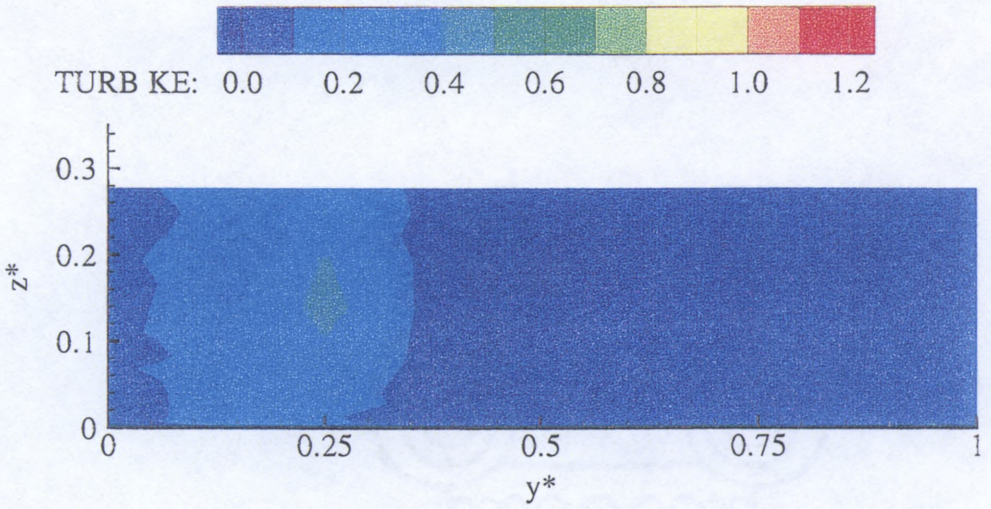

d) x* = -1.67

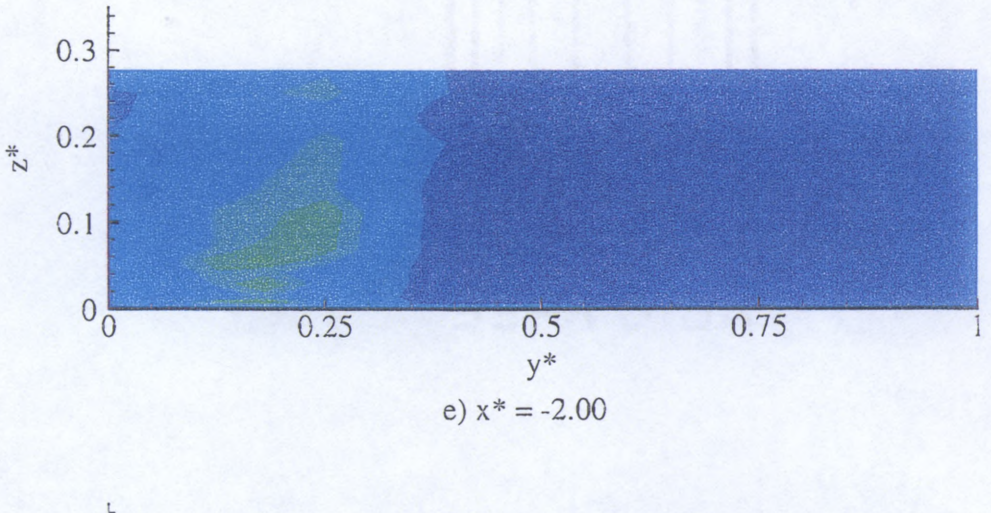

e) x* = -2.00

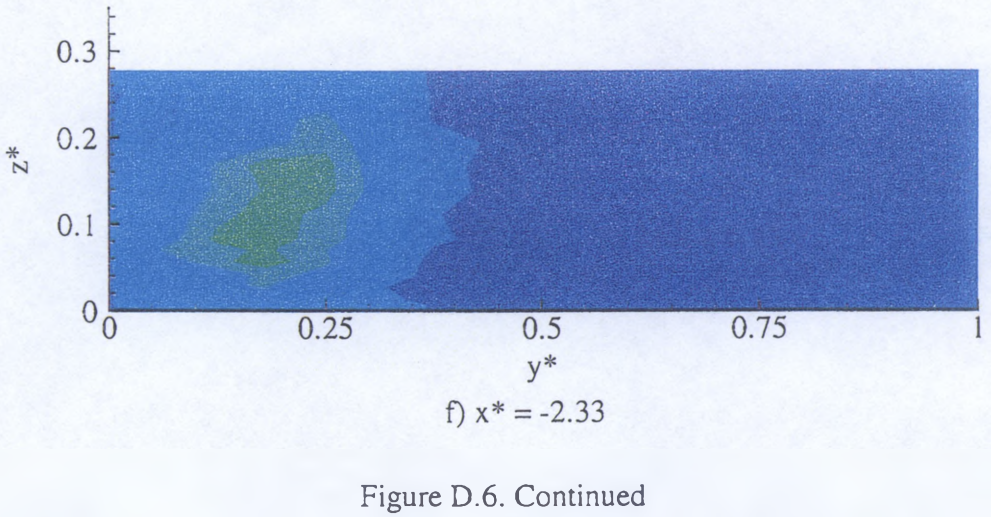

f) x* = -2.33

Figure D.6. Continued

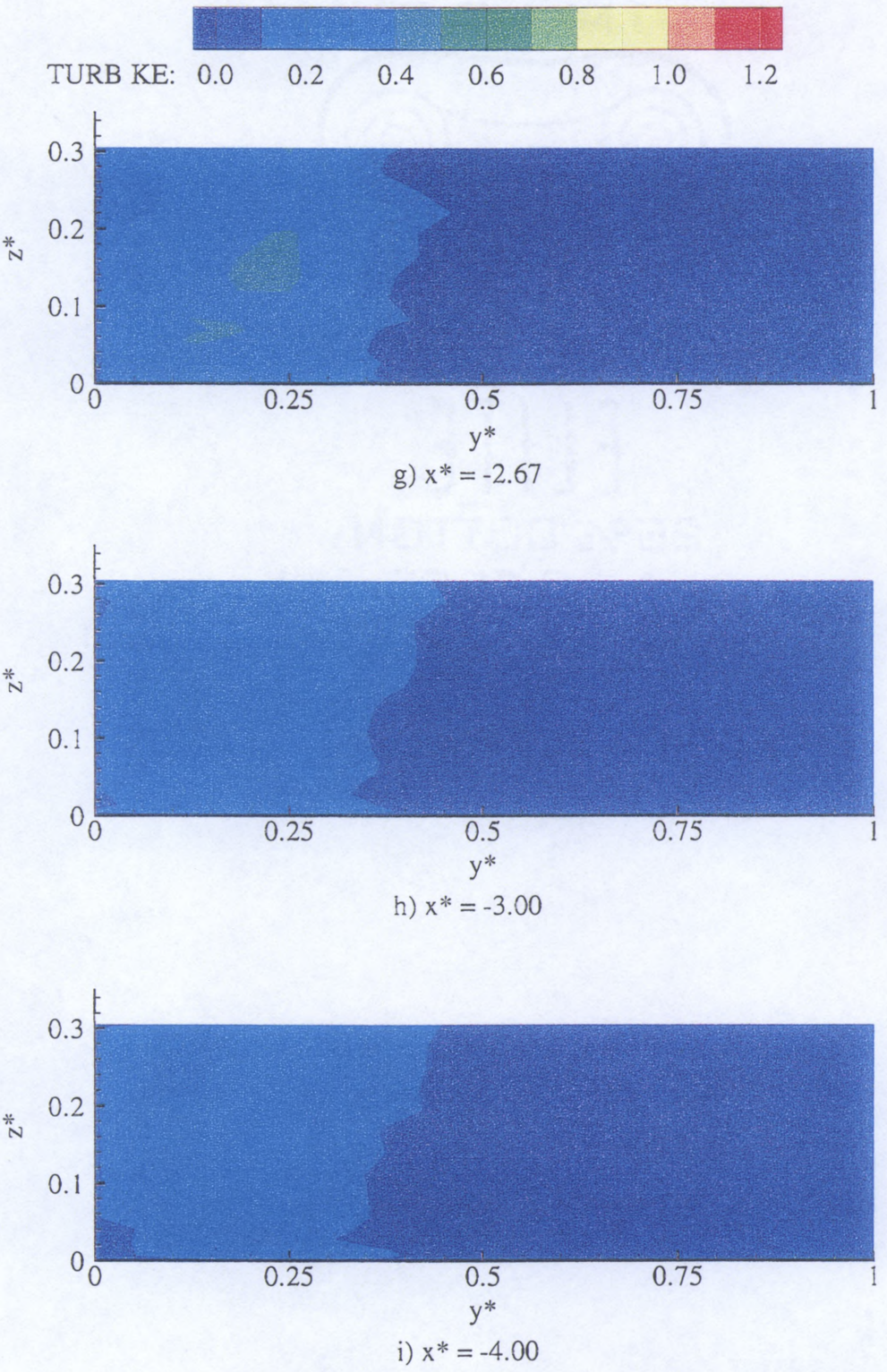

Figure D.6. Continued

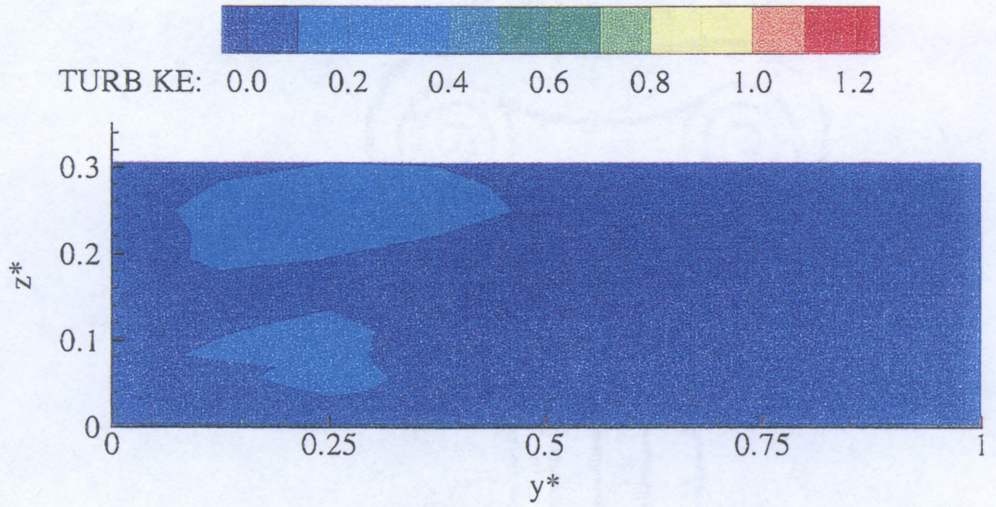

j) x* = -5.00

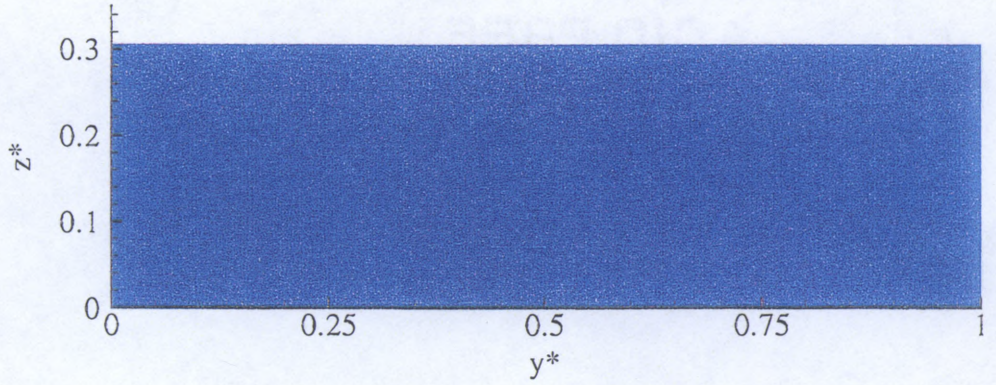

k) x* = -7.00

Figure D.6. Continued

APPENDIX E

DATA PLOTS FOR $q^* = 0.417$

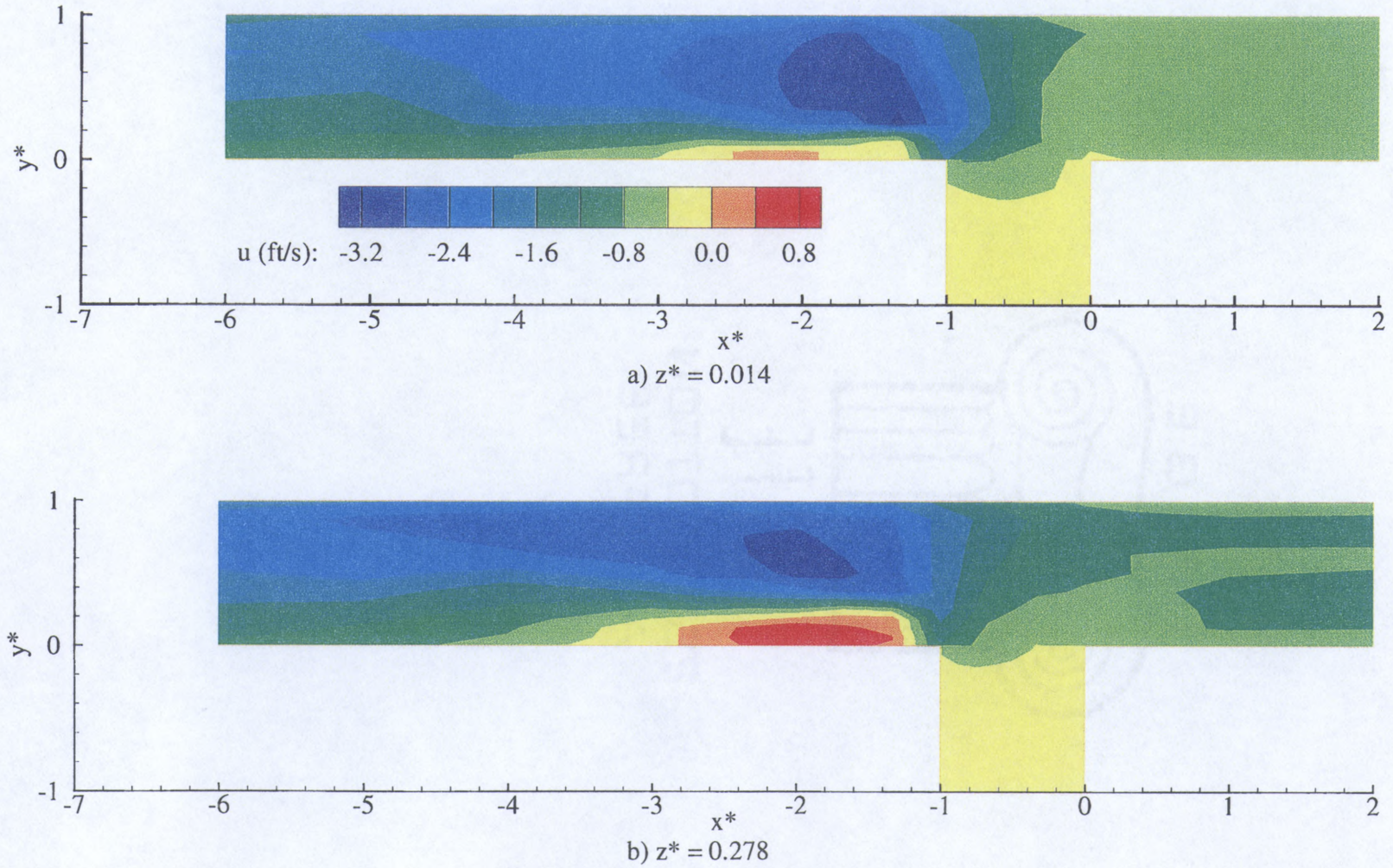

Figure E.1. u Velocity Plan View, q* = 0.417

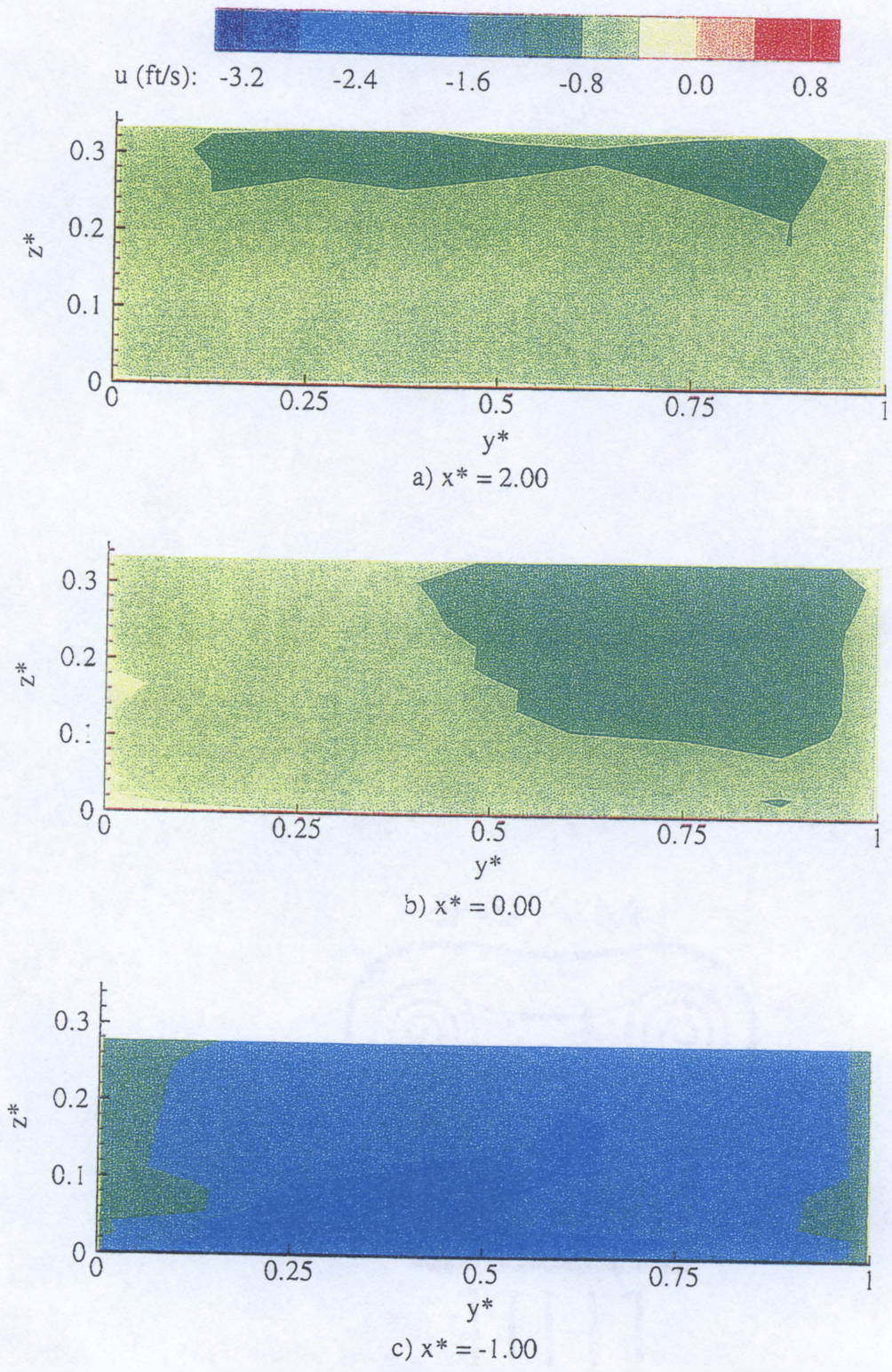

Figure E.2. u Velocity Cross-Sections, q* = 0.417

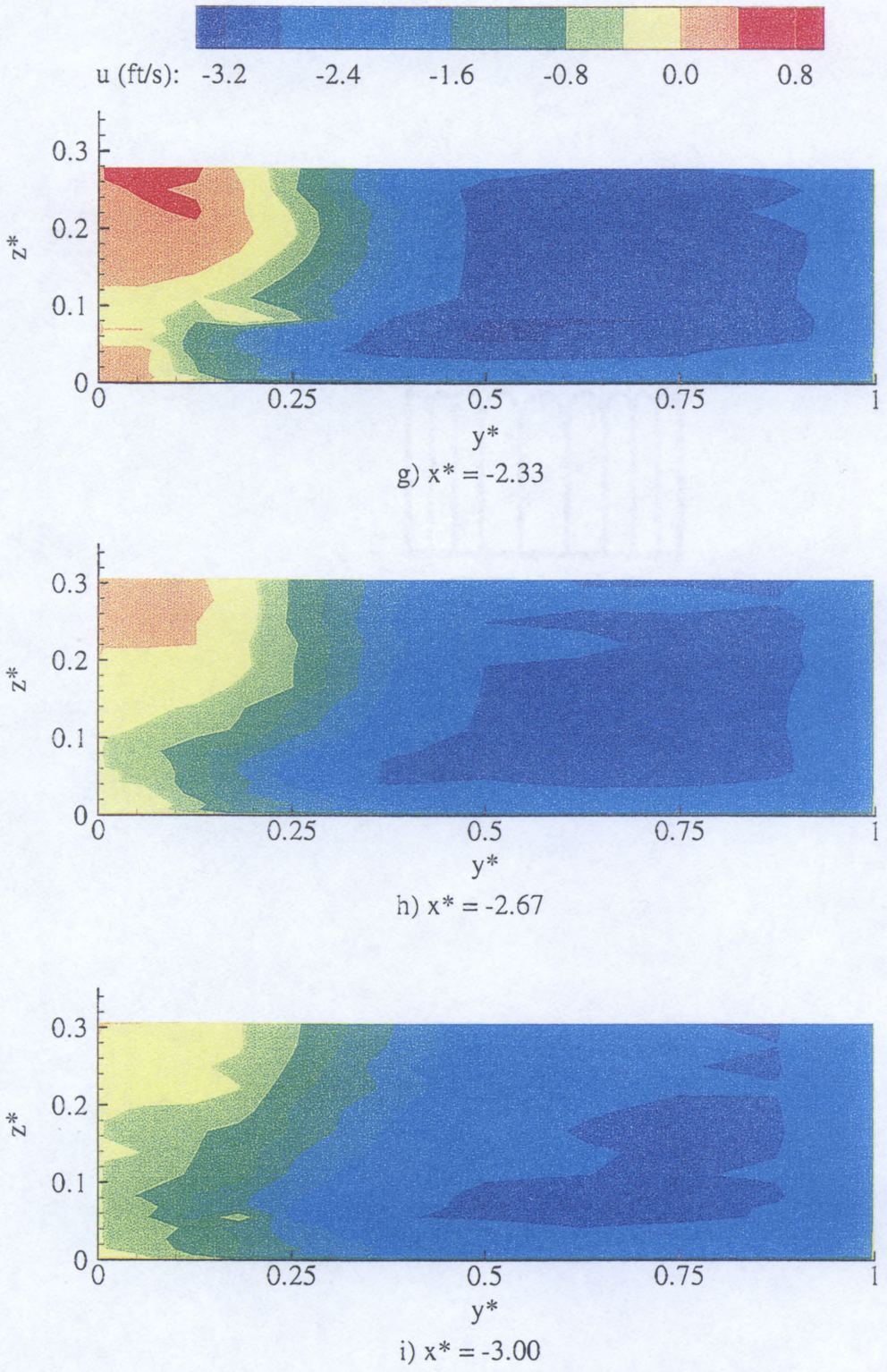

Figure E.2. Continued

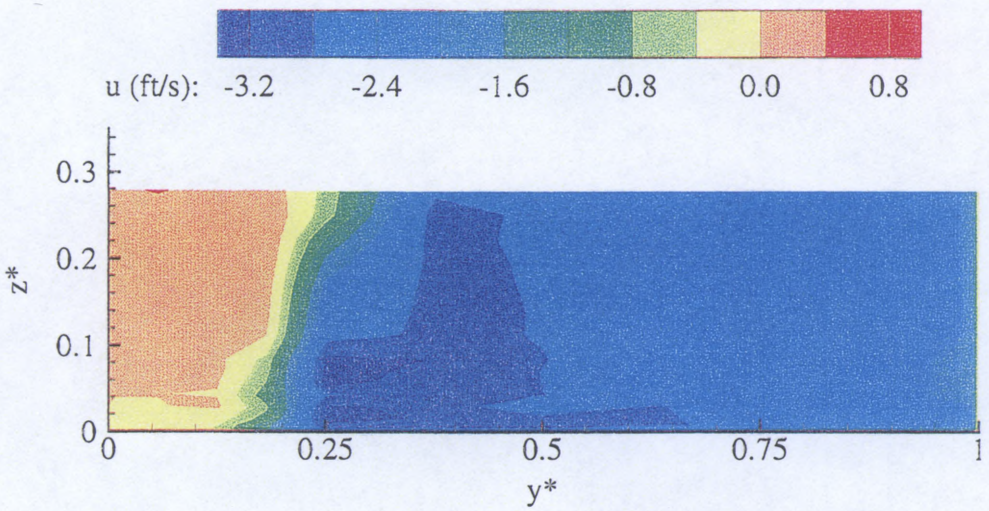

d) x* = -1.33

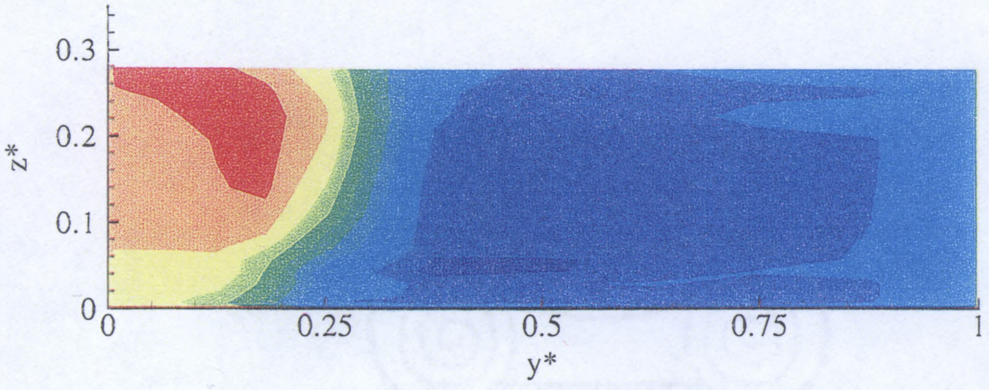

e) x* = -1.67

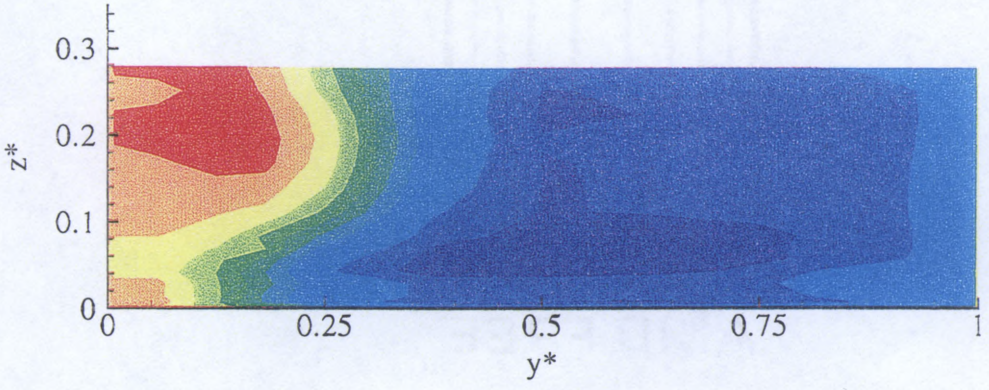

f) x* = -2.00

Figure E.2. Continued

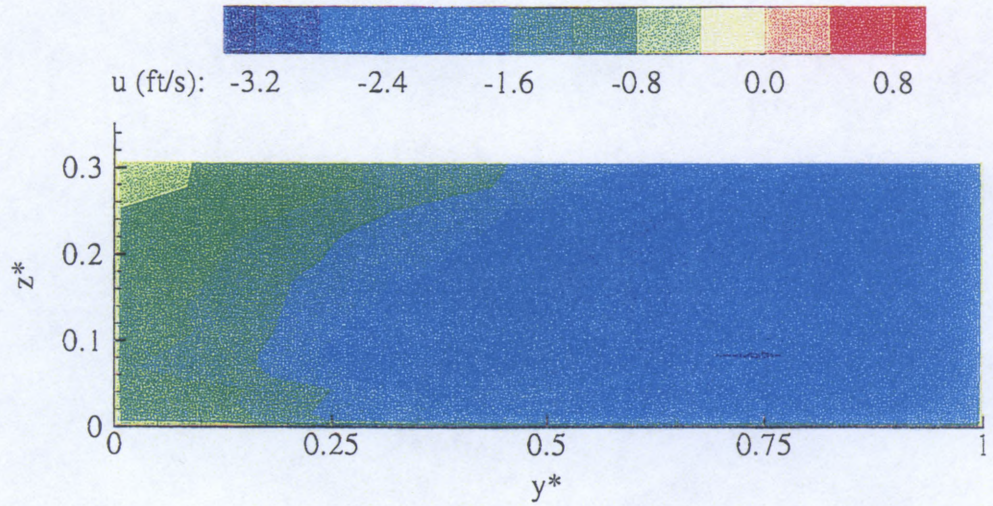

j) x* = -4.00

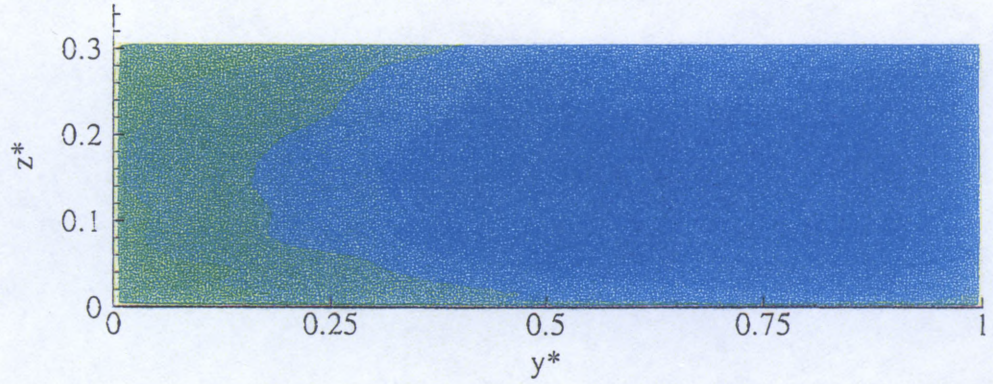

k) x* = -5.00

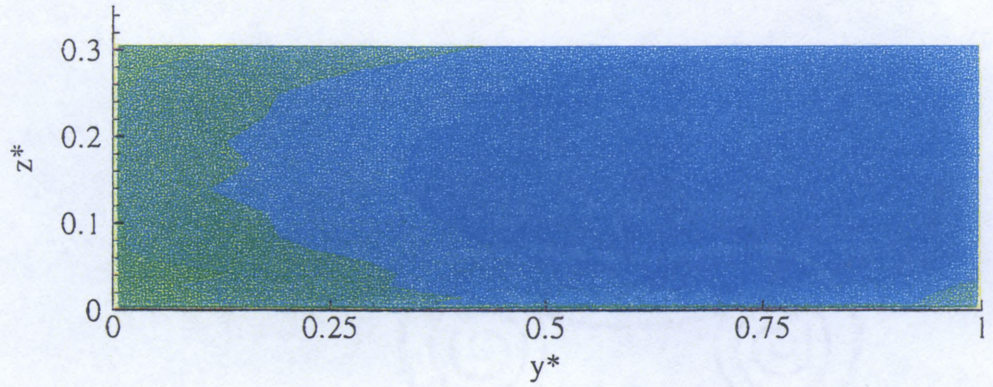

l) x* = -6.00

Figure E.2. Continued

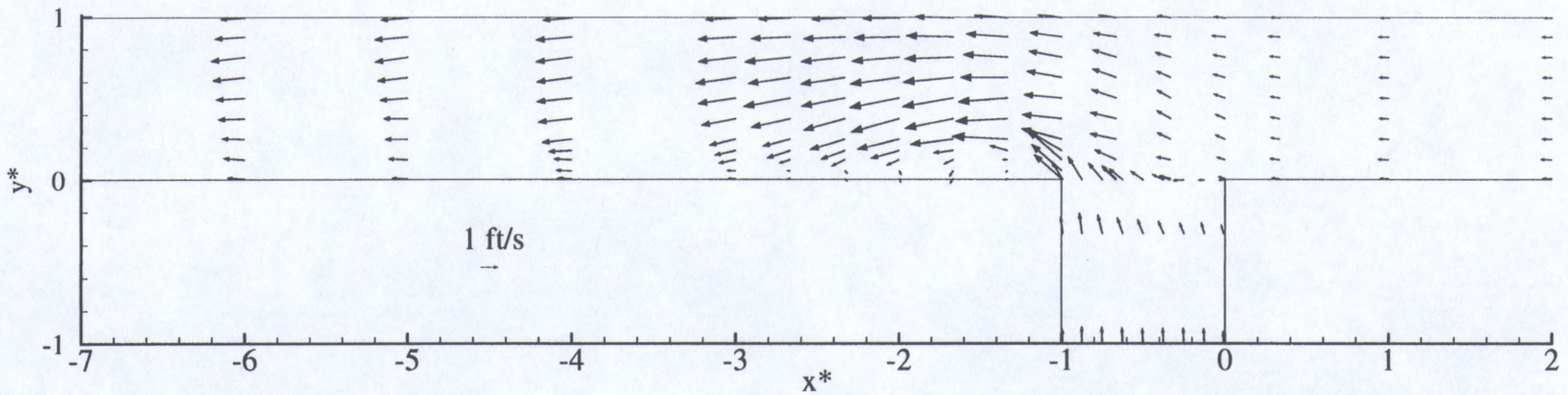

a) z* = 0.014

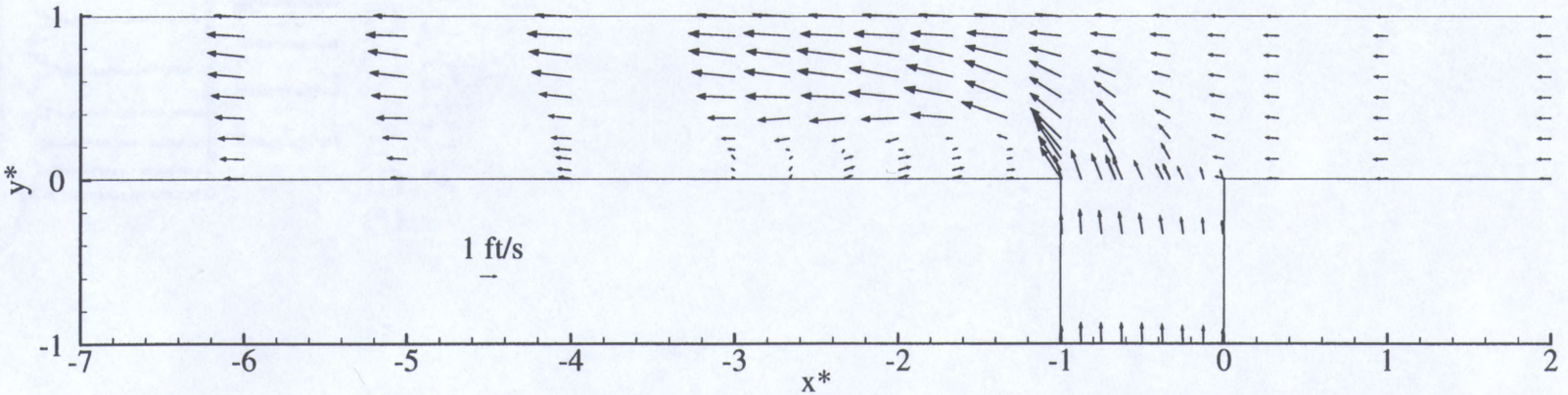

b) z* = 0.278

Figure E.3. u-v Vector Fields, q* = 0.417

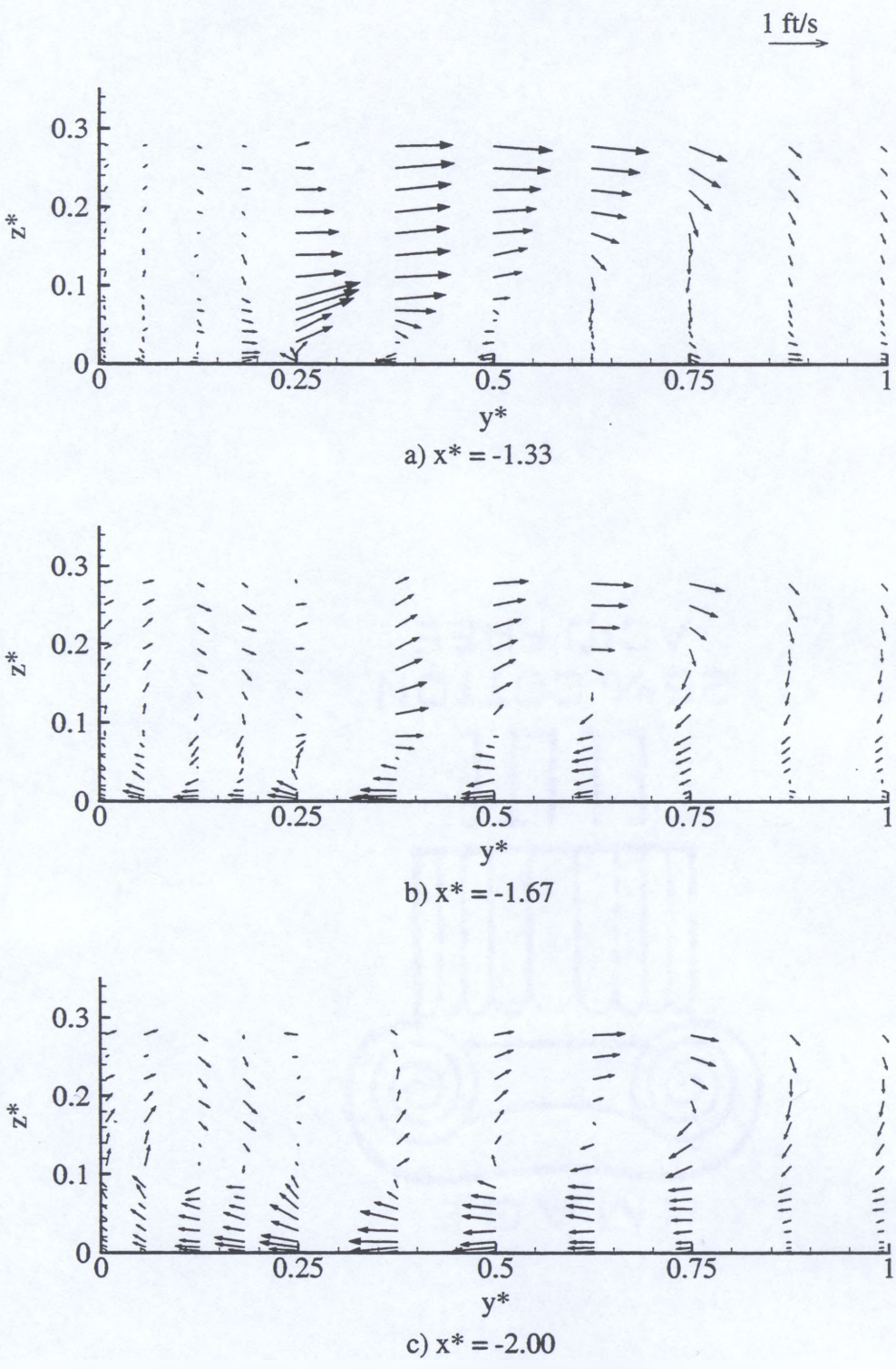

Figure E.4. v-w Vector Fields, q* = 0.417

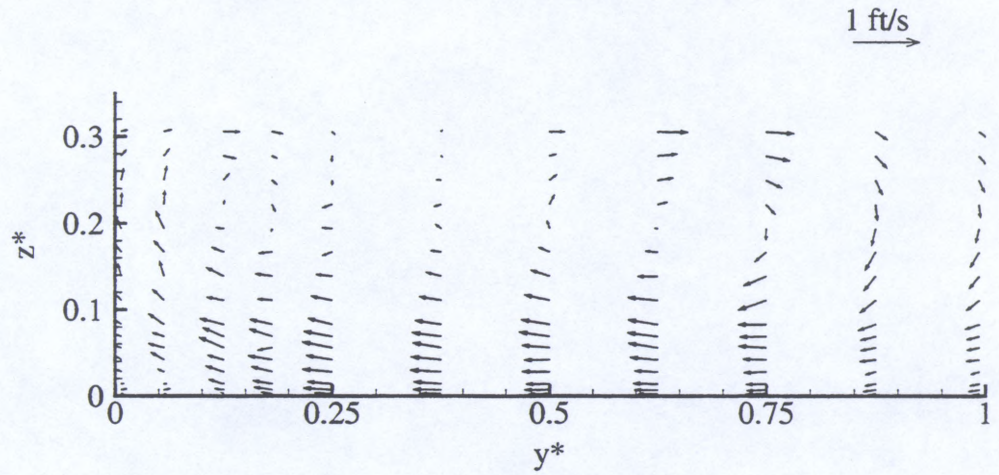

d) x* = -3.00

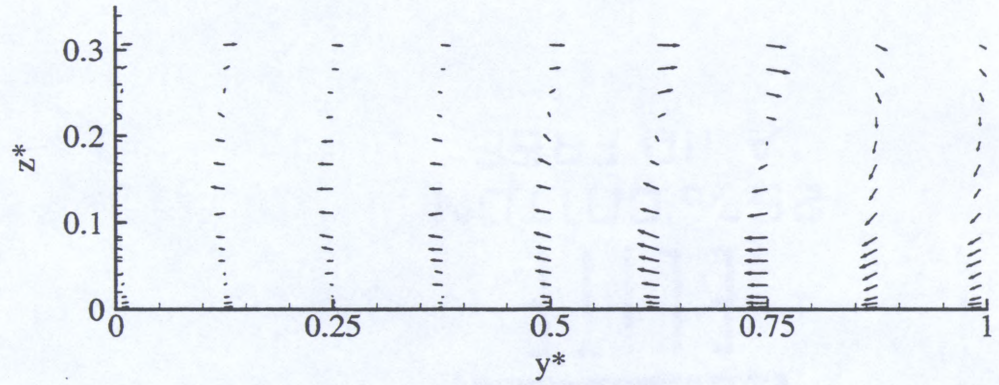

e) x* = -5.00

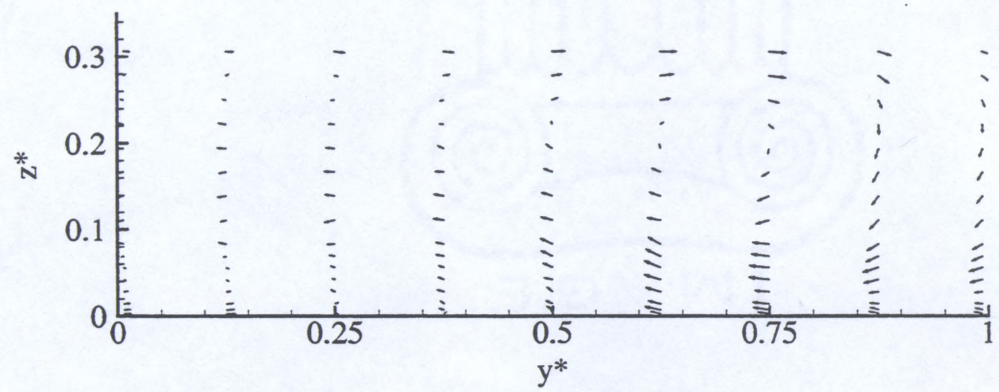

f) x* = -6.00

Figure E.4. Continued

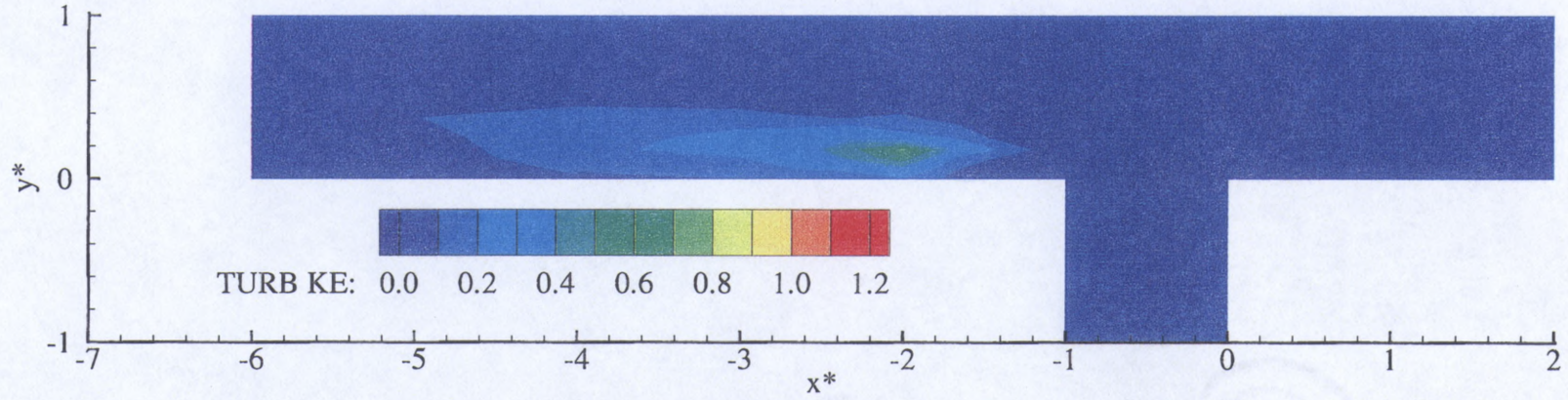

a) z* = 0.014

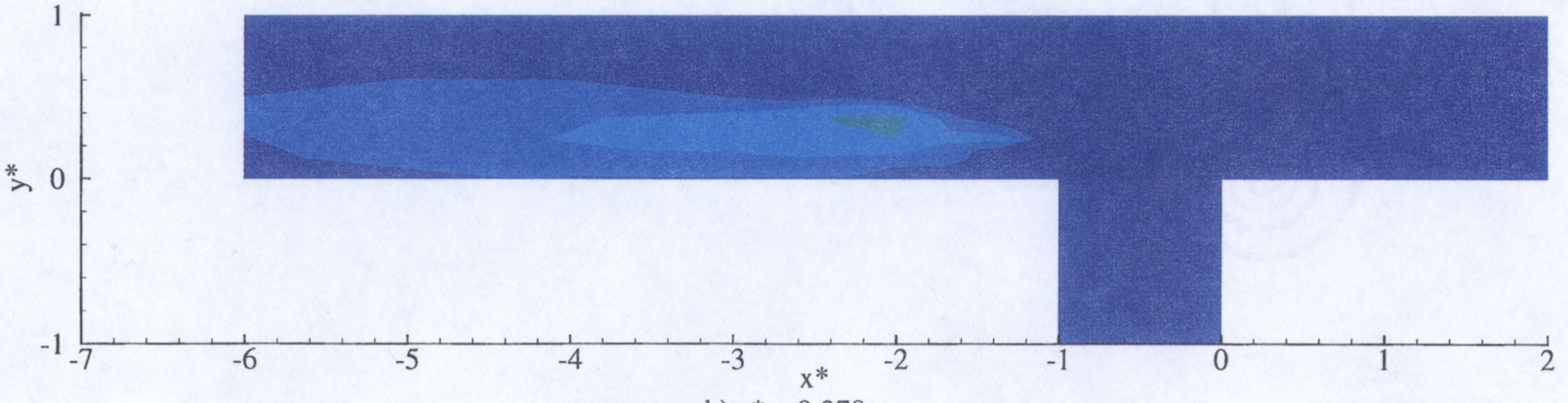

b) z* = 0.278

Figure E.5. Turbulent Kinetic Energy Plan View, q* = 0.417

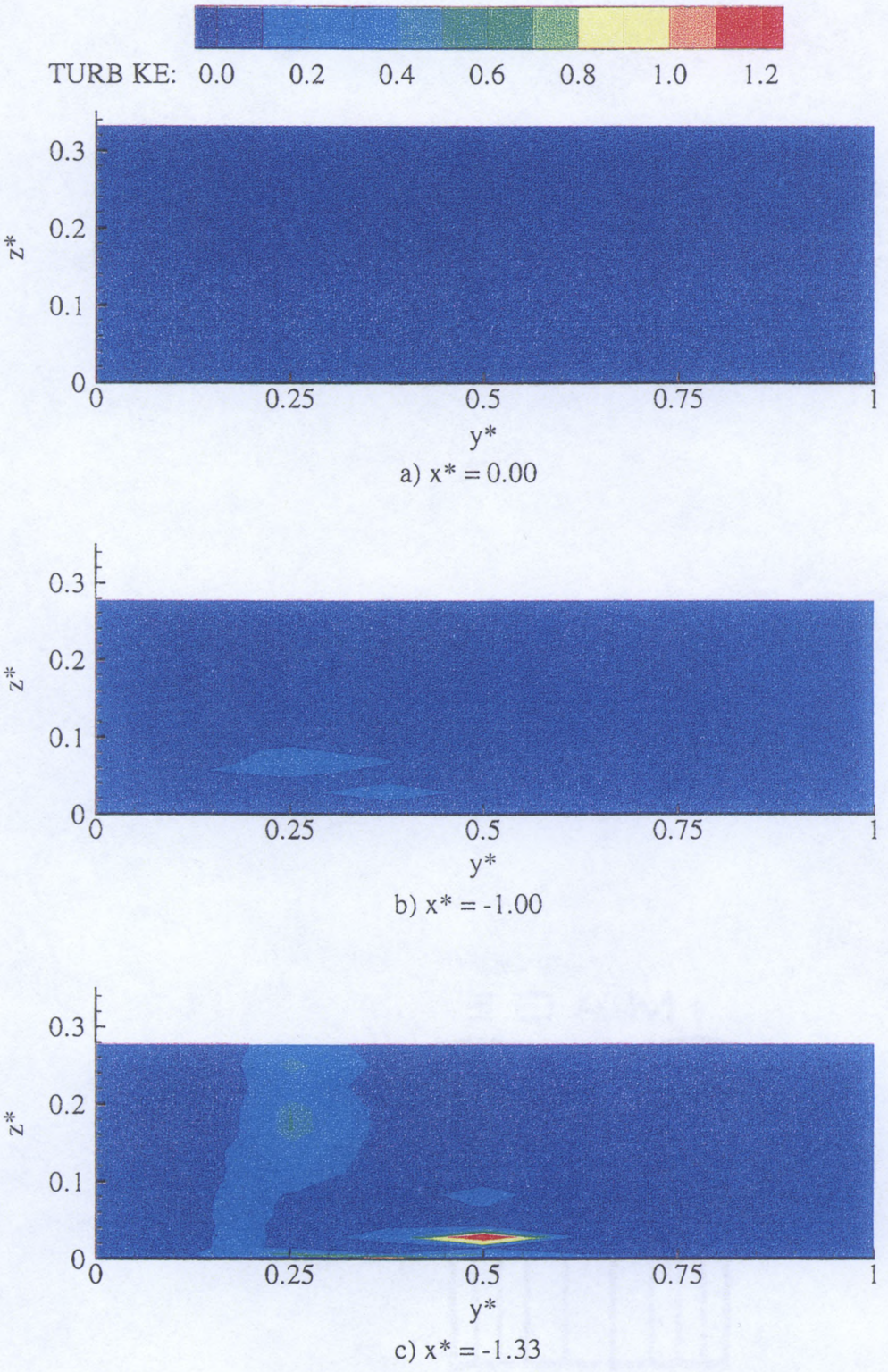

Figure E.6. Turbulent Kinetic Energy Cross-Sections, q* = 0.417

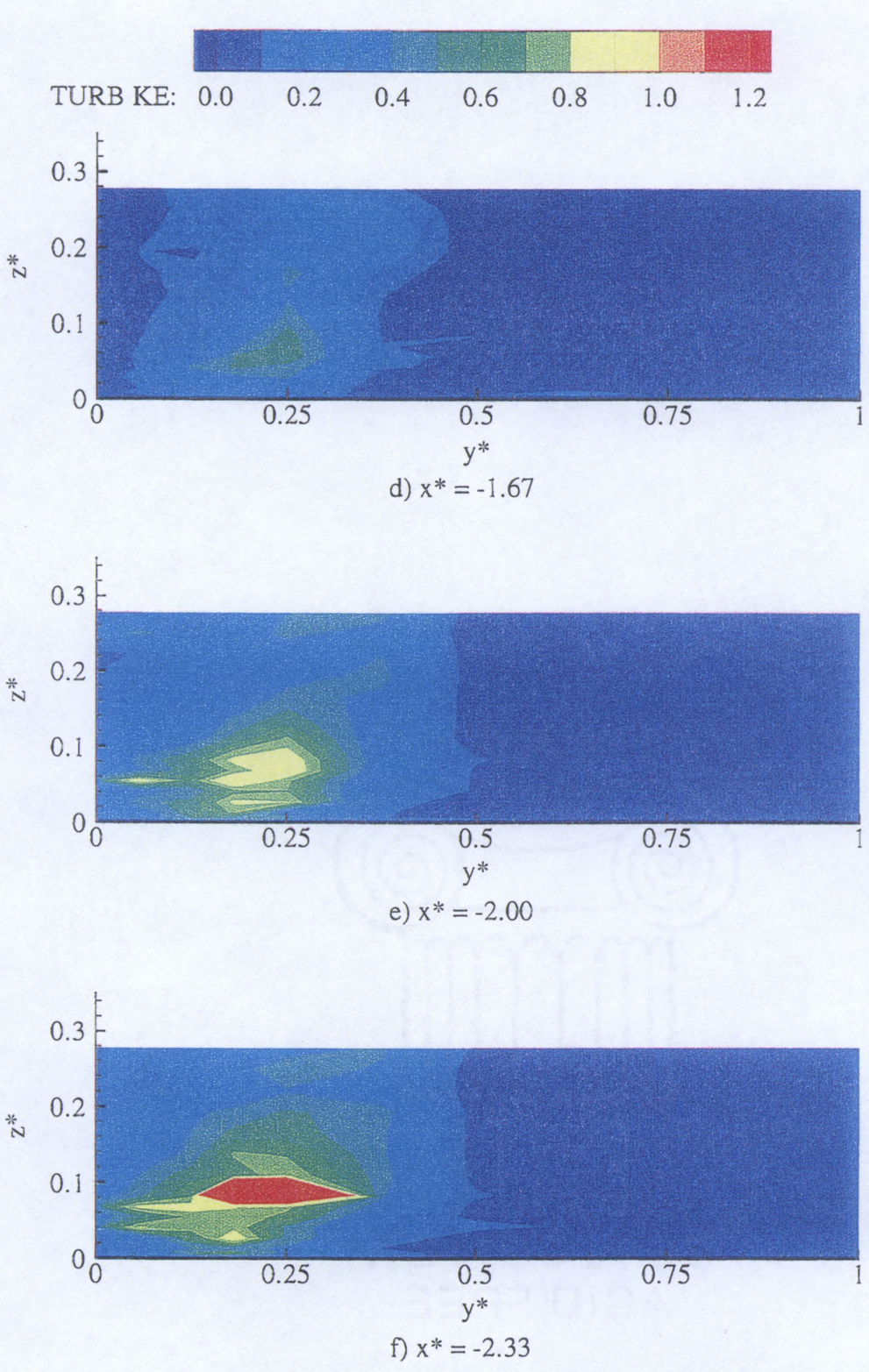

Figure E.6. Continued

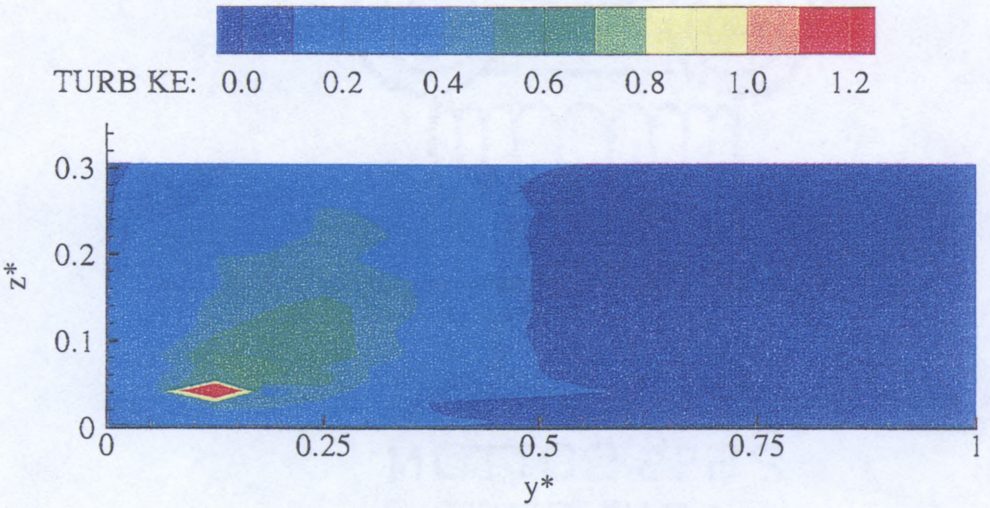

g) x* = -2.67

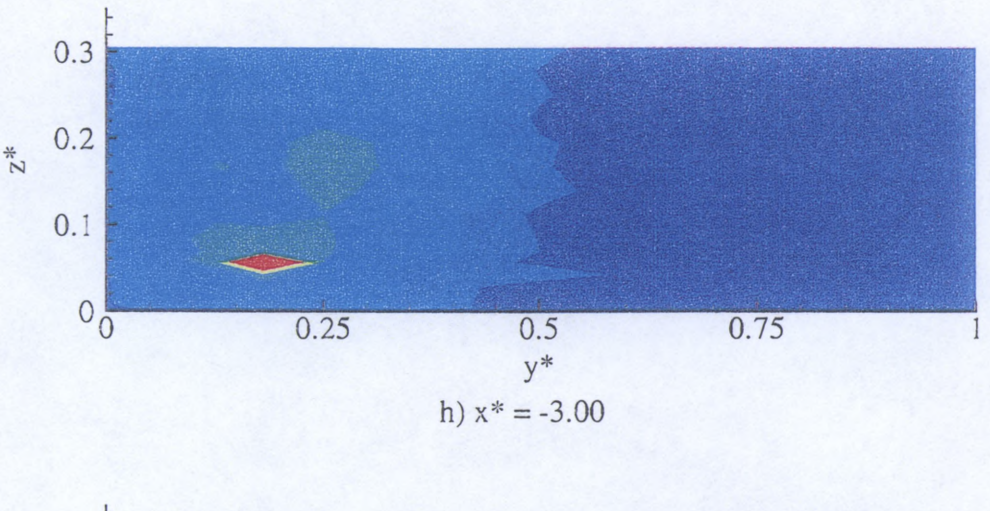

h) x* = -3.00

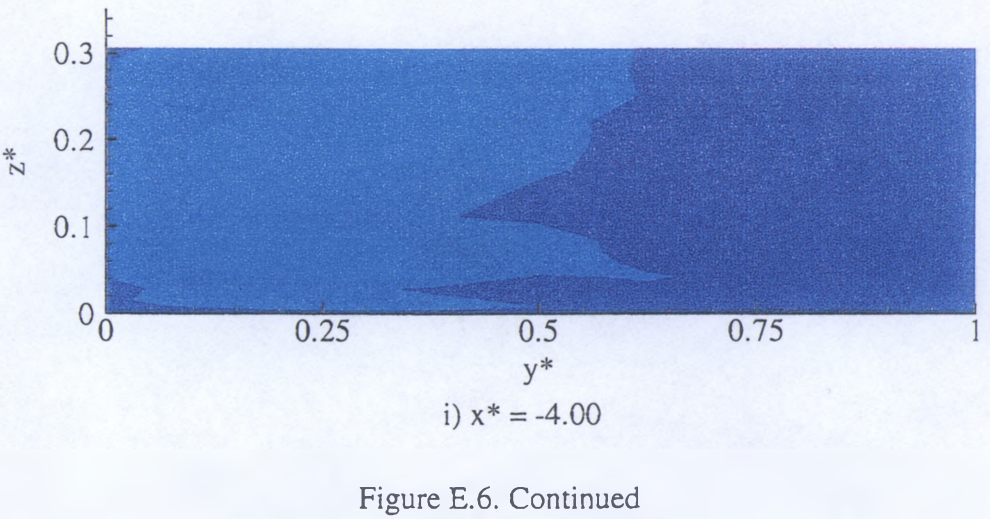

i) x* = -4.00

Figure E.6. Continued

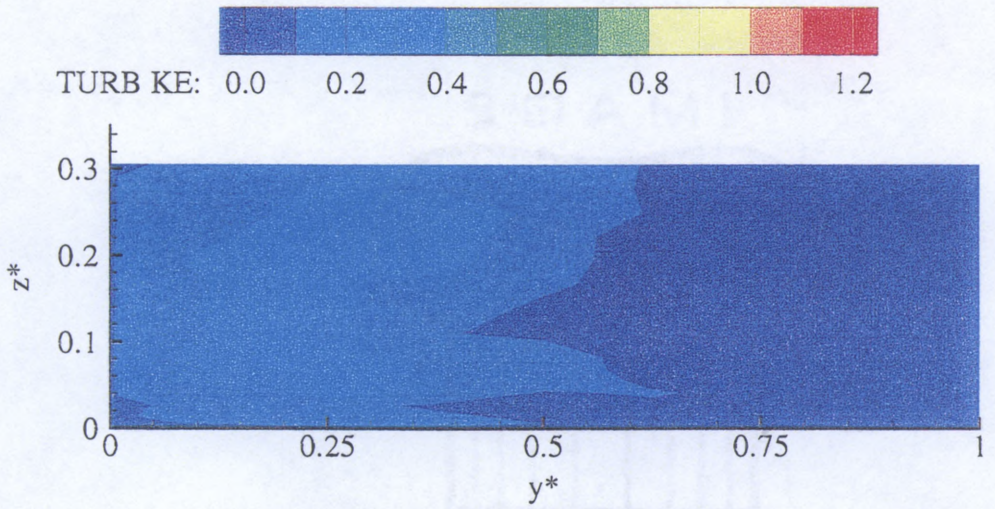

j) x* = -5.00

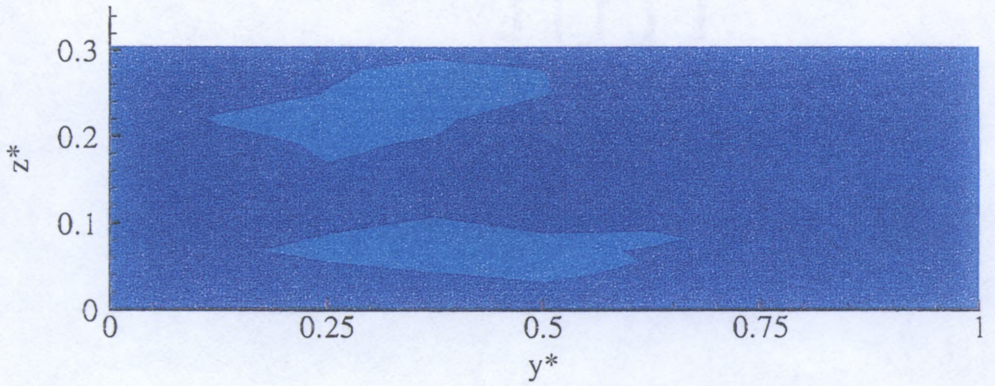

k) x* = -6.00

Figure E.6. Continued

APPENDIX F

DATA PLOTS FOR $q^* = 0.250$

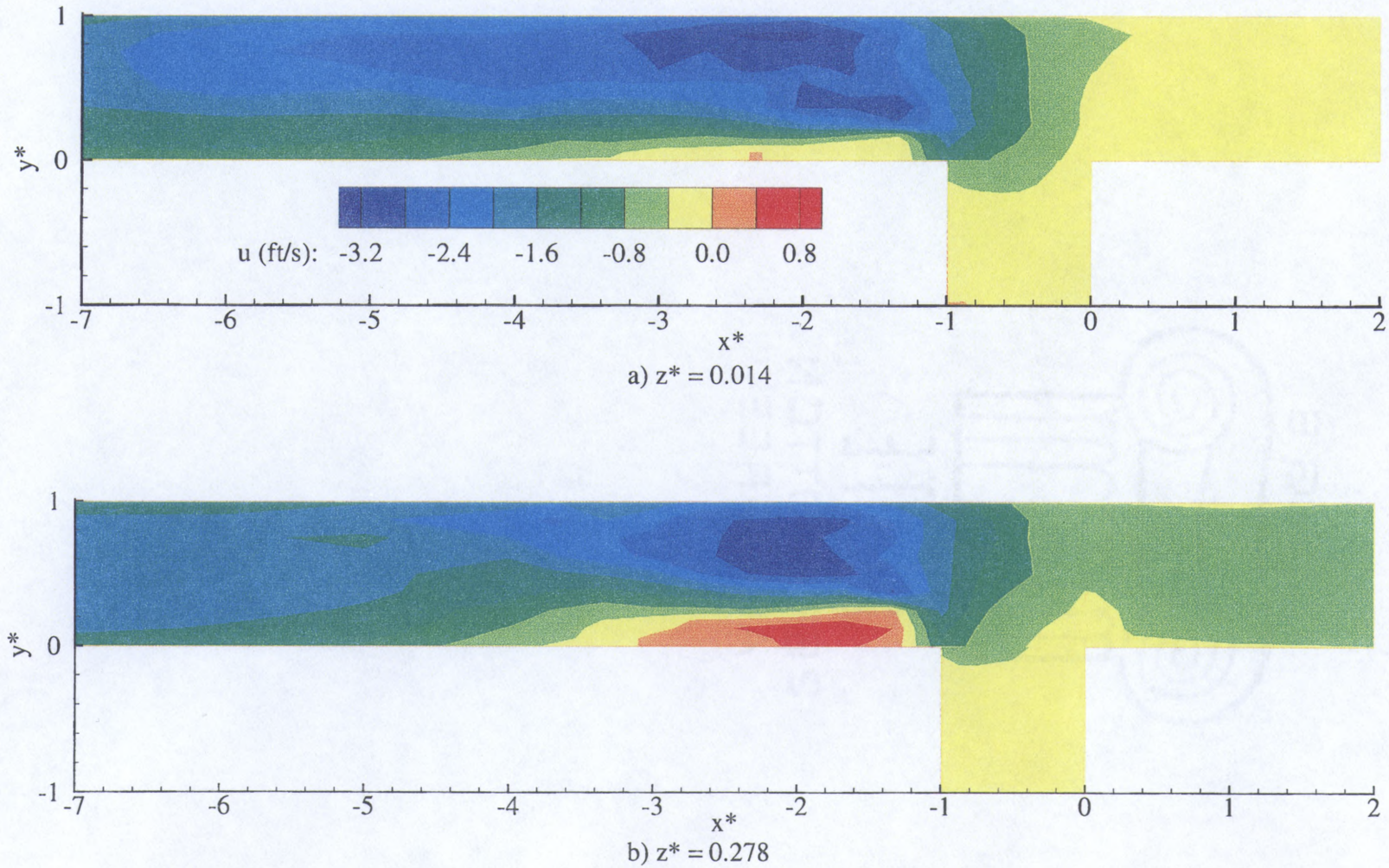

Figure F.1. u Velocity Plan View, q* = 0.250

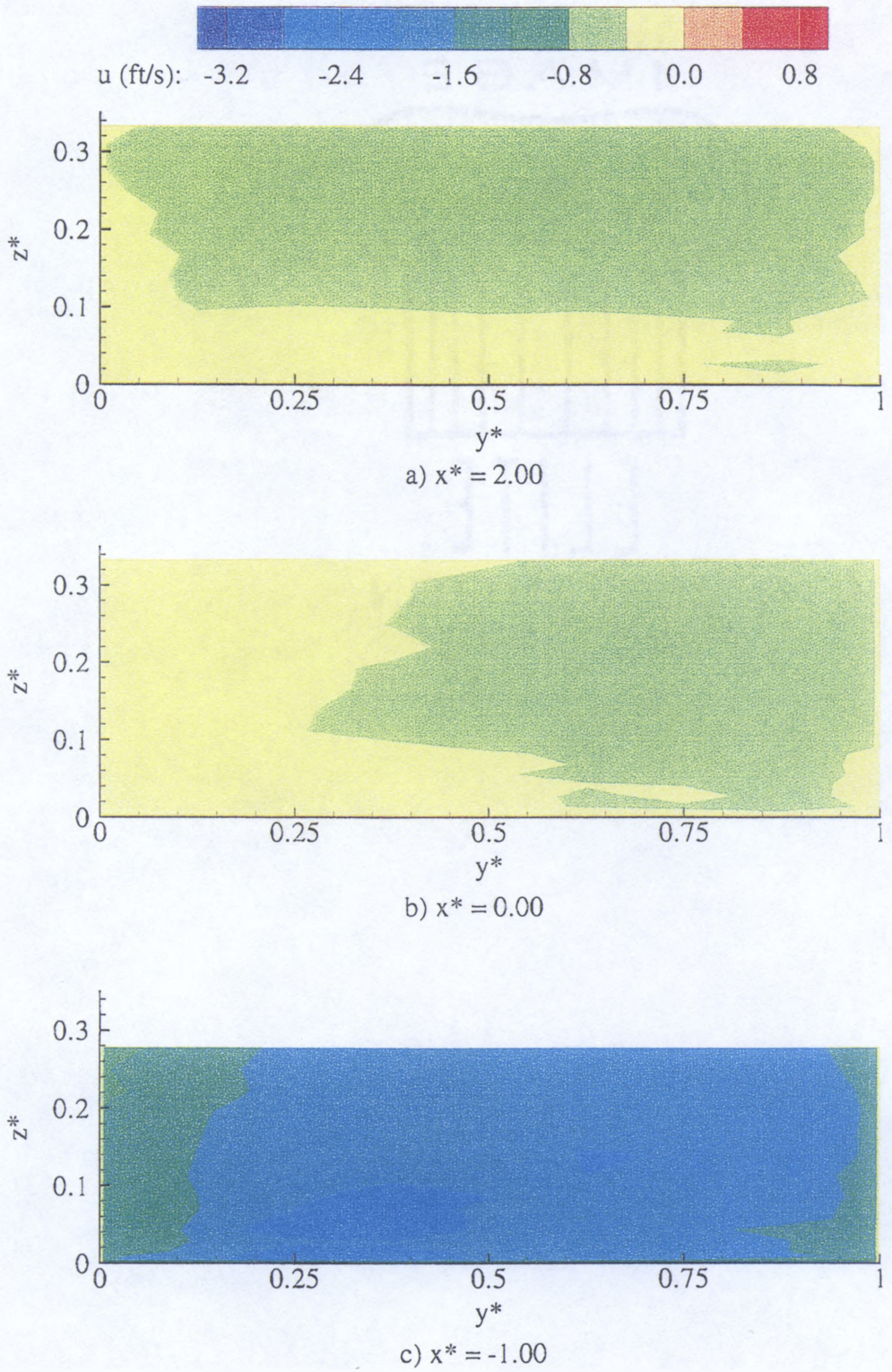

Figure F.2. u Velocity Cross-Sections, q* = 0.250

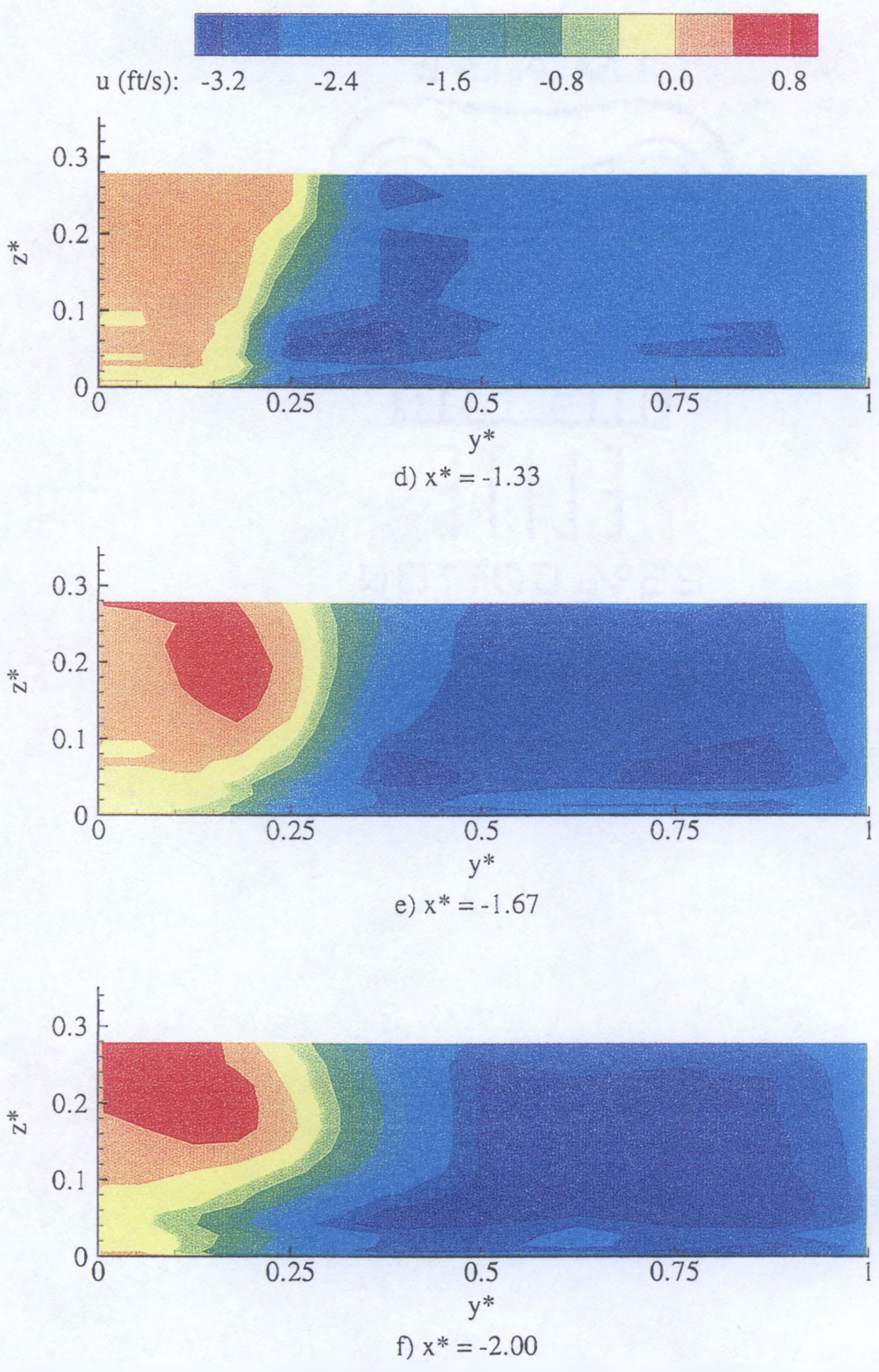

Figure F.2. Continued

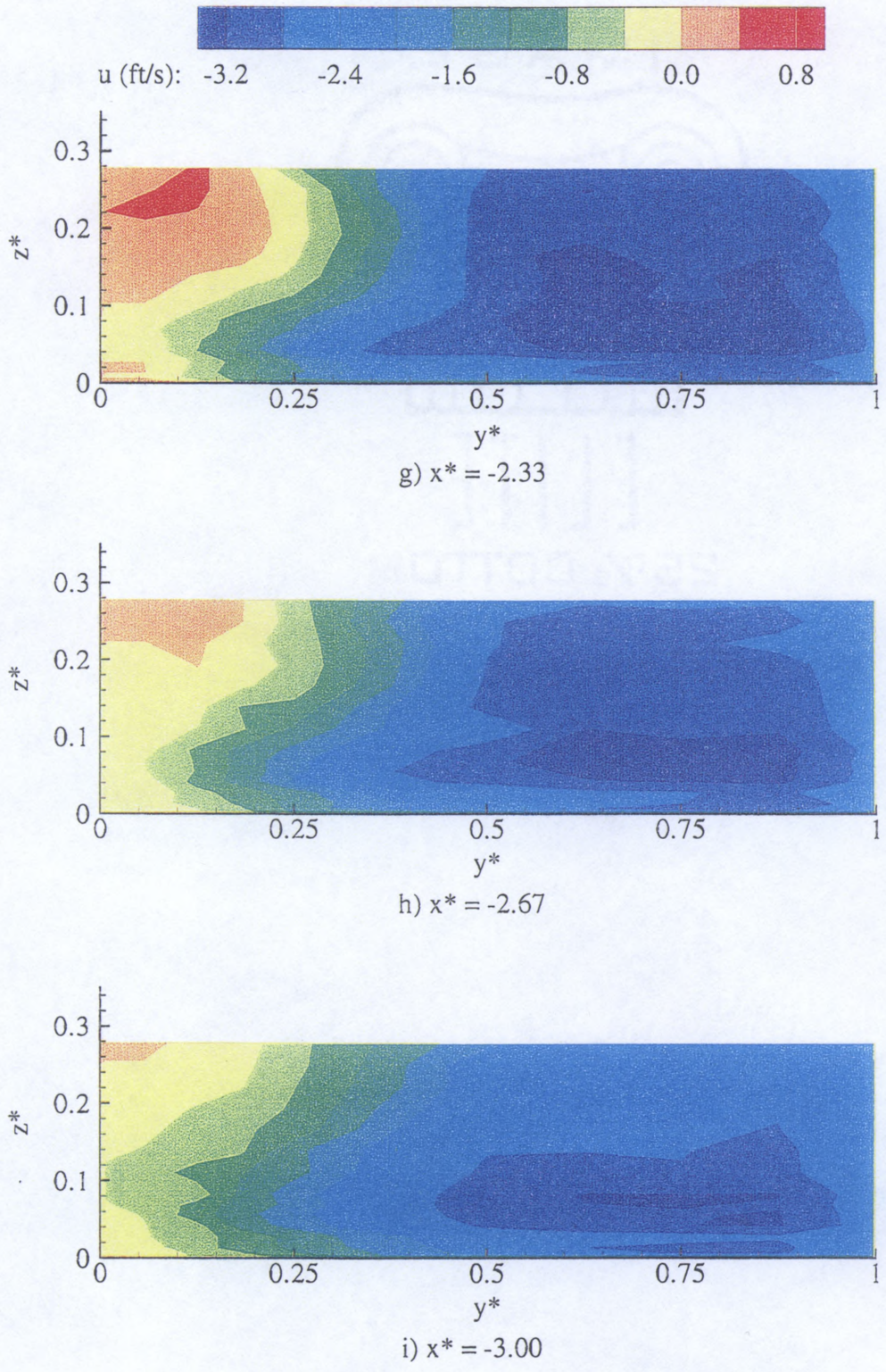

Figure F.2. Continued

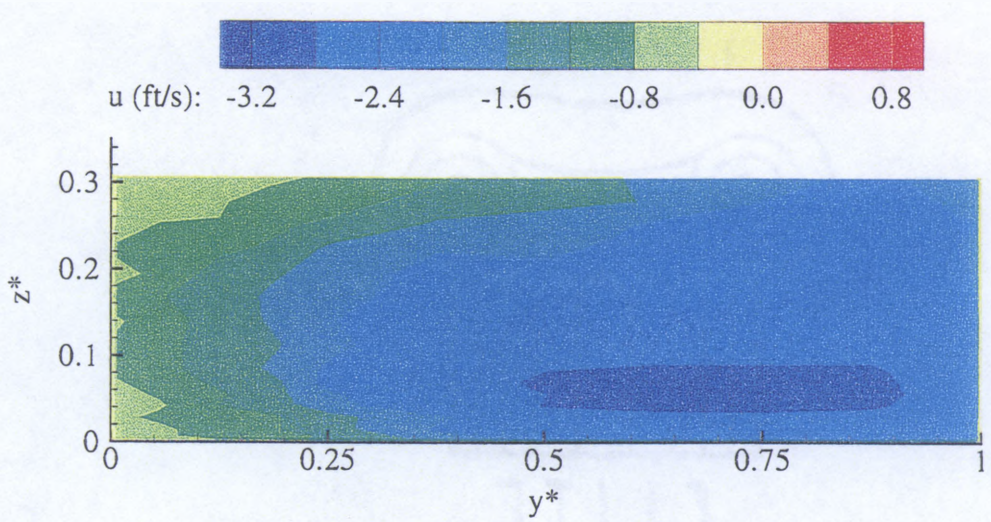

j) x* = -4.00

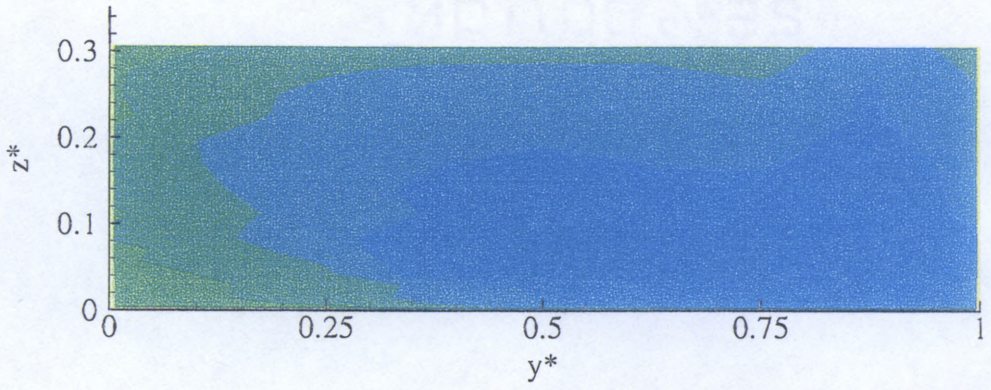

k) x* = -5.00

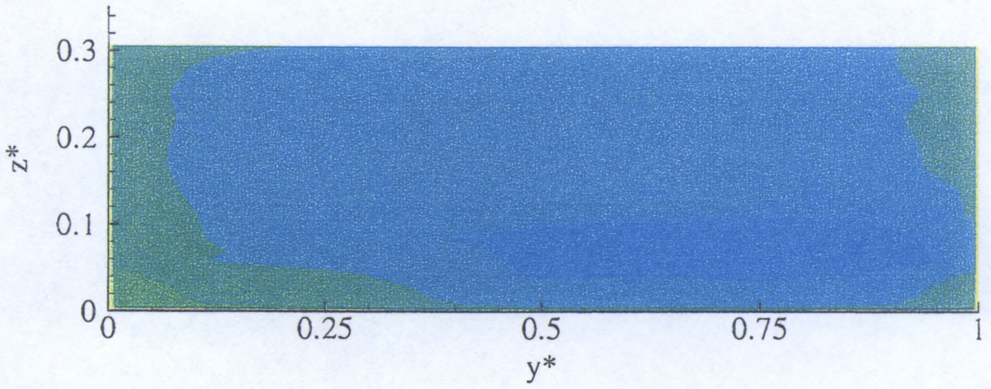

l) x* = -6.00

Figure F.2. Continued

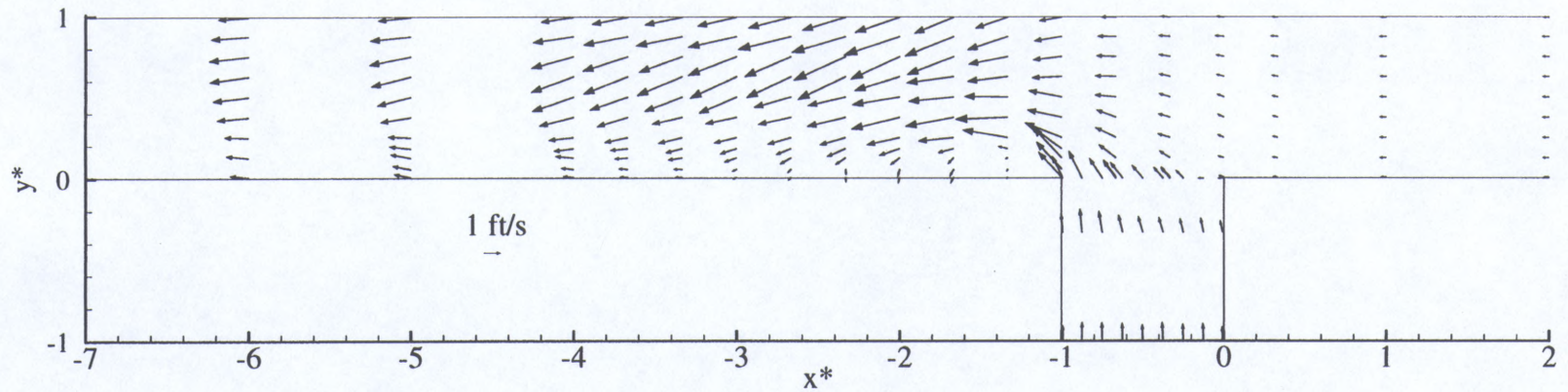

a) z* = 0.014

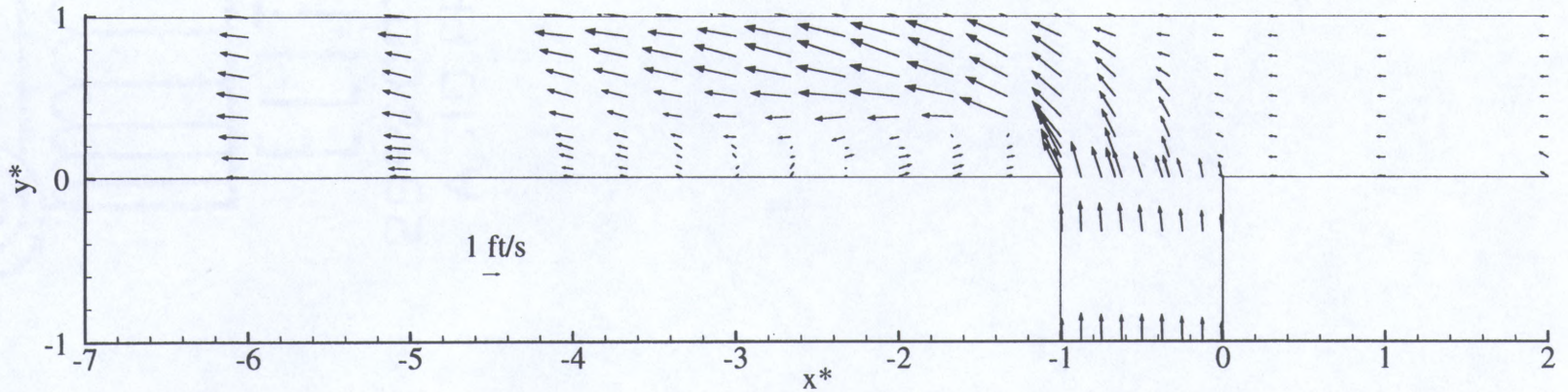

b) z* = 0.278

Figure F.3. u-v Vector Fields, q* = 0.250

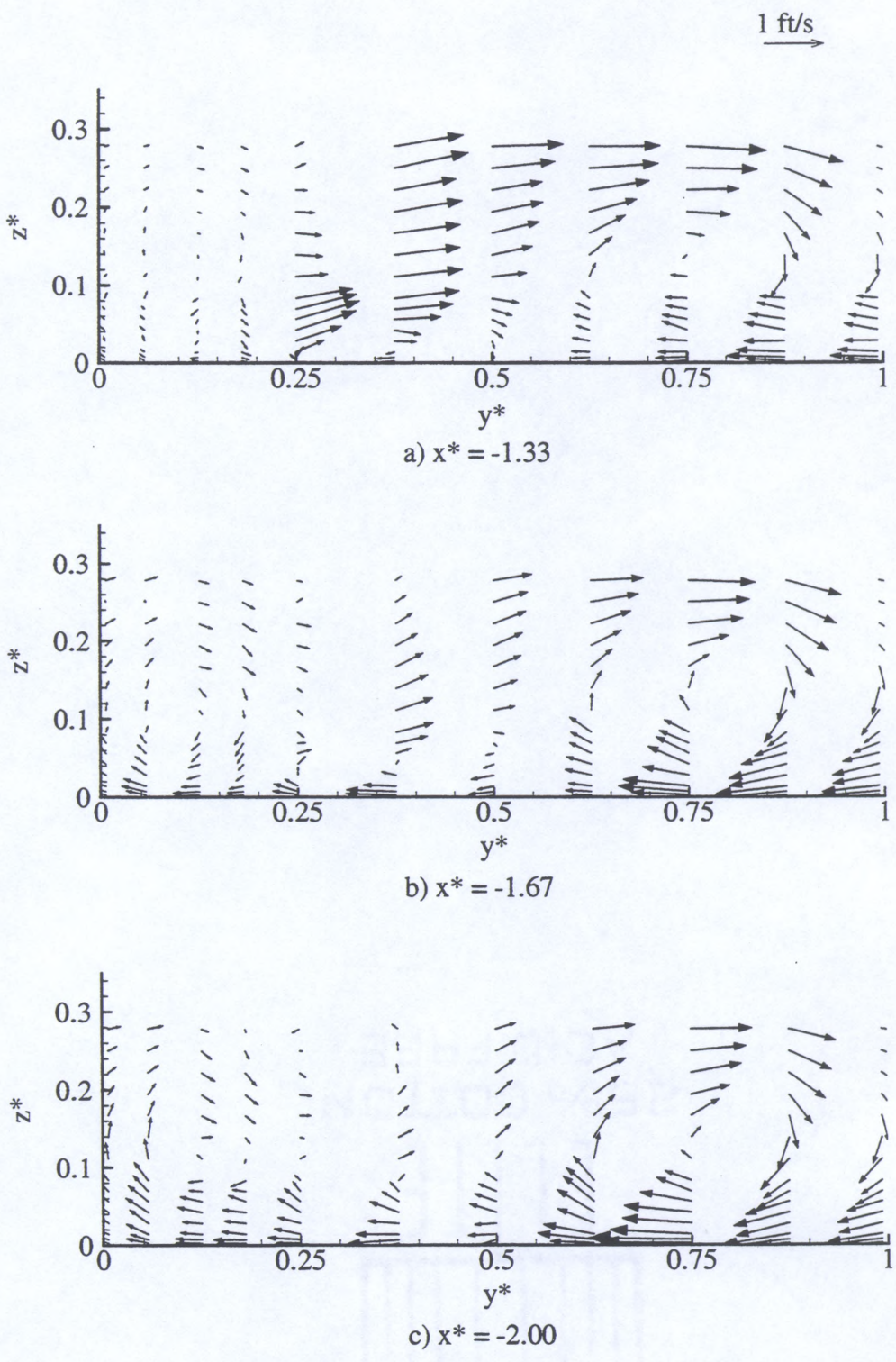

Figure F.4. v-w Vector Fields, q* = 0.250

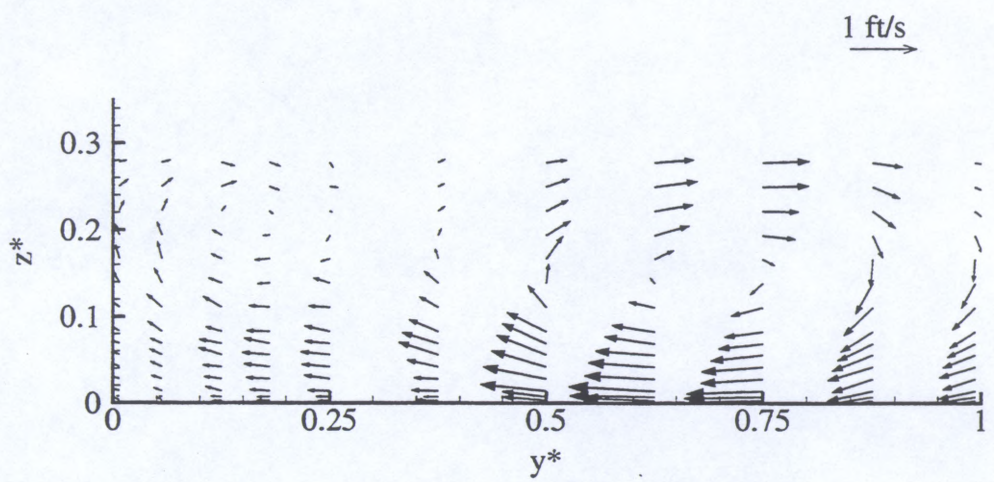

d) x* = -3.00

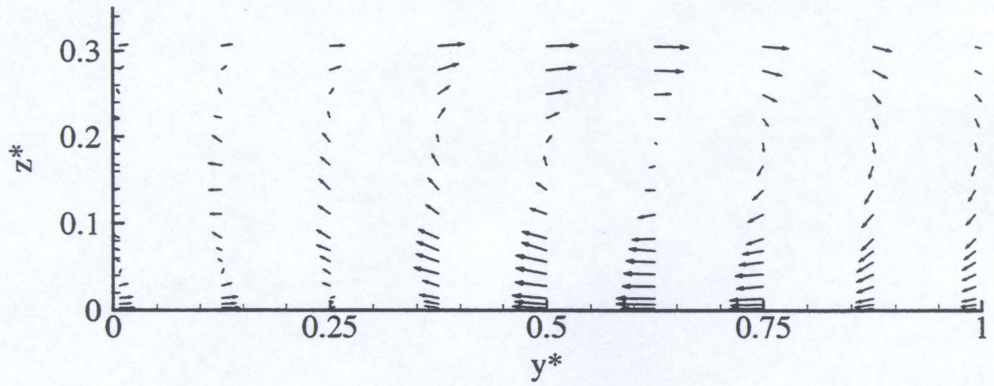

e) x* = -5.00

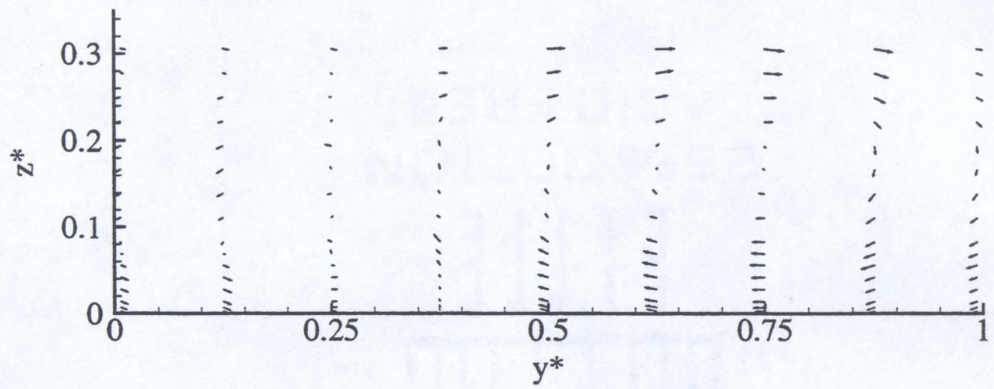

f) x* = -7.00

Figure F.4. Continued

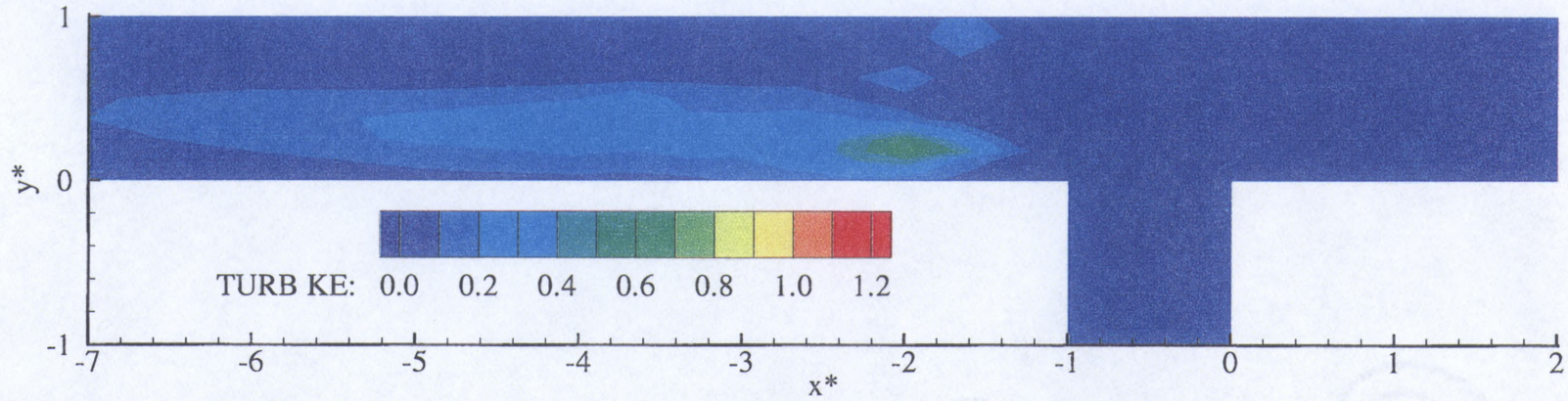

a) z* = 0.014

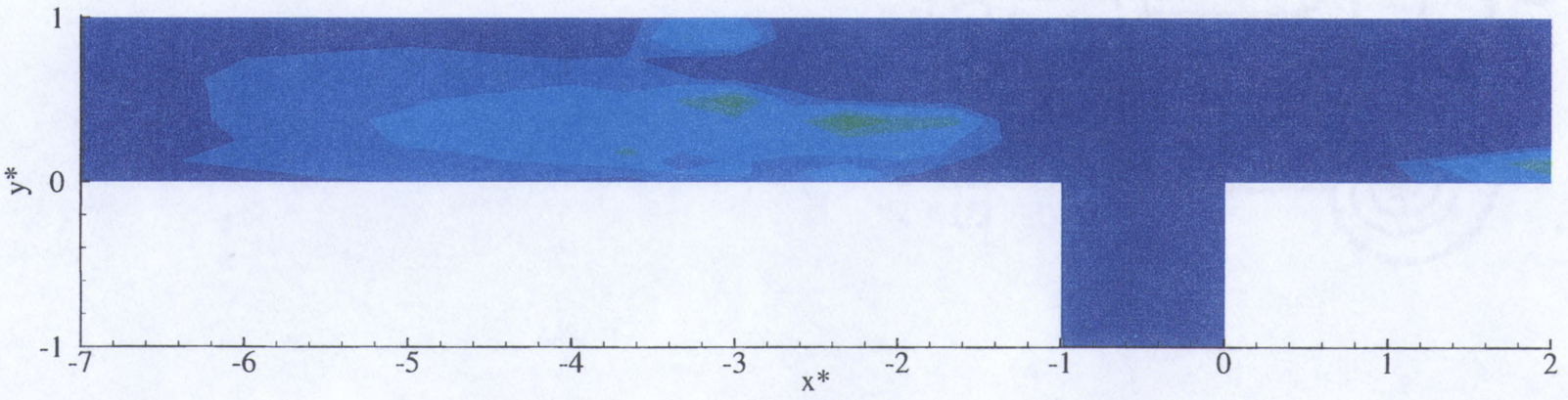

b) z* = 0.278

Figure F.5. Turbulent Kinetic Energy Plan View, q* = 0.250

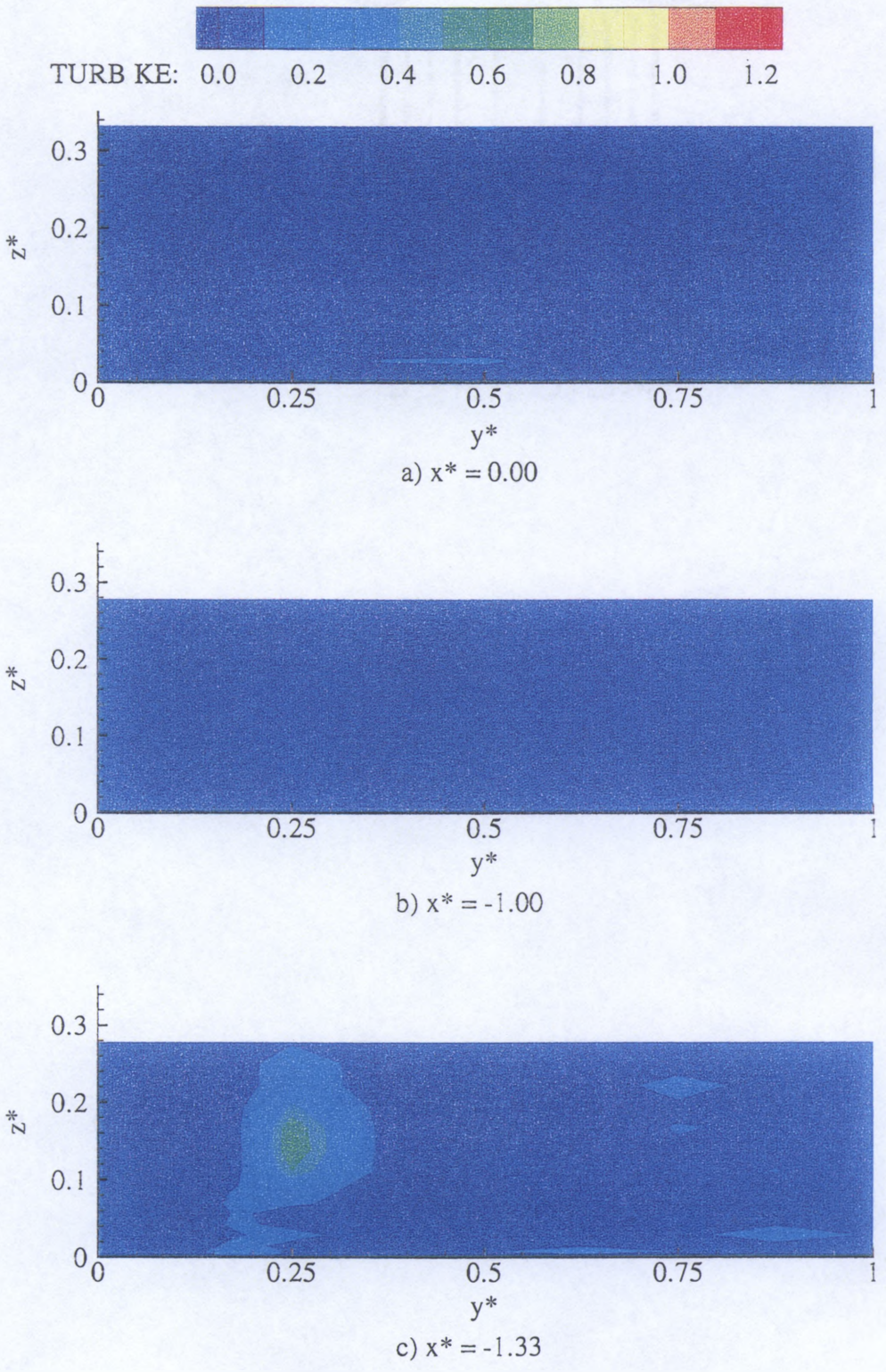

Figure F.6. Turbulent Kinetic Energy Cross-Sections, q* = 0.250

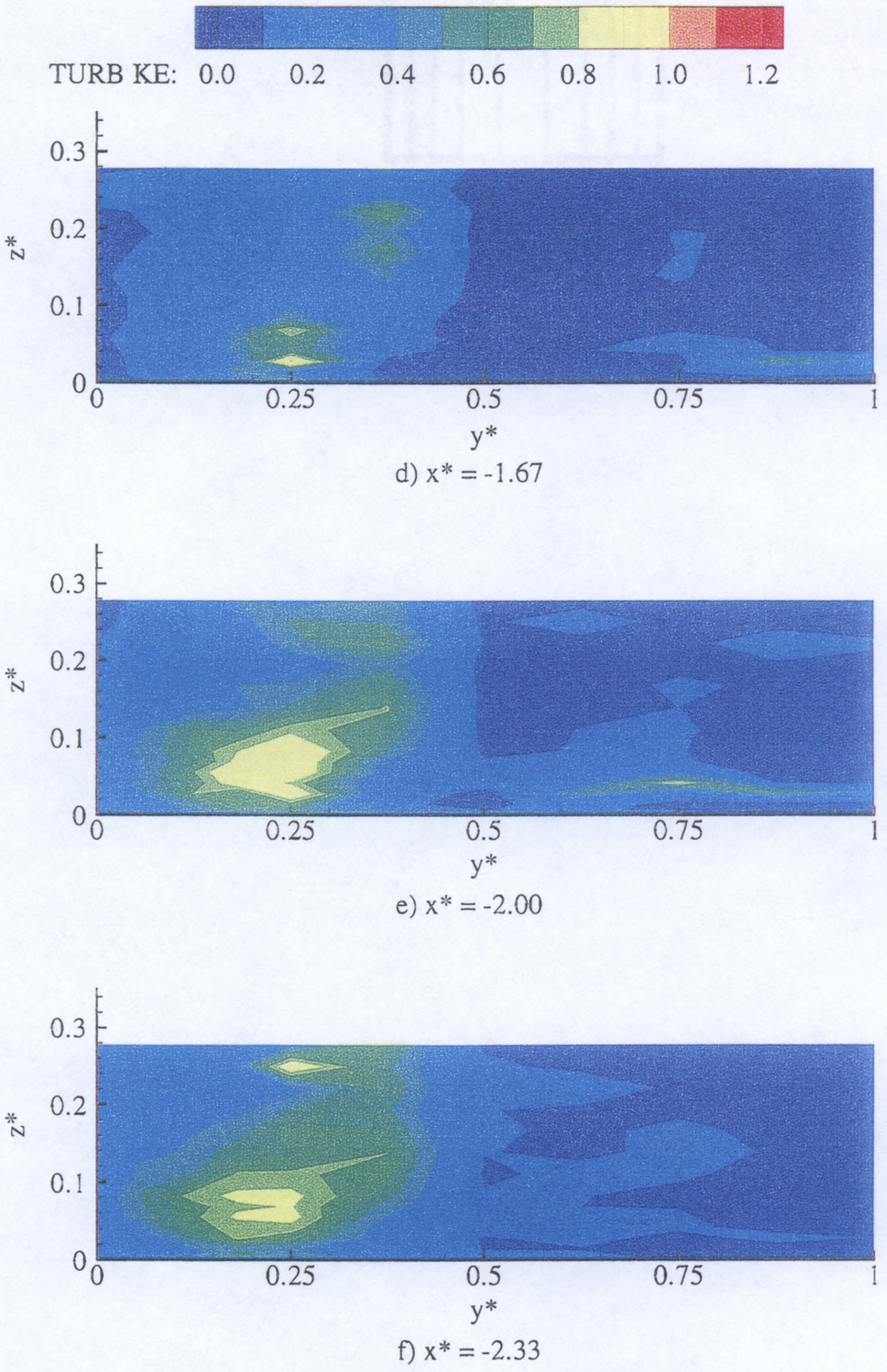

Figure F.6. Continued

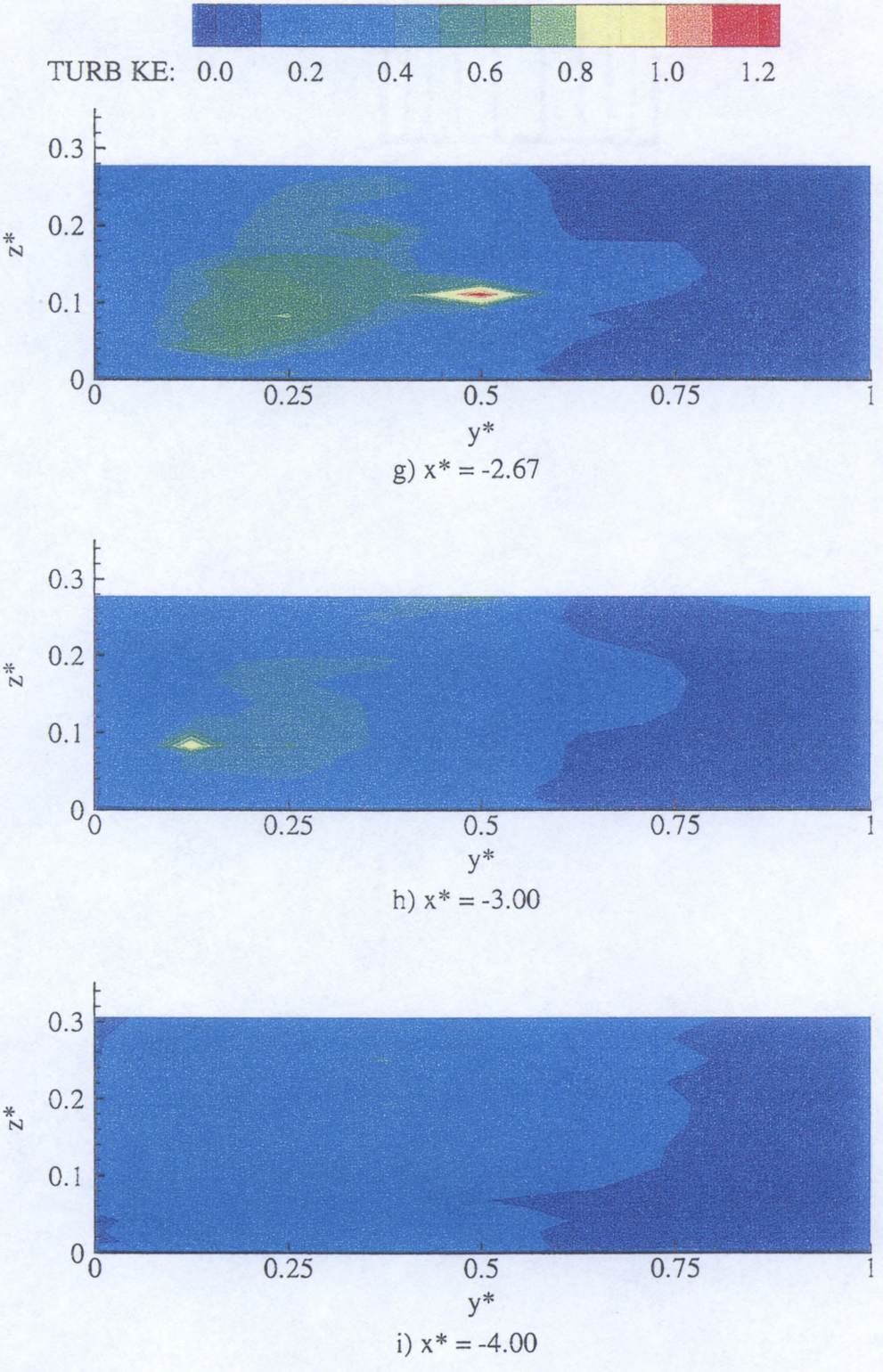

Figure F.6. Continued

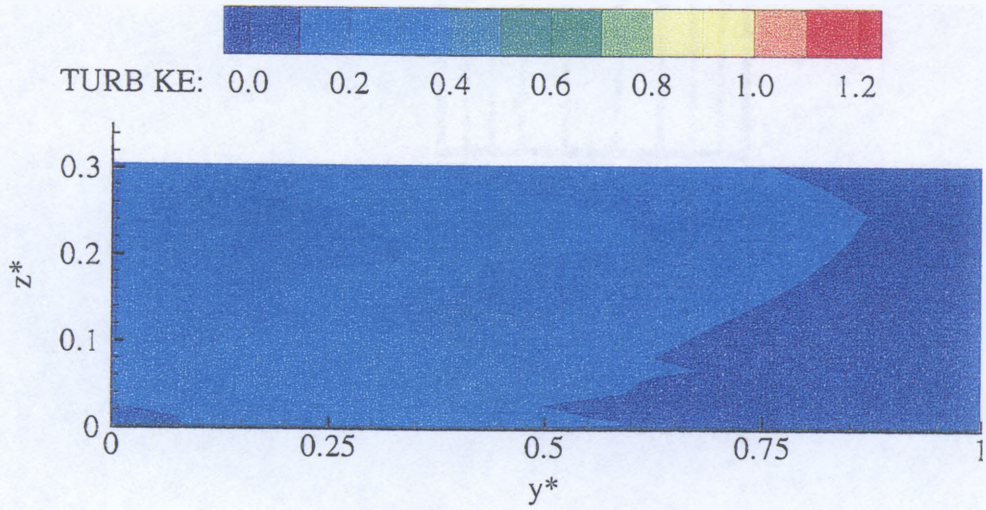

j) x* = -5.00

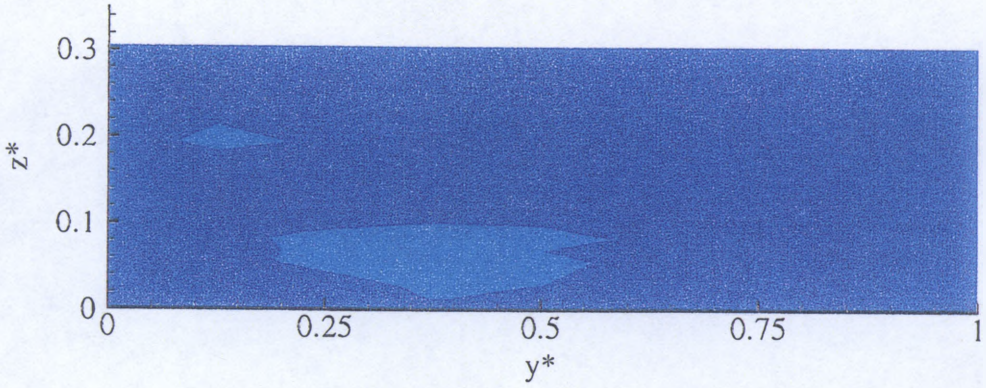

k) x* = -7.00

Figure F.6. Continued

APPENDIX G

DATA PLOTS FOR q* = 0.083

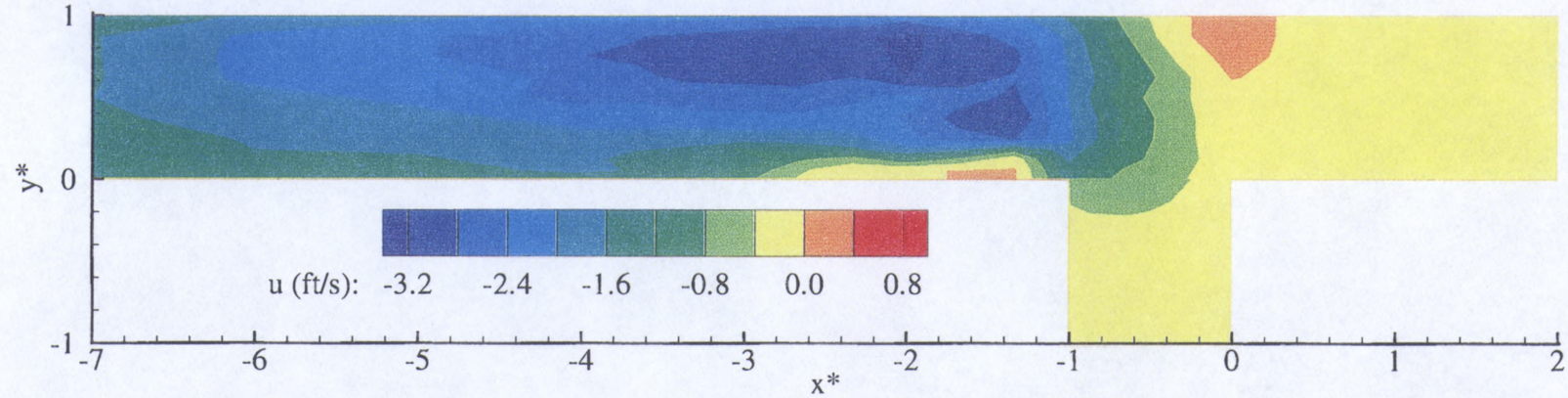

a) z* = 0.014

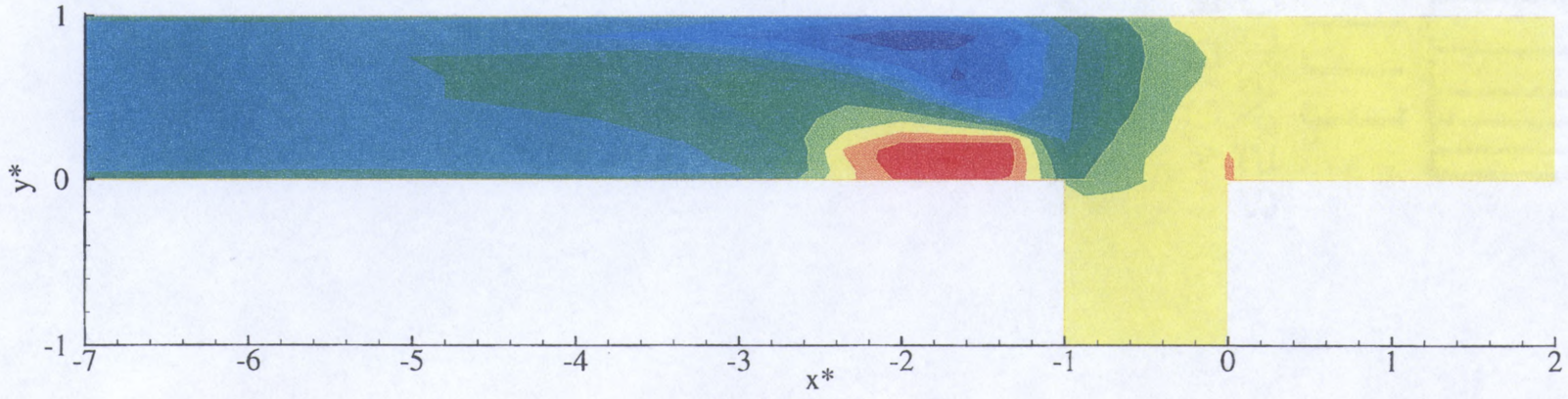

b) z* = 0.278

Figure G.1. u Velocity Plan View, q* = 0.083

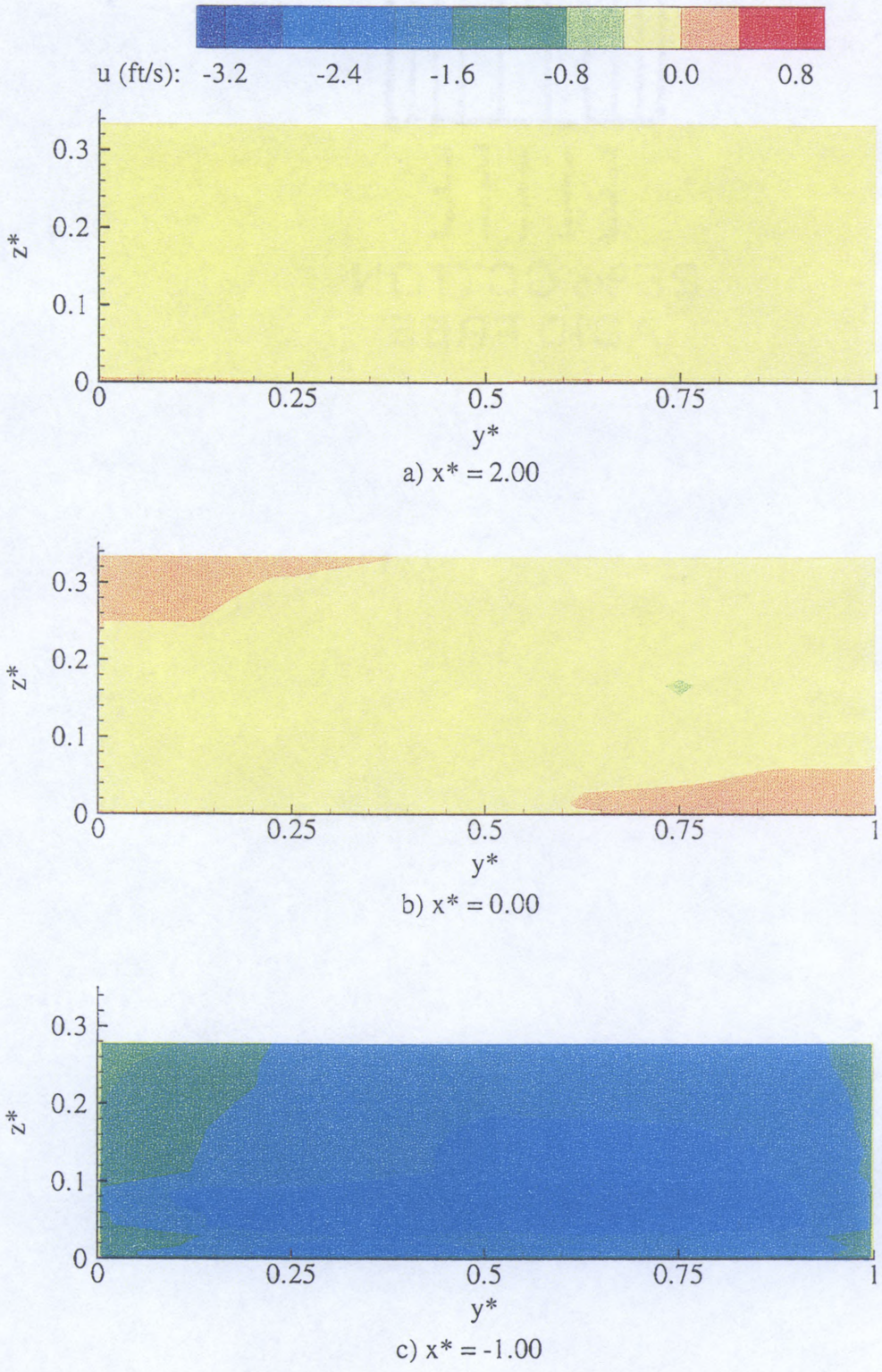

Figure G.2. u Velocity Cross-Sections, q* = 0.083

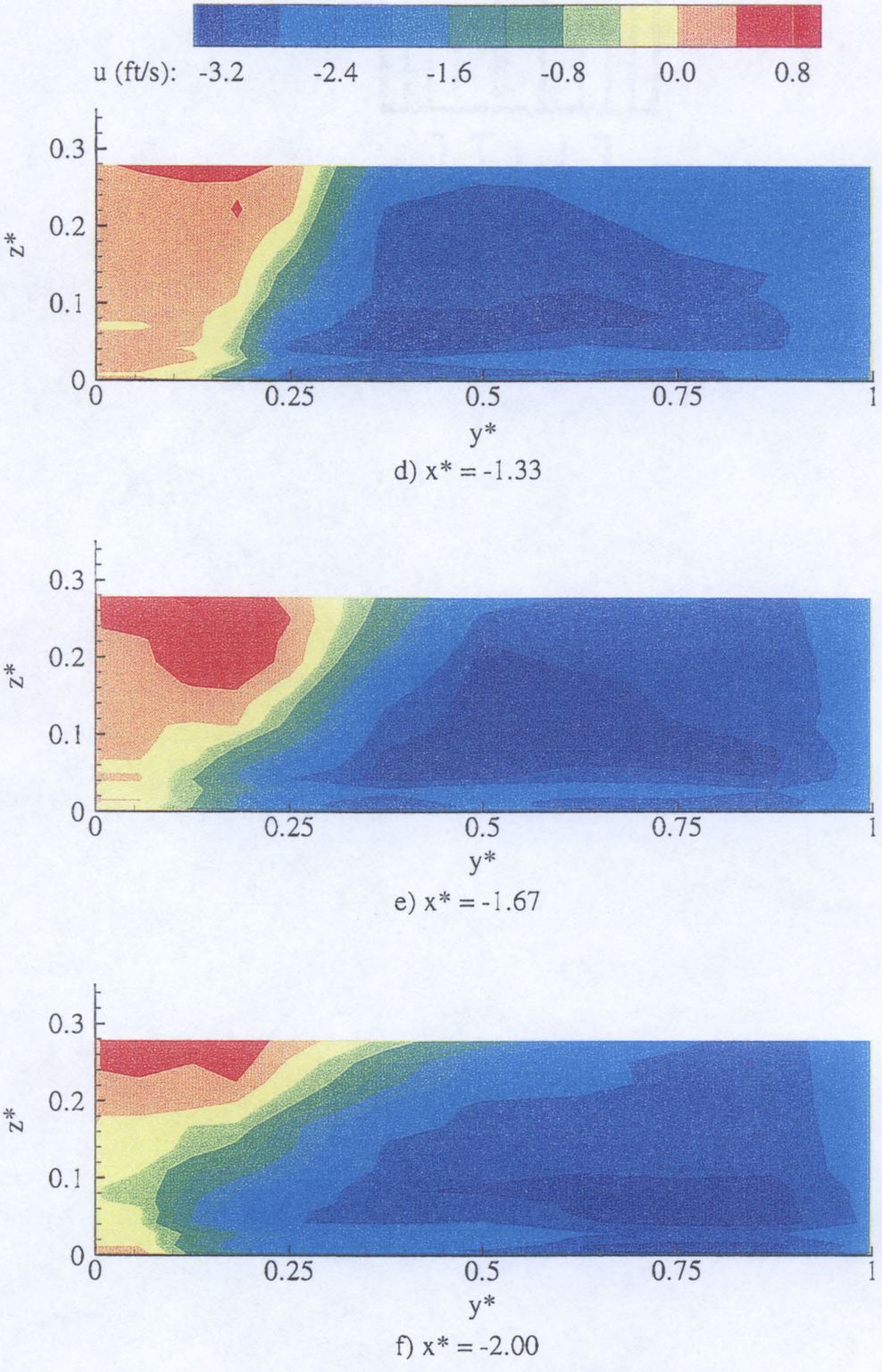

Figure G.2. Continued

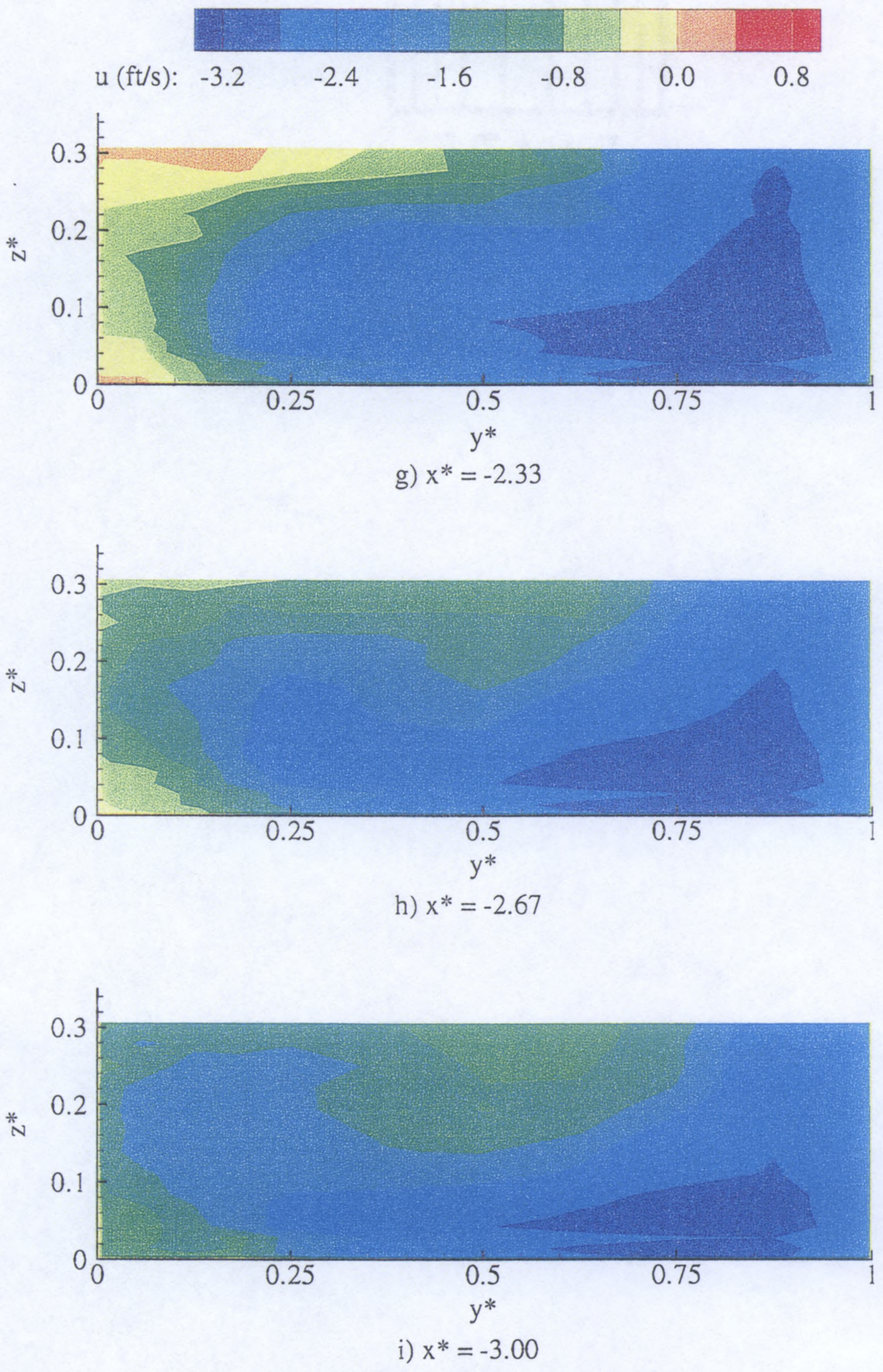

Figure G.2. Continued

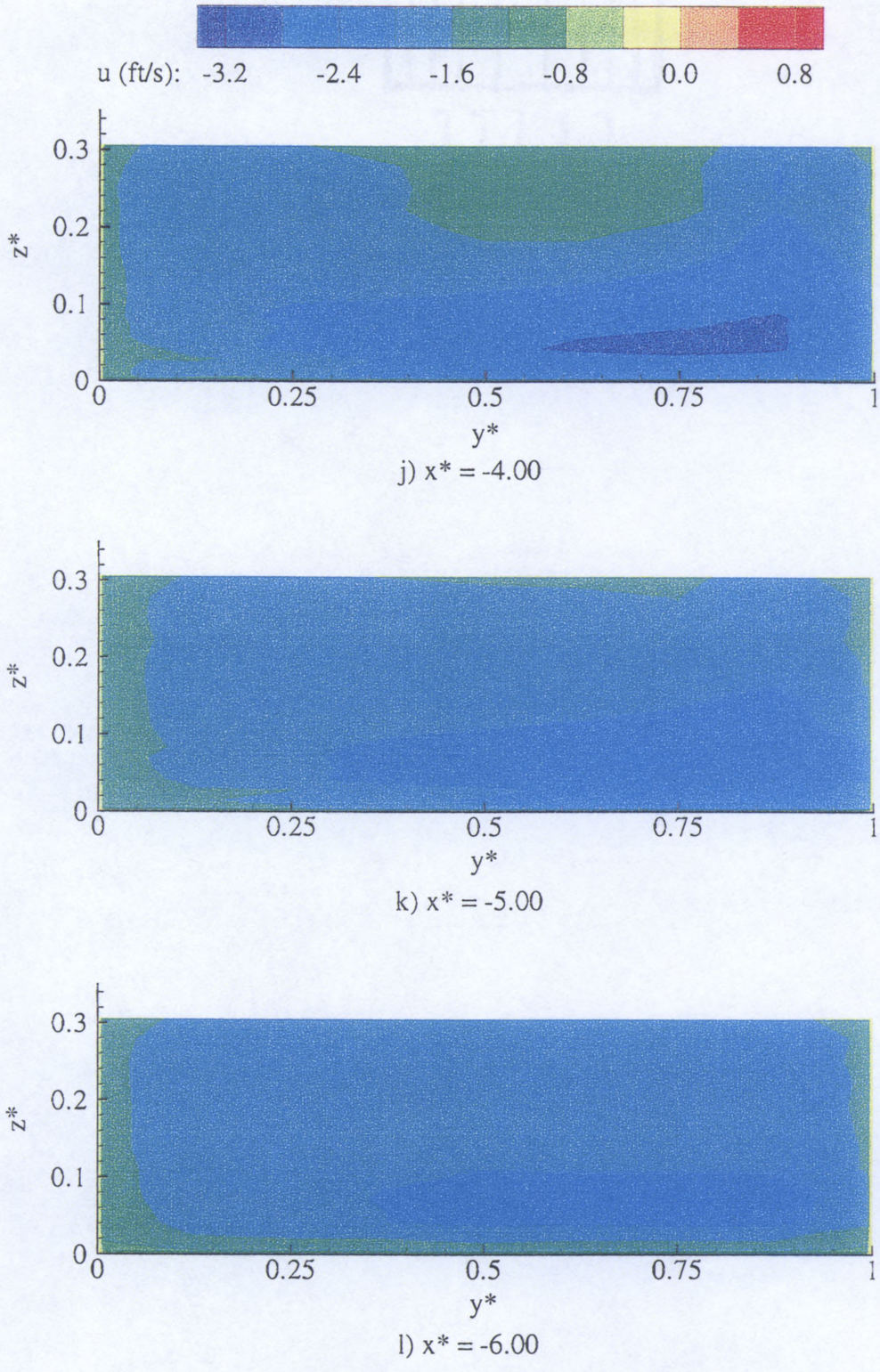

Figure G.2. Continued

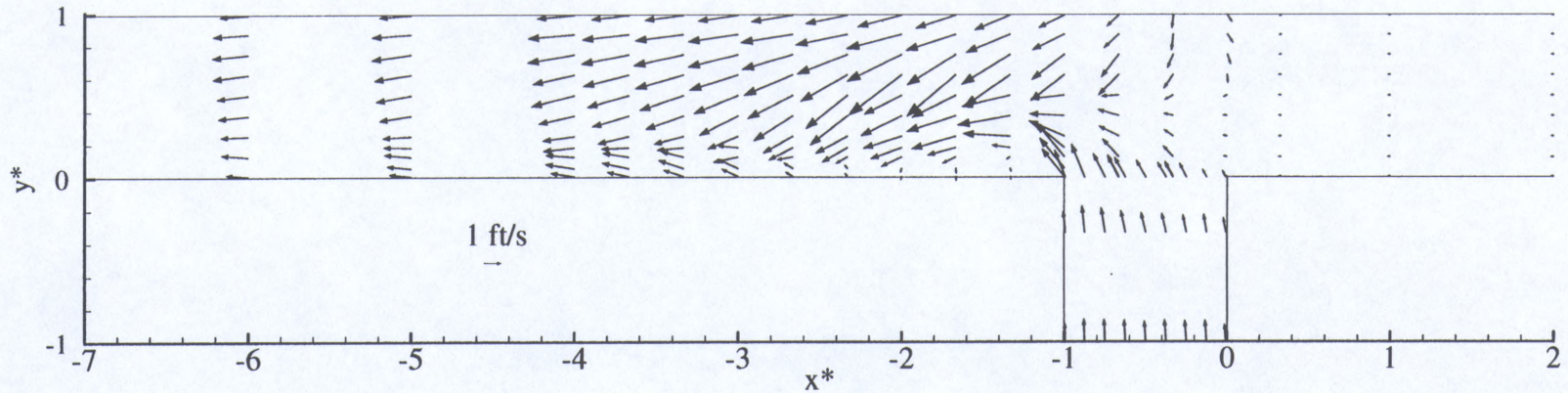

a) z* = 0.014

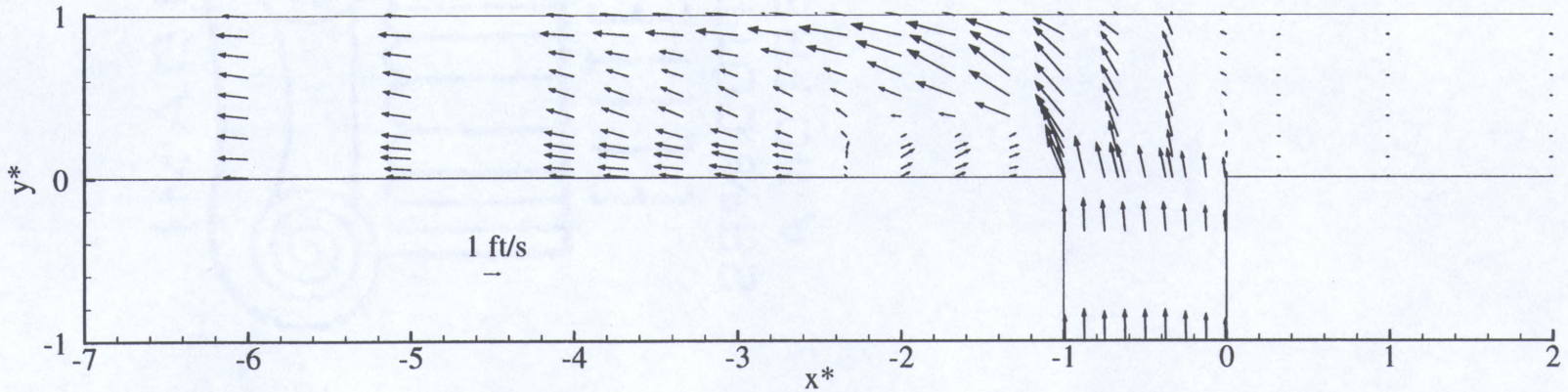

b) z* = 0.278

Figure G.3. u-v Vector Fields, q* = 0.083

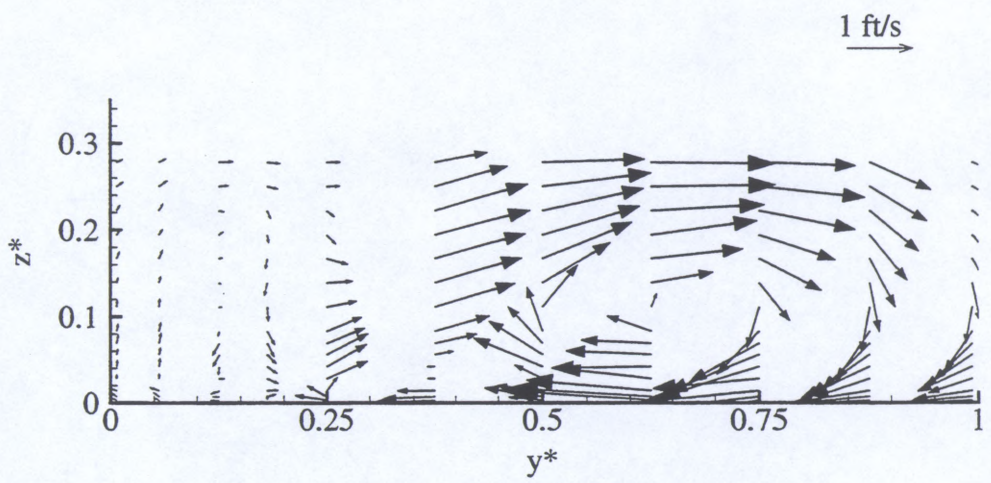

a) x* = -1.33

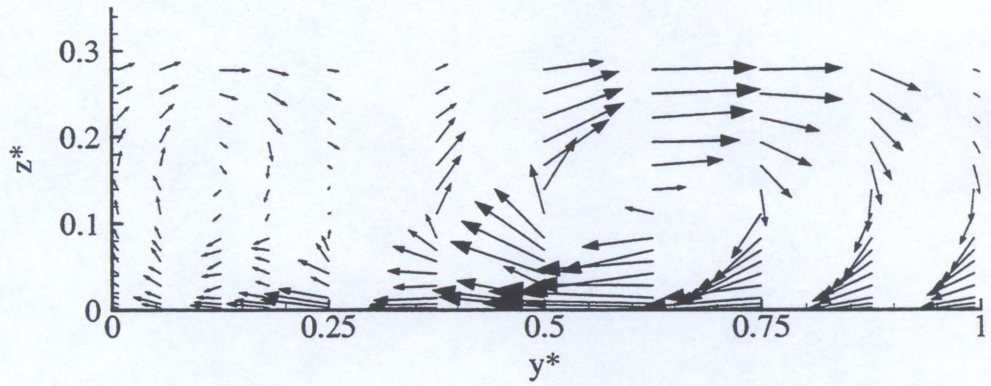

b) x* = -1.67

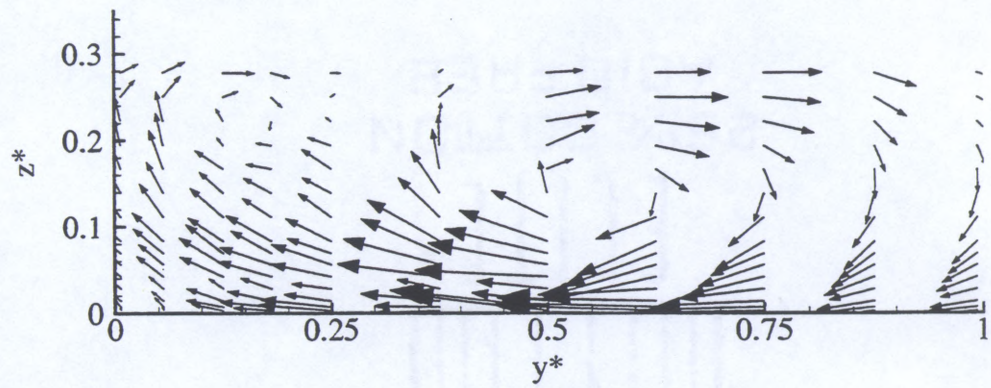

c) x* = -2.00

Figure G.4. v-w Vector Fields, q* = 0.083

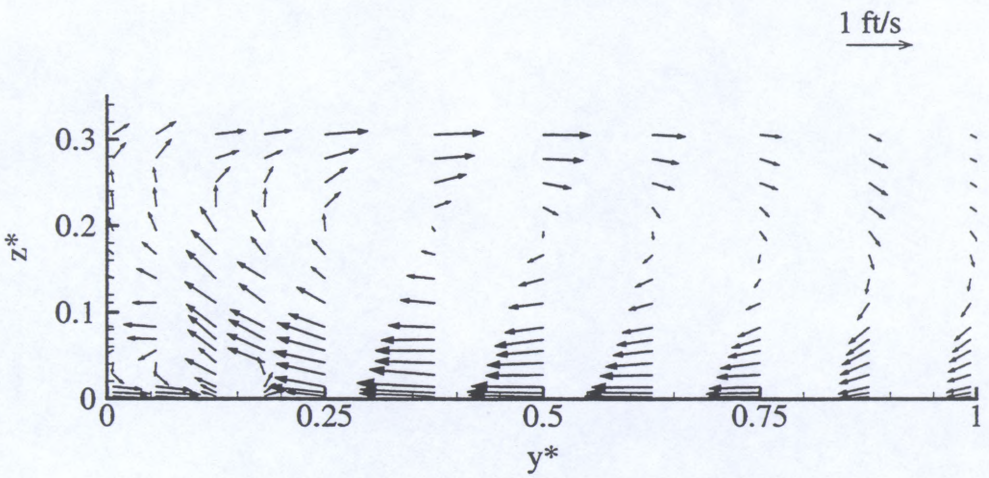

d) x* = -3.00

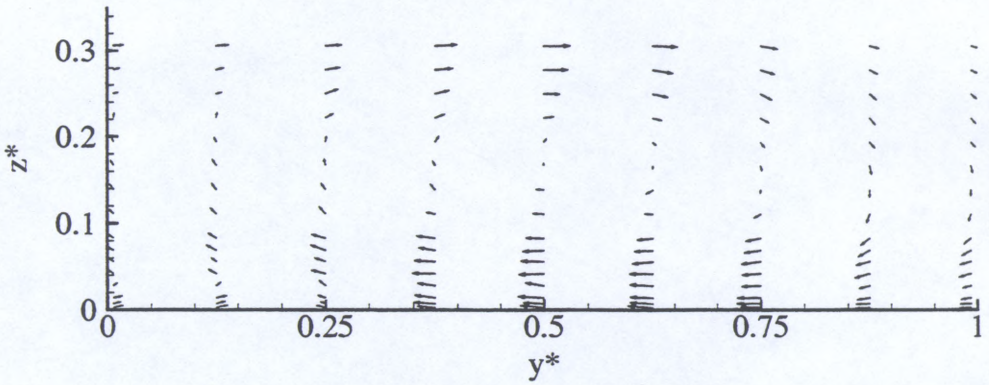

e) x* = -5.00

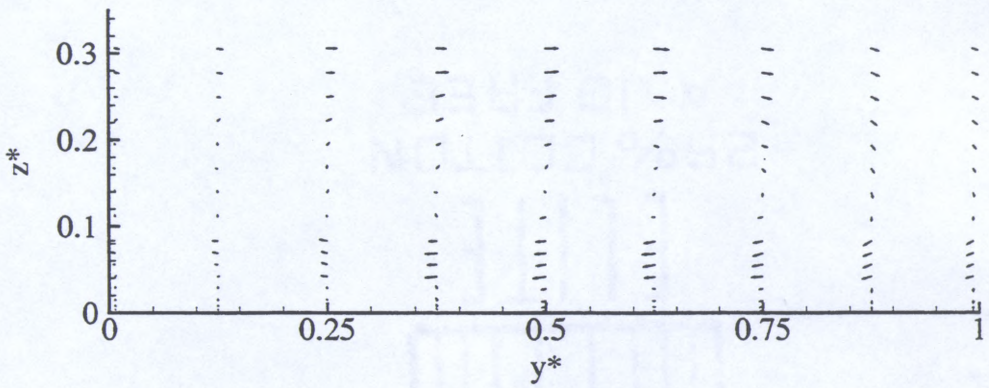

f) x* = -7.00

Figure G.4. Continued

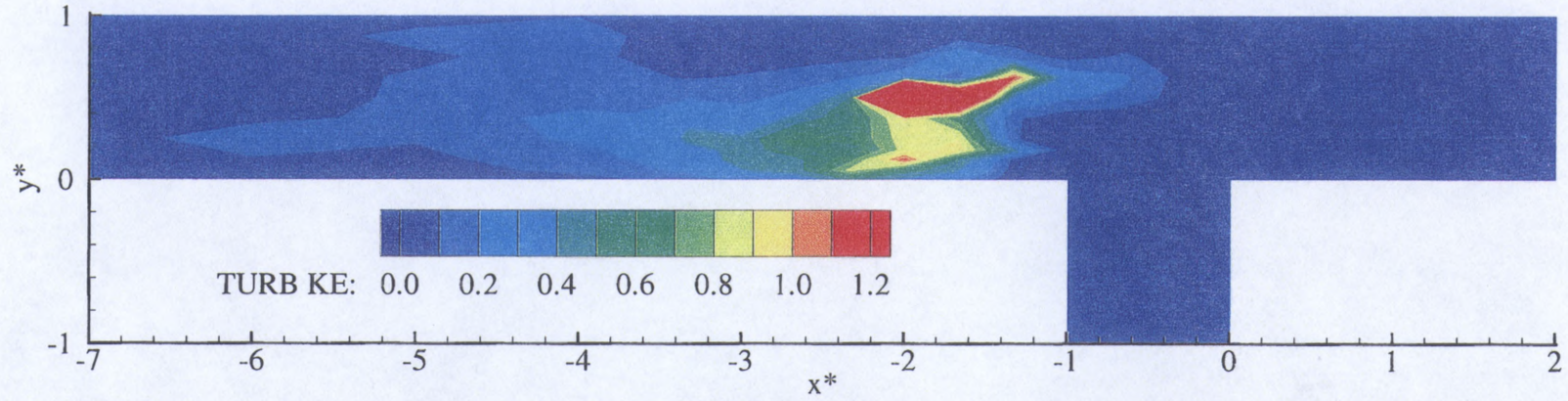

a) z* = 0.014

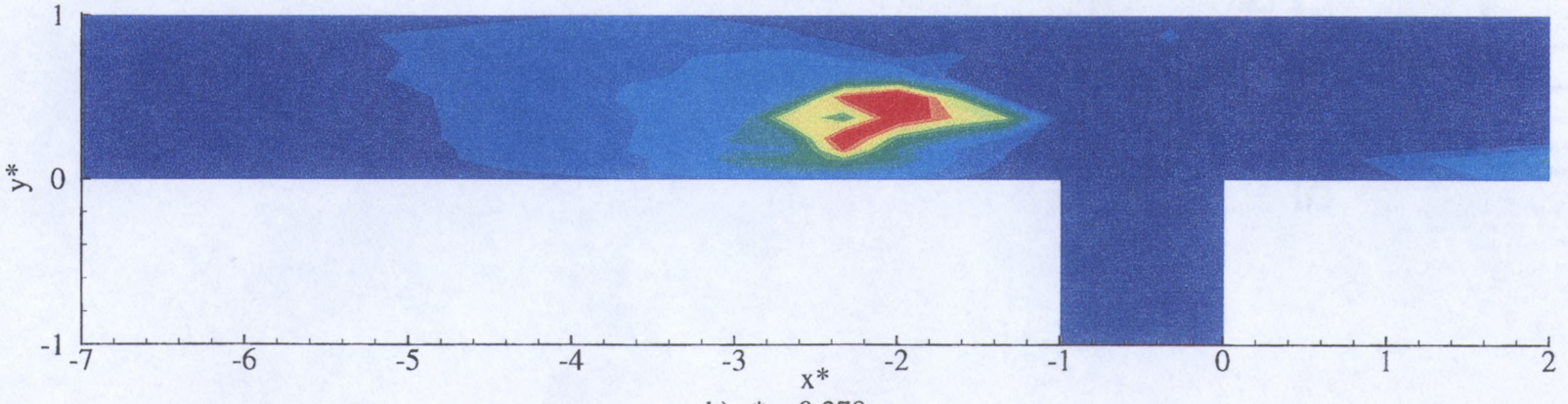

b) z* = 0.278

Figure G.5. Turbulent Kinetic Energy Plan View, q* = 0.083

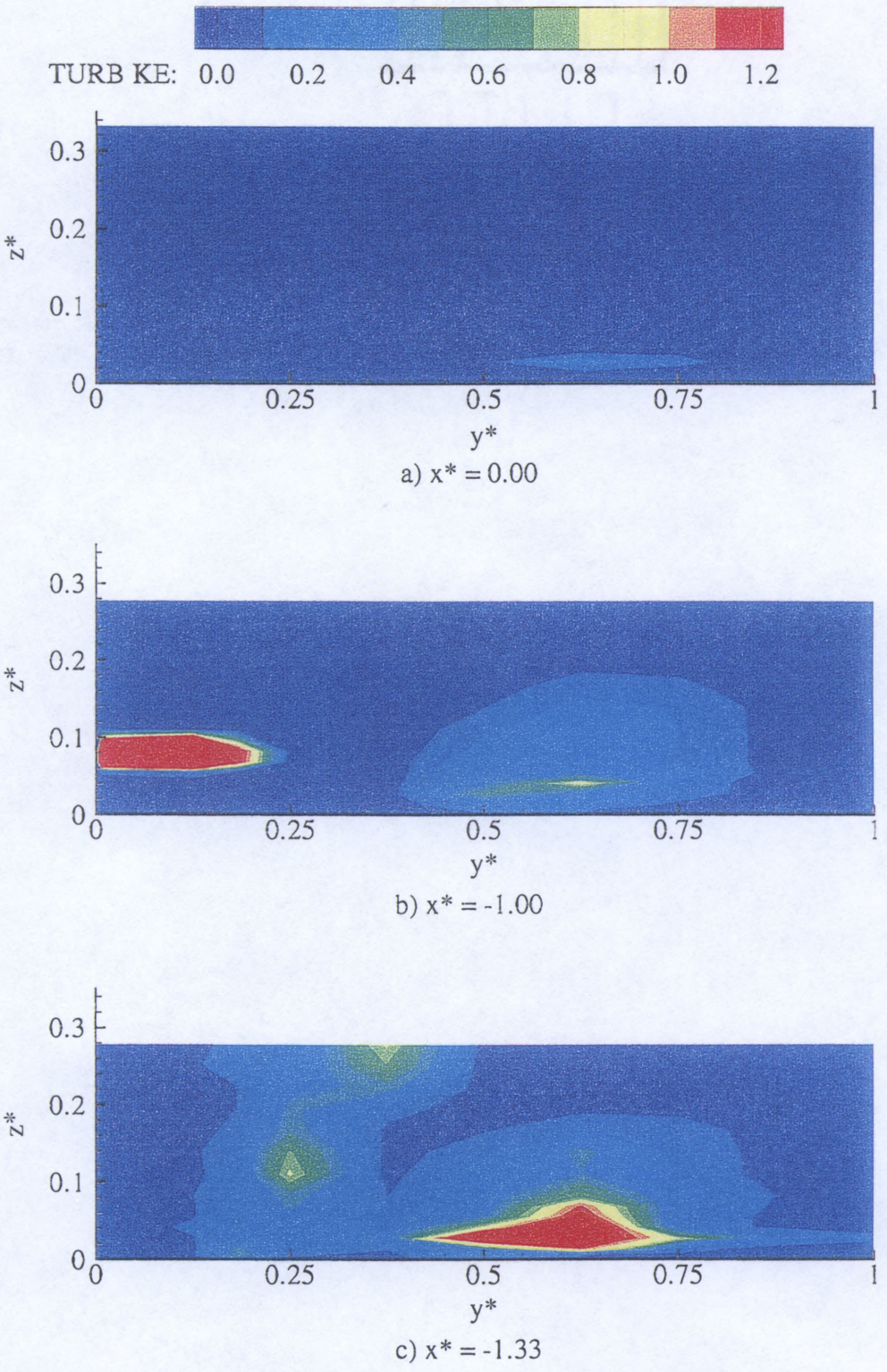

Figure G.6. Turbulent Kinetic Energy Cross-Sections, q* = 0.083

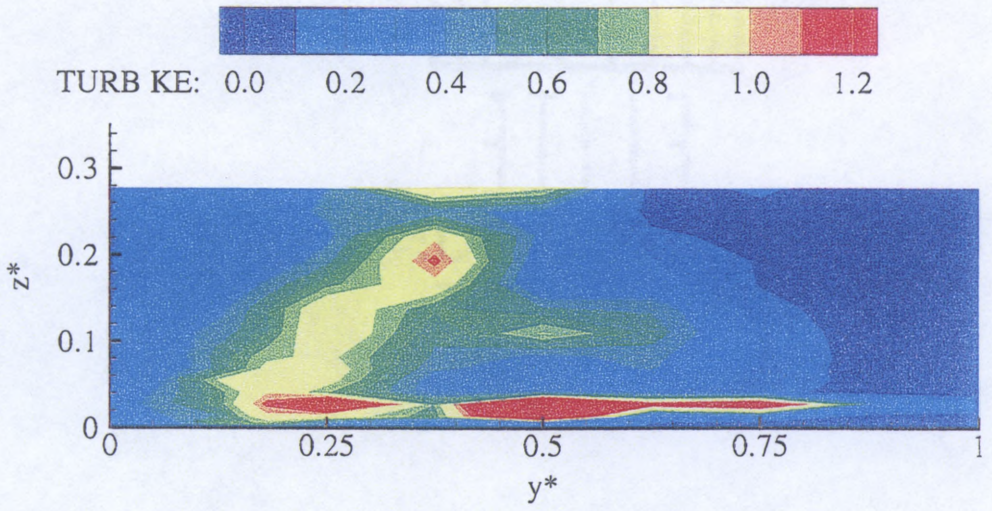

d) x* = -1.67

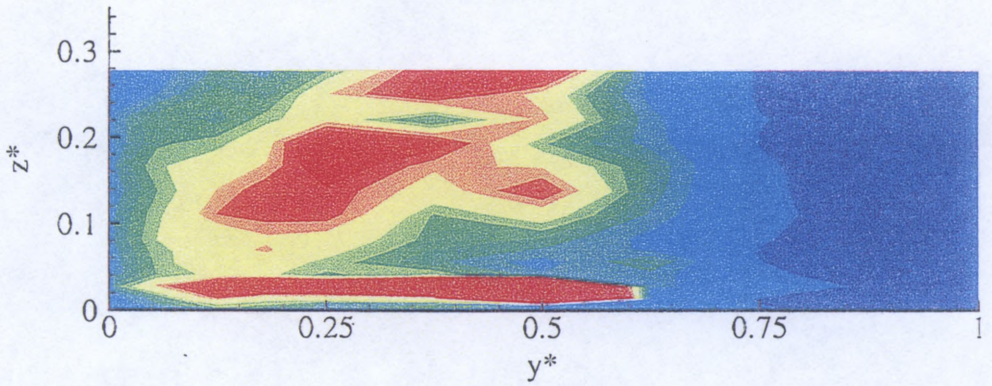

e) x* = -2.00

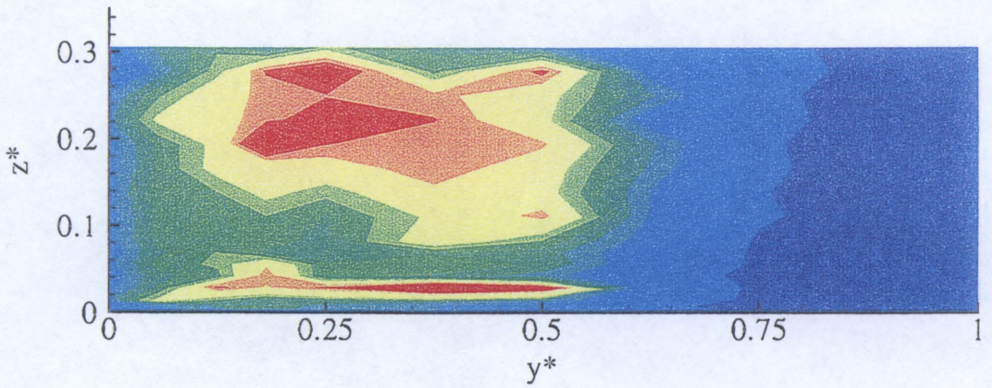

f) x* = -2.33

Figure G.6. Continued

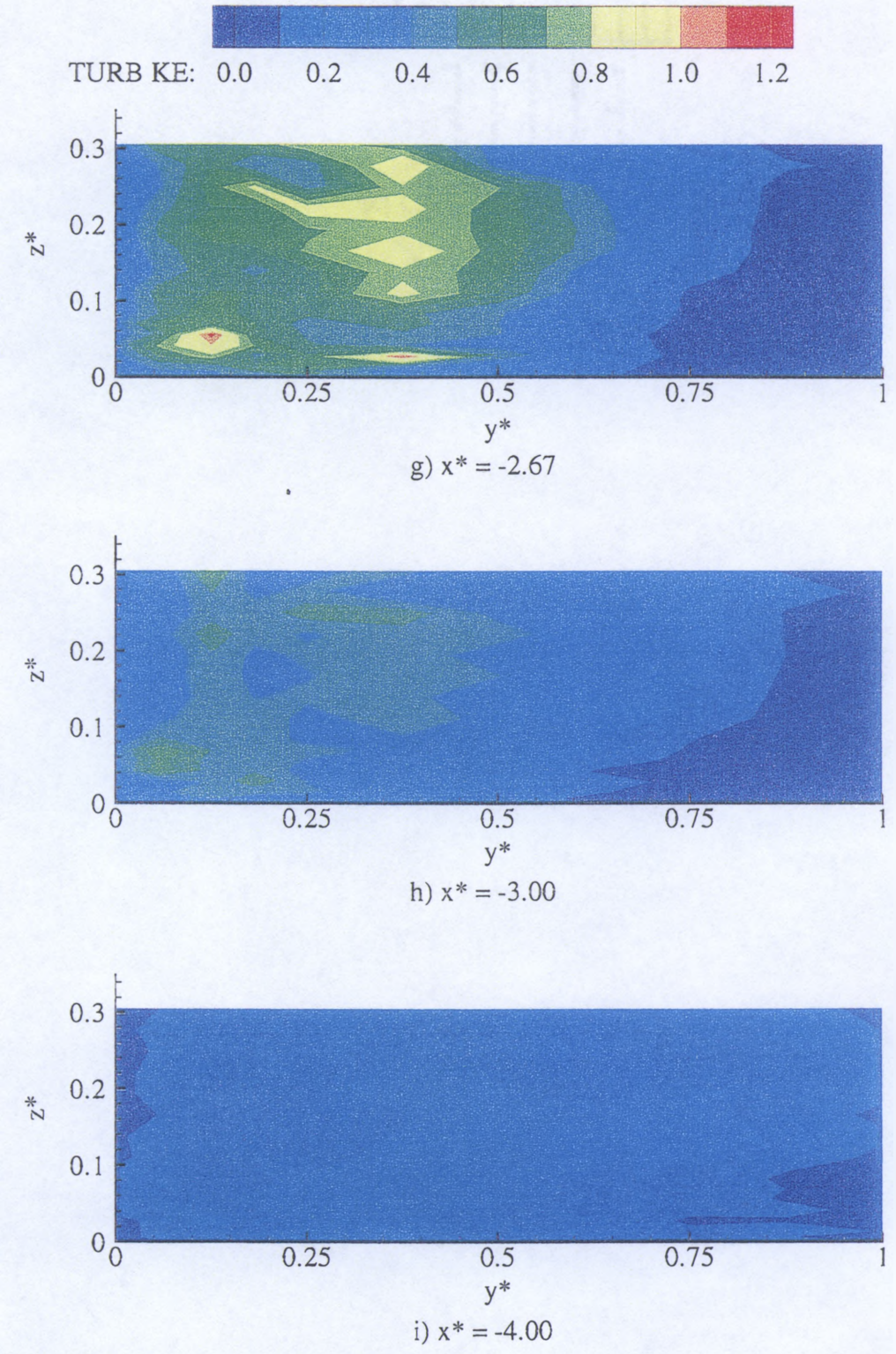

Figure G.6. Continued

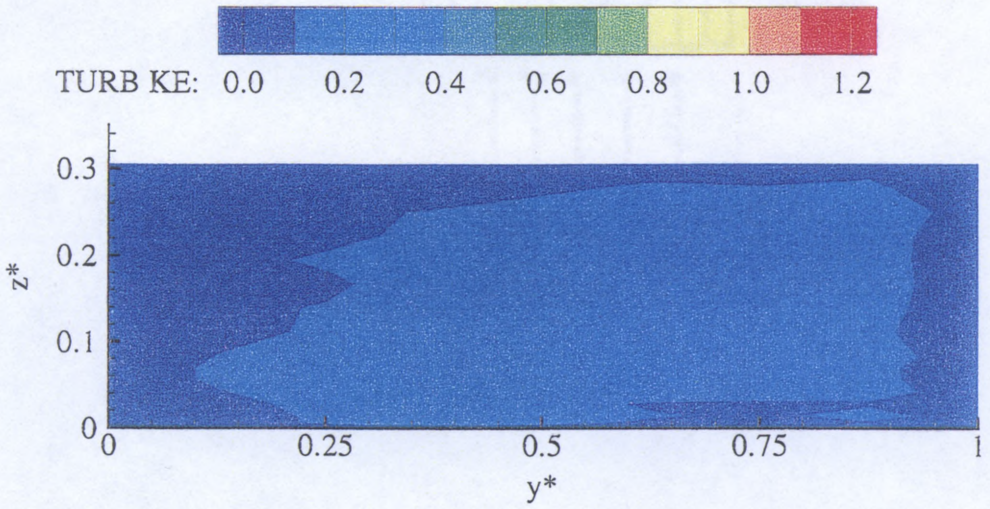

j) x* = -5.00

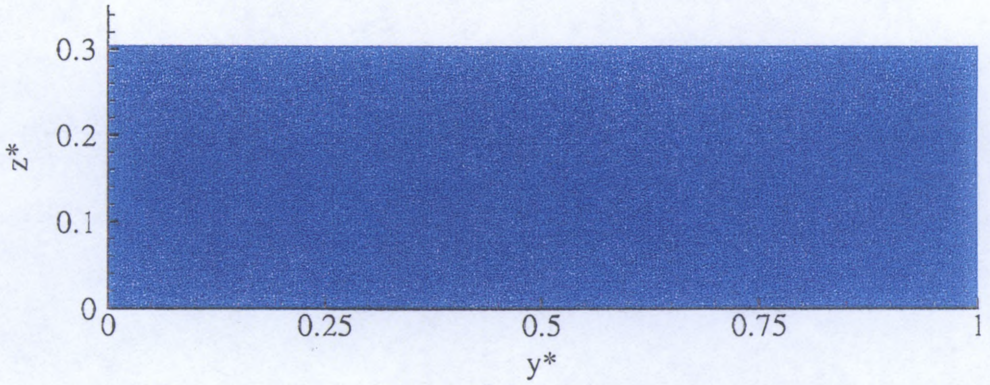

k) x* = -7.00

Figure G.6. Continued

REFERENCES

Best, J. L. and Reid, I. (1984). Separation Zone at Open-Channel Junctions. *Journal of Hydraulic Engineering*, ASCE, Vol. 110, No. 11, pp. 1588-1594.

Biron, P., Best, J. L. and Roy, A. G. (1996). Effects of Bed Discordance on Flow Dynamics at Open Channel Confluences. *Journal of Hydraulic Engineering*, ASCE, Vol. 122, No. 12, pp. 676-682.

Gurram, S. K., Karki, K. S. and Hager, W. H. (1997). Subcritical Junction Flow. *Journal of Hydraulic Engineering*, ASCE, Vol. 123, No. 5, pp. 447-455.

Hager, W. H. (1989). Transitional Flow in Channel Junctions. *Journal of Hydraulic Engineering*, ASCE, Vol. 115, No. 2, pp. 243-259.

Hsu, C. C., Wu, F. S. and Lee, W. J. (1998a). Flow at 90° Equal-Width Open-Channel Junction. *Journal of Hydraulic Engineering*, ASCE, Vol. 124, No. 2, pp. 186-191.

Hsu, C. C., Lee, W. J. and Chang, C. H. (1998b). Subcritical Open-Channel Junction Flow. *Journal of Hydraulic Engineering*, ASCE, Vol. 124, No. 8, pp. 847-855.

Joy, D. M. and Townsend, R. D. (1981). Improved Flow Characteristics at a 90° Channel Confluence. *5th Canadian Hydrotechnical Conference*, Fredericton, New Brunswick, pp. 781-799.

Lin, J. D. and Soong, H. K. (1979). Junction Losses in Open Channel Flows. *Water Resources Research*, Vol. 15, No. 2, pp. 414-418.

Kumar, S. G. (1993). Transitional Flow in Channel Junctions. *Journal of Hydraulic Research*, Vol. 31, No. 5, pp. 601-604.

Modi, P. N., Ariel, P. D. and Dandekar, M. M. (1981). Conformal Mapping for Channel Junction Flow. *Journal of the Hydraulics Division*, ASCE, Vol. 107, No. 12, pp. 1713-1733.

Ramamurthy, A. S., Carballada, L.B. and Tran, D. M. (1988). Combining Open Channel Flow at Right Angled Junctions. *Journal of Hydraulic Engineering*, ASCE, Vol. 114, No. 12, pp. 1449-1460.

Taylor, E. H. (1944). Flow Characteristics at Rectangular Open-Channel Junctions. *Transactions*, ASCE, 109,. pp. 893-902.

Webber, N. B. and Greated, C. A. (1966). An Investigation of Flow Behavior at the Junction of Rectangular Channels. *Proceedings of the Institution of Civil Engineers*, London, England, Vol. 34, pp. 321-334.